University of Iowa

Iowa Research Online

Theses and Dissertations

2006

A univariate decomposition method for higher-order reliability analysis and design optimization

Dong Wei
University of Iowa

A UNIVARIATE DECOMPOSITION METHOD FOR HIGHER-ORDER RELIABILITY ANALYSIS AND DESIGN OPTIMIZATION

by

Dong Wei

ABSTRACT

The objective of this research is to develop new stochastic methods based on most probable points (MPPs) for general reliability analysis and reliability-based design optimization of complex engineering systems. The current efforts involves: (1) univariate method with simulation for reliability analysis; (2) univariate method with numerical integration for reliability analysis; (3) multi-point univariate for reliability analysis involving multiple MPPs; and (4) univariate method for design sensitivity analysis and reliability-based design optimization.

Two MPP-based univariate decomposition methods were developed for component reliability analysis with highly nonlinear performance functions. Both methods involve novel function decomposition at MPP that facilitates higher-order univariate approximations of a performance function in the rotated Gaussian space. The first method entails Lagrange interpolation of univariate component functions that leads to an explicit performance function and subsequent Monte Carlo simulation. Based on linear or quadratic approximations of the univariate component function in the direction of the MPP, the second method formulates the performance function in a form amenable to an efficient reliability analysis by multiple one-dimensional integrations. Although both methods have comparable computational efficiency, the second method can be extended to derive analytical sensitivity of failure probability for design optimization. For reliability problems entailing multiple MPPs, a multi-point univariate decomposition method was also developed. In addition to the effort of identifying the MPP, the univariate methods require a small number of exact or numerical function evaluations at

selected input. Numerical results indicate that the MPP-based univariate methods provide accurate and/or computationally efficient estimates of failure probability than existing methods.

Finally, a new univariate decomposition method was developed for design sensitivity analysis and reliability-based design optimization subject to uncertain performance functions in constraints. The method involves a novel univariate approximation of a general multivariate function in the rotated Gaussian space; analytical sensitivity of failure probability with respect to design variables; and standard gradient-based optimization algorithms. In both reliability and sensitivity analyses, the proposed effort has been reduced to performing multiple one-dimensional integrations. Numerical results indicate that the proposed method provides accurate and computationally efficient estimates of the sensitivity of failure probability and leads to accurate design optimization of uncertain mechanical systems.

Abstract Approved: _____
Thesis supervisor

Professor /Mechanical and Industrial Engineering
Title and Department

July 12, 2006
Date

A UNIVARIATE DECOMPOSITION METHOD FOR HIGHER-ORDER

RELIABILITY ANALYSIS AND DESIGN OPTIMIZATION

by

Dong Wei

A thesis submitted in partial fulfillment
of the requirements for the Doctor of
Philosophy degree in Mechanical Engineering
in the Graduate College of
The University of Iowa

July 2006

Thesis Supervisor: Professor Sharif Rahman

Graduate College
The University of Iowa
Iowa City, Iowa

CERTIFICATE OF APPROVAL

_____

PH.D. THESIS

_____

This is to certify that the Ph.D. thesis of
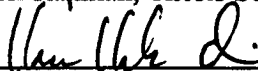
Dong Wei

has been approved by the Examining Committee for the
thesis requirement for the Doctor of Philosophy degree in
Mechanical Engineering at the July 2006 graduation.

Thesis committee: _____
                  Sharif Rahman, Thesis Supervisor

                  _____
                  Kyung K. Choi

                  _____
                  M. Asghar Bhatti

                  _____
                  Jia Lu

                  _____
                  Pavlo Krokhmal

To Li and Malcom

ACKNOWLEDGEMENTS

ABSTRACT

The objective of this research is to develop new stochastic methods based on most probable points (MPPs) for general reliability analysis and reliability-based design optimization of complex engineering systems. The current efforts involves: (1) univariate method with simulation for reliability analysis; (2) univariate method wit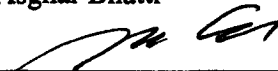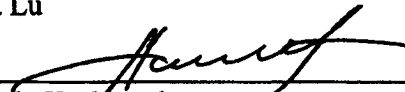h numerical integration for reliability analysis; (3) multi-point univariate for reliability analysis involving multiple MPPs; and (4) univariate method for design sensitivity analysis and reliability-based design optimization.

Two MPP-based univariate decomposition methods were developed for component reliability analysis with highly nonlinear performance functions. Both methods involve novel function decomposition at MPP that facilitates higher-order univariate approximations of a performance function in the rotated Gaussian space. The first method entails Lagrange interpolation of univariate component functions that leads to an explicit performance function and subsequent Monte Carlo simulation. Based on linear or quadratic approximations of the univariate component function in the direction of the MPP, the second method formulates the performance function in a form amenable to an efficient reliability analysis by multiple one-dimensional integrations. Although both methods have comparable computational efficiency, the second method can be extended to derive analytical sensitivity of failure probability for design optimization. For reliability problems entailing multiple MPPs, a multi-point univariate decomposition method was also developed. In addition to the effort of identifying the MPP, the univariate methods require a small number of exact or numerical function evaluations at

iv

selected input. Numerical results indicate that the MPP-based univariate methods provide accurate and/or computationally efficient estimates of failure probability than existing methods.

Finally, a new univariate decomposition method was developed for design sensitivity analysis and reliability-based design optimization subject to uncertain performance functions in constraints. The method involves a novel univariate approximation of a general multivariate function in the rotated Gaussian space; analytical sensitivity of failure probability with respect to design variables; and standard gradient-based optimization algorithms. In both reliability and sensitivity analyses, the proposed effort has been reduced to performing multiple one-dimensional integrations. Numerical results indicate that the proposed method provides accurate and computationally efficient estimates of the sensitivity of failure probability and leads to accurate design optimization of uncertain mechanical systems.

v

TABLE OF CONTENTS

LIST OF TABLES

LIST OF FIGURES

xiii

CHAPTER 1

INTRODUCTION

1.1 Background and Motivation

Balancing the requirements of reliability and cost is a dilemma for engineers in the design of complex engineering structures. Simply increasing the cost or weight of a structure does not always yield an improvement in reliability. Although traditional deterministic analysis and optimization techniques are well defined, they provide little or no assistance to a designer in consistently characterizing reliability. In other words, there is no systematic way for a deterministic design approach to predict structural safety probabilistically. Furthermore, optimization techniques based on a deterministic approach usually lead to a cost and/or weight savings, but an unreliable and/or unsafe design. There are many uncertainties, such as loads, material properties, geometry, and manufacturing tolerances that exist in engineering structures. The ability to accurately characterize and propagate these uncertainties is increasingly important in order to evaluate their effects on the probabilistic response and reliability of complex engineering structures. Figure 1.1 shows uncertainty propagation and probabilistic analysis in a physics-based simulation of such complex systems. Once designers are able to model uncertainties and predict their effects on response, reliability-based design optimization or robust design optimization can be conducted to solve the dilemma of cost and reliability.

Unfortunately, stochastic methods embedded in current reliability-based/robust design processes are inaccurate and/or computationally inefficient when: (1) the input-

output relationship is highly nonlinear; (2) the number of input random variables or fields is large; and (3) there are large statistical variations in input. For example, the most common approach to predict the failure probability involves first- and second- order reliability methods (FORM/SORM), which are not adequate for highly nonlinear problems. Simulation methods, which are usually employed for obtaining benchmark results, are not computationally efficient, and are not suitable to being embedded in optimization design processes. A new stochastic method is thus needed with greater accuracy and/or better efficiency than traditional methods. Such a method should be able to be integrated into the reliability-based optimization process to solve realistic design problems.

1.2 Objectives of the Study

The primary objective of this study is to develop a new stochastic method to solve highly nonlinear reliability problems, referred to as the most probable point (MPP)-based decomposition method, for reliability analysis and subsequent design optimization of complex engineering systems. The following four research directions have been pursued: (1) development of an MPP-based univariate method with simulation; (2) development of an MPP-based univariate method with numerical integration; (3) development of an MPP-based univariate method for solving multiple MPPs problems; (4) sensitivity analysis and reliability-based design optimization involving the new univariate method.

The proposed MPP-based decomposition method is new and will address highly nonlinear input-output transformation, unlimited number of dependent or correlated

random variables, and a large uncertainty of random input. The method involves a novel decomposition at the MPP that facilitates a univariate approximation of the general multivariate function, and probability estimation by simulation or numerical integration. This univariate approximation can be highly nonlinear, which includes all higher-order univariate terms, so it should provide better approximation around MPP than the linear (FORM) or quadratic (SORM) approximation. In addition to the effort of identifying the MPP, the method developed requires a small number of exact or numerical evaluations of performance function at a selected input. Hence, the proposed method will not only provide accurate solutions, but also create computationally efficient results compared with existing methods.

1.3 Organization of the Thesis

Chapter 2 presents mathematical generalities and notations required by reliability analysis and a state-of-the-art review of methods for reliability analysis and reliability-based-optimization-design. The need for fundamental research is emphasized.

Chapter 3 presents an MPP-based univariate method with simulation. The following topics are discussed: multivariate function decomposition at MPP, response surface generation by Lagrange interpolation, and Monte Carlo simulation.

Chapter 4 proposes an MPP-based univariate method with numerical integration. This method involves univariate decomposition of the performance function and univariate integration for failure probability estimation.

Chapter 5 discusses the extension of the MPP-based univariate method in multiple MPPs problems. This application involves a global optimization method entailing the barrier method, univariate decomposition at multiple MPPs, and system reliability analysis.

Chapter 6 presents reliability-based design optimization with univariate decomposition. The proposed RBDO process involves reliability analysis by univariate decomposition, design sensitivity analysis by univariate decomposition, and standard gradient-based design optimization.

Chapter 7 provides conclusions from the present work and recommendations for the future studies.
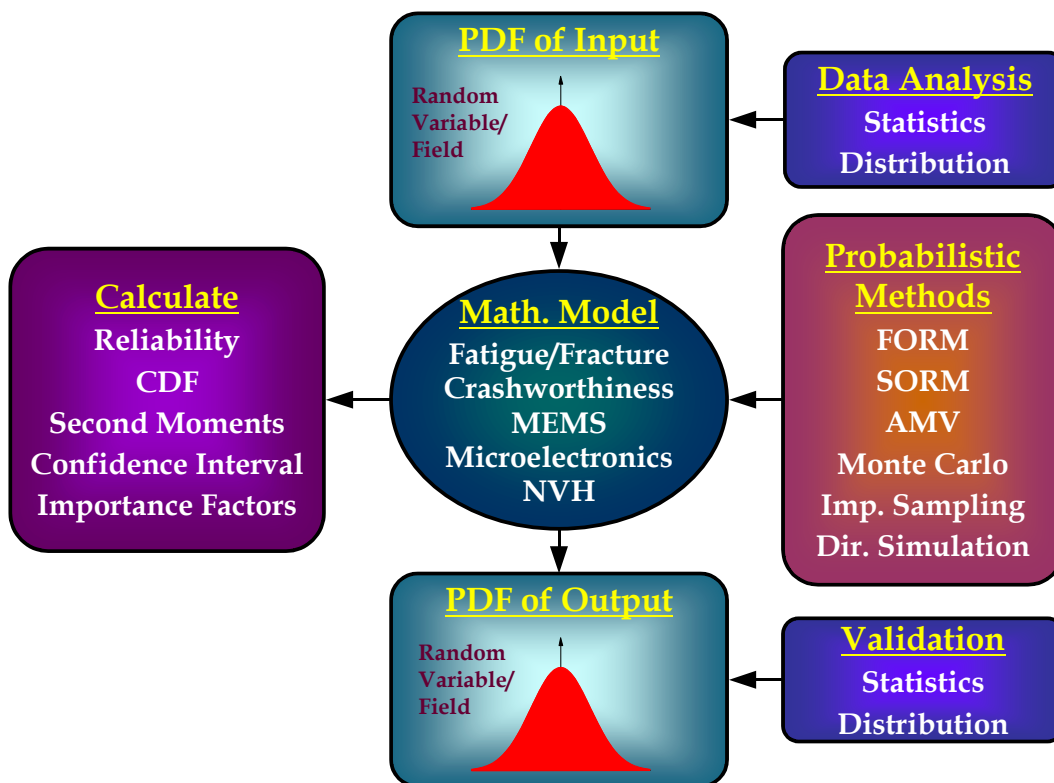
Figure 1.1 Uncertainty propagation and probabilistic analysis

CHAPTER 2

STATE-OF-THE-ART REVIEW

2.1 Generalities

This section introduces mathematical generalities and notations that are required by the probabilistic methods presented in subsequent sections.

2.1.1 Probability Space

The observation of a random phenomenon is classically referred to as a trial. All possible outcomes of a trial from the sample space of the phenomenon are denoted by Ω. An event is defined as a subset of Ω containing all outcomes $\omega \in \Omega$. If there is no outcome in one event, then the event is null set, and denoted by $\varnothing$. Events A and B are disjoint events if $A \cap B = \varnothing$. Events A and B are equal if and only if $A \subseteq B$ and $B \subseteq A$. Probability theory aims at associating numbers with events, i.e., their probability of occurrence. Let P denote the probability measure. An σ-algebra $\mathcal{F}$ is a nonempty collection of subsets of Ω such that the following holds: (1) The empty set $\varnothing$ is in $\mathcal{F}$. (2) If A is in $\mathcal{F}$, then so is the complement of A. (3) If A_i, $i = 1, 2, \ldots$ is a sequence of elements of $\mathcal{F}$, then the union of A_i is in $\mathcal{F}$. The probability space constructed by these notions is denoted by a triple $(\Omega, \mathcal{F}, P)$.

2.1.2 Random Variable

Consider a probability space $(\Omega, \mathcal{F}, P)$ and a real-valued random variable X defined on this space. The cumulative distribution function (CDF), denoted by $F_X(x)$,

of the random variable X is defined by the mapping $X : \Omega \to \mathbb{R}$ and the probability measure P, i.e., $F_X(x) \equiv P(X \le x)$. If $F_X(x)$ is continuous in $\mathbb{R}$, then the probability density function (PDF), denoted by $f_X(x)$, is $f_X(x) = dF_X(x)/dx$.

For function $g(X) = X^l$, where g is continuous in $\mathbb{R}$, the lth statistical moment or moment of order l of X is defined as

$$m_l \equiv \mathbb{E}\left[X^l \right] \equiv \int_{-\infty}^{+\infty} x^l f_X(x) dx , \tag{2.1}$$

where $\mathbb{E}$ is the expectation operator. If function $g(X) = (X - m_1)^l$ is considered, then the results in Equation (2.1) define the central moments of order l of X. The moments

$$\mu_X \equiv m_1 , \qquad \sigma_X \equiv \mathbb{E}[X - \mu_X]^2 , \qquad \nu \equiv \sigma_X / \mu_X , \qquad \gamma_3 \equiv \mathbb{E}[X - \mu_X]^3 / \sigma_X^3 , \qquad \text{and}$$

$\gamma_4 \equiv \mathbb{E}[X - \mu_X]^4 / \sigma_X^4$ are called the mean, variance, coefficient of variation, coefficient of skewness, and coefficient of kurtosis, respectively. These moments can be calculated by direct integration, as expressed in Equation (2.1). The positive square root of the variance is called standard deviation and is denoted by σ_X.

2.1.3 Random Vector

Let $\boldsymbol{X} = \{X_1, \cdots, X_N\}^T \in \mathbb{R}^N$ be a real-valued random vector on the probability space $(\Omega, \mathcal{F}, P)$. The joint cumulative distribution function, denoted by $F_X(\boldsymbol{x})$, of $\boldsymbol{X}$ is defined by the mapping $\boldsymbol{X} : \Omega \to \mathbb{R}^N$ and the probability measure P, i.e.,

$F_X(x) \equiv P\left(\bigcap_{i=1}^{N}\{X_i \le x_i\}\right)$. If $F_X(x)$ is such that $f_X(x) = \partial^N F_X(x)/\partial x_1 \cdots \partial x_N$ exists, then $f_X(x)$ is called the joint probability density function of X.

Consider continuous function $g(X) = \prod_{i=1}^{N} X_i^{l_i}$, where $l_i \ge 0, i = 1, \cdots, N$ are integers. The lth statistical moment or moment of order $l = \sum_{i=1}^{N} l_i$ of X is

$$m_{l_1, \cdots, l_N} \equiv \mathbb{E}\left[g(X)\right] \equiv \mathbb{E}\left[\prod_{i=1}^{N} X_i^{l_i}\right]. \tag{2.2}$$

For example, the first and second moment properties, such as mean μ_{X_i} of X_i, correlation ρ_{ij} of (X_i, X_j), covariance γ_{ij} of (X_i, X_j), and variance $\sigma_{X_i}^2$ of X_i, can be easily obtained from Equation (2.2) as

$$\mu_{X_i} \equiv \mathbb{E}\left[X_i\right] = m_{l_1, \cdots, l_N} \text{ for } l_i = 1, l_j = 0, j \ne i, \tag{2.3}$$

$$\rho_{ij} \equiv \mathbb{E}\left[X_i X_j\right] = m_{l_1, \cdots, l_N} \text{ for } l_i = l_j = 1, l_k = 0, k \ne i, j, \tag{2.4}$$

$$\gamma_{ij} \equiv \mathbb{E}\left[\left(X_i - \mu_{X_i}\right)\left(X_j - \mu_{X_j}\right)\right] = \rho_{ij} - \mu_{X_i}\mu_{X_j}, \tag{2.5}$$

and

$$\sigma_{X_i}^2 \equiv \mathbb{E}\left[X_i - \mu_{X_i}\right]^2 = \gamma_{ii}. \tag{2.6}$$

2.2 Reliability Analysis

2.2.1 Basic Random Variables and Limit State Function

Consider a system with uncertain mechanical characteristics that is subject to random loads. Denote by X an N-dimensional vector of *basic random variables* with

components $\{X_1, \ldots, X_N\}$ describing the randomness in geometry, material properties and loading. To assess the reliability of the structural system, a *limit state function g* that depends on basic random vector $\boldsymbol{X}$ defined as follows: $g(\boldsymbol{X}) > 0$, which defines the safe state of the structure, and $g(\boldsymbol{X}) \leq 0$ defines the failure state. The values of $\boldsymbol{X}$ satisfying $g(\boldsymbol{X}) = 0$ define the limit state surface of the structure in the original space.

2.2.2 Component and System Reliability Analyses

A fundamental problem in time-invariant *component reliability analysis* entails calculation of a multi-fold integral (Madsen, et. al, 1986)

$$P_F \equiv P\left[g(\boldsymbol{X}) < 0\right] = \int_{g(\boldsymbol{x}) < 0} f_X(\boldsymbol{x}) d\boldsymbol{x}, \tag{2.7}$$

where $\boldsymbol{X} = \{X_1, \cdots, X_N\}^T \in \mathbb{R}^N$ is a real-valued, *N*-dimensional random vector defined on a probability space $(\Omega, \mathcal{F}, P)$ comprising the sample space Ω, the σ-field $\mathcal{F}$, and the probability measure P; $g(\boldsymbol{x})$ is the performance function, such that $g(\boldsymbol{x}) < 0$ represents the failure domain; P_F is the probability of failure; and $f_X(\boldsymbol{x})$ is the joint probability density function of $\boldsymbol{X}$, which typically represents loads, material properties, and geometry, respectively.

In general, any engineering system has to satisfy more than one performance criterion. *System reliability* evaluations are used to consider multiple failure modes and/or multiple component failures. A complete reliability analysis includes both

component- and system-level estimates. If there are M failure modes or multiple component failures, series, parallel and mixed system are described by

series system

$$F = \bigcup_{i=1}^{M} F_i \,, \tag{2.8}$$

parallel system

$$F = \bigcap_{i=1}^{M} F_i \,, \tag{2.9}$$

parallel systems in series

$$F = \bigcup_{i=1}^{l} \bigcap_{j=1}^{m_i} F_{ij} \,, \ \sum_{i=1}^{l} m_i = M \,, \tag{2.10}$$

and series systems in parallel

$$F = \bigcap_{i=1}^{l} \bigcup_{j=1}^{m_i} F_{ij} \,, \ \sum_{i=1}^{1} m_i = M \,, \tag{2.11}$$

where $F_i \equiv g_i(X) < 0$ is the failure event of the ith system component, $g_i(X)$ is the ith performance function, and F is the system failure event.

If Equation (2.10) is a minimal set, it can be denoted by a minimal *cut set*. Cut sets are minimal if they contain no other cut sets as a genuine subset. Analogously, Equation (2.11) is called a *tie set*. Such sets are minimal if no tie set contains another tie set as a genuine subset.

For a series system made of M independent events, the failure probability is given by

$$P_F = P\left[\bigcup_{i=1}^{M} F_i \right] = 1 - \prod_{i=1}^{M} \left(1 - P(F_i)\right). \tag{2.12}$$

Similarly, for a parallel system consisting of M independent events, the failure probability is

$$P_F = P\left[\bigcap_{i=1}^{M} F_i\right] = \prod_{i=1}^{M} P(F_i).$$ (2.13)

In the case of fully dependent events,

$$P_F = P\left[\bigcup_{i=1}^{M} F_i\right] = \max_i \{P(F_i)\}, \ i = 1, \cdots, M,$$ (2.14)

and

$$P_F = P\left[\bigcap_{i=1}^{M} F_i\right] = \min_i \{P(F_i)\}, \ i = 1, \cdots, M.$$ (2.15)

For arbitrary cases of series system (failure domain is given by the intersection of componental failure domains), the failure probability can be estimated by

$$P_F = P\left[\bigcap_{i=1}^{M} F_i\right] \cong \Phi_M(-\boldsymbol{\beta}; \boldsymbol{R}),$$ (2.16)

where $\Phi_n(\bullet)$ is the joint CDF of an M-dimensional Gaussian vector, $\boldsymbol{\beta} = \{\beta_1, \cdots, \beta_M\}^T$ is a vector of *reliability indices* obtained by FORM/SORM (will be discussed in section 2.4.2) for each failure event, and $\boldsymbol{R}$ is the correlation matrix.

Furthermore, if the failure events can be reduced to the minimal cut set and the cut sets all have small failure probabilities, then the narrow probability bounds can be derived as

$$P_{F,L} \le P_F \le P_{F,U},$$ (2.17a)

where the lower bound $P_{F,L}$ and the upper bound $P_{F,U}$ are

$$P_{F,L} = P(F_1) + \sum_{i=2}^{M} \max\left\{0, P(F_i) - \sum_{i=2}^{M} P(F_i \cap F_j)\right\}$$ (2.17b)

and

$$P_{F,U} = P(F_1) + \sum_{i=2}^{M} \left\{ P(F_i) - \max_{j<i} \left\{ P(F_i \cap F_j) \right\} \right\}. \qquad (2.17c)$$

2.2.3 Early Reliability Analyses

Early structural reliability analysis aimed at determining the failure probability in terms of second moment statistics of resistance and load variables. Suppose that performances of a structural system can be lumped into two random variables denoted by resistance R and load S respectively. The safety margin is defined by

$$Z \equiv R - S. \qquad (2.18)$$

Cornell's reliability index (Cornell, 1969) is then defined by

$$\beta_C = \frac{\mu_Z}{\sigma_Z}, \qquad (2.19)$$

where μ_Z and σ_Z are mean and standard deviation respectively of Z. It can be given the following interpretation: if R and S are jointly normal, so is Z. The failure probability is given by

$$P_F = P(Z \le 0) = P\left(\frac{Z - \mu_Z}{\sigma_Z} \le -\frac{\mu_Z}{\sigma_Z} \right) \equiv \Phi(-\beta_C), \qquad (2.20)$$

where $\Phi(\cdot)$ is the standard normal cumulative distribution function. In this case, β_C can be described as a function of the second moment statistics of R and S, given by

$$\beta_C = \frac{\mu_R - \mu_S}{\sqrt{\sigma_R^2 + \sigma_S^2 - 2\rho_{RS}\sigma_R\sigma_S}}, \qquad (2.21)$$

where μ_R, σ_R are mean and standard deviation respectively of R, μ_S, σ_S are mean and standard deviation respectively of S, and ρ_{RS} is the correlation coefficient of R and S.

The general case would be that Z is a limit state function of random vector $\boldsymbol{X}$, $Z \equiv g(\boldsymbol{X})$, where $\boldsymbol{X} = \{X_1, \cdots, X_N\}^T \in \mathbb{R}^N$, and the mean vector $\boldsymbol{\mu}_X$ and covariance matrix $\boldsymbol{R}$ are known. If g-function is nonlinear, using Taylor expansion around the mean and only keeping the linear term will lead to the so-called *mean value first order reliability index*

$$\beta_{MVFOSM} = \frac{g(\boldsymbol{\mu}_X)}{\sqrt{\left(\nabla g\big|_{X=\mu_X}\right)^T \boldsymbol{R} \, \nabla g\big|_{X=\mu_X}}} \ . \tag{2.22}$$

Where $\nabla = \{\partial/\partial X_1, \cdots, \partial/\partial X_N\}^T$.

2.2.4 Methods of Reliability Analysis

For most practical problems, the exact evaluation of the integral in Equation (2.7), either analytical or numerical, is not possible because N is large, $f_X(\boldsymbol{x})$ is generally non-Gaussian, and $g(\boldsymbol{x})$ is highly nonlinear function of $\boldsymbol{x}$. Therefore, some approximation and simulation methods have been developed, which will be discussed in detail in subsequent sections. These methods include mean-value methods, first-, second-, and higher-order reliability methods, simulation methods, response surface methods, and recently developed decomposition methods.

2.3 Mean-Value Methods

Using mean values as the approximation point is a conventional method for estimating the mean and standard deviation of the response, and is the basic idea behind mean-value methods. These methods usually provide an approximate CDF analysis.

2.3.1 Mean-Value Method

Assuming that a Z-function is continuous and smooth around the mean-values point, the first-order Taylor's series expansion is

$$Z_{MV1}(\boldsymbol{X}) = Z(\boldsymbol{\mu_X}) + \sum_{i=1}^{N} \left(\frac{\partial Z}{\partial X_i} \right) \Bigg|_{\boldsymbol{X}=\boldsymbol{\mu_X}} \left(X_i - \mu_{X_i} \right). \tag{2.23}$$

where $\boldsymbol{X} = \{X_1, \cdots, X_N\}^T \in \mathbb{R}^N$, and $\boldsymbol{\mu_X} = \{\mu_{X_1}, \cdots, \mu_{X_N}\}^T$ is the mean vector of $\boldsymbol{X}$. Since the Z_{MV1} function is linear and explicit, its CDF, as well as the reliability analysis, can be computed effectively.

For nonlinear g-functions, the solution based on (2.23) is, in general, not adequately accurate. Higher-order expansions need to be considered, for example, the second-order approximations

$$Z_{MV2}(\boldsymbol{X}) = Z_{MV1}(\boldsymbol{X}) + \frac{1}{2} \sum_{i=1}^{N} \left(\frac{\partial^2 Z}{\partial X_i^2} \right) \Bigg|_{\boldsymbol{X}=\boldsymbol{\mu_X}} \left(X_i - \mu_{X_i} \right)^2, \tag{2.24}$$

and

$$Z_{MV3}(\boldsymbol{X}) = Z_{MV2}(\boldsymbol{X}) + \sum_{\substack{i,j=1 \\ i \neq j}}^{N} \left(\frac{\partial^2 Z}{\partial X_i \partial X_j} \right) \Bigg|_{\boldsymbol{X}=\boldsymbol{\mu_X}} \left(X_i - \mu_{X_i} \right)\left(X_i - \mu_{X_j} \right), \tag{2.25}$$

where Z_{MV2} and Z_{MV3} are partial and full second order Taylor expansions. Third and higher-order approximations are not recommended because of a lack of efficiency and

numerical issues. Based on Equation (2.23), or (2.24) and (2.25), the mean value probabilistic solution is defined as mean-value (MV) method.

2.3.2 Advanced-Mean Method

The Advanced Mean-Value (AMV) method was proposed by Wu (1990) primarily to improve the MV solution with slightly more computational effort. By using a simple correction term, AMV compensates for the expansion truncation error. The AMV model can be simply expressed by

$$Z_{AMV}(X) = Z_{MV}(X) + H(Z_{MV}), \qquad (2.26)$$

where $H(Z_{MV})$ is defined as the correction term for higher order expansion terms. $H(Z_{MV})$ denotes the difference between the exact value of Z computed at the MPP, and the approximation of Z computed at the MPP determined by the MV method. The accuracy of AMV depends on the accuracy of the approximate MPP.

2.3.3 Advanced-Mean Value Method+

The AMV procedure can be considered an MV method in the first iteration when the linearization is performed at the mean point. If subsequent iterations are carried out to improve results, the AMV procedure becomes the so-called AMV+. The AMV+ procedure uses the MPP, but not the mean point in the original x-space as the expansion point in subsequent iterations (Wu et al., 1994). Iterations will continue to perform until the approximate MPP converges to the exact value.

2.4 First-, Second-, and Higher-Order Reliability Methods

2.4.1 Transformation

2.4.1.1 Independent Random Variables

Consider a random component X_i with CDF $F_{X_i}(x_i), i = 1, \cdots, N$. Let U_i be a standard normal random variable with its CDF $\Phi(u_i)$. From the definition

$$F_{X_i}(x_i) \equiv P[X_i \leq x_i] = p, \tag{2.27}$$

If

$$\Phi(u_i) \equiv P[U_i \leq u_i] = p, \tag{2.28}$$

then the mapping between x_i and u_i can be obtained from

$$\Phi(u_i) \equiv F_{X_i}(x_i), \tag{2.29}$$

which yields

$$u_i = \Phi^{-1}\left[F_{X_i}(x_i)\right] \tag{2.30}$$

or the inverse mapping

$$x_i = F_{X_i}^{-1}\left[\Phi(u_i)\right]. \tag{2.31}$$

As long as $F_{X_i}(x_i)$ can be inverted, either analytically or numerically, a performance function described in the x-space can easily be mapped onto u-space.

2.4.1.2 Dependent Random Variables – Rosenblatt Transformation

Consider an N-dimensional random vector X with a generic joint distribution function $F_X(x)$. Let $T : X \to U$ denote a transformation from x-space to u-space,

where *U* is an *N*-dimensional standard Gaussian random vector. According to Rosenblatt (1952), the transformation is given by

$$T : \begin{cases} u_1 & = & \Phi^{-1}\left[F_{X_1}(x_1)\right] \\ u_2 & = & \Phi^{-1}\left[F_{X_2}(x_2|x_1)\right] \\ \vdots & \vdots & \vdots \\ u_N & = & \Phi^{-1}\left[F_{X_N}(x_N|x_1,x_2,\cdots,x_{N-1})\right] \end{cases}, \qquad (2.32)$$

where $F_{X_i}(x_i|x_1,x_2,\cdots,x_{i-1}), i=2,\cdots,N$ is the CDF of X_i conditional on $X_1 = x_1, X_2 = x_2, \cdots, X_{i-1} = x_{i-1}$ and $\Phi(\bullet)$ is the CDF of a standard Gaussian random variable. The conditional distribution function $F_{X_i}(x_i|x_1,x_2,\cdots,x_{i-1})$ can be obtained from

$$F_{X_i}(x_i|x_1,x_2,\cdots,x_{i-1}) = \frac{\int_{-\infty}^{x_i} f_{X_1 X_2 \cdots X_i}(x_1,x_2,\cdots,x_{i-1},\xi)d\xi}{f_{X_1 X_2 \cdots X_{i-1}}(x_1,x_2,\cdots,x_{i-1})}, \qquad (2.33)$$

where $f_{X_1 X_2 \cdots X_{i-1}}(x_1,x_2,\cdots,x_{i-1})$ is the joint probability density function of $\{X_1,X_2,\cdots,X_{i-1}\}^T$. The inverse transformation can be obtained in a stepwise manner as

$$T^{-1} : \begin{cases} x_1 & = & F_{X_1}^{-1}\left[\Phi(u_1)\right] \\ x_2 & = & F_{X_2}^{-1}\left[\Phi(u_2|x_1)\right] \\ \vdots & \vdots & \vdots \\ x_N & = & F_{X_N}^{-1}\left[\Phi(u_n|x_1,x_2,\cdots,x_{N-1})\right] \end{cases}. \qquad (2.34)$$

2.4.1.3 Dependent Random Variables – Nataf Transformation

Consider a dependent random vector *X*, for which the marginal cumulative distribution functions $F_{X_i}(x_i), i=1,\cdots,N$ and the correlation coefficient matrix

$P_X = \{\rho_{ij}\}$ are known. It may have been described by an approximate but completely specified joint probability distribution function $F_X(x)$. X may also be transformed to the standard normal random vector Y in y-space, given by

$$y_i = \Phi^{-1}\left[F_{X_i}(x_i)\right]. \tag{2.35}$$

where $Y = \{Y_1, \cdots, Y_N\}^T$ is an N-dimensional standard normal random vector with joint probability density function $\phi_N(y, P_Y)$ having zero means, unit standard deviations, and correlation coefficient matrix $P_Y = \{\rho'_{ij}\}$. Then, given the usual rules for transformation of random variables, the approximate joint density function $f_X(x)$ in x-space is (Nataf, 1962)

$$f_X(x) = \phi_N(y, P_Y) \cdot |J| \tag{2.36}$$

with

$$|J| = \frac{\partial(y_1, y_2, \cdots, y_N)}{\partial(x_1, x_2, \cdots, x_N)} = \frac{f_{X_1}(x_1) \cdot f_{X_2}(x_2) \cdots f_{X_N}(x_N)}{\phi(y_1)\phi(y_2)\cdots\phi(y_N)}. \tag{2.37}$$

To solve P_Y in Equation (2.36), consider any two random variables (X_i, X_j) and the correlation coefficient between them as

$$\rho_{ij} = \frac{\gamma_{ij}}{\sigma_{X_i}\sigma_{X_j}} = \mathbb{E}\left[Z_i Z_j\right] = \int_{-\infty}^{\infty}\int_{-\infty}^{\infty} z_i z_j \phi_2\left(y_i, y_j; \rho'_{ij}\right) dy_i dy_j, \tag{2.38}$$

where $Z_i = (X_i - \mu_{X_i})/\sigma_{X_i}$. Here the correlation coefficient matrix $P_Y = \{\rho'_{ij}\}$ can be obtained from the known $P_X = \{\rho_{ij}\}$ iteratively from (2.38).

Once $\boldsymbol{P}_Y$ is determined for any pair of $\left(X_i, X_j\right)$, Equation (2.35) can be used to obtain the correlated standard normal distribution in $\boldsymbol{y}$-space. Furthermore, an orthogonal transformation can be used to obtain independent standard normal distribution in $\boldsymbol{u}$-space, which will be discussed in the following.

2.4.1.4 Transformation between Dependent and Independent Normal Variables

Let $\boldsymbol{X} = \left(X_1, \cdots, X_N\right)$ be an N-dimensional normal random vector with joint probability density function $\phi_n\left(\boldsymbol{x}, \boldsymbol{C}_X\right)$ having mean vector $\boldsymbol{\mu}_X$, and covariance matrix $\boldsymbol{C}_X$. Let $\boldsymbol{U} = \left(U_1, \cdots, U_N\right)$ be an N-dimensional independent standard random vector. Then, the transformation between $\boldsymbol{X}$ and $\boldsymbol{U}$ can be expressed by

$$\boldsymbol{X} = \boldsymbol{A}\boldsymbol{U} + \boldsymbol{\mu}_X . \tag{2.39}$$

Since $\boldsymbol{C}_X$ is positive definite and symmetric, the orthogonal transformation matrix ($\boldsymbol{A}^T = \boldsymbol{A}^{-1}$) can be defined by

$$\boldsymbol{C}_X = \boldsymbol{A}\boldsymbol{A}^T . \tag{2.40}$$

Because $\boldsymbol{C}_X$ is known, Equation (2.40) can be obtained by Cholesky decomposition.

2.4.2 Most Probable Point (MPP)

A most probable point (MPP) is defined as the point $\boldsymbol{u}^*$ on the limit state surface closest to the origin in standard normal space (Figure 2.1). This point leads to the definition of the *reliability index* β as

$$\beta = \left\| \boldsymbol{u}^* \right\|. \tag{2.41}$$

The determination of MPP $\boldsymbol{u}^*$ can be formulated as a constrained optimization problem, defined by

$$\begin{array}{c} \min\limits_{\boldsymbol{u} \in \mathbb{R}^N} \left\| \boldsymbol{u} \right\| \\ \text{s. t. } g_U(\boldsymbol{u}) = 0 \end{array}, \tag{2.42}$$

where $\left\| \boldsymbol{u} \right\| = \sqrt{\sum\limits_{i=1}^{N} u_i^2}$ is the Euclidean L_2-norm of the N-dimensional vector $\boldsymbol{u}$ and $g_U(\boldsymbol{u})$ is

the transformed performance function in $\boldsymbol{u}$-space.

2.4.2.1 Early Approaches

The constrained optimization problem defined in (2.42) is equivalent to

$$\min\limits_{\boldsymbol{u} \in \mathbb{R}^N, \lambda \in \mathbb{R}} L(\boldsymbol{u}, \lambda), \tag{2.43}$$

where λ is the Lagrange multiplier and

$$L(\boldsymbol{u}, \lambda) = \frac{1}{2} \left\| \boldsymbol{u} \right\|^2 + \lambda g_U(\boldsymbol{u}). \tag{2.44}$$

Assuming the optimization solution is $\left(\boldsymbol{u}^*, \lambda^* \right)$ and sufficient smoothness is found for the function involved, the partial derivatives of $L(\boldsymbol{u}, \lambda)$ have to be zero at the solution point. Hence

$$\left\| \boldsymbol{u}^* \right\| + \lambda^* \nabla g_U \left(\boldsymbol{u}^* \right) = 0 \tag{2.45}$$

and

$$g_U \left(\boldsymbol{u}^* \right) = 0. \tag{2.46}$$

The positive Lagrange multiplier λ can be obtained from (2.45), and then substituted in the same equation. This yields the first order optimality condition:

$$\boldsymbol{u}^* \cdot \left\| \nabla g_U \left(\boldsymbol{u}^* \right) \right\| + \left\| \boldsymbol{u}^* \right\| \cdot \nabla g_U \left(\boldsymbol{u}^* \right) = 0 \,. \tag{2.47}$$

This condition means that the normal to the limit state surface at the MPP should point towards to the origin of *u*-space. Many standard algorithms are available for solving the Lagrange optimal problem defined in (2.43). However, the first-order method may converge to an infeasible point; Newton's method requires second-order information. These difficulties suggest that the Lagrange method may not be a good optimization technique for the reliability problem.

2.4.2.2 Hasofer-Lind Method

Hasofer and Lind (1974) proposed an iterative algorithm to solve (2.43), which was later used by Rackwitz and Fiessler (1978) in conjunction with probability transformation techniques. This algorithm generates a sequence of points $\boldsymbol{u}_i$ from the recursive rule

$$\boldsymbol{u}_{i+1} = \frac{\nabla g_U \left(\boldsymbol{u}_i \right)^T \cdot \boldsymbol{u}_i - g_U \left(\boldsymbol{u}_i \right)}{\left\| \nabla g_U \left(\boldsymbol{u}_i \right) \right\|} \frac{\nabla g_U \left(\boldsymbol{u}_i \right)}{\left\| \nabla g_U \left(\boldsymbol{u}_i \right) \right\|} \,. \tag{2.48}$$

At the current iterative point $\boldsymbol{u}_i$, the limit state surface is linearized, i.e. replaced by the trace in the *u*-space of the hyperplane tangent to $g_U \left(\boldsymbol{u} \right)$ at $\boldsymbol{u} = \boldsymbol{u}_i$. Equation (2.48) is the solution to this linearized optimization problem, which corresponds to the orthogonal projection of $\boldsymbol{u}_i$ onto the trace of the tangent hyperplane. The Hasofer-Lind method is widely used due to its simplicity. However, it may not converge in some cases.

2.4.2.3 Improved Hasofer-Lind method

Zhang and Der Kiureghian (1995,1997) proposed an improved version of the Hasofer-Lind method for which unconditional convergence could be proven. It is based on the following reformulation of the recursive definition of Equation (2.48):

$$\boldsymbol{u}_{i+1} = \boldsymbol{u}_i + \lambda_i \boldsymbol{d}_i, \lambda_i = 1 \tag{2.49}$$

and

$$\boldsymbol{d}_i = \frac{\nabla g_U \left(\boldsymbol{u}_i\right)^T \cdot \boldsymbol{u}_i - g_U \left(\boldsymbol{u}_i\right)}{\left\|\nabla g_U \left(\boldsymbol{u}_i\right)\right\|} \frac{\nabla g_U \left(\boldsymbol{u}_i\right)}{\left\|\nabla g_U \left(\boldsymbol{u}_i\right)\right\|} - \boldsymbol{u}_i, \tag{2.50}$$

where $\boldsymbol{d}_i$ and λ_i are the searching direction and the step size respectively. The original Hasofer-Lind method can be improved by computing an optimal step size $\lambda_i \neq 1$. For this purpose, a merit function $m(\boldsymbol{u})$ is introduced. During each iteration, after computing (2.50), a line search is carried out to find λ_i such that merit function is minimized. That is, find λ_i to satisfy minimizing $m(\boldsymbol{u}_i + \lambda \boldsymbol{d}_i)$. The unconstrained optimization problem (Equation (2.43)) is replaced by the problem of finding a value λ_i such that the merit function is sufficiently reduced (if not minimal). The so-called Armijo rule (Luenberger, 1986) is an efficient technique, which is written by

$$\lambda_i = \max_{k \in \mathbb{R}} \left\{ b^k \left| m\left(\boldsymbol{u}_i + b^k \boldsymbol{d}_i\right) - m\left(\boldsymbol{u}_i\right) \leq -ab^k \left\|\nabla m\left(\boldsymbol{u}_i\right)\right\|^2 \right. \right\}, \tag{2.51}$$

where $a, b \in (0,1)$ are pre-selected parameters and k is an integer.

Zhang and Ker Kiureghian (1995,1997) proposed the following merit function:

$$m(\boldsymbol{u}) = \frac{1}{2}\|\boldsymbol{u}\|^2 + c\left|g_U(\boldsymbol{u})\right|. \tag{2.52}$$

This expression has two properties:

(1) The search direction $\boldsymbol{d}$ defined in (2.50) satisfies:

$$\forall \boldsymbol{u},\ \nabla m(\boldsymbol{u})^{T} \cdot \boldsymbol{d} \leq 0 \text{ provides } c > \frac{\|\boldsymbol{u}\|}{\|\nabla g_{U}(\boldsymbol{u})\|}. \tag{2.53}$$

(2) The merit function attains its minimum at the MPP provided that the same condition is fulfilled on c.

Both properties are sufficient to ensure that the global algorithm defined by (2.49), (2.50) and (2.51) is unconditionally convergent (Luenberger, 1986).

2.4.2.4 Others

With the exception of the Hasofer-Lind method and its variants, Liu and Kiureghian (1986,1991) discussed other algorithms in structural reliability analysis, including the gradient projection method, the augmented Lagrange method, and sequential quadratic programming (SQP) method. Based on results of numerical examples, they recommended the SQP and improved/modified Hasofer-Lind method because of their convergence and computational efficiency.

Other recently proposed intelligent algorithms for reliability analysis include neural networks (Shao and Morutso, 1997), and evolutionary algorithms (Elegbede, 2005). These methods still need further investigation.

2.4.3 First-Order Reliability Method

The first–order reliability method (FORM) is based on the first-order linear approximation of the limit state surface $g(x) = 0$, tangent to the closest point of the surface to the origin. The determination of this point involves nonlinear constrained optimization, and is usually performed in the standard Gaussian image of the original space, which can be obtained by the Rosenblatt transformation (Rosenblatt, 1952). The FORM algorithm involves several steps; they will be described briefly assuming a generic N-dimensional random vector X.

First, the space x of uncertain parameters X is transformed into a new N-dimensional u space of independent standard Gaussian variables U. The original limit state $g(x) = 0$ then becomes mapped into the new limit state $g_U(u) = 0$ in u space.

Second, the point u^* on the limit state $g_U(u) = 0$ that has the shortest distance to the origin of the u space is determined by using an appropriate nonlinear optimization algorithm. This point is referred to as the design or beta point, and has a distance β_{HL} (known as the reliability index) to the origin of u space.

Third, the limit state, $g_U(u) = 0$, is approximated by a hyperplane (linear or first-order), $g_L(u) = 0$, tangent to it at the design point.

Finally, the probability of failure P_F is thus approximated by $P_{F,1} = P\left[g_L(U) < 0 \right]$ in FORM and given as:

$$P_{F,1} = P\left[g_L(U) < 0 \right] = \Phi\left(-\beta_{HL}\right), \tag{2.54}$$

where

$$\Phi(u) = \frac{1}{\sqrt{2\pi}} \int_{-\infty}^{u} \exp\left(-\frac{1}{2}\xi^2\right) d\xi \qquad (2.55)$$

is the cumulative distribution function (CDF) of a standard Gaussian random variable.

2.4.4 Second-Order Reliability Method

Second–order reliability methods (SORM) are proposed as a natural extension of FORM. The idea is to approximate the limit state surface by a quadratic surface whose probabilistic content is known analytically.

<u>2.4.4.1 General Quadratic Approximation</u>

For a standard Gaussian random vector $\boldsymbol{U} \mapsto N(\boldsymbol{0}, \boldsymbol{I}) \in \mathbb{R}^N$, its joint PDF is

$$f_U(\boldsymbol{u}) = \phi(\boldsymbol{u}) = (2\pi)^{-\frac{N}{2}} \exp\left[-\frac{1}{2}\boldsymbol{u}^T\boldsymbol{u}\right]. \qquad (2.56)$$

Assuming that $g_U(\boldsymbol{u})$ is continuous, smooth, and at least twice differentiable, its second-order Taylor series expansion about MPP ($\boldsymbol{u}^*$) is

$$g_U(\boldsymbol{u}) \cong g_U(\boldsymbol{u}^*) + \nabla g_U(\boldsymbol{u}^*)^T(\boldsymbol{u} - \boldsymbol{u}^*) + \frac{1}{2}(\boldsymbol{u} - \boldsymbol{u}^*)^T \boldsymbol{H}(\boldsymbol{u}^*)(\boldsymbol{u} - \boldsymbol{u}^*) \equiv g_Q(\boldsymbol{u}), \qquad (2.57)$$

where $\nabla g_U(\boldsymbol{u}^*)$ is the gradient vector and $\boldsymbol{H}(\boldsymbol{u}^*)$ is the Hessian matrix, both evaluated at the MPP. Since $g_U(\boldsymbol{u}^*) = 0$,

$$g_Q(\boldsymbol{u}) = \left(-\nabla g_U{}^T\boldsymbol{u}^* + \frac{1}{2}\boldsymbol{u}^{*T}\boldsymbol{H}\boldsymbol{u}^*\right) - \left(-\nabla g_U{}^T + \boldsymbol{u}^{*T}\boldsymbol{H}\right)\boldsymbol{u} + \frac{1}{2}\boldsymbol{u}^T\boldsymbol{H}\boldsymbol{u}, \qquad (2.58)$$

in which the argument "$(\boldsymbol{u}^*)$" has been dropped for notational convenience. At the MPP

$$\frac{\boldsymbol{u}^*}{\beta_{HL}} = -\frac{\nabla g_U}{\|\nabla g_U\|} = \boldsymbol{\alpha}^*, \tag{2.59}$$

where $\beta_{HL} = \|\boldsymbol{u}^*\|$ and $\boldsymbol{\alpha}^*$ is unit vector to MPP. Dividing equation (2.59) by $\|\nabla g_U\|$ yields

$$\frac{g_Q(\boldsymbol{u})}{\|\nabla g_U\|} = \left(\beta_{HL} + \frac{\beta_{HL}^2}{2}\boldsymbol{\alpha}^{*T}\frac{\boldsymbol{H}}{\|\nabla g_U\|}\boldsymbol{\alpha}^*\right) - \left(\boldsymbol{\alpha}^{*T} + \beta_{HL}\boldsymbol{\alpha}^{*T}\frac{\boldsymbol{H}}{\|\nabla g_U\|}\right)\boldsymbol{u} + \frac{1}{2}\boldsymbol{u}^T\frac{\boldsymbol{H}}{\|\nabla g_U\|}\boldsymbol{u}. \tag{2.60}$$

2.4.4.2 Parabolic Approximation

Construct an orthogonal matrix $\boldsymbol{R} \in \mathbb{L}\left(\mathbb{R}^N \times \mathbb{R}^N\right)$, whose Nth column is $\boldsymbol{\alpha}^*$, i.e.,

$$\boldsymbol{R} \in \left[\boldsymbol{R}_1 | \boldsymbol{\alpha}^*\right], \tag{2.61}$$

where $\boldsymbol{R}_1 \in \mathbb{L}\left(\mathbb{R}^N \times \mathbb{R}^{N-1}\right)$ satisfies

$$\boldsymbol{\alpha}^{*T}\boldsymbol{R}_1 = \boldsymbol{0}_{1\times(N-1)}. \tag{2.62}$$

The matrix $\boldsymbol{R}$ can be obtained by Gram-Schmidt orthogonalization.

Consider the orthogonal transformation

$$\boldsymbol{u} = \boldsymbol{R}\boldsymbol{v}, \tag{2.63}$$

and partitioning

$$\boldsymbol{v} = \left\{\begin{matrix} \tilde{\boldsymbol{v}} \\ v_N \end{matrix}\right\}, \tag{2.64}$$

where

$$\tilde{V} \mapsto N\left(\boldsymbol{0}_{N-1}, \boldsymbol{I}_{N-1}\right) \in \mathbb{R}^{N-1} \text{ and } V_N \mapsto N\left(0,1\right). \tag{2.65}$$

Hence, equation (2.60) becomes

$$\frac{g_Q(\boldsymbol{u})}{\|\nabla g_U\|} = \left(\beta_{HL} + \frac{\beta_{HL}^2}{2}\boldsymbol{\alpha}^{*T}\frac{\boldsymbol{H}}{\|\nabla g_U\|}\boldsymbol{\alpha}^*\right) - \left(v_N + \beta_{HL}\boldsymbol{\alpha}^{*T}\frac{\boldsymbol{H}}{\|\nabla g_U\|}\boldsymbol{Rv}\right) + \boldsymbol{v}^T\boldsymbol{Av}, \quad (2.66)$$

where $\boldsymbol{A} = \dfrac{1}{2}\dfrac{\boldsymbol{R}^T\boldsymbol{HR}}{\|\nabla g_U\|} \in \mathbb{L}\left(\mathbb{R}^N \times \mathbb{R}^N\right)$.

Consider the partition of $\boldsymbol{A}$

$$\boldsymbol{A} = \begin{bmatrix} \tilde{\boldsymbol{A}}_{N-1} & \tilde{\boldsymbol{A}}_{1N} \\ \tilde{\boldsymbol{A}}_{1N} & \tilde{\boldsymbol{A}}_{NN} \end{bmatrix}, \quad (2.67)$$

where $\tilde{\boldsymbol{A}}_{N-1} \in \mathbb{L}\left(\mathbb{R}^{N-1} \times \mathbb{R}^{N-1}\right), \tilde{\boldsymbol{A}}_{N1} = \tilde{\boldsymbol{A}}_{1N}^T \in \mathbb{L}\left(\mathbb{R}^1 \times \mathbb{R}^{N-1}\right)$, and $\tilde{A}_{NN} \in \mathbb{R}$. In view of this

partition, the general quadratic equation reads

$$\frac{g_Q(\boldsymbol{u})}{\|\nabla g_U\|} = -v_N + \beta_{HL} + \tilde{\boldsymbol{v}}^T\tilde{\boldsymbol{A}}_{N-1}\tilde{\boldsymbol{v}} + \frac{\beta_{HL}^2}{2}\boldsymbol{\alpha}^{*T}\frac{\boldsymbol{H}}{\|\nabla g_U\|}\boldsymbol{\alpha}^* - \beta_{HL}\boldsymbol{\alpha}^{*T}\frac{\boldsymbol{H}}{\|\nabla g_U\|}\boldsymbol{Rv} + 2v_N\tilde{\boldsymbol{A}}_{N1}\tilde{\boldsymbol{v}} + \tilde{A}_{NN}v_N^2. \quad (2.68)$$

Madsen et al. (1986) proposed a parabolic approximation of (2.68) by neglecting

any cross terms and second order terms of v_n and β_{HL}. Only the first three terms are left,

leading to

$$\frac{\tilde{g}_Q}{\|\nabla g_U\|} \cong -v_N + \beta_{HL} + \tilde{\boldsymbol{v}}^T\tilde{\boldsymbol{A}}_{N-1}\tilde{\boldsymbol{v}}. \quad (2.69)$$

This parabolic approximation has been used by many researchers, such as, Breitung

(1984), Hohenbeichler and Rackwitz(1988), Tvedt (1990), Cai and Elishakoff(1994),

Koyluoglu and Nielsen (1994), Adhikari (2004), and others.

2.4.4.3 Failure Probability Evaluation - Asymptotic Solutions

Using (2.69) as the parabolic approximation of the failure surface, the second order estimate of the failure probability is

$$P_{F,II} = P\left[\frac{\tilde{g}_Q}{\|\boldsymbol{\nabla} g_U\|} < 0\right] \cong P\left[V_N > \beta_{HL} + \tilde{\boldsymbol{V}}^T \tilde{\boldsymbol{A}}_{N-1} \tilde{\boldsymbol{V}}\right]. \qquad (2.70)$$

Define a random variable $Z : \mathbb{R}^{N-1} \mapsto \mathbb{R}$ by

$$Z \equiv \tilde{\boldsymbol{V}}^T \tilde{\boldsymbol{A}}_{N-1} \tilde{\boldsymbol{V}}, \qquad (2.71)$$

as the quadratic mapping of a standard Gaussian vector $\tilde{\boldsymbol{V}} \mapsto N\left(\boldsymbol{0}_{N-1}, \boldsymbol{I}_{N-1}\right) \in \mathbb{R}^{N-1}$. Therefore

$$P_{F,II} \cong P\left[V_N > \beta_{HL} + Z\right] = \mathbb{E}\left[\Phi\left(-\beta_{HL} - Z\right)\right]. \qquad (2.72)$$

Unfortunately, the exact probability density function of the quadratic form Z is in general not available in closed form. For this reason, it is difficult to calculate the expectation $\mathbb{E}\left[\Phi\left(-\beta_{HL} - Z\right)\right]$ analytically.

The function $\Phi\left(-\beta_{HL} - Z\right)$ is continuous and differentiable (of any order) for $z \in \mathbb{R}$. Expanding $\ln\left[\Phi\left(-\beta_{HL} - Z\right)\right]$ at $Z = 0$ and keeping only the linear term

$$\ln\left[\Phi\left(-\beta_{HL} - Z\right)\right] \cong \ln\left[\Phi\left(-\beta_{HL}\right)\right] - \frac{\phi\left(\beta_{HL}\right)}{\Phi\left(-\beta_{HL}\right)} Z. \qquad (2.73)$$

where $\phi\left(u\right) = \frac{1}{\sqrt{2\pi}}\exp\left(-\frac{1}{2}u^2\right)$ is the probability density function (PDF) of a standard Gaussian random variable. Hence,

$$\Phi\left(-\beta_{HL}-Z\right)\cong\Phi\left(-\beta_{HL}\right)\exp\left[-\frac{\phi\left(\beta_{HL}\right)}{\Phi\left(-\beta_{HL}\right)}Z\right]. \qquad (2.74)$$

The moment generation function $M_Z(s)$ of a random variable Z is defined as

$$M_Z(s)\equiv\mathbb{E}\left[\exp\left(sZ\right)\right]. \qquad (2.75)$$

For a quadratic form $Z\equiv\tilde{V}^T\tilde{A}_{N-1}\tilde{V}$ of Gaussian variables, it is elementary to show

$$M_Z(s)\equiv\mathbb{E}\left[\exp\left(sZ\right)\right]=\left|\boldsymbol{I}_{N-1}-2s\tilde{A}_{N-1}\right|^{-\frac{1}{2}}. \qquad (2.76)$$

From Equation (2.72)

$$\begin{aligned}
P_{F,II}&\cong\mathbb{E}\left[\Phi\left(-\beta_{HL}-Z\right)\right]\\
&\cong\mathbb{E}\left[\Phi\left(-\beta_{HL}\right)\exp\left(-\frac{\phi\left(\beta_{HL}\right)}{\Phi\left(-\beta_{HL}\right)}Z\right)\right]\\
&=\Phi\left(-\beta_{HL}\right)\left|\boldsymbol{I}_{N-1}+2\frac{\phi\left(\beta_{HL}\right)}{\Phi\left(-\beta_{HL}\right)}\tilde{A}_{N-1}\right|^{-\frac{1}{2}}
\end{aligned} \qquad (2.77)$$

Let $a_i, i=1,\cdots,N-1$ be the eigenvalues of $\tilde{A}_{N-1}$, it can be proved that eigenvalues of $\boldsymbol{I}_{N-1}+2\left(\phi\left(\beta_{HL}\right)\big/\Phi\left(-\beta_{HL}\right)\right)\tilde{A}_{N-1}$ are $1+2\left(\phi\left(\beta_{HL}\right)\big/\Phi\left(-\beta_{HL}\right)\right)a_i, i=1,\cdots,N-1$. Thus, Equation (2.77) can be rewritten as

$$P_{F,II}\cong\Phi\left(-\beta_{HL}\right)\prod_{i=1}^{n-1}\left(1+2\frac{\phi\left(\beta_{HL}\right)}{\Phi\left(-\beta_{HL}\right)}a_i\right)^{-\frac{1}{2}}. \qquad (2.78)$$

Hohenbichler and Rackwitz (1988) gave the improved asymptotic solution as

$$P_{F,II}\approx\Phi\left(-\beta_{HL}\right)\prod_{i=1}^{n-1}\left(1+\kappa_i\frac{\phi\left(\beta_{HL}\right)}{\Phi\left(-\beta_{HL}\right)}\right)^{-\frac{1}{2}}, \qquad (2.79)$$

which is the same formula as (2.78), if the principal curvatures at the MPP are denoted by $\kappa_i = 2a_i$. The sign convention is such that curvature is positive when the surface curves are away from the origin.

Further, consider when $\beta_{HL} \to \infty$, so that $\dfrac{\phi(\beta_{HL})}{\Phi(-\beta_{HL})} \to \beta_{HL}$. Equation (2.79) is simplified as the same asymptotic solution given by Breitung (1984), which is

$$P_{F,II} \approx \Phi(-\beta_{HL}) \prod_{i=1}^{n-1} (1 + \kappa_i \beta_{HL})^{-\frac{1}{2}}. \tag{2.80}$$

2.4.4.4 Least-Squares' Non-Asymptotic Solution

Consider an approximation of $\Phi(-\beta_{HL} - Z)$ by

$$\Phi(-\beta_{HL} - Z) \cong c_1 \exp(-c_2 Z), \tag{2.81}$$

such that the error in this approximation is in some sense minimized. The error in representing $\Phi(-\beta_{HL} - Z)$ by (2.81) is given by

$$\varepsilon(Z; c_1, c_2) = \Phi(-\beta_{HL} - Z) - c_1 \exp(-c_2 Z). \tag{2.82}$$

Define the objective function

$$\Psi(c_1, c_2) = \int_{\mathbb{R}} \left[\varepsilon(z; c_1, c_2) \right]^2 dz = \int_{\mathbb{R}} \left[\Phi(-\beta_{HL} - z) - c_1 \exp(-c_2 z) \right]^2 dz. \tag{2.83}$$

To minimize (2.83) and simultaneously satisfy

$$\frac{\partial \Psi(c_1, c_2)}{\partial c_1} = 0 \text{ and } \frac{\partial \Psi(c_1, c_2)}{\partial c_2} = 0. \tag{2.84}$$

Further simplification of Equation (2.85) reveals that a system of nonlinear equations must be solved to obtain optimal parameters c_1 and c_2. An exact solution of (2.84) does not exist. However, a numerical solution can be obtained easily using widely available nonlinear equation solvers (MATLAB, IMSL, et al.), Hence, the SORM failure probability estimate is (Adhikari, 2004)

$$P_{F,II} \cong c_1 \left| \boldsymbol{I}_{N-1} + 2c_2 \tilde{A}_{N-1} \right|^{-\frac{1}{2}} = c_1 \prod_{i=1}^{N-1} \left(1 + \kappa_i c_2\right)^{-\frac{1}{2}}, \qquad (2.85)$$

where $\kappa_i, i = 1, \cdots, N-1$ are the principal curvatures.

The least-squares' method degenerates to Breitung's and Hohenbichler's asymptotic solutions when $\beta_{HL} \to \infty$, $c_1 \to \Phi\left(-\beta_{HL}\right), c_2 \to \phi\left(\beta_{HL}\right)/\Phi\left(-\beta_{HL}\right)$ (Hohenbichler's) or $c_2 \to \beta_{HL}$ (Breitung's).

2.4.4.5 Other Non-Asymptotic Solutions

For parabolic failure surface, the only sources of error in Equation (2.72) are from the approximation of $\Phi\left(-\beta_{HL} - Z\right)$ by first order Taylor expansion, which is asymptotically correct when $\beta_{HL} \to \infty$. If this condition is not well satisfied, other methods exist to improve this approximation.

Tvedt (1990) extended Breitung's asymptotic solution to obtain a three-term solution given by

$$P_{F,II} \cong \Phi\left(-\beta_{HL}\right)\prod_{i=1}^{N-1}\left(1+\kappa_i\beta_{HL}\right)^{-\frac{1}{2}}$$

$$+\left[\beta_{HL}\Phi\left(-\beta_{HL}\right)-\phi\left(\beta_{HL}\right)\right]\left[\prod_{i=1}^{N-1}\left(1+\kappa_i\beta_{HL}\right)^{-\frac{1}{2}}-\prod_{i=1}^{N-1}\left(1+\left(\beta_{HL}+1\right)\kappa_i\right)^{-\frac{1}{2}}\right]$$

$$+\left(\beta_{HL}+1\right)\left[\beta_{HL}\Phi\left(-\beta_{HL}\right)-\phi\left(\beta_{HL}\right)\right]\left[\prod_{i=1}^{N-1}\left(1+\kappa_i\beta_{HL}\right)^{-\frac{1}{2}}-\mathrm{Re}\left[\prod_{i=1}^{N-1}\left(1+\left(\beta_{HL}+i\right)\kappa_i\right)^{-\frac{1}{2}}\right]\right] \qquad , \quad (2.86)$$

where $i=\sqrt{-1}$. It can be shown that second and third terms of (2.86) vanish when $\beta_{HL}\to\infty$, which results in only the first term remaining: Breitung's asymptotic solution (2.80). Tvedt also derived an alternative formulation in a complex domain for a general quadratic failure surface; however, because this formulation is not in closed form, numerical integration is needed.

Koyluoglu and Nielsen (1994) derived a series solution for SORM using higher-order approximations of $\Phi\left(-\beta_{HL}-Z\right)$.

$$P_{F,II} \cong \Phi\left(-\beta_{HL}\right)\prod_{i=1}^{N-1}\frac{1}{\sqrt{1+\kappa_i/c_{0,1}}}$$

$$\times\left\{1+\frac{1}{2}c_{1,1}\sum_{k=1}^{N-1}\frac{\kappa_k}{1+\kappa_k/c_{0,1}}+\frac{1}{4}c_{2,1}\left[\left(\sum_{k=1}^{N-1}\frac{\kappa_k}{1+\kappa_k/c_{0,1}}\right)^2+2\sum_{k=1}^{N-1}\left(\frac{\kappa_k}{1+\kappa_k/c_{0,1}}\right)^2\right]\right.$$

$$\left.+\frac{1}{8}c_{3,1}\left[\left(\sum_{k=1}^{N-1}\frac{\kappa_k}{1+\kappa_k/c_{0,1}}\right)^3+2\left(\sum_{k=1}^{N-1}\frac{\kappa_k}{1+\kappa_k/c_{0,1}}\right)\left(\sum_{k=1}^{N-1}\left(\frac{\kappa_k}{1+\kappa_k/c_{0,1}}\right)^2\right)+12\sum_{k=1}^{N-1}\left(\frac{\kappa_k}{1+\kappa_k/c_{0,1}}\right)^3\right]+\cdots\right\} \qquad , (2.87)$$

where $c_{i,j}$ are coefficients that can be expressed solely in terms of β_{HL}.

Cai and Elishakoff (1994) also derived a series solution for a parabolic failure surface based on the Taylor expansion of $\Phi\left(-\beta_{HL}-Z\right)$ as

$$P_{F,II}\approx\Phi\left(-\beta_{HL}\right)+\frac{1}{\sqrt{2\pi}}\exp\left(-\frac{\beta_{HL}^{2}}{2}\right)\left(D_1+D_2+D_3+\cdots\right) , \qquad (2.88)$$

$$D_1 = \sum_{i=1}^{N-1} \kappa_i$$

$$\text{where} \qquad D_2 = -\frac{1}{2}\beta_{HL}\left[3\sum_{i=1}^{N-1}\kappa_i^2 + \sum_{i,j=1,i\neq j}^{N-1}\kappa_i\kappa_j \right] \qquad . \quad (2.89)$$

$$D_3 = \frac{1}{6}\left(\beta_{HL}^{\;2}-1\right)\left[15\sum_{i=1}^{N-1}\kappa_i^3 + 9\sum_{i,j=1,i\neq j}^{N-1}\kappa_i^{\;2}\kappa_j + \sum_{i,j,k=1,i\neq j\neq k}^{N-1}\kappa_i\kappa_j\kappa_k \right]$$

The series solution also converges to an exact solution of failure probability for a parabolic failure surface.

2.4.5 Higher-Order Reliability Method

For those cases, in which the limit-state surface has a large curvature (a high nonlinearity) around the MPP, both FORM and SORM can have large errors in their estimates of failure probability. For example, if the MPP is an inflection point (cubic form), or the limit-state surface is a flat hyperplane around the MPP, then curvature-fitted parabola of SORM is reduced to the tangent hyperplane, thus providing no improvement over FORM. Wang and Grandhi (1998) proposed a higher-order reliability method (HORM), which can be used for problems with highly nonlinear limit state functions, or with an inflection point of MPP. The flow chart in Fig. 2.2 illustrates the procedure of this method. In the rotated standard Gaussian space, two-point adaptive nonlinear approximation was used to approximate highly nonlinear limit state functions, and then based on the approximation given by Koyluoglu and Nielsen (1994) for $\Phi(\beta_{HL} + Z) - \Phi(\beta_{HL})$, the failure probability by numerical integrations was calculated.

In Figure 2.2, when *m* = 2, this method is simplified to the same SORM solution proposed by Koyluoglu and Nielsen (1994).

2.4.6 Multiple MPP Problems

The previously discussed methods only consider the case of a single MPP. If multiple MPPs exist, or if there are contributions from other regions around local minimums besides the region around a single MPP (Figure 2.3), these methods can fail to provide a correct estimation of failure probability. The existence of multiple MPPs may cause the following problems: (1) the optimization algorithm may converge to a local MPP (local minimum), in which case FORM/SORM and the MPP-based method will miss the region of dominant contribution to the failure probability; (2) even if the global MPP is found, other significant contributions to the failure probability may exist in the neighborhoods of other local MPPs; and (3) suppose that all MPPs are identified successfully, system FORM/SORM may not be sufficient accurate if there are highly nonlinearities around these MPPs.

To handle multiple MPPs problems, two steps need to be investigated: (1) global optimization techniques to find all MPPs, and (2) system reliability that consider the correlation of the piecewise approximation limit-state surface based on these MPPs. The following sections discuss possible strategies to solve multiple MPPs problems.

2.4.6.1 Multi-Point FORM/SORM

The arbitrary failure set defined in Equation (2.7) may exhibit large calculation difficulties. As suggested by Ditlevsen and Madsen (1996), this set can be approximated

by multiple first-order or second order approximations. A reliability calculation can then be undertaken with less difficulty for a simpler failure set. To use this method, all local minimums need to be determined in advance and the quality of the solution depends on the accuracy of these approximations.

2.4.6.2 System Reliability Method

Once multiple MPPs are identified successfully, system reliability methods can be used to estimate the failure probability. If the failure region is given by an intersection of failure domains, system reliability can be estimated using Equation (2.16). If the failure domain is a union of failure domains, a bound technique can be used, as described in Equation (2.43). More complicated failure regions can also be considered, which are discussed in detail in section 2.2.2.

2.4.6.3 Sampling Based MPP Search

Thacker (2001) proposed a simple sampling technique to locate all MPPs for a given level, and then the system approach can be used. The procedure runs as follows: (1) estimate the probability of failure using coarse sampling; (2) convert the realizations in the failure region to u-space (standard Gaussian space); (3) evaluate the distance to the origin for each realization; and (4) sort the results and report those realizations with the shortest distance. Although this method is not very efficient, since the sampling technique is much easier and more stable, it was implemented with structural reliability software such as NESSUS.

2.4.6.4 Multiple Linearization

Mahadevan and Shi (2001) proposed a simple multipoint linearization method for nonlinear reliability analysis in order to improve the failure probability approximation of FORM. The method is based on four main concepts: (1) approximate the limit state using multiple hyperplanes; (2) search for the multiple linearization points on the limit state; (3) seek computational efficiency through the investigation of correlated hyperplane; (4) estimate the failure probability through union and/or intersection operations, depending on the limit state definition. The difficulty with this method is how to select and search the multiple linearization points on the limit state.

2.4.6.5 "Barrier" Optimal Method

In optimization theory, a common trick to find multiple solutions for a problem is to construct "barriers" around previously found solutions, thereby forcing the algorithm to seek a new solution. In reliability problems, the objective function is the distance from the limit state surface to the origin. A "barrier" around the first solution can be constructed by moving the limit state in the neighborhood away from the origin. Consequently, following "barriers" can be constructed to find the new solutions. Der Kiureghian and Dakessian (1998) proposed this method to solve multiple MPPs problems and suggested a "barrier" function $B_i(\boldsymbol{u})$ like the following:

$$B_i(\boldsymbol{u}) = \begin{cases} s_i\left(r_i^2 - \|\boldsymbol{u} - \boldsymbol{u}_i^*\|^2\right)^2, & \|\boldsymbol{u} - \boldsymbol{u}_i^*\| \le r_i \\ 0, & \text{elsewhere} \end{cases} \tag{2.90}$$

where r_i is the radius of the bulge and s_i is a positive scale factor, $\boldsymbol{u}_i^*$ is the vector form of ith solution.

2.4.6.6 Global Response Surface Method

The basic idea behind this method, proposed by Gupta and Manohar (2004), is to construct a response surface for the limit state by using global information, rather than the local information around a single MPP. The algorithm is described as follows: (1) define a new set of coordinates to be identified for each point, which includes translating the origin a prescribed distance along one of the axes and the number of shifting origins depends on the number of points one wishes to identify; (2) the Bucher (1990) approach is subsequently used to identify the design point of the new performance function in the new coordinate system; (3) a polynomial response surface is obtained, whose coefficients are determined by a least square regression analysis; and (4) Monte Carlo simulations are carried out on the response surface to obtain estimates of failure probability.

2.5 Simulation Methods

Simulation methods that involve sampling and estimation are well known in the statistics and reliability literature. Direct Monte Carlo simulation (MCS) is the most widely used simulation method, which involves the generation of independent samples of all input random variables, repeated deterministic trials to obtain corresponding simulated samples of response variables, and standard statistical analysis to estimate probabilistic

characteristics of response. In order to improve the computational efficiency of direct MCS, many strategies are applied to reduce the number of samplings.

2.5.1 Direct Monte Carlo Simulation

For structural reliability analysis involving a random vector $X = \{X_1, \cdots, X_N\}$ with joint density $f_X(x)$, the probability of failure defined by limit state function $g(X)$ can be estimated from M independent samples $x_1, \cdots, x_M$ generated from the density function $f_X(x)$. If there are an M^* number of samples among them satisfying $g(x) \leq 0$, then the probability of failure is approximated by

$$P_F = P\big[g(X) \leq 0\big] \cong \frac{M^*}{M}. \tag{2.91}$$

and the reliability is

$$P_S = 1 - P_F \cong \frac{M - M^*}{M}. \tag{2.92}$$

By direct MCS, a large number of samples are required to estimate accurately for the small probability of failure.

2.5.2 Importance Sampling

The idea of importance sampling is to generate samples, not from the probability density function $f_X(x)$ of random vector X, but from another sampling distribution. It is expected that better approximation can be obtained for probability of failure from the

new density function. The probability of failure defined in Equation (2.7) can be rewritten as

$$P_F = \int_{g(x) \leq 0} f_X(x) dx = \int_{g(x) \leq 0} w(x) h(x) dx, \qquad (2.93)$$

where $w(x) = f_X(x)/h(x)$. By using the importance sampling method with an M number of samples, the probability of failure is given by

$$P_F = \frac{1}{M} \sum_{i=1}^{M} \left(w(x_i) \big| g(x_i) \leq 0 \right). \qquad (2.94)$$

A simple and widely employed approach of importance sampling is to move the sampling center from the origin in standard Gaussian space to the design point (MPP) on the failure surface (Scheller and Stix, 1987). Other sampling distribution and sampling centers were discussed by Engelund and Rackwitz (1993).

2.5.3 Stratified Sampling

In stratified sampling, the domain of integration is divided into several regions (Melcher, 1999). Emphasis can be attributed by implementing more simulation in regions that contribute to the failure event. Consequently, the total domain of integration can be divided into m regions, i.e., $R_1, R_2, \cdots, R_m$. Using the total probability theorem, the probability of failure can be estimated as

$$P_F = \sum_{j=1}^{m} \left[P(R_j) \frac{1}{N_j} \sum_{i=1}^{N_j} \mathcal{I}(x) \right], \qquad (2.95)$$

where $\mathcal{I}(\boldsymbol{x}) = \begin{cases} 0, & \text{if } g(\boldsymbol{x}) > 0 \\ 1, & \text{if } g(\boldsymbol{x}) < 0 \end{cases}$ is the indication function with respect to the performance

function $g(\boldsymbol{x})$, $P(R_j)$ is the failure probability of region R_j, and N_j is the number of simulations performed in region R_j. Since the failure region may not be known in advance, a trial and error method is necessary to implement this strategy.

2.5.4 Directional Simulation

Consider a reliability problem with a limit state function $g(\boldsymbol{X})$ involving N normally distributed random variables. If length R and direction $\boldsymbol{A}$ of a vector $\boldsymbol{X} = R\boldsymbol{A}$ are defined, then R^2 is Chi-square distributed with the CDF $\chi_N^2(r)$ having N degrees of freedom. Probability of failure defined in Equation (2.7) can be given by an integration of the conditional failure probability in the direction $\boldsymbol{A} = \boldsymbol{a}$ as (Bjerager, 1988)

$$
\begin{aligned}
P_F &= P\big[g(\boldsymbol{X}) \le 0\big] = P\big[g(R\boldsymbol{A}) \le 0\big] \\
&= \int_{\text{All direction}} P\big[g(R\boldsymbol{a}) \le 0 \,|\, \boldsymbol{A} = \boldsymbol{a}\big] f_A(\boldsymbol{a}) \, d\boldsymbol{a}, \\
&= \int_{\text{All direction}} \Big[1 - \chi_N^2(r_a^2)\Big] f_A(\boldsymbol{a}) \, d\boldsymbol{a}
\end{aligned}
\tag{2.96}
$$

where $\boldsymbol{a}$ is a realization of a random unit vector $\boldsymbol{A}$ uniformly distributed on the N dimensional unit hypersphere $\boldsymbol{\Omega}_N$ and centered around the origin, and $f_A(\boldsymbol{a})$ is the uniformly density function, given by

$$
f_A(\boldsymbol{a}) = \frac{1}{S} = \frac{\Gamma(N/2)}{2\pi^{N/2}},
\tag{2.97}
$$

where S is the surface area of $\mathbf{\Omega}_N$, $\Gamma(\bullet)$ is the Gamma function, and r_a is the distance from the origin to the limit state surface in the direction $\boldsymbol{a}$. Suppose the unit hypersphere is divided evenly into M subsurfaces with the same area S / M and a representative direction $\boldsymbol{a}_i$. From Equation (2.97), the failure probability can be approximated by

$$P_F \cong \frac{1}{M} \sum_{i=1}^{M} \left[1 - \chi_N^2 \left(r_{\boldsymbol{a}_i}^2 \right) \right]. \tag{2.98}$$

The key issue for this method is to generate M evenly distributed $\boldsymbol{a}_i$ directions. There are two approaches available: (1) generate M vectors of N independent Gaussian random variables and normalize these vectors to unit length; or (2) generate M vectors of N independent uniform random variables by using the rejection method, such that a vector is retained only if its length is no greater than one, in which case all vectors are normalized. The directional simulation method is very efficient, because the distance from the origin to the limit state surface in any direction can be obtained efficiently, as pointed out by Ditlevsen (1990).

2.5.5 Latin Hypercube Sampling

Latin hypercube sampling, first proposed by McKay (1979) and further developed by Stein (1987) and Olsson and Sandberg (2002), uses a stratified sampling procedure to sample the values of the random variables from their probability density functions. For a problem involving N random variables, if M is the required number of samples, then an $M \times N$ matrix $\boldsymbol{P}$ can be created, in which each of the N columns is a random permutation

of $1, 2, \cdots, M$, and an $M \times N$ matrix $\boldsymbol{R}$ of independent random numbers from the uniform

$(0,1)$ distribution are established by standard MCS. A matrix $\boldsymbol{S}$ is obtained as

$$S = \frac{1}{M}\left(\boldsymbol{P} - \boldsymbol{R}\right). \tag{2.99}$$

Then, realization of the random vectors become

$$\boldsymbol{x}_i = \left(x_{i1}, \cdots, x_{iN}\right), \; i = 1, \cdots, M, \tag{2.100}$$

in which $x_{ij} = F_{x_j}^{-1}\left(S_{ij}\right)$, where $F_{x_j}^{-1}(\bullet)$ is the inverse of the CDF for random variable X_j.

There is a risk that some spurious correlation will appear, and Olsson (2003) proposed

some methods to reduce it.

2.5.6 Markov Chain Monte Carlo Simulation

The Markov chain MCS method, also called subset simulation, was applied by Au

and Beck (2001) to estimate small failure probability using a modified Metropolis

algorithm (Metropolis, 1953, Fisherman, 1996). This method transfers the evaluation of

failure probability to the evaluation of a sequence of simulations of more frequent events

in conditional probability spaces. For a given failure event F, construct

$F_1 \supset F_2 \supset \cdots \supset F_m = F$ as a decreasing sequence of failure events, so that

$F_k = \bigcap_{i=1}^{k} F_i, \; k = 1, 2, \cdots, m$. According to the definition of conditional probability, failure

probability becomes

$$P_F = P[F_m] = P\left[\bigcap_{i=1}^{m} F_i\right]$$
$$= P\left[F_m\middle|\bigcap_{i=1}^{m-1} F_i\right]P\left[\bigcap_{i=1}^{m-1} F_i\right] \qquad (2.101)$$
$$= P[F_1]P[F_2|F_1]P[F_3|F_2]\cdots P[F_m|F_{m-1}]$$

The major task is to simulate the conditional samples efficiently, which was achieved using the modified Metropolis algorithm (Au and Beck, 2001). This method is found robust up to the number of random variables and efficient in computing small probabilities. However, the proposed PDFs involved in the Metropolis algorithm have to be carefully chosen because the spread affects the size of the region covered by the Markov chain samples and, consequently, the efficiency. A small spread tends to increase the dependence between two successive samples due to their proximity, and an excessively large spread may reduce the acceptance rate and increase the number of repeated Markov chain samples. In both cases, convergence could be slow.

2.6 Response Surface Methods

The practicality of reliability methods for a specific limit state depends on the complexity of the formulation of the limit state. Often the limit state function is not available in explicit form, but rather defined implicitly through a complicated numerical procedure, given for example by the finite element analysis. For such limit state formulations, the needed calculations may require prohibitive large computational efforts. One way to solve such complex problem is to approximate the limit state surface in a numerical-experimental way by using a surface in explicitly mathematical form, and then implementing a reliability analysis. This procedure is called the *response surface method*.

2.6.1 Basic Principle of Response Surface Method

Let $X = \{X_1, \cdots, X_N\}$ be the vector of basic random variables. The central idea of the response surface method is to approximate the exact limit state function $g(X)$, which is usually known through an algorithmic procedure, by a polynomial function $\hat{g}(X)$. In practice, quadratic functions are used in the form

$$g(x) \cong \hat{g}(x) = a_0 + \sum_{i=1}^{N} a_i x_i + \sum_{i=1}^{N} a_{ii} x_i^2 + \sum_{i=1}^{N} \sum_{j=1, j \neq i}^{N} a_{ij} x_i x_j , \qquad (2.102)$$

where the set of coefficients $a = \{a_0, a_i, a_{ii}, a_{ij}\}$, which correspond to the constant, linear, square, and cross terms, respectively, are to be determined.

A limited number of evaluations of the limit state function are required to build the surface. A reliability analysis can then be performed by means of the analytical expression in Equation (2.102), instead of the true limit state function. This approach is particularly attractive when simulation methods such as importance sampling (Bucher and Bourgund, 1990) are used to obtain the reliability results.

2.6.2 Building the Response Surface

The determination of the unknown coefficients a is performed by using the least squares method. After choosing a set of fitting points x_k, $k = 1, \cdots, n$, for which the exact value $y_k = g(x_k)$ is computed, the error $\varepsilon(a)$, defined by

$$\varepsilon(a) = \sum_{i=1}^{n} \left(y_k - \hat{g}(x_k) \right)^2 , \qquad (2.103)$$

is minimized with respect to $\boldsymbol{a}$. Reformulating Equation (2.103) in the form

$$\hat{g}(X) = \{1, x_i, x_i^2, x_i x_j\}^T \cdot \{a_0, a_i, a_{ii}, a_{ij}\} \equiv V^T(\boldsymbol{x}) \cdot \boldsymbol{a}, \qquad (2.104)$$

where $i, j = 1, \cdots, N$ and $j \neq i$. The least squares problem becomes:

$$\min \left\{ \sum_{i=1}^{n} \left(y_k - V^T(\boldsymbol{x}_k) \cdot \boldsymbol{a} \right)^2 \right\}. \qquad (2.105)$$

After some basic algebra (Faravelli, 1989), the solution to the above problem yields

$$\boldsymbol{a} = \left(\boldsymbol{v}^T \boldsymbol{v} \right)^{-1} \boldsymbol{v}^T \boldsymbol{y}, \qquad (2.106)$$

where $\boldsymbol{v}$ is the matrix whose rows are the vectors $V(\boldsymbol{x}_k)$ and $\boldsymbol{y}$ is the vector whose components are $y_k = g(\boldsymbol{x}_k)$.

The various response surface methods proposed in the literature differ only in the terms retained in the polynomial expression (2.102), and the selection of the coordinates of the fitting points, i.e., the experimental design used in the regression analysis. It is emphasized that $n \geq N$ is required to solve (2.105). Furthermore, the fitting points have to be chosen in a consistent way in order to get independent equations.

2.6.3 Various Types of Response Surface Approaches

Early applications of the response surface method involved the so-called factorial experimental design. For each random variable X_i, lower and upper values of realizations (x_i^-, x_i^+) are selected. Overall, 2^N fitting points are defined by all possible combinations

$\{x_1^{\pm}, \cdots, x_N^{\pm}\}$. The number of fitting points increases exponentially with the number of random variables N involved in the reliability problem under consideration.

In order to reduce the number of fitting points for cases in which N is large, Bucher and Bourgund (1990) proposed a simplified quadratic expression without cross terms, which is defined by only $(2N+1)$ coefficients $\boldsymbol{a} = \{a_0, a_i, a_{ii}\}$. In the first step, the mean vector $\boldsymbol{\mu}_X$ is chosen as the center point of the response surface. Exact $(2N+1)$ fitting points are selected "along the axes," described by

$$\begin{cases} \boldsymbol{x}_1 = \boldsymbol{\mu}_X \\ \boldsymbol{x}_{2i} = \boldsymbol{\mu}_X - f\sigma_i \boldsymbol{e}_i, \; i = 1, \cdots, N \\ \boldsymbol{x}_{2i+1} = \boldsymbol{\mu}_X + f\sigma_i \boldsymbol{e}_i, \; i = 1, \cdots, N \end{cases} \tag{2.107}$$

where σ_i is the standard deviation of the ith random variable, $\boldsymbol{e}_i$ is the ith basis vector of the space of parameters, whose coordinates are $\{0, \cdots, 0, 1, 0, \cdots 0\}$, and f is an arbitrary number (set to 3 by Bucher and Bourgund (1990)).

From this first response surface, an estimate of the design point $\boldsymbol{x}^*$ is computed. Then, a new center point $\boldsymbol{x}_M$ is obtained as a linear interpolation between $\boldsymbol{\mu}_X$ and $\boldsymbol{x}^*$ by

$$\boldsymbol{x}_M = \boldsymbol{\mu}_X + (\boldsymbol{x}^* - \boldsymbol{\mu}_X) \frac{g(\boldsymbol{\mu}_X)}{g(\boldsymbol{\mu}_X) - g(\boldsymbol{x}^*)}. \tag{2.108}$$

A second response surface is then generated around $\boldsymbol{x}_M$. As a whole, the approach requires only $(4N+3)$ evaluations of the limit state function, and can thus be carried out for structural systems involving a great number of random variables. Finally, importance sampling is used to obtain the reliability results.

Later, Rajashekhar and Ellingwood (1993) considered the same approach by Bucher and Bourgund (1990) as the first two steps of an iterative procedure until full convergence. They also added cross terms to the response surface definition, obtaining better results in numerical examples.

Kim and Na (1997) observed that in previous research, the fitting points are selected around a preselected point (i.e., the mean value of the basic random vector) and arranged along the axes or "diagonals" of the space of parameters, without considering the orientation of the original limit state surface. The authors argued that in some cases these procedures might not converge to the true design point. Alternatively, they proposed to determine a series of linear response surfaces as follows: in each iteration, the fitting points used in the previous step are projected onto the previous response surface, and the projection points that are obtained (which are closer to the actual limit state surface) are used for generating the next response surface. In each iteration, an approximate reliability index is readily available, since the response surface is linear. In some sense, this method finds the design point without solving the minimization problem usually associated with FORM. This method is called the *vector projection method*.

Starting from the idea of Kim and Na (1997), Das and Zhang (2000) proposed enhancing the linear response surface by adding square terms. The fitting points defining the final linear response surface are reused to produce the quadratic surface. SORM analysis is then performed.

Lemaire (1997) presents a synthetic summary of the response surface method and draws the following conclusions: (1) it is better to cast the response surface in standard

normal space, rather than in the original space because regression can be controlled better; (2) provided enough fitting points, the choice of the type of experimental design is not fundamental; and (3) the quality of the response surface has to be checked. Different indicators are proposed to estimate the accuracy: (1) the back-transformation of the fitting points from standard normal space to the original space, in order to exclude non-physical points; (2) the conditioning of the experimental matrix $v^T v$ in Equation (2.106); (3) the quality of the regression measured by a correlation coefficient; and (4) the extent to which the obtained design point belongs to the original limit state surface.

2.7 Mean-Point-based Decomposition Methods

Recently, Rahman and Xu (2004) developed new decomposition methods that can solve highly nonlinear reliability problems more accurately or more efficiently than FORM/SORM and simulation methods. A major advantage of these decomposition methods over FORM/SORM, so far they are based on the mean point of random input as a reference point, is that higher-order approximations of performance functions can be obtained without calculating the MPP or the gradients.

2.7.1 Multivariate Function Decomposition

Consider a continuous, differentiable, real-valued function $y(\boldsymbol{x})$ that depends on $\boldsymbol{x}$ = $\{x_1,\ldots,x_N\} \in \mathbb{R}^N$. Suppose that $y(\boldsymbol{x})$ has convergent Taylor series expansion at an arbitrary reference point $\boldsymbol{x} = \boldsymbol{c} = \{c_1,\cdots,c_N\}^T$, expressed by

$$y(\boldsymbol{x}) = y(\boldsymbol{c}) + \sum_{j=1}^{\infty} \frac{1}{j!} \sum_{i=1}^{N} \frac{\partial^j y}{\partial x_i^j}(\boldsymbol{c})(x_i - c_i)^j + R_2 \qquad (2.109)$$

or

$$y(\boldsymbol{x}) = y(\boldsymbol{c}) + \sum_{j=1}^{\infty} \frac{1}{j!} \sum_{i=1}^{N} \frac{\partial^j y}{\partial x_i^{\,j}}(\boldsymbol{c})(x_i - c_i)^j$$
$$+ \sum_{j_1,j_2 > 0}^{\infty} \frac{1}{j_1! \, j_2!} \sum_{i_1 < i_2} \frac{\partial^{j_1 + j_2} y}{\partial x_{i_1}^{\,j_1} \partial x_{i_2}^{\,j_2}}(\boldsymbol{c})(x_{i_1} - c_{i_1})^{j_1}(x_{i_2} - c_{i_2})^{j_2} + R_3 \qquad (2.110)$$

where the remainder R_2 denotes all terms with dimension two and higher and the remainder R_3 denotes all terms with dimension three and higher.

2.7.1.1 Univariate Approximation

Consider a univariate approximation of $y(\boldsymbol{x})$, denoted by

$$\hat{y}_1(\boldsymbol{x}) \equiv \hat{y}_1(x_1, \cdots, x_N) = \sum_{i=1}^{N} y(c_1, \cdots, c_{i-1}, x_i, c_{i+1}, \cdots, c_N) - (N-1)y(\boldsymbol{c}), \quad (2.111)$$

where each term in the summation is a function of only one variable and can be subsequently expanded in a Taylor series at $\boldsymbol{x} = \boldsymbol{c}$, yielding

$$\hat{y}_1(\boldsymbol{x}) = y(\boldsymbol{c}) + \sum_{j=1}^{\infty} \frac{1}{j!} \sum_{i=1}^{N} \frac{\partial^j y}{\partial x_i^{\,j}}(\boldsymbol{c})(x_i - c_i)^j . \qquad (2.112)$$

A comparison between Equations (2.109) and (2.112) indicates that univariate approximation leads to the residual error $y(\boldsymbol{x}) - \hat{y}_1(\boldsymbol{x}) = R_2$, which includes contributions from terms of dimension two and higher. For sufficiently smooth $y(\boldsymbol{x})$ with a convergent Taylor series, the coefficients associated with higher-dimensional terms are usually much smaller those with one-dimensional terms. In that case, higher-dimensional terms contribute less to the function, and therefore, can be neglected.

2.7.1.2 Bivariate Approximation

In a similar way, consider the bivariate approximation

$$
\begin{aligned}
\hat{y}_2(\boldsymbol{x}) \quad \equiv \quad & \sum_{i_1<i_2} y(c_1,\cdots,c_{i_1-1},x_{i_1},c_{i_1+1},\cdots,c_{i_2-1},x_{i_2},c_{i_2+1},\cdots,c_N) \\
& -(N-2)\sum_{i=1}^{N} y(c_1,\cdots,c_{i-1},x_i,c_{i+1},\cdots,c_N)+\frac{(N-1)(N-2)}{2}y(\boldsymbol{c})
\end{aligned}
\quad , \quad (2.113)
$$

of $y(\boldsymbol{x})$, where each term on the right hand side is a function of at most two variables, and

can be subsequently expanded in a Taylor series at $\boldsymbol{x}=\boldsymbol{c}$, yielding

$$
\begin{aligned}
\hat{y}_2(\boldsymbol{x}) \quad = \quad & y(\boldsymbol{c})+\sum_{j=1}^{\infty}\frac{1}{j!}\sum_{i=1}^{N}\frac{\partial^j y}{\partial x_i^{\,j}}(\boldsymbol{c})(x_i-c_i)^j \\
& +\sum_{j_1,j_2>0}^{\infty}\frac{1}{j_1!\,j_2!}\sum_{i_1<i_2}\frac{\partial^{j_1+j_2}y}{\partial x_{i_1}^{\,j_1}\partial x_{i_2}^{\,j_2}}(\boldsymbol{c})(x_{i_1}-c_{i_1})^{j_1}(x_{i_2}-c_{i_2})^{j_2}
\end{aligned}
\quad . \quad (2.114)
$$

Again, a comparison of Equations (2.110) and (2.114) indicates that the bivariate

approximation leads to the residual error $y(\boldsymbol{x})-\hat{y}_2(\boldsymbol{x})=R_3$, in which remainder R_3

includes terms of dimension three and higher. The bivariate approximation includes all

terms with no more than two variables, thus leading to a higher rate of accuracy than the

univariate approximation.

2.7.1.3 Generalized *S*-Variate Approximation

The procedure for univariate and bivariate representations described above can be

generalized to an *S*-variate representation for any integer $1\leq S\leq N$. The generalized *S*-

variate approximation of $y(\boldsymbol{x})$ is

$$
\hat{y}_S(\boldsymbol{x})\equiv\sum_{i=0}^{S}(-1)^i\binom{N-S+i-1}{i}y_{S-i}(\boldsymbol{x}),
\quad (2.115)
$$

where

$$y_R = \sum_{k=0}^{R} \binom{N-k}{R-k} t_k; \ \ 0 \le R \le S \ \ , \tag{2.116}$$

with

$$
\begin{aligned}
t_0 \ &= \ y(\boldsymbol{c}) \\
t_1 \ &= \ \sum_{j_1} \frac{1}{j_1!} \sum_{i_1=1}^{N} \frac{\partial^{j_1} y}{\partial x_{i_1}^{j_1}}(\boldsymbol{c})(x_{i_1}-c_{i_1})^{j_1} \\
t_2 \ &= \ \sum_{j_1,j_2} \frac{1}{j_1! j_2!} \sum_{i_1<i_2} \frac{\partial^{j_1+j_2} y}{\partial x_{i_1}^{j_1} \partial x_{i_2}^{j_2}}(\boldsymbol{c})(x_{i_1}-c_{i_1})^{j_1}(x_{i_2}-c_{i_2})^{j_2} \\
&\vdots \ \ \vdots \ \ \vdots \\
t_S \ &= \ \sum_{j_1,j_2,\cdots,j_S} \frac{1}{j_1! j_2!\cdots j_S!} \sum_{i_1<i_2<\cdots<i_S} \frac{\partial^{j_1+j_2+\cdots+j_S} y}{\partial x_{i_1}^{j_1} \partial x_{i_2}^{j_2}\cdots \partial x_{i_S}^{j_S}}(\boldsymbol{c})(x_{i_1}-c_{i_1})^{j_1}(x_{i_2}-c_{i_2})^{j_2}\cdots(x_{i_S}-c_{i_S})^{j_S}
\end{aligned}
\tag{2.117}
$$

Using a multivariate function theorem, it can be shown that $\hat{y}_S(\boldsymbol{x})$ in Equation (2.115) consists of all terms of the Taylor series of $y(\boldsymbol{x})$ that have less than or equal to S variables. The expanded form of Equation (2.115), when compared with the Taylor expansion of $y(\boldsymbol{x})$, indicates that the residual error in the S-variate approximation is $y(\boldsymbol{x}) - \hat{y}_S(\boldsymbol{x}) = R_{S+1}$, where the remainder R_{S+1} includes terms of dimension $S+1$ and higher. When $S = 1, 2$, Equation (2.115) degenerates to univariate and bivariate approximation. Similarly, trivariate, quadrivariate, and other higher-variate approximations can be derived by appropriately selecting the value of S. At the limit, when $S = N$, Equation (2.115) converges to the exact function $y(\boldsymbol{x})$. In other words, the proposed approximation generates convergent representation of $y(\boldsymbol{x})$.

2.7.1.4 Remarks

The decomposition of a general multivariate function $y(\boldsymbol{x})$ can be viewed as a finite sum

$$y(\boldsymbol{x}) = \underbrace{\underbrace{y_0 + \sum_{i=1}^{N} y_i(x_i)}_{=\hat{y}_1(\boldsymbol{x})} + \sum_{\substack{i_1,i_2=1 \\ i_1<i_2}}^{N} y_{i_1 i_2}(x_{i_1}, x_{i_2}) + \cdots + \sum_{\substack{i_1,\cdots,i_S=1 \\ i_1<\cdots<i_S}}^{N} y_{i_1\cdots i_S}(x_{i_1},\cdots,x_{i_S})}_{=\hat{y}_S(\boldsymbol{x})} + \cdots + y_{12\cdots N}(x_1,\cdots,x_N)}_{=\hat{y}_2(\boldsymbol{x})}, \quad (2.118)$$

where y_0 is a constant, $y_i(x_i)$ is a univariate component function representing an independent contribution by input variable v_i, $y_{i_1 i_2}(x_{i_1}, x_{i_2})$ is a bivariate component function describing cooperative influence of two input variables x_{i_1} and x_{i_2}, $y_{i_1\cdots i_S}(x_{i_1},\cdots,x_{i_S})$ is an S-variate component function quantifying cooperative effects of S input variables $x_{i_1},\cdots,x_{i_S}$, and so on. By comparing Equations (2.111) and (2.113) with Equation (2.118), the univariate and bivariate approximations provide two- and three-term approximants, respectively, of the finite decomposition. In general, the S-variate approximation in Equation (2.115) yields the S+1-term approximant of the decomposition. The fundamental conjecture underlying this work is that component functions arising in the proposed decomposition will exhibit insignificant higher-dimensional effects.

It is worth noting that the univariate approximation in Equation (2.111) should not be viewed as first- or second-order Taylor series expansions and does not limit the nonlinearity of $y(\boldsymbol{x})$. According to Equation (2.112), *all* higher-order univariate terms of $y(\boldsymbol{x})$ are included in the proposed approximation. In fact, the univariate component

function $y_i(x_i)$ can be highly nonlinear and, therefore, in general should provide higher-order representation of a performance function than those by FORM or SORM. Furthermore, the approximations contain contributions from *all* input variables.

2.7.2 Response Surface Generation

Consider the univariate terms $y_i(x_i) \equiv y(c_1, \cdots, c_{i-1}, x_i, c_{i+1}, \cdots, c_N)$ in Equations (2.112) and (2.113). If for $x_i = x_i^{(j)}$, n function values

$$y_i(x_i^{(j)}) = y(c_1, \cdots, c_{i-1}, x_i^{(j)}, c_{i+1}, \cdots, c_N); j = 1, 2, \cdots, n \qquad (2.119)$$

are given, the function value for arbitrary x_i can be obtained using the Lagrange interpolation as

$$y_i(x_i) = \sum_{j=1}^{n} \phi_j(x_i) y_i(x_i^{(j)}), \qquad (2.120)$$

where the shape function $\phi_j(x_i)$ is defined as

$$\phi_j(x_i) = \frac{(x_i - x_i^{(1)}) \cdots (x_i - x_i^{(j-1)})(x_i - x_i^{(j+1)}) \cdots (x_i - x_i^{(n)})}{(x_i^{(j)} - x_i^{(1)}) \cdots (x_i^{(j)} - x_i^{(j-1)})(x_i^{(j)} - x_i^{(j+1)}) \cdots (x_i^{(j)} - x_i^{(n)})}. \qquad (2.121)$$

By using Equation (2.120), many function values of $y_i(x_i)$ can be arbitrarily generated if n function values are given. The same idea can be applied to the bivariate terms $y_{i_1 i_2}(x_{i_1}, x_{i_2}) \equiv y(c_1, \cdots, c_{i_1-1}, x_{i_1}, c_{i_1+1}, \cdots, c_{i_2-1}, x_{i_2}, c_{i_2+1}, \cdots, c_N)$ in Equation (2.116). If for $x_{i_1} = x_{i_1}^{(j_1)}$ and $x_{i_2} = x_{i_2}^{(j_2)}$, n^2 function values

$$y_{i_1 i_2}(x_{i_1}^{j_1}, x_{i_2}^{j_2}) \equiv y(c_1, \cdots, c_{i_1-1}, x_{i_1}^{j_1}, c_{i_1+1}, \cdots, c_{i_2-1}, x_{i_2}^{j_2}, c_{i_2+1}, \cdots, c_N);$$
$$j_1 = 1, 2, \cdots, n; j_2 = 1, 2, \cdots, n \qquad (2.122)$$

are given, the function value $y_{i_1 i_2}(x_{i_1}, x_{i_2})$ for arbitrary point (x_{i_1}, x_{i_2}) can be obtained using the Lagrange interpolation as

$$y_{i_1 i_2}(x_{i_1}, x_{i_2}) = \sum_{j_2=1}^{n} \sum_{j_1=1}^{n} \phi_{j_1}(x_{i_1}) \phi_{j_2}(x_{i_2}) y_{i_1 i_2}(x_{i_1}^{j_1}, x_{i_2}^{j_2}), \qquad (2.123)$$

where shape functions $\phi_{j_1}(x_{i_1})$ and $\phi_{j_2}(x_{i_2})$ are defined in Equation (2.121). Note that there are n and n^2 performance function evaluations involved in Equation (2.119) and Equation (2.122), respectively. Therefore, the total cost for univariate approximation entails $nN+1$ function evaluations, and for bivariate approximation, $N(N-1)n^2/2 + nN + 1$ function evaluations are required. More accurate multivariate approximations can be developed in a similar way, but with a much higher cost.

2.7.3 Monte Carlo Simulation

For component reliability analysis, the Monte Carlo estimates $P_{F,1}$ and $P_{F,2}$ of failure probability, employing univariate and bivariate representations, respectively, are

$$P_{F,1} = \frac{1}{N_S} \sum_{i=1}^{N_S} \mathcal{I}\left[\hat{y}_1\left(\boldsymbol{x}^{(i)} \right) < 0 \right] \qquad (2.124)$$

and

$$P_{F,2} = \frac{1}{N_S} \sum_{i=1}^{N_S} \mathcal{I}\left[\hat{y}_2\left(\boldsymbol{x}^{(i)} \right) < 0 \right], \qquad (2.125)$$

where $\boldsymbol{x}^{(i)}$ is the ith realization of $\boldsymbol{X}$, N_S is the sample size, and $\mathcal{I}[\cdot]$ is an indicator function such that $\mathcal{I} = 1$ if $\boldsymbol{x}^{(i)}$ is in the failure set (*i.e.*, when $\hat{y}_1(\boldsymbol{x}^{(i)}) < 0$ for univariate

representation and when $\hat{y}_2(\boldsymbol{x}^{(i)}) < 0$ for bivariate representation of the performance function) and *zero* otherwise.

Since univariate or bivariate representations facilitate lower-dimensional response surface approximations, the subsequent Monte Carlo simulation can be conducted for any sample size. However, the accuracy and efficiency of failure probability calculations using Equations (2.124) and (2.125) depend on both the decomposition and response surface approximation.

2.8 Sensitivity Analysis

Sensitivity analysis provides a measure of a specific input variable's importance to the reliability results. The deterministic input variables and the parameters in the distributions of random input variables are denoted as input parameters. The sensitivity of the reliability measure with respect to changes in these parameters is important for reliability-based design optimization. This can easily be evaluated as a change of reliability for a given change in the design. In combination with an optimization procedure that aims at minimizing total cost, the sensitivities can be also used with iterative solution methods.

2.8.1 Derivative of Reliability Index –One Parameter

Consider a performance function $g(\boldsymbol{u};\theta)$, where θ is a single parameter, for an MPP $\boldsymbol{u}^*$ on the limit-state surface in the standard Gaussian space, the following equations exist

$$\boldsymbol{u}^* = \boldsymbol{\alpha}\beta, \tag{2.126}$$

$$\boldsymbol{\alpha} = -\frac{\nabla g(\boldsymbol{u}^*;\theta)}{\left\|\nabla g(\boldsymbol{u}^*;\theta)\right\|},\tag{2.127}$$

$$\boldsymbol{\alpha}^T\boldsymbol{\alpha} = 1,\tag{2.128}$$

$$g\left(\boldsymbol{u}^*;\theta\right) = 0,\tag{2.129}$$

where $\nabla = \left\{\partial/\partial u_1,\cdots,\partial/\partial u_N\right\}^T$. It follows that β is also a function of θ. The sensitivity

of β with respect to changes in θ is measured by the derivative $d\beta/d\theta$.

From Equations (2.126) and (2.128)

$$\beta = \boldsymbol{\alpha}^T\boldsymbol{u}^*,\tag{2.130}$$

which, on taking derivative with respect to θ, given

$$\frac{d\beta}{d\theta} = \frac{d\boldsymbol{\alpha}^T}{d\theta}\boldsymbol{u}^* + \boldsymbol{\alpha}^T\frac{d\boldsymbol{u}}{d\theta}\bigg|_{u=u^*}.\tag{2.131}$$

The first term on the right-hand side of Equation (2.131) is zero because

$d\boldsymbol{\alpha}/d\theta$ and $\boldsymbol{\alpha}$ are mutually orthogonal and $\boldsymbol{u}^* = \boldsymbol{\alpha}\beta$. The orthogonality is verified

directly by differentiation of Equation (2.128). Differentiation of Equation (2.129) gives

$$\frac{dg(\boldsymbol{u}^*;\theta)}{d\theta} = \frac{\partial g}{\partial \theta} + \nabla g^T\frac{d\boldsymbol{u}}{d\theta}\bigg|_{u=u^*} = 0.\tag{2.132}$$

This, after divided by $\left\|\nabla g\right\|$ on both sides, yields

$$\frac{1}{\left\|\nabla g\right\|}\frac{\partial g}{\partial \theta} + \frac{\nabla g^T}{\left\|\nabla g\right\|}\frac{d\boldsymbol{u}}{d\theta}\bigg|_{u=u^*} = 0,\tag{2.133}$$

By comparing Equation (2.133) and (2.131), gives

$$\frac{d\beta}{d\theta} = \frac{1}{\left\|\nabla g\right\|}\frac{\partial g}{\partial \theta}.\tag{2.134}$$

That is the sensitivity of reliability index with respect to parameter θ.

There are two different cases of application for Equation (2.134).

(1) Case I: θ is a deterministic input variable

Hence, θ is a parameter that concerns the definition of the limit state. The limit-state function in standard Gaussian space and original space satisfy

$$g(\boldsymbol{u};\theta) = g[T(\boldsymbol{x});\theta] = G(\boldsymbol{x};\theta),$$

(2.135)

where $\boldsymbol{u} = T(\boldsymbol{x})$ is the given transformation. It then follows that $\partial g/\partial\theta = \partial G/\partial\theta$.

(2) Case II: *θ* is a distribution parameter

Such a parameter has no influence on the limit state in original space, but has influence on the limit state in the standard Gaussian space through the transformation $\boldsymbol{u} = T(\boldsymbol{x};\theta)$. That means:

$$g(\boldsymbol{u};\theta) = G(\boldsymbol{x}),$$

(2.136)

where the right side is independent of . Therefore, the partial derivative of the left hand side of Equation (2.136) with respect to θ is zero, written as

$$\nabla g^T \frac{\partial \boldsymbol{u}}{\partial\theta} + \frac{\partial g}{\partial\theta} \equiv 0.$$

(2.137)

By application of (2.127), Equation (2.134) gives

$$\frac{d\beta}{d\theta} = \boldsymbol{\alpha}^T \frac{\partial \boldsymbol{u}}{\partial\theta}\bigg|_{\boldsymbol{u}=\boldsymbol{u}^*}.$$

(2.138)

2.8.2 Derivative of FORM Approximation to Failure Probability

The FORM based approximation to the probability of failure is

$$P_{F,1} = \Phi(-\beta). \tag{2.139}$$

The derivative of the failure probability is

$$\frac{dP_{F,1}}{d\theta} = -\phi(-\beta)\frac{d\beta}{d\theta}. \tag{2.140}$$

Correspondingly, the derivative of the natural logarithm to $P_{F,1}$ is

$$\frac{d\log P_{F,1}}{d\theta} = -\frac{\phi(-\beta)}{\Phi(-\beta)}\frac{d\beta}{d\theta}. \tag{2.141}$$

For large values of β the asymptotic formula $\phi(-\beta)/\Phi(-\beta) \cong \beta$ is valid, whereby the results of (2.141) can be simplified.

If $P_{F,1}$ is viewed as a function of an input parameter, the image is in most cases strongly curved. However, if β or $\log P_{F,1}$ is mapped as a function of the input parameter, most often the image is only slightly curved. Assume that the probability of failure is known for a value θ of the input parameter. We want to determine the probability of failure corresponding to the parameter value $\theta + \Delta\theta$. A calculation based on

$$P_{F,1}\big|_{\theta+\Delta\theta} \cong P_{F,1}\big|_{\theta} + \frac{dP_{F,1}}{d\theta}\Delta\theta, \tag{2.142}$$

often will be quite inaccurate except for very small values of $\Delta\theta$. However, a calculation based on

$$P_{F,1}\big|_{\theta+\Delta\theta} = \Phi\left(-\left(\beta+\Delta\beta\right)\right) \cong \Phi\left(-\left(\beta+\frac{d\beta}{d\theta}\Delta\theta\right)\right) \qquad (2.143)$$

is often a reasonable approximation even for large values of $\Delta\theta$. Similarly another reasonable approximation is

$$P_{F,1}\big|_{\theta+\Delta\theta} \cong \exp\left\{\log P_{F,1}\big|_{\theta} + \frac{d\log P_{F,1}\big|_{\theta}}{d\theta}\Delta\theta\right\}. \qquad (2.144)$$

2.9 Reliability-based Design Optimization

2.9.1 Introduction

Stochastic optimization is a mathematical framework for solving general optimization problems in the presence of uncertainty, typically manifested by the probabilistic description of objective and constraint functions. A special case of stochastic optimization, frequently encountered in structural design, is referred to as reliability–based design optimization (RBDO). According to Royset et al. (2001), there are three types of formulation for solving an RBDO problem:

Type I: Minimize the cost of the design, subject to reliability and structural constraints;

Type II: Maximize the reliability of the design, subject to cost and structural constraints; and

Type III: Minimize the initial cost of the design plus the expected cost of failure, subject to reliability and structural constraints.

Of these three types, the first formulation is widely studied, typically involving a time-invariant reliability analysis. The basic mathematical model of Type I RBDO can be written as

$$\begin{aligned} \min_{\boldsymbol{d} \in \mathcal{D} \subseteq \mathbb{R}^K} \quad & c_0(\boldsymbol{d}) \\ \text{subject to} \quad & c_i(\boldsymbol{d}) \equiv P\left[g_i(\boldsymbol{X};\boldsymbol{d}) \geq 0\right] \leq R_i; \quad i = 1, \cdots, n_c, \\ & \boldsymbol{d}_l \leq \boldsymbol{d} \leq \boldsymbol{d}_u \end{aligned} \qquad (2.145)$$

where $\boldsymbol{d} = \{d_1, \cdots, d_k\}^T \in \mathcal{D}$ is a K-dimensional vector of design variables with a nonempty closed set $\mathcal{D} \subseteq \mathbb{R}^K$; $\boldsymbol{X} = \{X_1, \cdots, X_N\}^T \in \mathbb{R}^N$ is an N-dimensional random vector with mean and joint probability density function defined on a probability space $(\Omega, \mathcal{F}, P)$; f is the objective function that depends on $\boldsymbol{d}$; $g_i(\boldsymbol{X};\boldsymbol{d}), i = 1, \cdots, n_c$ is the ith performance function that depends on $\boldsymbol{d}$; and $0 \leq R_i \leq 1, i = 1, \cdots, n_c$ are target probabilities. The design vector $\boldsymbol{d}$ can be deterministic parameters of objective and constraint functions and/or distribution parameters of $\boldsymbol{X}$ (e.g., the mean). The lower and upper bounds of $\boldsymbol{d}$ are denoted by $\boldsymbol{d}_l$ and $\boldsymbol{d}_u$, respectively. According to Equation (2.145), the objective and constraint functions are both deterministic; however, the evaluation of constraints requires a reliability analysis.

2.9.2 FORM-based Optimization Methods

Traditionally, RBDO formulation is based on the FORM, due to its simplicity and computational efficiency. The constraint of Equation (2.145) can then be expressed by

$$P\left[g_i(\boldsymbol{X};\boldsymbol{d}) \leq 0\right] = F_{g_i}(0) \leq \Phi(-\beta_t) \quad i = 1, \cdots, n_c, \qquad (2.146)$$

where β$_t$ is the target reliability index and the cumulative distribution function $F_{g_i}(0)$ is described as

$$F_{g_i}(0) = \int_{g_i(X;d) \leq 0} \cdots \int f_X(x) dx \ i = 1, \cdots, n_c \ , \tag{2.147}$$

and $f_X(x)$ is the joint probability density function (JPDF) of X.

2.9.2.1 Double-Loop Approach

The classical double-loop RBDO method employs two nested optimization loops: the design optimization loop (outer) and the reliability assessment loop (inner). The inner loop is needed to evaluate each probabilistic constraint in Equation (2.145), which together with the outer loop make the double-loop RBDO computationally very expensive.

The probabilistic constraint in Equation (2.145) can be further expressed through inverse transformations in two alternative ways:

$$\beta_i = \left(-\Phi^{-1}\left(F_{g_i}(0)\right)\right) \geq \beta_t \tag{2.148}$$

$$g_{P_i} = F_{g_i}^{-1}\left(\Phi(-\beta_t)\right) \geq 0 \tag{2.149}$$

where β$_i$ and g_{P_i} are called the safety index and the probabilistic performance measure for the ith probabilistic constraint, respectively. If Equation (2.148) is employed to describe the probabilistic constraint in equation (2.145), it is called reliability index approach (RIA). The reliability index β is the minimum distance of a point u on the limit state $g_U(u) = 0$ from the origin of the standard normal space. Therefore, it can be calculated from the following reliability minimization problem

$$\beta = \min_{u} \|u\|$$
$$\text{s.t. } g_U(u) = 0$$

(2.150)

Similarly, Equation (2.149) can replace the probabilistic constrain with the performance measure, which is referred to as the performance measure approach (PMA). In PMA, the performance measure is calculated from the following reliability minimization problem

$$g_{P_i} = \min_{u} g_U(u)$$
$$\text{s.t. } \|u\| = \beta_t$$

(2.151)

Methods to solve (2.150) are discussed in section 2.4.2. Methods to solve (2.151) were summarized by Youn, et al.(2003), which included the variations of mean-value methods.

2.9.2.2 Single-Loop Approach

An equivalent formulation of the general RBDO problem (2.145) can be stated as

$$\min_{d \in \mathcal{D} \subseteq \mathbb{R}^K} c_0(d)$$
$$\text{subject to } g_i^R(X;d) \geq 0, i = 1, \cdots, n_c,$$
$$d_l \leq d \leq d_u$$

(2.152)

where g^R is the R-percentile of the constraint $g(X;d)$. It is defined as

$$P[g(X;d) \geq g^R] = R,$$

(2.153)

where R is the target reliability for the constraint. If $g^R \geq 0$, $P[g(X;d) \geq 0] \geq R$. Therefore, $g^R \geq 0$ provides an equivalent deterministic expression of the probabilistic constraints in Equation (2.145). The R-percentile g^R is evaluated using the PMA method

(Liang, et al., 2004) of Equation (2.151). After the MPP is calculated, the R-percentile is given by

$$g^R = g\left(X_{MPP};d\right). \tag{2.154}$$

Thus, the optimization problem of (2.152) becomes

$$\begin{aligned}
&\min_{d \in \mathscr{D} \subseteq \mathbb{R}^K} \; c_0\left(d\right) \\
&\text{subject to} \;\; g_i\left(X_{MPP};d\right) \geq 0, i = 1, \cdots, n_c \,, \\
&\qquad\qquad d_l \leq d \leq d_u
\end{aligned} \tag{2.155}$$

where $\mu_X = X_{MPP_i} - U_{MPP_i}\sigma$ and X_{MPP_i}, U_{MPP_i} are the MPP for the ith constraint in x and u spaces, respectively and σ is the vector of standard deviations.

Using the PMA approach, an inner loop of the double-loop method solves the optimization problem described by Equation (2.151). At the optimal point, the following Karush-Kuhn-Tacker (KKT) optimality condition is satisfied

$$\nabla g_U\left(u\right) + \lambda \nabla H\left(u\right) = 0, \tag{2.156}$$

where $H\left(u\right) = \|u\| - \beta$ is an equality constraint and λ is the corresponding Lagrange multiplier. The derivation gives

$$u = -\beta_t\alpha, \tag{2.157}$$

where $\alpha = \nabla g_U\left(X;d\right)/\left\|\nabla g_U\left(X;d\right)\right\|$ is the constrain normalized gradient in u space. The transformation of x to u space yields the following relationships

$$X = \mu_X - \sigma\beta_t\alpha, \tag{2.158}$$

where $\alpha = \sigma \nabla g_X (X;d) / \|\sigma \nabla g_X (X;d)\|$. Using (2.158), the RBDO formulation of Equation (2.155) can be transformed to the following single-loop, equivalent deterministic optimization problem

$$\min_{d \in \mathcal{D} \subseteq \mathbb{R}^K} c_0(d)$$
$$\text{subject to } g_i(X_i;d) \geq 0, i = 1, \cdots, n_c \qquad (2.159)$$

where $X_i = \mu_X - \sigma \beta_{t_i} \alpha_i$, $\alpha_i = \sigma \nabla g_{i_X}(X;d) / \|\sigma \nabla g_{i_X}(X;d)\|$, $d_l \leq d \leq d_u$, and β_{t_i} is the target reliability index for the ith constraint, α_i is the normalized gradient of the ith constraint. The single loop method does not search for the MPP of each constraint at each iteration. Instead, the MPP of the active constraints are correctly identified at the optimum. This dramatically improves the efficiency of the proposed single loop method without compromising accuracy.

2.9.3 Sequential Methods for RBDO

To avoid a nested optimization problem, sequential RBDO methods have been developed, which decouple the upper level design optimization from the reliability analysis (Agarwal, 2004). The design optimization and the search of the MPPs are performed separately and the procedure is repeated until a desired convergence is achieved. The idea is to find a consistent reliable design at lower computational cost as compared with the nested approach (double-loop). A consistent reliable design is a feasible design that satisfies all the reliability constraints. The reliability analysis is employed to check if a given design meets the desired reliability level. In most

sequential techniques of RBDO, a design obtained by performing a deterministic optimization is updated based on the information obtained from the reliability analysis, and the updated design is used as a starting point for the next cycle.

Chen and Du (2002) proposed a sequential optimization and reliability assessment methodology (SORA). In SORA, boundaries of the violated constraints are shifted into the feasible direction based on the reliability information obtained by previous iteration. Both RIA and PMA can be used for reliability assessment if FORM is deserved adequately. The PMA approach was reported to be computationally more efficient than RIA approach. In SORA, a first order reliability analysis is performed to obtain the MPP for each failure driven constraint. Therefore, a consistent reliable design provides an approximate solution. However, a true local optimum cannot be guaranteed, because the MPP for active constraints are obtained from the previous design point. Consequently, an MPP update has been suggested, but it may lead to spurious optimal design.

2.9.4 Simulation-based Optimization Methods

In RBDO, a particular source of difficulty is constructing approximating expressions for the failure probability that can be used in conjunction with optimization algorithms. Two approaches for such approximations are described as follows.

2.9.4.1 Sample Average Approximation

A sample average approximation method is constructed by replacing the failure probabilities in the original RBDO problem with Monte Carlo sampling estimates. The results associated with such approximations give asymptotic properties of minimizes of

sample average approximation problems as the number of samples goes to infinity, and give error estimates for finite sample sizes.

Royset and Polak (2004) described the RBDO problem with component failure probabilities as

$$
\begin{aligned}
&\min_{\boldsymbol{x} \subseteq \mathbb{R}^N} \; c_0(\boldsymbol{x}) + \sum_{k=1}^{K} c_k(\boldsymbol{x}) p_k(\boldsymbol{x}) \\
&\text{subject to } p_k(\boldsymbol{x}) \le \hat{p}_k, \; k = 1, \cdots, K, \\
&\qquad\qquad f_j(\boldsymbol{x}) \le 0, \; j = 1, \cdots, J
\end{aligned}
\tag{2.160}
$$

where $f_j(\boldsymbol{x})$ is the jth deterministic continuously differentiable, constraint function; $c_k(\boldsymbol{x}), k = 1, \cdots K$ is the continuously differentiable cost function associated with the failure of the kth component; $\hat{p}_k$ is the pre-defined bound for the kth component failure probability and $c_0(\boldsymbol{x})$ is the initial cost function. The difficulty associated with solving (2.160) is that the failure probabilities cannot be computed exactly and hence has to be approximated. In addition, expressions, if they exist, are difficult to obtain for the gradients of the failure probabilities and their approximations. Due to this reason, a direct application of the standard optimization algorithm is impossible.

Royset and Polak (2004) gave approximations of the integrals for probability of failure and its gradient by using sampling techniques. To improve efficiency, they prefer importance sampling rather than original direct Monte Carlo simulation. Through these estimates, combined with the Polak-He algorithm (2004), a new algorithm was proposed and proved to converge with a sample size that tends to infinity.

<u>2.9.4.2 Response Surface Approximation</u>

Simulation-based methods are easy to implement into a reliability analysis. However, these methods also produce noisy responses that make them difficult to use in gradient-based optimization algorithms. Response surface approximations can help solve two problems of simulation-based methods: simulation cost and the noise from random sampling. To solve RBDO of composite laminates in cryogenic environments, Qu and Haftka (2001, 2003) proposed a method based on response surface approximations. Two types of response surfaces need to be created. The first type is analysis response surface (ARS), which is fitted to the performance response in terms of both design variables and random variables. When ARS is used, the probability of failure at each design point can be calculated efficiently. The second type is design response surface (DRS), which is fitted to probability of failure as a function of design variables. The DRS is created to filter out noise generated by simulation-based methods and is used to calculate the reliability constraint in the design optimization procedure.

2.9.5 Others

Xu and Rahman (2004) recently proposed new decomposition methods to solve RBDO problems. The application involves lower-dimensional approximations of general multi-variate functions, response surface approximations, and Monte Carlo simulation. Since the probability of failure is estimated from the mean point based decomposition approximation of failure surface, there is no need for an inner optimization loop of the reliability assessment. The new method does not depend on FORM/SORM to conduct

reliability analysis, and it requires only a small number of function evaluations. Numerical examples show the proposed method is both accurate and efficient. The cost for function evaluations in the proposed method can be predetermined, while other optimization methods cannot predict the cost for optimization procedure.

Recently, Zou and Mahadevan (2006) proposed a new decoupling approach, for decoupling the optimization and reliability analysis iterations in traditional nested formulations. The reliability constraints are approximated by first-order Taylor series expansion based on reliability analysis results, so that the outer loop only performs deterministic optimization. The advantage of this method is that any reliability methods can be employed in inner loop for reliability analysis. The computational efficiency depends on the reliability method used and accuracy of the approximation for reliability constraints.

2.10 Summary of Review and Future Research Needs

2.10.1 Conclusions from Existing Research

Accuracy and efficiency are the two major concerns in existing structural reliability and probabilistic design research. In practical applications, the number of design/random variables is large, the limit state/constraint function could be highly nonlinear, and local minimums in optimal design could exist, in addition to other possible complications. The following provides a summary of review of existing methods for both reliability analysis and reliability-based design optimization.

<u>Reliability Analysis</u>

(1) Mean-Value methods are desirable for computational efficiency and usually used to predict the CDF of the response. Since original MV methods are first/second order Taylor expansions of the performance function at the mean point, they can only solve linear or slightly nonlinear problems. Although AMV compensates for the expansion truncation error by using a correction term, the difference between the approximate MPP and exact MPP can be enormous. Because AMV+ uses Taylor expansion based on an exact MPP, reliability estimation can be much improved. However, since AMV+ is a second order estimation, it cannot produce acceptable solutions in highly nonlinear problems.

(2) Classical FORM/SORM methods are widely used in reliability calculations. The advantage of FORM is computational efficiency and the information provided by MPP. For most reliability problems, SORM can improve FORM by providing curvature information around the MPP, which increases the computational effort needed to calculate the second derivatives of performance function with respect to random variables. For highly nonlinear problems, the linear/quadratic approximation in FORM/SORM can cause errors in the estimation of probability. For example, if the MPP is an inflection point, or if the failure surface around the MPP is very flat, then FORM/SORM can lead to a very large error in probability calculation. HORM was proposed to improve point-fitted SORM and approximates the highly nonlinear surface by using so-called two point adaptive nonlinear approximation. This method can solve simple, highly nonlinear problems. However, for practical applications,

when the number of random variables is large and response calculation is time consuming, the computational efficiency of HORM is low, and may not be useful for solving industrial-scale structural reliability problems.

(3) Simulation methods are applied when no feasible analytical solution is possible, or when some approximate methods need to be verified. Direct Monte Carlo simulation generally requires a large number of simulations to calculate small probability, and is impractical when each simulation involves expensive finite-element, boundary-element, or mesh-free calculations. As a result, researchers have developed or examined faster simulation methods (see section 2.5). The most difficulty of these sampling methods is, they need to determine the most probable failure region, or chose an appropriate PDF in advance, depending on the failure region. Hence, simulation methods are useful when alternative methods are inapplicable or inaccurate, and have been traditionally employed as a benchmark for evaluating approximate methods.

(4) For most practical applications, the performance/response is usually implicit. Such a deterministic prediction can be very time consuming (e.g., large-scale finite element analysis), and prevents the implementation of simulation methods. The response surface method provides an approximation of performance/response by using fitted polynomials. Then, based on explicit functions, a broad range of analytical methods/simulation methods can be used efficiently. Since most response surface methods are second order, they may not be adequate for highly nonlinear problems; the model's accuracy cannot be adequately assessed and controlled outside selected

data regions. The required number of original model evaluations increasing dramatically for those response surface methods with full cross terms in the case of a large number of random variables.

(5) The major advantage of mean-point-based decomposition methods over FORM/SORM is that higher order approximations of a performance function can be achieved without calculating the MPP or gradients. Thus, these methods can solve highly nonlinear reliability problems more accurately and/or more efficiently. However, for a certain class of reliability problems these methods may require computationally demanding higher-variate (bivariate, trivariate, etc.) decomposition to adequately represent performance function, which will add computational effort significantly.

Reliability-based Design Optimization

(6) Solving RBDO with the double-loop approach is expensive because of the inherent computational expense required for a reliability analysis in the inner loop. For a large-scale multidisciplinary system with a large number of random/design variables and failure modes, this method is not practical due to high computational costs. Although the decoupled method (e.g. sequential optimization reliability assessment) and the single-loop approach with the KKT condition improve the computational efficiency, these methods may not yield required accuracy and convergence. If the reliability problem is highly nonlinear or multiple MPPs exist, then FORM-based RBDO methods may obtain an undesirable probabilistic optimal design.

(7) Simulation-based RBDO approaches yield better accuracy than FORM-based RBDO approaches. However, the huge computational cost of sampling only makes them applicable to simple problems. Additionally, the optimization algorithm associated with the outer loop may face difficulty in searching the optimum, due to the sampling errors of derivatives of probabilistic constraints. Even though response surface approximation of the derivatives may overcome some of these difficulties generated from sampling, another source of approximation is involved.

(8) The existing mean-point-based decomposition methods introduced recently in RBDO can improve both efficiency and accuracy for highly nonlinear problems. The cost of function evaluations in the proposed method can be predetermined, while most existing optimization methods cannot predict the cost of the optimization procedure apriori. Based on the same comment associated with the reliability analysis for the mean-point-based decomposition method, a higher-variate approximation, if required, may increase the computational costs of RBDO significantly.

2.10.2 Need for Fundamental Research

Based on the review described in the preceding sections, the following fundamental research should be pursued:

(1) The decomposition methods for reliability analysis depend on the selected reference or expansion point. It is elementary to show that an improper or careless selection of the reference point can spoil the approximation. Past work indicates that the mean point of random input is a good candidate for defining the reference point. However,

for certain class of reliability problems, existing mean-point-based decomposition methods may require computationally demanding bivariate or trivariate decompositions to adequately represent performance functions. Hence, developing univariate methods, capable of producing computationally efficient, yet sufficiently adequate performance functions, is a major motivation of the current work. The present work is motivated by the argument that using MPP as the reference point may provide an improved function approximation, however, with the additional expense of identifying the MPP.

(2) The mean point- or MPP-based decomposition methods involve further layers of approximations, due to both response-surface generation of univariate or bivariate component functions and Monte Carlo simulation. However, the MPP-based univariate decomposition, if appropriately cast in the rotated Gaussian space, permits an efficient evaluation of the failure probability by closed-form solutions. In other words, it is possible to perform a general failure probability analysis, which represents a multi-dimensional integration over an arbitrary region, by multiple one-dimensional integrations. Therefore, developing closed-form solutions of reliability without relying on response surface generation or Monte Carlo simulation is proposed.

(3) The existence of multiple MPPs in reliability analysis can result in large errors by currently available methods. Even if all MPPs can be identified, the high nonlinearity around some or all MPPs may lead to inadequate accuracy or unacceptable efficiency by using existing multi-point FORM/SORM. Therefore, developing a univariate

decomposition method that can handle multiple MPPs and yield superior accuracy or computational efficiency than existing methods is highly desirable. The proposed research will extend the MPP-based univariate method for solving multiple MPP problems.

(4) A major by-product of formulating closed-form solutions for determining failure probability by MPP-based univariate decomposition method is the likelihood of developing analytical sensitivities of reliability with respect to design variables. Such sensitivities are useful for subsequent reliability-based design optimization and should be developed.

(5) The ultimate goal of a reliability analysis is design optimization of mechanical and structural systems in the presence of uncertainties. If the results of both reliability and sensitivity are accurate and/or computationally efficient, the associated reliability-based design optimization will also be effective. Therefore, the final goal of the proposed research is to develop a new RBDO methodology employing the MPP-based univariate decomposition method.
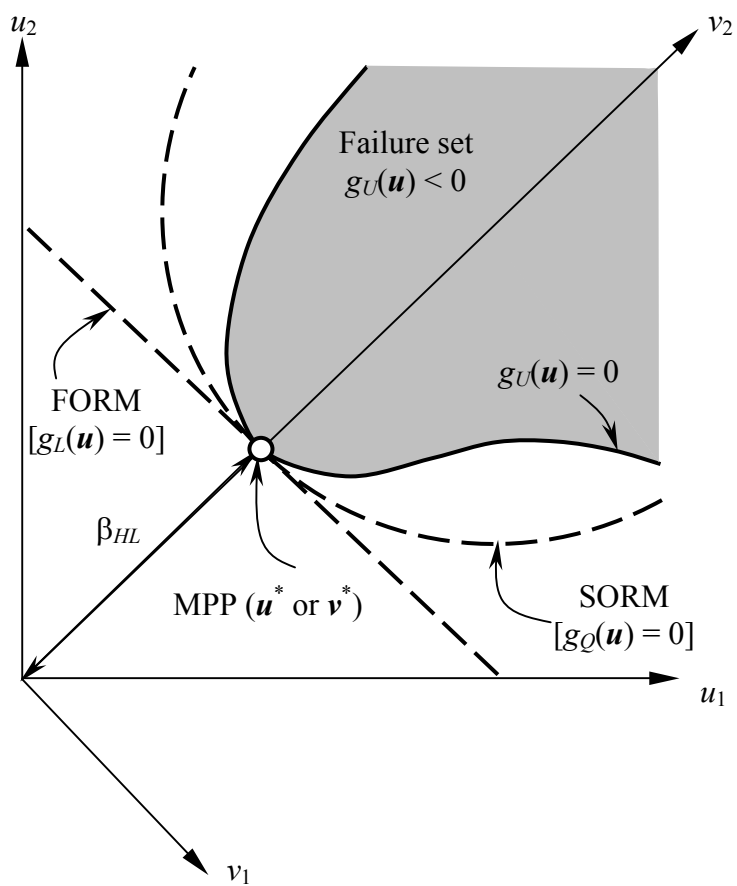
Figure 2.1 MPP at the 2D standard normal space

```
        ┌─────────────────────────┐
        │      Search for MPP      │
        └─────────────────────────┘
                    │
                    ▼
        ┌─────────────────────────┐
        │ Coordinates Transformation │
        │          Y = RU          │
        └─────────────────────────┘
                    │
                    ▼
      ┌──────────────────────────────┐
      │ Select two additional points, and │
      │ construct an adaptive approximation │
      └──────────────────────────────┘
                    │
                    ▼
```

Construct
$$\tilde{y}_n = \beta + \sum_{i=1}^{n-1} a_i y_i^m$$

Estimate of failure probability by Gauss Hermite integral

| m- even a_i- poistive | m- even a_i-negative | m- even a_i-postive & negative | m- odd a_i-all postive or all negative | m- odd a_i-postive & negative |
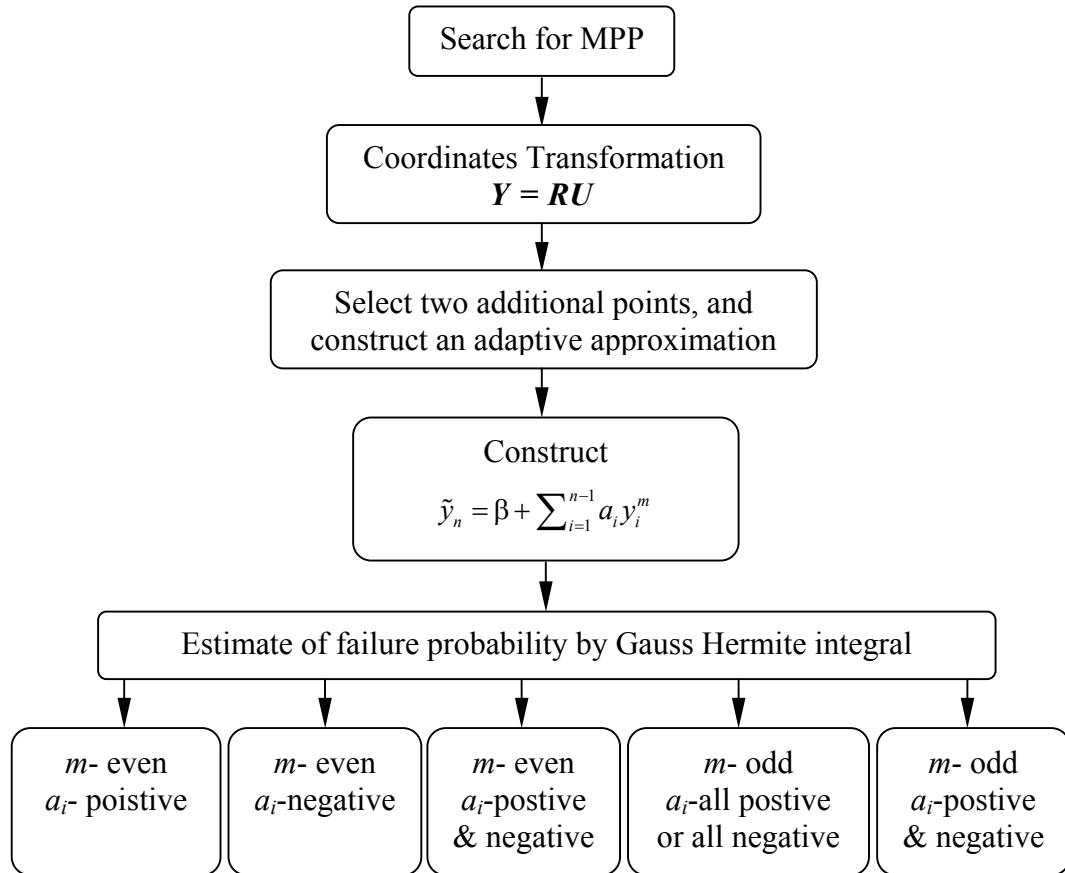
Figure 2.2 Schematic flowchart for HORM

2 MPPs

4 MPPs

1 MPP, but 2 important regions

Infinite MPPs
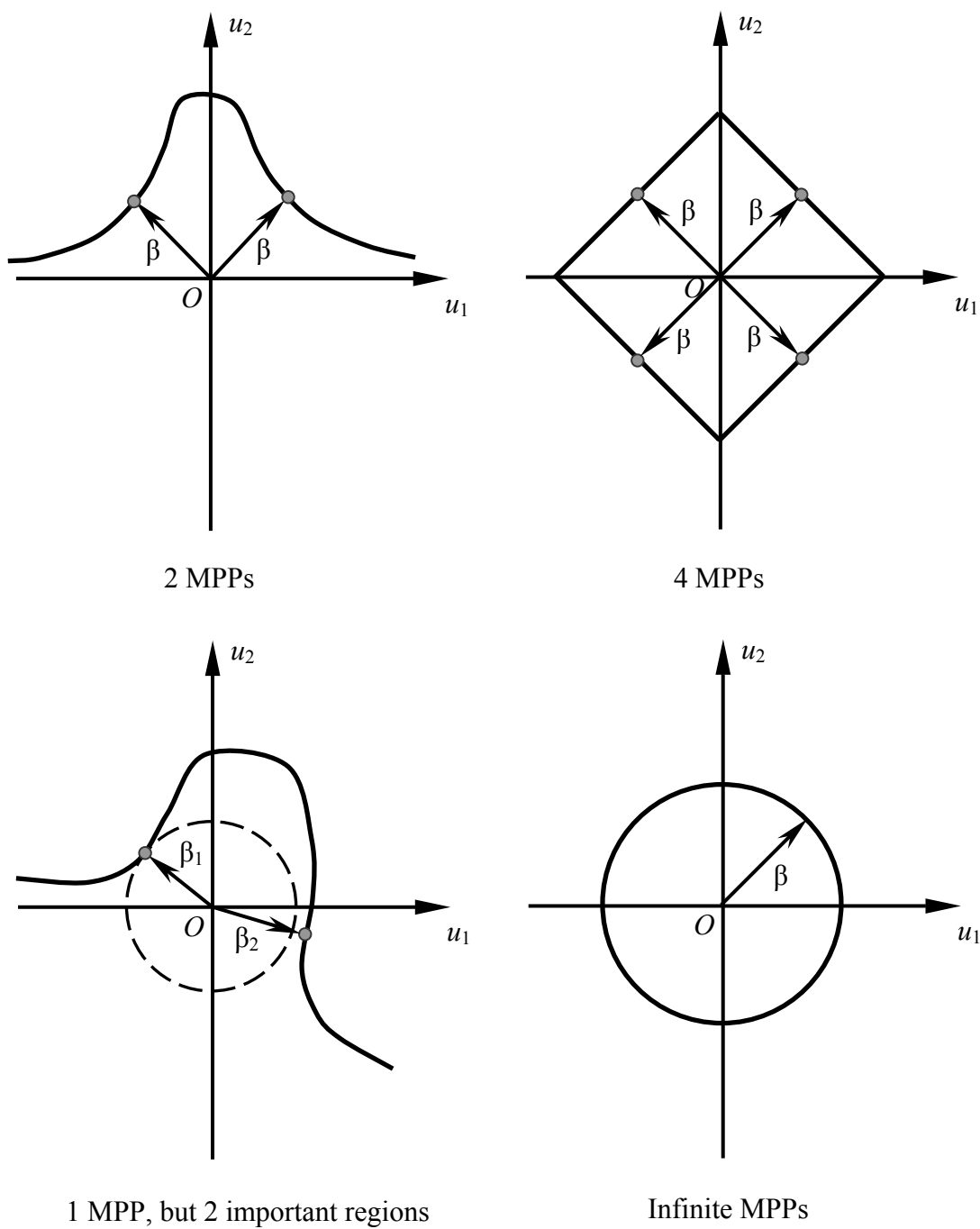
Figure 2.3 Multiple MPPs

CHAPTER 3

MPP-BASED UNIVARIATE METHOD WITH SIMULATION

3.1 Multivariate Function Decomposition at MPP

Consider a continuous, differentiable, real-valued performance function $g(\boldsymbol{x})$ that depends on $\boldsymbol{x} = \{x_1, \cdots, x_N\}^T \in \mathbb{R}^N$. If $\boldsymbol{u} = \{u_1, \cdots, u_N\}^T \in \mathbb{R}^N$ is the standard Gaussian space, let $\boldsymbol{u}^* = \left\{u_1^*, \cdots, u_N^*\right\}^T$ denote the MPP or beta point, which is the closest point on the limit-state surface to the origin. The MPP has a distance β_{HL}, which is commonly referred to as the Hasofer-Lind reliability index (Madsen et al., 1986), is determined by a standard nonlinear constrained optimization. Construct an orthogonal matrix $\boldsymbol{R} \in \mathbb{R}^{N \times N}$ whose Nth column is $\boldsymbol{\alpha}^* \equiv \boldsymbol{u}^*/\beta_{HL}$, i.e., $\boldsymbol{R} = \left[\boldsymbol{R}_1 \middle| \boldsymbol{\alpha}^*\right]$, where $\boldsymbol{R}_1 \in \mathbb{R}^{N \times N-1}$ satisfies $\boldsymbol{\alpha}^{*T}\boldsymbol{R}_1 = \boldsymbol{0} \in \mathbb{R}^{1 \times N-1}$. The matrix $\boldsymbol{R}$ can be obtained, for example, by Gram-Schmidt orthogonalization. For a orthogonal transformation $\boldsymbol{u} = \boldsymbol{R}\boldsymbol{v}$, let $\boldsymbol{v} = \{v_1, \cdots, v_N\}^T \in \mathbb{R}^N$ represent the rotated Gaussian space with the associated MPP $\boldsymbol{v}^* = \left\{v_1^*, \cdots, v_{N-1}^*, v_N^*\right\}^T = \left\{0, \cdots, 0, \beta_{HL}\right\}^T$. The transformed limit states $h(\boldsymbol{u}) = 0$ and $y(\boldsymbol{v}) = 0$ are therefore the maps of the original limit state $g(\boldsymbol{x}) = 0$ in the standard Gaussian space ($\boldsymbol{u}$ space) and the rotated Gaussian space ($\boldsymbol{v}$ space), respectively. Figure 3.1 depicts FORM and SORM approximations of a limit-state surface at MPP for $N = 2$.

Suppose that $y(\boldsymbol{v})$ has a convergent Taylor series expansion at MPP $\boldsymbol{v}^* = \left\{v_1^*, \cdots, v_N^*\right\}^T$ and can be expressed by

$$y(\boldsymbol{v}) = y\left(\boldsymbol{v}^*\right) + \sum_{j=1}^{\infty} \frac{1}{j!} \sum_{i=1}^{N} \frac{\partial^j y}{\partial v_i^{\ j}}\left(\boldsymbol{v}^*\right)\left(v_i - v_i^{\ *}\right)^j + \mathcal{R}_2 \qquad (3.1)$$

or

$$\begin{aligned}
y(\boldsymbol{v}) &= y\left(\boldsymbol{v}^*\right) + \sum_{j=1}^{\infty} \frac{1}{j!} \sum_{i=1}^{N} \frac{\partial^j y}{\partial v_i^{\ j}}\left(\boldsymbol{v}^*\right)\left(v_i - v_i^{\ *}\right)^j \\
&+ \sum_{j_1, j_2 > 0}^{\infty} \frac{1}{j_1! j_2!} \sum_{i_1 < i_2} \frac{\partial^{j_1 + j_2} y}{\partial v_{i_1}^{\ j_1} \partial v_{i_2}^{\ j_2}}\left(\boldsymbol{v}^*\right)\left(v_{i_1} - v_{i_1}^{\ *}\right)^{j_1}\left(v_{i_2} - v_{i_2}^{\ *}\right)^{j_2} + \mathcal{R}_3
\end{aligned}, \qquad (3.2)$$

where the remainder $\mathcal{R}_2$ denotes all terms with dimension two and higher and the remainder $\mathcal{R}_3$ denotes all terms with dimension three and higher.

3.1.1 Univariate Approximation

Consider a univariate approximation of $y(\boldsymbol{v})$, denoted by

$$\hat{y}_1(\boldsymbol{v}) \equiv \hat{y}_1(v_1, \cdots, v_N) = \sum_{i=1}^{N} y(v_1^{\ *}, \cdots, v_{i-1}^{\ *}, v_i, v_{i+1}^{\ *}, \cdots, v_N^{\ *}) - (N-1)y(\boldsymbol{v}^*), \quad (3.3)$$

where each term in the summation is a function of only one variable and can be subsequently expanded in a Taylor series at $\boldsymbol{v} = \boldsymbol{v}^*$, yielding

$$\hat{y}_1(\boldsymbol{v}) = y(\boldsymbol{v}^*) + \sum_{j=1}^{\infty} \frac{1}{j!} \sum_{i=1}^{N} \frac{\partial^j y}{\partial x_i^{\ j}}\left(\boldsymbol{v}^*\right)(v_i - v_i^{\ *})^j . \qquad (3.4)$$

Comparison of Equations (3.1) and (3.4) indicates that the univariate approximation leads to the residual error $y(\boldsymbol{v}) - \hat{y}_1(\boldsymbol{v}) = \mathcal{R}_2$, which includes contributions from terms of dimension two and higher. For sufficiently smooth $y(\boldsymbol{v})$ with convergent Taylor series, the coefficients associated with higher-dimensional terms are usually much smaller than that with one-dimensional terms. As such, higher-dimensional terms contribute less to the function, and therefore, can be neglected. Nevertheless, Equation (3.4) includes all

higher-order univariate terms, as compared with FORM and SORM, which only retain linear and quadratic terms, respectively. Hence, $\hat{y}_1(\boldsymbol{v})$ yields more accurate representation of $y(\boldsymbol{v})$ than FORM/SORM. Furthermore, Equation (3.4) represents exactly the same function as $y(\boldsymbol{v})$ when $y(\boldsymbol{v}) = \sum y_i(v_i)$, *i.e.*, when $y(\boldsymbol{v})$ can be additively decomposed into functions $y_i(v_i)$ of single variables.

3.1.2 Bivariate Approximation

In a similar manner, consider a bivariate approximation

$$
\begin{aligned}
\hat{y}_2(\boldsymbol{v}) = &\sum_{i_1 < i_2} y\left(v_1^*, \cdots, v_{i_1-1}^*, v_{i_1}, v_{i_1+1}^*, \cdots, v_{i_2-1}^*, v_{i_2}, v_{i_2+1}^*, \cdots, v_N^*\right) \\
&-(N-2)\sum_{i=1}^{N} y\left(v_1^*, \cdots, v_{i-1}^*, v_i, v_{i+1}^*, \cdots, v_N^*\right) + \frac{(N-1)(N-2)}{2} y\left(\boldsymbol{v}^*\right)
\end{aligned}
\tag{3.5}
$$

of $y(\boldsymbol{v})$, where each term on the right hand side is a function of at most two variables and can be expanded in a Taylor series at $\boldsymbol{v} = \boldsymbol{v}^*$, yielding

$$
\hat{y}_2(\boldsymbol{v}) = y\left(\boldsymbol{v}^*\right) + \sum_{j=1}^{\infty} \frac{1}{j!} \sum_{i=1}^{N} \frac{\partial^j y}{\partial v_i^{\,j}}\left(\boldsymbol{v}^*\right)(v_i - v_i^*)^j + \sum_{j_1, j_2 > 0}^{\infty} \frac{1}{j_1! j_2!} \sum_{i_1 < i_2} \frac{\partial^{j_1+j_2} y}{\partial v_{i_1}^{\,j_1} \partial v_{i_2}^{\,j_2}}\left(\boldsymbol{v}^*\right)\left(v_{i_1} - v_{i_1}^*\right)^{j_1}\left(v_{i_2} - v_{i_2}^*\right)^{j_2}.
$$

(3.6)

Again, the comparison of Equations (3.2) and (3.6) indicates that the bivariate approximation leads to the residual error $y(\boldsymbol{v}) - \hat{y}_2(\boldsymbol{v}) = \mathcal{R}_3$, in which the remainder $\mathcal{R}_3$ includes terms of dimension three and higher. The bivariate approximation includes all terms with no more than two variables, thus yielding higher accuracy than the univariate approximation. Furthermore, Equation (3.6) exactly represents $y(\boldsymbol{v}) = \sum \sum y_{ij}(v_i, v_j)$,

i.e., when $y(\boldsymbol{v})$ can be additively decomposed into functions $y_{ij}(v_i, v_j)$ of at most two variables.

3.1.3 Generalized *S*-variate Approximation

The procedure for univariate and bivariate approximations described in the preceding can be generalized to an *S*-variate approximation for any integer $1 \leq S \leq N$. The generalized *S*-variate approximation of $y(\boldsymbol{v})$ is

$$\hat{y}_S(\boldsymbol{v}) \equiv \sum_{i=0}^{S} (-1)^i \binom{N-S+i-1}{i} \sum_{k_1 < \cdots < k_{S-i}} y(v_1^*, \cdots, v_{k_1-1}^*, v_{k_1}, v_{k_1+1}^*, \cdots, v_{k_{S-i}-1}^*, v_{k_{S-i}}, v_{k_{S-i}+1}^*, \cdots, v_N^*).$$

(3.7)

If $\quad y_R \equiv y(v_1^*, \cdots, v_{k_1-1}^*, v_{k_1}, v_{k_1+1}^*, \cdots, v_{k_R-1}^*, v_{k_R}, v_{k_R+1}^*, \cdots, v_N^*); \ 0 \leq R \leq S$, a

multivariate function decomposition theorem, developed by the first author's group, leads to (Xu and Rahman, 2004)

$$y_R = \sum_{k=0}^{R} \binom{N-k}{R-k} t_k; \ 0 \leq R \leq S \ , \tag{3.8}$$

where

$$
\begin{aligned}
t_0 &= y(\boldsymbol{v}^*) \\
t_1 &= \sum_{j_1} \frac{1}{j_1!} \sum_{i_1=1}^{N} \frac{\partial^{j_1} y}{\partial v_{i_1}^{j_1}} (\boldsymbol{v}^*) (v_{i_1} - v_{i_1}^*)^{j_1} \\
t_2 &= \sum_{j_1, j_2} \frac{1}{j_1! j_2!} \sum_{i_1 < i_2} \frac{\partial^{j_1+j_2} y}{\partial v_{i_1}^{j_1} \partial v_{i_2}^{j_2}} (\boldsymbol{v}^*) (v_{i_1} - v_{i_1}^*)^{j_1} (v_{i_2} - v_{i_2}^*)^{j_2} \\
&\vdots \quad \vdots \quad \vdots \\
t_S &= \sum_{j_1, \cdots, j_S} \frac{1}{j_1! \cdots j_S!} \sum_{i_1 < \cdots < i_S} \frac{\partial^{j_1+\cdots+j_S} y}{\partial v_{i_1}^{j_1} \cdots \partial v_{i_S}^{j_S}} (\boldsymbol{v}^*) (v_{i_1} - v_{i_1}^*)^{j_1} \cdots (v_{i_S} - v_{i_S}^*)^{j_S}
\end{aligned}
$$
. (3.9)

Using Equations (3.8) and (3.9), it can be shown that $\hat{y}_S(\mathbf{v})$ in Equation (3.7) consists of all terms of the Taylor series of $y(\mathbf{v})$ that have less than or equal to S variables (Xu and Rahman, 2004). The expanded form of Equation (3.7), when compared with the Taylor expansion of $y(\mathbf{v})$, indicates that the residual error in the S-variate approximation is $y(\mathbf{v}) - \hat{y}_S(\mathbf{v}) = \mathcal{R}_{S+1}$, where the remainder $\mathcal{R}_{S+1}$ includes terms of dimension $S+1$ and higher. When $S = 1$, Equation (3.7) degenerates to the univariate approximation (Equation (3.3)). When $S = 2$, Equation (3.7) becomes the bivariate approximation (Equation (3.5)). Similarly, trivariate, quadrivariate, and other higher-variate approximations can be derived by appropriately selecting the value of S. In the limit, when $S = N$, Equation (3.7) converges to the exact function $y(\mathbf{v})$. In other words, the decomposition technique generates a convergent sequence of approximations of $y(\mathbf{v})$.

3.1.4 Remarks

The decomposition of a general multivariate function $y(\mathbf{v})$ can be viewed as a finite sum

$$y(\mathbf{v}) = \underbrace{\underbrace{y_0 + \sum_{i=1}^{N} y_i(v_i)}_{=\hat{y}_1(\mathbf{v})} + \sum_{\substack{i_1,i_2=1 \\ i_1<i_2}}^{N} y_{i_1 i_2}(v_{i_1}, v_{i_2}) + \cdots + \sum_{\substack{i_1,\cdots,i_S=1 \\ i_1<\cdots<i_S}}^{N} y_{i_1\cdots i_S}(v_{i_1},\cdots,v_{i_s})}_{=\hat{y}_S(\mathbf{v})} + \cdots + y_{12\cdots N}(v_1,\cdots,v_N) \ ,$$

$$\tag{3.10}$$

where y_0 is a constant, $y_i(v_i)$ is a univariate component function representing independent contribution to $y(\mathbf{v})$ by input variable v_i acting alone, $y_{i_1 i_2}(v_{i_1}, v_{i_2})$ is a bivariate component function describing cooperative influence of two input variables v_{i_1} and v_{i_2}, $y_{i_1 \cdots i_S}(v_{i_1}, \cdots, v_{i_S})$ is an S-variate component function quantifying cooperative effects of S input variables $v_{i_1}, \cdots, v_{i_S}$, and so on. By comparing Equations (3.3) and (3.5) with Equation (3.10), the univariate and bivariate approximations provide two- and three-term approximants, respectively, of the finite decomposition. In general, the S-variate approximation in Equation (3.7) yields the S+1-term approximant of the decomposition. The fundamental conjecture underlying this work is that component functions arising in the proposed decomposition will exhibit insignificant higher-dimensional effects cooperatively.

It is worth noting that the univariate approximation in Equation (3.3) should not viewed as first- or second-order Taylor series expansions nor does it limit the nonlinearity of $y(\mathbf{v})$. According to Equation (3.4), *all* higher-order univariate terms of $y(\mathbf{v})$ are included in the proposed approximation. In fact, the univariate component function $y_i(v_i)$ can be highly nonlinear and therefore should provide in general higher-order representation of a performance function than those by FORM or SORM. Furthermore, the approximations contain contributions from *all* input variables.

Finally, the decomposition presented here depends on the selected reference point. It is elementary to show that an improper or careless selection of the reference point can spoil the approximation. The authors' past work indicates that the mean point of random

input is a good candidate for defining the reference point (Xu and Rahman, 2005). This present work is motivated by the argument that using MPP as the reference point may provide an improved function approximation, however, with the additional expense of identifying the MPP.

3.2 Response Surface Generation

Consider the univariate component function $y_i(v_i) \equiv y(v_1^*, \cdots, v_{i-1}^*, v_i, v_{i+1}^*, \cdots, v_N^*)$ in Equation (3.4). If for $v_i = v_i^{(j)}$, n function values

$$y_i(v_i^{(j)}) = y(v_1^*, \cdots, v_{i-1}^*, v_i^{(j)}, v_{i+1}^*, \cdots, v_N^*); j = 1, 2, \cdots, n \qquad (3.11)$$

are given, the function value for arbitrary v_i can be obtained using the Lagrange interpolation as

$$y_i(v_i) = \sum_{j=1}^{n} \phi_j(v_i) y_i(v_i^{(j)}), \qquad (3.12)$$

where the shape function $\phi_j(v_i)$ is defined as

$$\phi_j(v_i) = \frac{\prod_{k=1, k \neq j}^{n} \left(v_i - v_i^{(k)} \right)}{\prod_{k=1, k \neq j}^{n} \left(v_i^{(j)} - v_i^{(k)} \right)}. \qquad (3.13)$$

By using Equations (3.13) and (3.14), arbitrarily many values of $y_i(v_i)$ can be generated if n values of that component function are given. The same procedure is repeated for all univariate component functions, *i.e.*, for all $y_i(v_i)$, $i = 1, \cdots, N$. Therefore, the total cost

for the univariate approximation in Equation (3.4), in addition to that required for locating MPP, entails a *maximum* of $nN + 1$ function evaluations.

More accurate bivariate or multivariate approximations (*e.g*., Equations (3.6) or (3.8)) can be developed in a similar way. However, because of much higher cost of multivariate approximations, only the univariate approximation will be examined in this paper.

3.3 Monte Carlo Simulation

For component reliability analysis, the Monte Carlo estimate $P_{F,1}$ of the failure probability employing the proposed univariate approximation is

$$P_{F,1} = \frac{1}{N_S} \sum_{i=1}^{N_S} \mathcal{I}\left[\hat{y}_1\left(\boldsymbol{v}^{(i)}\right) < 0 \right], \tag{3.14}$$

where $\boldsymbol{v}^{(i)}$ is the *i*th realization of $\boldsymbol{V}$, N_S is the sample size, and $\mathcal{I}[\cdot]$ is an indicator function such that $\mathcal{I} = 1$ if $\boldsymbol{v}^{(i)}$ is in the failure set (*i.e.*, when $\hat{y}_1(\boldsymbol{v}^{(i)}) < 0$) and *zero* otherwise. Similar failure probability estimates can be developed using higher-variate models if required. In addition, similar approximations can be employed for system reliability analysis (Xu and Rahman, 2005).

The decomposition method involving univariate approximation (Equation (3.4)), *n*-point Lagrange interpolation (Equations (3.13) and (3.14)), and Monte Carlo simulation (Equation (3.15)) is defined as the *MPP-based univariate method* in this chapter. Since the univariate method leads to explicit response-surface approximation of a performance function, the embedded Monte Carlo simulation can be conducted for any sample size.

However, the accuracy and efficiency of the resultant failure-probability calculation depend on both the univariate and response surface approximations. They will be evaluated using several numerical examples, as follows.

3.4 Numerical Examples

Four numerical examples involving explicit functions from mathematical or solid-mechanics problems (Examples 1 and 2) and implicit functions from structural or solid-mechanics problems (Examples 3 and 4), are presented to illustrate the MPP-based univariate response-surface method developed. Whenever possible, comparisons have been made with existing mean-point-based univariate response-surface method, FORM/SORM, and simulation methods to evaluate the accuracy and computational efficiency of the proposed method. For the MPP-based univariate response-surface method, n (= 3, 5, or 7) uniformly distributed points $v_i^* - (n-1)/2, v_i^* - (n-3)/2, \cdots, v_i^*, \cdots, v_i^* + (n-3)/2, v_i^* + (n-1)/2$ were deployed at v_i-coordinate, leading to $(n-1)N$ function evaluations in addition to those required for locating the MPP.

When comparing computational efforts by various methods, the number of original performance function evaluations is chosen as the primary metric in this paper. For the direct Monte Carlo simulation, the number of original function evaluations is the same as the sample size. However, in univariate response-surface methods, they are different, because the Monte Carlo simulation (although with same sample size as in direct Monte Carlo simulation) embedded in the proposed method is conducted using

their response surface approximations. The difference in CPU times in evaluating an original function and its response surface approximation is significant when a calculation of the original function involves expensive finite-element analysis, as in Examples 3 and 4. However, the difference becomes trivial when analyzing explicit performance functions, as in Examples 1 and 2. Hence, the computational effort expressed in terms of function evaluations alone should be carefully interpreted for explicit performance functions. Nevertheless, the number of function evaluations provides an objective measure of the computational effort for reliability analysis of realistic problems.

3.4.1 Example Set I – Mathematical Functions (Example 1)

Consider a cubic and a quartic performance functions (Grandhi and Wang, 1999), expressed respectively by

$$g(X_1, X_2) = 2.2257 - \frac{0.025\sqrt{2}}{27}(X_1 + X_2 - 20)^3 + \frac{33}{140}(X_1 - X_2) \quad (3.15)$$

and

$$g(X_1, X_2) = \frac{5}{2} + \frac{1}{216}(X_1 + X_2 - 20)^4 - \frac{33}{140}(X_1 - X_2), \quad (3.16)$$

where $X_i \mapsto N(10,3)$, $i = 1,2$ are independent, Gaussian random variables, each with mean $\mu = 10$ and standard deviation $\sigma = 3$. From an MPP search, $v^* = \{0, 2.2257\}^T$ and $\beta_{HL} = \|v^*\| = 2.2257$ for the cubic function and $v^* = \{0, 2.5\}^T$ and $\beta_{HL} = \|v^*\| = 2.5$ for the quartic function, as shown in Figures 3.2(a) and 3.2(b), respectively. In addition, Figures 3.2(a) and 3.2(b) plot exact limit-state surfaces and their various approximations by FORM/SORM (Breitung, 1984; Hohenbichler et al., 1987; Cai and Elishakoff, 1994),

mean-point-based univariate response-surface method (Xu and Rahman, 2005), and proposed MPP-based univariate response-surface method. For univariate response-surface methods, a value of $n = 5$ was selected, resulting 9 function evaluations. According to Figures 3.2(a) and 3.2(b), the MPP-based univariate response-surface method yields exact limit-state equations, since both performance functions considered are univariate functions and at most consist of fourth-order polynomial in the rotated Gaussian space. For the cubic function, the limit-state equation by mean-point based univariate method matches the exact equation only at MPP. However, for the quartic function, the mean-point-based limit-state equation is non-negative, leading to a null failure set. FORM and SORM yield grossly inaccurate representation of both limit-state equations, due to zero (inflection point of the cubic function) or very small (highly nonlinearity of the quartic function) curvatures at MPP.

Tables 3.1 and 3.2 show the results of the failure probability calculated by FORM, SORM due to Breitung (1984), Hohenbichler (1987), and Cai and Elishakoff (1994), mean-point-based univariate response-surface method (Xu and Rahman, 2005), proposed MPP-based univariate response-surface method, and direct Monte Carlo simulation using 10^6 samples. The MPP-based univariate response-surface method predicts exact probability of failure. The univariate response-surface method using mean point, which yields poor approximations of performance functions [see Figures 3.2(a) and 3.2(b)], underpredicts (cubic function) or fails (quartic function) to provide a solution. Other commonly used reliability methods, such as FORM and SORM, underpredict failure probability by 31 percent and overpredict failure probability by 117 percent when

compared with direct Monte Carlo results. The SORM results are the same as the FORM results, indicating that there is no improvement over FORM for problems involving inflection points or high nonlinearity.

3.4.2 Example Set II – Solid Mechanics Problems

3.4.2.1 Example 2 – Burst Margin of a Rotating Disk

Consider an annular disk of inner radius R_i, outer radius R_o, and constant thickness $t \ll R_o$ (plane stress), as shown in Figure 3.3. The disk is subject to an angular velocity ω about an axis perpendicular to its plane at the center. The maximum allowable angular velocity ω_a when tangential stresses through the thickness reach the material ultimate strength S_u factored by a material utilization factor α_m is (Boresi and Schmidt, 2003)

$$\omega_a = \left[\frac{3\alpha_m S_u \left(R_o - R_i \right)}{\rho \left(R_o^{\,3} - R_i^{\,3} \right)} \right]^{1/2}, \tag{3.17}$$

where ρ is the mass density of the material. According to an SAE G-11 standard, the satisfactory performance of the disk is defined when the burst margin M_b, defined as

$$M_b \equiv \frac{\omega_a}{\omega} = \left[\frac{3\alpha_m S_u \left(R_o - R_i \right)}{\rho \omega^2 \left(R_o^{\,3} - R_i^{\,3} \right)} \right]^{1/2}, \tag{3.18}$$

exceeds a critical threshold of 0.37473 (Penmetsa and Grandhi, 2003). If random variables $X_1 = \alpha_m$, $X_2 = S_u$, $X_3 = \omega$, $X_4 = \rho$, $X_5 = R_o$, and $X_6 = R_i$, and have their statistical properties defined in Table 3.3, the performance function becomes

$$g(X) = M_b(X_1, X_2, X_3, X_4, X_5, X_6) - 0.37473., \tag{3.19}$$

Table 3.4 presents predicted failure probability of the disk and associated computational effort using MPP- and mean-point-based univariate response-surface methods, mean-point-based bivariate response-surface method, FORM, Hohenbichler's SORM (Hohenbichler et al., 1987), and direct Monte Carlo simulation (10^6 samples). For univariate and bivariate response-surface methods, a value of $n = 7$ was selected. The results indicate that the proposed MPP-based univariate method and mean-point-based bivariate method produce the most accurate solution. The mean-point based univariate method significantly overpredicts the failure probability, whereas FORM and SORM slightly underpredict the failure probability. The MPP-based univariate response-surface method surpasses both the accuracy (although marginally) and efficiency of SORM and mean-point-based bivariate response-surface method in solving this reliability problem.

3.4.2.2 Example 3 – 10-Bar Truss Structure

A ten-bar, linear-elastic, truss structure, shown in Figure 3.4, was studied in this example to examine the accuracy and efficiency of the proposed reliability method. The Young's modulus of the material is 10^7 psi. Two concentrated forces of 10^5 lb are applied at nodes 2 and 3, as shown in Figure 3.4. The cross-sectional area $X_i, i = 1, \cdots, 10$ for each bar follows truncated normal distribution clipped at $x_i = 0$ and has mean $\mu = 2.5$ in^2 and standard deviation $\sigma = 0.5$ in^2. According to the loading condition, the maximum displacement $[(v_3(X_1, \cdots, X_{10})]$ occurs at node 3, where a permissible displacement is limited to 18 in. Hence, the performance function is

$$g(X) = 18 - v_3(X_1, \cdots, X_{10}).$$ (3.20)

From the MPP search involving finite-difference gradients, the reliability index is $\beta_{HL} = \|v^*\| = 1.3642$. Table 3.5 shows the failure probability of the truss, calculated using the proposed MPP-based univariate response-surface method, mean-point based univariate response-surface method (Xu and Rahman, 2005), FORM, three variants of SORM due to Breitung (1984), Hohenbeichler et al. (1987) and Cai and Elishakoff (1994), and direct Monte Carlo simulation (10^6 samples). For univariate response-surface methods, a value of $n = 7$ was selected. As can be seen from Table 5, both versions of the univariate response-surface method predict the failure probability more accurately than FORM and all three variants of SORM. This is because univariate methods are able to approximate the performance function more accurately than FORM and SORM. A comparison of the number of function evaluations, also listed in Table 3.5, indicates that the mean-point-based univariate response-surface method is the most efficient method. The number of function evaluations by the MPP-based univariate response-surface method is slightly larger than FORM, but much less than SORM.

3.4.2.3 Example 4 – Fracture Mechanics of Functionally Graded Material

The final example involves an edge-cracked plate, presented to illustrate mixed-mode probabilistic fracture-mechanics analysis using the univariate response-surface method. As shown in Figure 3.5(a), a plate of length $L = 16$ units, width $W = 7$ units was fixed at the bottom and subjected to a far-field and a shear stress τ^{∞} applied at the top. A $2b_1 \times 2b_2$ domain with $2b_1 = 2b_2 = 3.5$ units, required to calculate the M-integral. The

elastic modulus and Poisson's ratio were 1 unit and 0.25, respectively. A plane strain condition was assumed. The statistical property of the random input $X = \{a/W, \tau^\infty, K_{Ic}\}^T$ is defined in Table 3.6.

Due to the far-field shear stress τ^∞, the plate is subjected to mixed-mode deformation involving fracture modes I and II (Anderson, 1995). The mixed-mode stress-intensity factors $K_I(X)$ and $K_{II}(X)$ were calculated using an interaction integral method (Yau et al. 1980). The plate was analyzed using the finite element method (FEM) involving a total of 832 8-noded, regular, quadrilateral elements and 48 6-noded, quarter-point (singular), triangular elements at the crack-tip, as shown in Figure 3.5(b).

The failure criterion is based on a mixed-mode fracture initiation using the maximum tangential stress theory (Anderson, 1995), which leads to the limit-state equation

$$g(X) = K_{Ic} - \left[K_I(X)\cos^2\frac{\Theta(X)}{2} - \frac{3}{2}K_{II}(X)\sin\Theta(X) \right]\cos\frac{\Theta(X)}{2}, \quad (3.21)$$

where K_{Ic} is a deterministic fracture toughness, typically measured from small-scale fracture experiments under mode-I and plane strain conditions, and $\Theta_c(X)$ is the direction of crack propagation, given by

$$\Theta_c(X) = \begin{cases} 2\tan^{-1}\left(\dfrac{1-\sqrt{1+8\left[K_{II}(X)/K_I(X)\right]^2}}{4K_{II}(X)/K_I(X)} \right), & \text{if } K_{II}(X) > 0 \\[4mm] 2\tan^{-1}\left(\dfrac{1+\sqrt{1+8\left[K_{II}(X)/K_I(X)\right]^2}}{4K_{II}(X)/K_I(X)} \right), & \text{if } K_{II}(X) < 0 \end{cases} . \quad (3.22)$$

Failure probability estimates of $P_F = P[g(X) < 0]$, obtained using the proposed MPP-based univariate method, mean-point-based univariate and bivariate methods, FORM, Hohenbeichler's SORM, and direct Monte Carlo simulation, are compared in Figure 3.6 and are plotted as a function of $\mathbb{E}[\tau^\infty]$, where $\mathbb{E}$ is the expectation operator. For each reliability analysis (i.e., each point in the plot), FORM and SORM require 29 and 42 function evaluations (finite-element analysis). Using $n = 9$, the mean-point-based and MPP-based univariate methods require only 25 and 53 ($= 29 + 24$) function evaluations, respectively, whereas 211 and 50,000 finite-element analyses are needed by the mean-point-based bivariate method and Monte Carlo simulation, respectively. The results clearly show that MPP-based univariate method is more accurate than other methods, particularly when the failure probability is low. The computational effort by MPP-based univariate method is much lower than that by mean-point-based bivariate or simulation methods.

3.5 Fatigue Reliability Applications

The objective of this section is to illustrate the effectiveness of the proposed univariate response-surface method in solving a large-scale practical engineering problem. The problem involves mechanical fatigue durability and reliability analyses of a lever arm in a wheel loader.

3.5.1 Problem Definition and Input

Figure 3.7(a) shows a wheel loader commonly used in the heavy construction industry. A major structural problem entails fatigue life evaluation of lever arms, also

depicted in Figure 3.7(a). The loading and boundary conditions of a single lever arm are shown in Figure 3.7(b). The load F_E at pin E can be viewed as an input load due to other mechanical components of the wheel loader. The deterministic constant-amplitude load cycles at pin E vary from -800 to 3200 kN and are shown in Figure 3.7(c). The lever arm is made of cast steel with deterministic elastic properties, as follows: (1) Young's modulus $E = 203$ GPa, (2) Poisson's ratio $\nu = 0.3$. In general, the random input vector X, which comprises casting defect characteristics and material properties, include defect radius r, ultimate strength S_u, fatigue strength coefficient σ'_f, fatigue strength exponent b, fatigue ductility coefficient ε'_f, and fatigue ductility exponent c. Table 3.7 defines statistical properties of X. The objective is to predict fatigue durability and reliability of the lever arm. A value of $n = 3$ was selected for the proposed univariate method.

3.5.2 Fatigue Reliability Analysis

The von Mises strain-life method was employed for fatigue durability analysis (Stephens et al., 2001). According to this method, the Coffin-Manson-Morrow equation for determining fatigue crack-initiation life N_f at a point is (Stephens et al., 2001)

$$\frac{\Delta\varepsilon}{2} = \frac{\sigma'_f - \sigma_m}{E}\left(2N_f\right)^b + \varepsilon'_f\left(2N_f\right)^c, \tag{3.23}$$

where $\Delta\varepsilon$ is the equivalent strain range and σ_m is the equivalent mean stress, both of which depend on strain and stress fields. Appendix A provides a brief exposition of calculating $\Delta\varepsilon$ and σ_m, which requires results of linear-elastic finite-element stress

analysis.   Appendix B describes how defect size can be estimated from casting simulation.

Once $\Delta\varepsilon$ and σ_m are calculated, the fatigue life $N_f(X)$, which depends on random input X, can be calculated by solving Equation (3.23).   The fatigue failure is defined when $N_f(X)$ exceeds a design threshold n_0.   Hence, the performance function becomes

$$g(X) = N_f(X) - n_0. \tag{3.24}$$

A value of $n_0 = 10^7$ cycles was employed in this study.

3.5.3 Results

3.5.3.1 Without Defects

Figure 3.8(a) shows a three-dimensional finite-element mesh of the lever arm involving 77,154 tetrahedral elements and 17,089 nodes, which was generated using the ABAQUS commercial software (ABAQUS, 2002).   Using the FEM-based stress analysis and following the procedure described in Appendix A, Figures 3.8(b) and 3.8(c) present contours of equivalent alternating strain ($=$ half of equivalent strain range $= \Delta\varepsilon/2$) and equivalent mean stress (σ_m), respectively, of the lever arm.

The MPP-based univariate response-surface method was applied to calculate the probability of fatigue failure $P_F \equiv P\left[N_f(X) < n_0 \right]$.   Since no defects are considered initially, only four random variables comprising fatigue strength coefficient, fatigue strength exponent, fatigue ductility coefficient, and fatigue ductility exponent are required. Figure 3.9 shows the contour plot of the reliability index $\beta \equiv \Phi^{-1}\left(1 - P_F\right)$ of the

entire lever arm. Results indicate that the reliability indices are relatively small (*i.e.*, failure probabilities are relatively large) in Region A where there are large strains (see Figure 3.8(a)) or in Region B where there are large mean stress (see Figure 3.8(b)) and are expected. A further comparative analysis indicates that largest failure probabilities in Regions A and B are 0.0127 and 0.00466, respectively. Therefore, if the lever arm is redesigned, a natural tendency is to modify the shape or size of Region A until the failure probability is lowered to a target value.

3.5.3.2 With Defects

The probabilistic analysis described in the preceding can also be employed when casting-induced shrinkage defects are considered. However, any detrimental effect of defect size on $\Delta\varepsilon$ and σ_m and two additional random variables, such as defect radius and ultimate strength S_u, (see Appendix A) must be accounted for in subsequent reliability analysis. Figure 3.10 shows the contour plot of porosity distribution in the lever arm and was generated using the MAGMASOFT commercial software (MAGMASOFT, 2002). The MAGMASOFT simulation predicts larger porosity in Region B in this particular lever arm. By following the procedure of Appendix B, the mean radius (μ_r) of equivalent spherical defects at three internal (near surface) locations 1, 2, and 3, sketched in Figure 10, are estimated to be 14.4 mm, 5.5 mm, and 11.5 mm, respectively. The 10 percent coefficient of variation and lognormal distribution of *r* were defined arbitrarily.

Table 3.8 presents predicted failure probabilities at locations 1, 2, and 3, calculated with and without considering casting-induced shrinkage porosity. Results

suggest that the presence of defect can alter failure probability by 3 to 4 orders of magnitude. It is interesting to note that the largest failure probability of 0.0782, which occurs in Region B due to the presence of defect, has now become larger than the largest failure probability of 0.0127 in Region A. In other words, larger failure probability may occur at other seemingly non-critical regions when casting-induced defects are considered. Therefore, mechanical fatigue design processes that do not account for casting-induced defects may neither improve design nor provide a truly reliable solution.

Table 3.1 Failure probability for cubic performance function

Method	Failure Probability	Number of function evaluations[a]
MPP-based univariate method	0.01907	29[b]
Mean-point-based univariate method (Xu and Rahman, 2005)	0.01558	9[c]
FORM	0.01302	21
SORM (Breitung, 1984)	0.01302	204
SORM (Hohenbichler, 1987)	0.01302	204
SORM (Cai and Elishakoff, 1994)	0.01302	204
Direct Monte Carlo simulation	0.01907	1,000,000

(a) Total number of times the original performance function is calculated.

(b) $21 + (n-1) \times N = 21 + (5-1) \times 2 = 29$

(c) $(n-1) \times N + 1 = (5-1) \times 2 + 1 = 9$

Table 3.2 Failure probability for quartic performance function

Method	Failure Probability	Number of function evaluations[a]
MPP-based univariate method	0.002886	29[b]
Mean-point-based univariate method (Xu and Rahman, 2005)	_[c]	_[c]
FORM	0.006209	21
SORM (Breitung, 1984)	0.006208	212
SORM (Hohenbichler, 1987)	0.006208	212
SORM (Cai and Elishakoff, 1994)	0.006206	212
Direct Monte Carlo simulation	0.002886	1,000,000

(a) Total number of times the original performance function is calculated.

(b) $21 + (n-1) \times N = 21 + (5-1) \times 2 = 29$

(c) Fails to provide a solution.

Table 3.3 Statistical properties of random input for rotating disk

Random Variable	Mean	Standard Deviation	Probability Distribution
α_m	0.9377	0.0459	Weibull[a]
S_u, ksi	220	5	Gaussian
ω, rpm	24	0.5	Gaussian
ρ, lb-sec^2/in^4	0.29/g[b]	0.0058/g[b]	Uniform[c]
R_o, in	24	0.5	Gaussian
R_i, in	8	0.3	Gaussian

(a) Scale parameter = 25.508; shape parameter = 0.958

(b) $g = 385.82$ in/sec^2

(c) Uniformly distributed over (0.28,0.3).

Table 3.4 Failure probability of rotating disk

Method	Failure Probability	Number of function evaluations[a]
MPP-based univariate method	0.00101	167[b]
Mean-point-based univariate method (Xu and Rahman, 2005)	0.00159	37[c]
Mean-point-based bivariate method (Xu and Rahman, 2005)	0.00103	577[d]
FORM	0.000894	131
SORM (Hohenbichler, 1987)	0.000970	378
Direct Monte Carlo simulation	0.00104	1,000,000

(a) Total number of times the original performance function is calculated.

(b) $131 + (n-1) \times N = 131 + (7-1) \times 6 = 167$

(c) $(n-1) \times N + 1 = (7-1) \times 6 + 1 = 37$

(d) $N \times (N-1) \times (n-1)^2 / 2 + (n-1) \times N + 1 = 6 \times (6-1) \times (7-1)^2 / 2 + (7-1) \times 6 + 1 = 577$

Table 3.5 Failure probability of ten-bar truss structure

Method	Failure Probability	Number of function evaluations[a]
MPP-based univariate method	0.1465	187[b]
Mean-point-based univariate method (Xu and Rahman, 2005)	0.1357	61[c]
FORM	0.0862	127
SORM (Breitung, 1984)	0.1286	506
SORM (Hohenbichler, 1987)	0.1524	506
SORM (Cai and Elishakoff, 1994)	0.1467	506
Direct Monte Carlo simulation	0.1394	1,000,000

(a) Total number of times the original performance functions is calculated.

(b) $127 + (n-1) \times N = 127 + (7-1) \times 10 = 187$

(c) $(n-1) \times N + 1 = (7-1) \times 10 + 1 = 61$

Table 3.6 Statistical properties of random input for an edge-cracked plate

Random Variable	Mean	Standard Deviation	Probability Distribution
a/W	0.5	0.2309	Uniform[a]
τ^∞	Variable [b]	0.1	Gaussian
K_{Ic}	200	0.1	Lognormal

(a) Uniformly distributed over (0.3, 0.7).

(b) Varies from 2.6 to 3.1.

Table 3.7 Statistical properties of random input for lever arm

Random Variable[a]	Mean	Coefficient of Variation	Probability Distribution
σ'_f, MPa	1,332	0.1	Lognormal
b	-0.1085	0.1	Lognormal
ε'_f	0.375	0.1	Lognormal
c	-0.6354	0.1	Lognormal
S_u, MPa	847	0.05	Lognormal
r, mm	Variable[b]	0.1	Lognormal

(a) Random variables S_u and r are active only when casting defects are considered.

(b) Varies as follows: 14.4, 5.5, and 11.5 mm at locations 1, 2, and 3, respectively (see Figure 10).

Table 3.8 Probability of fatigue failure of lever arm at locations 1, 2, and 3

Location	Mean Defect Radius, mm	Probability of Fatigue Failure	
		Without Defect[a]	With Defect[b]
1	14.4	3.396×10^{-6}	2.829×10^{-2}
2	5.5	2.294×10^{-5}	7.818×10^{-2}
3	11.5	3.433×10^{-6}	2.779×10^{-2}

(a) Random input vector: $\boldsymbol{X} = \{\sigma'_f, b, \varepsilon'_f, c\}^T \in \mathbb{R}^4$

(a) Random input vector: $\boldsymbol{X} = \{\sigma'_f, b, \varepsilon'_f, c, S_u, r\}^T \in \mathbb{R}^6$
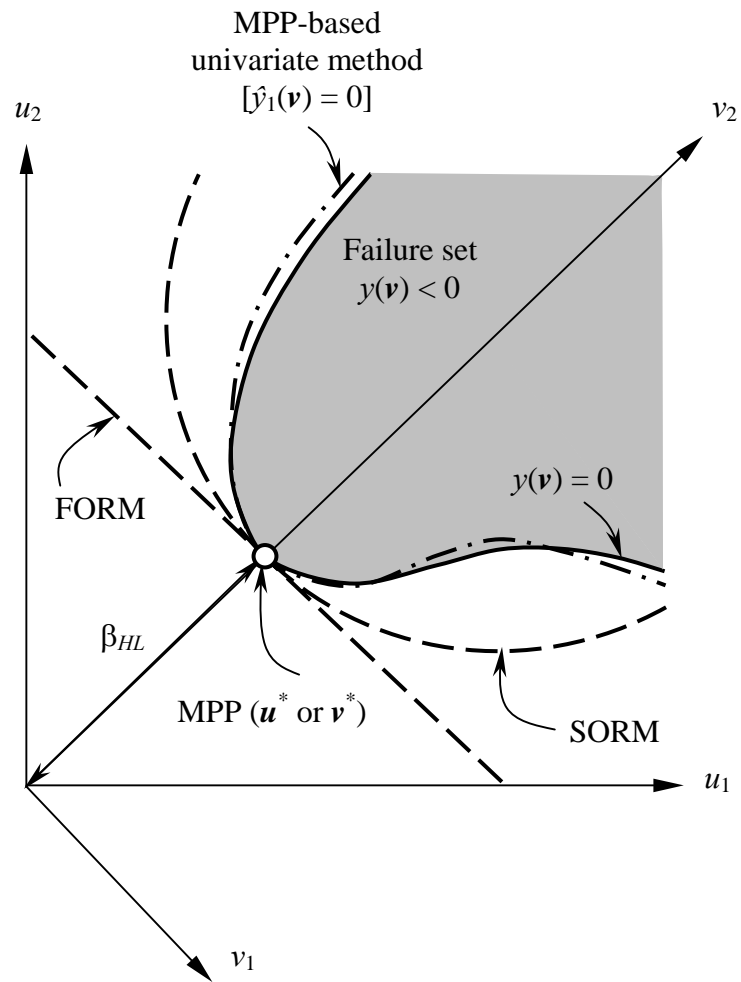
Figure 3.1 Performance function approximations by various methods
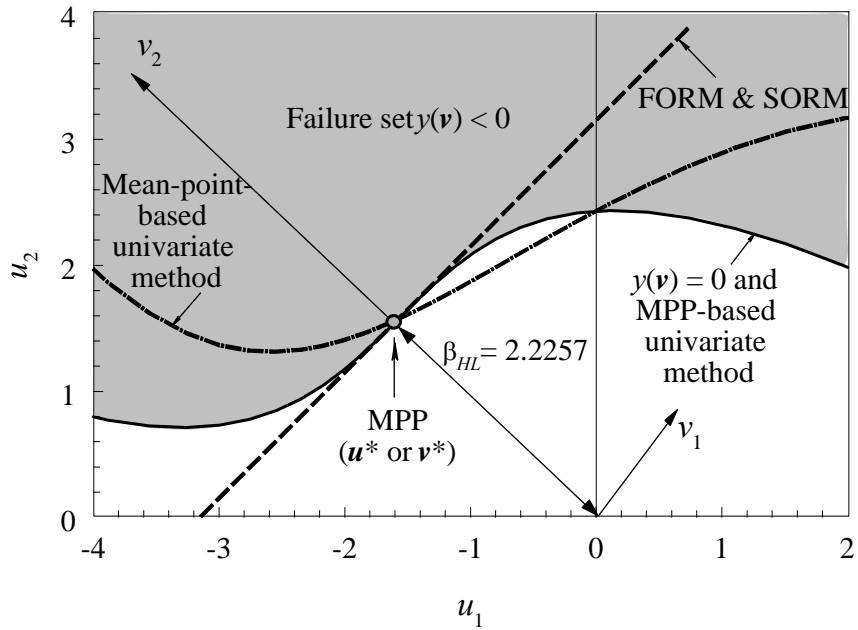
(a)
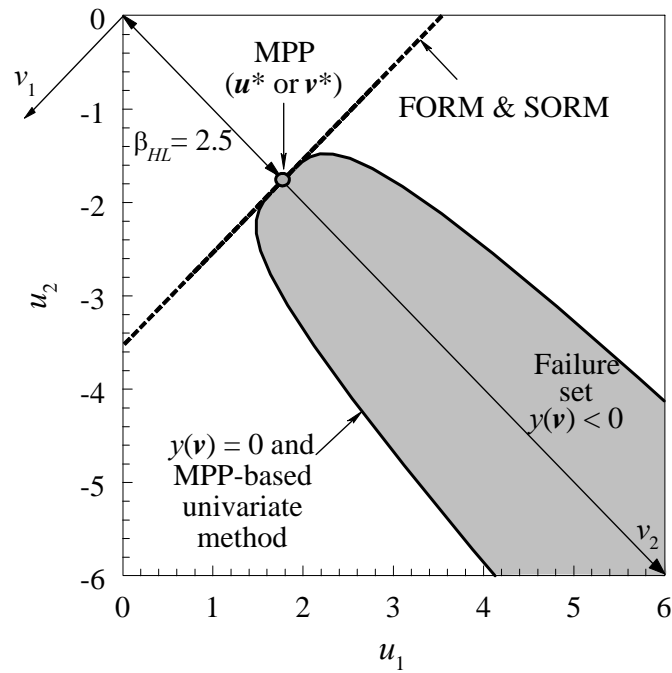
(b)

Figure 3.2 Approximate performance functions by various methods; (a) cubic function; (b) quartic function
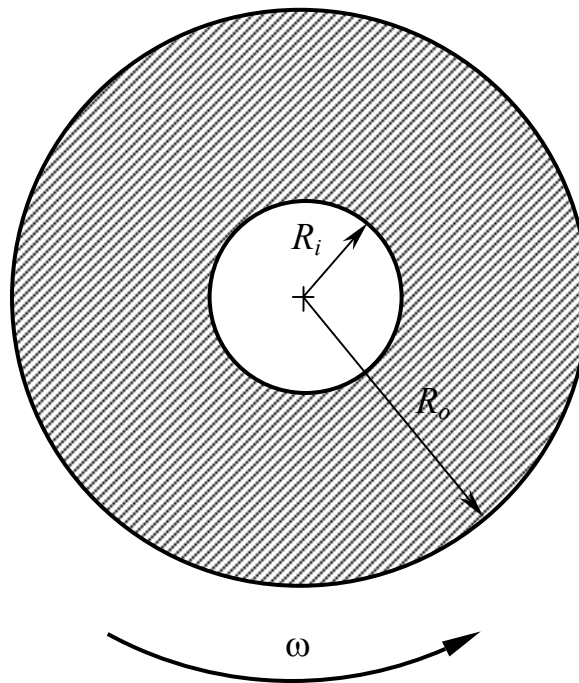
Figure 3.3 Rotating annular disk subject to angular velocity
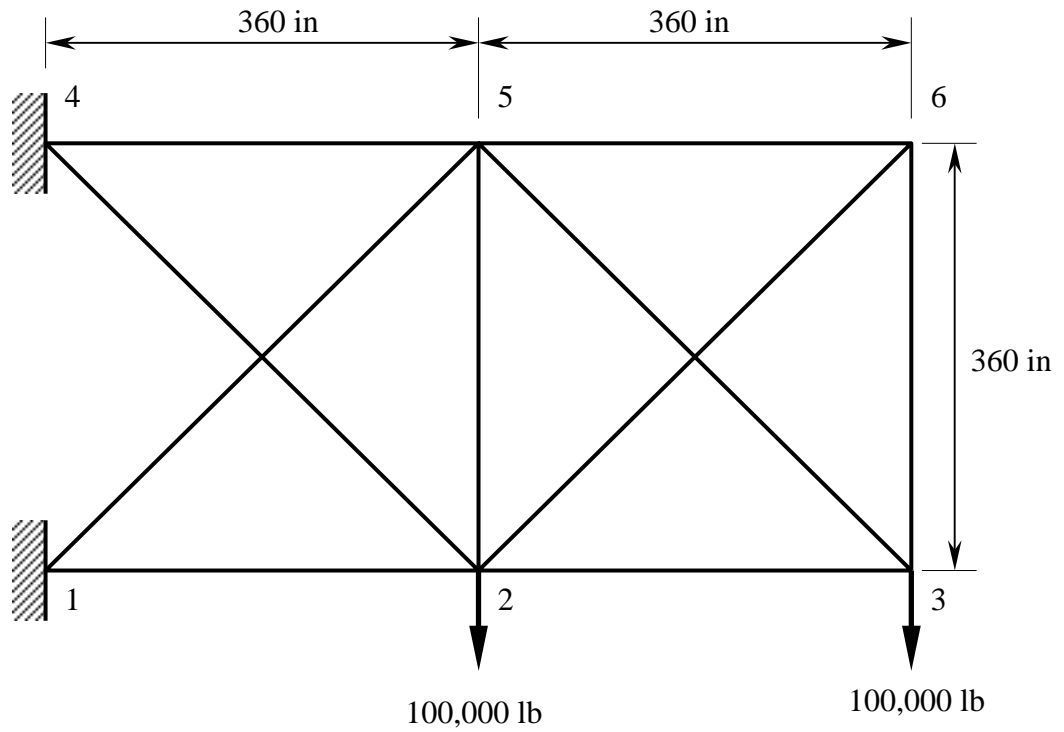
Figure 3.4 A ten-bar truss structure
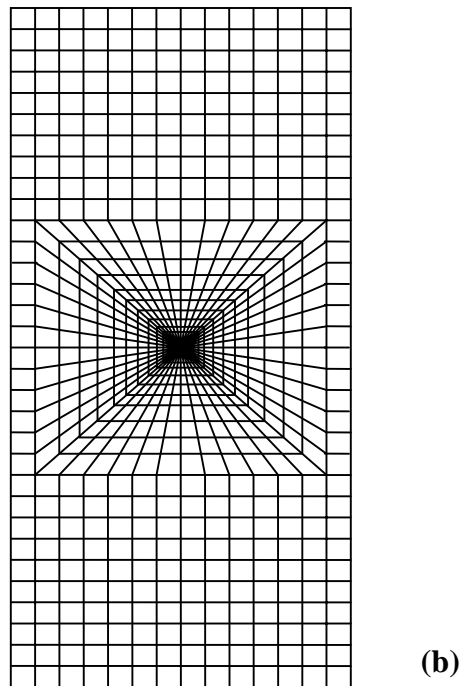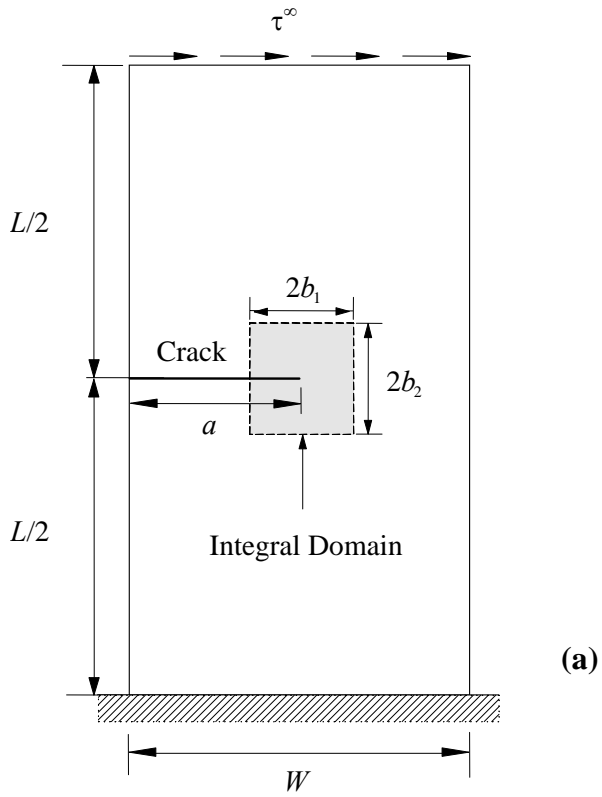
**Figure 3.5 An edge-cracked plate subject to mixed-mode deformation;
(a) geometry and loads; (b) finite-element discretization**
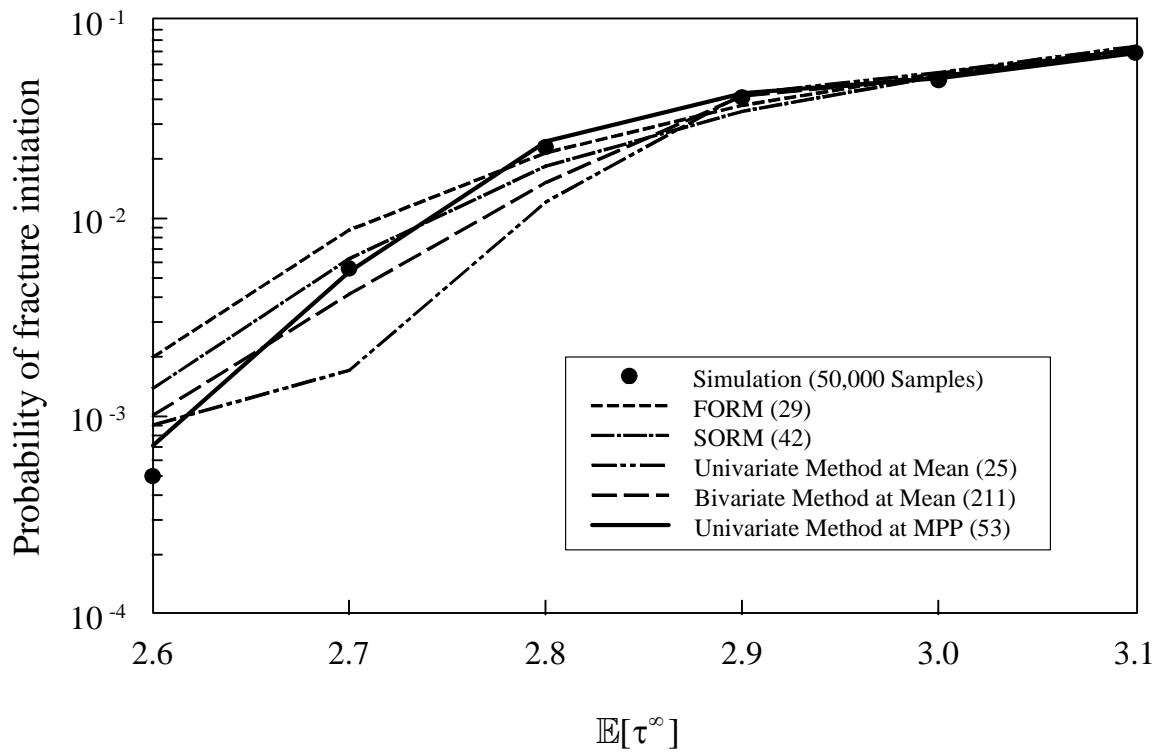
Figure 3.6 Probability of fracture initiation in an edge-cracked plate
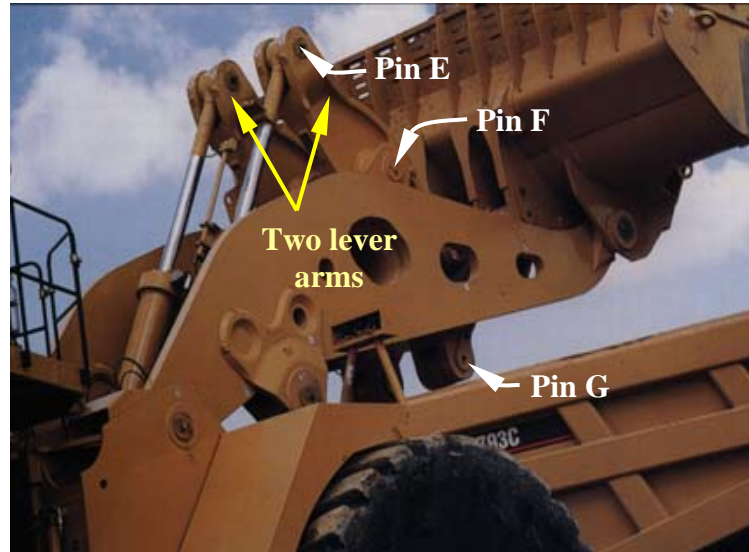
(a)
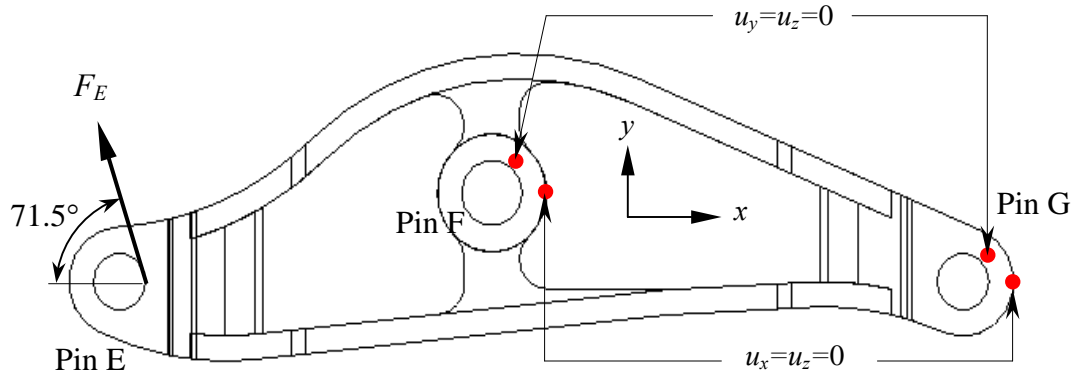
(b)
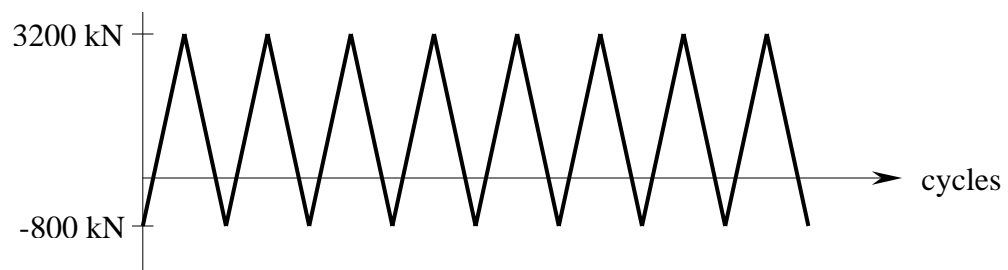
(c)

Figure 3.7 A wheel loader under cyclic loads; (a) two lever arms; (b) loading and boundary conditions of a lever arm; (c) constant-amplitude cyclic loads at pin E

(a)
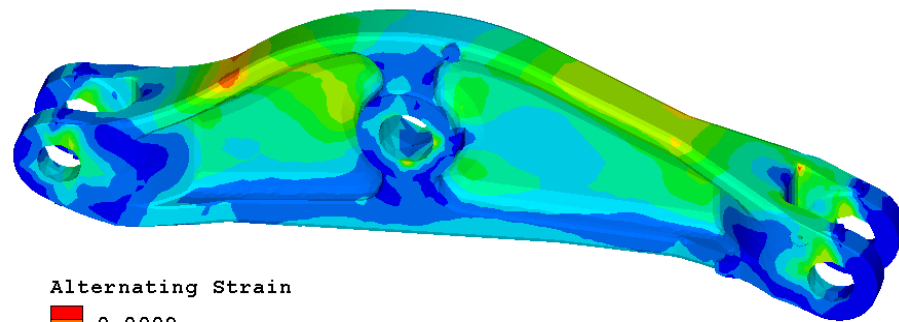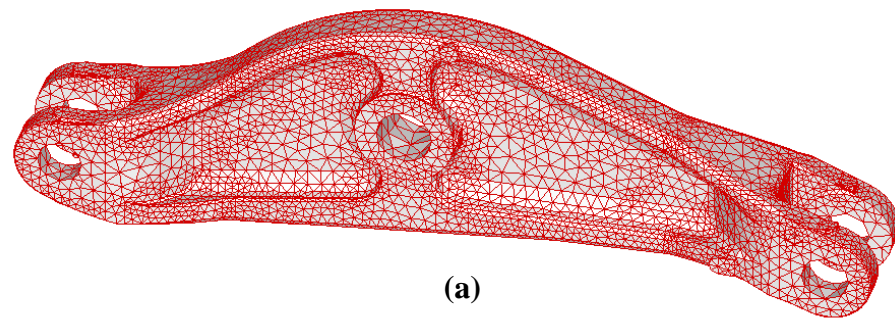
(b)
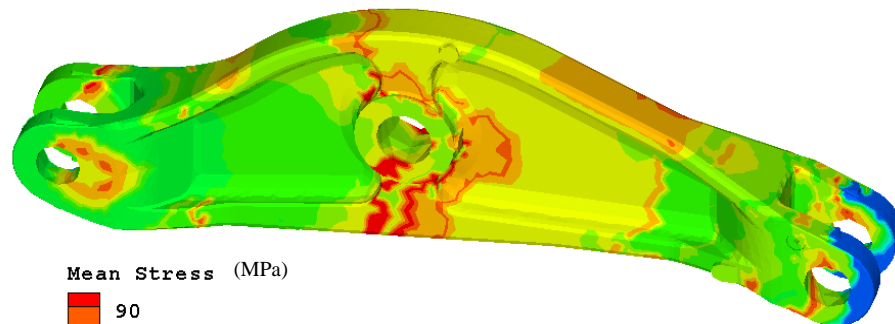
(c)

Figure 3.8 Finite element analysis of a lever arm; (a) mesh (77,154 elements; 17,089 nodes);(b) equivalent alternating strain ($\Delta\varepsilon/2$) contour; (c) equivalent mean stress (σ_m) contour

Region A
(Maximum $P_F = 0.0127$)

Region B
(Maximum $P_F = 0.00466$)

Reliability Index

9
8
7
6
5.5
5
4.5
4
3.5
3
2.5
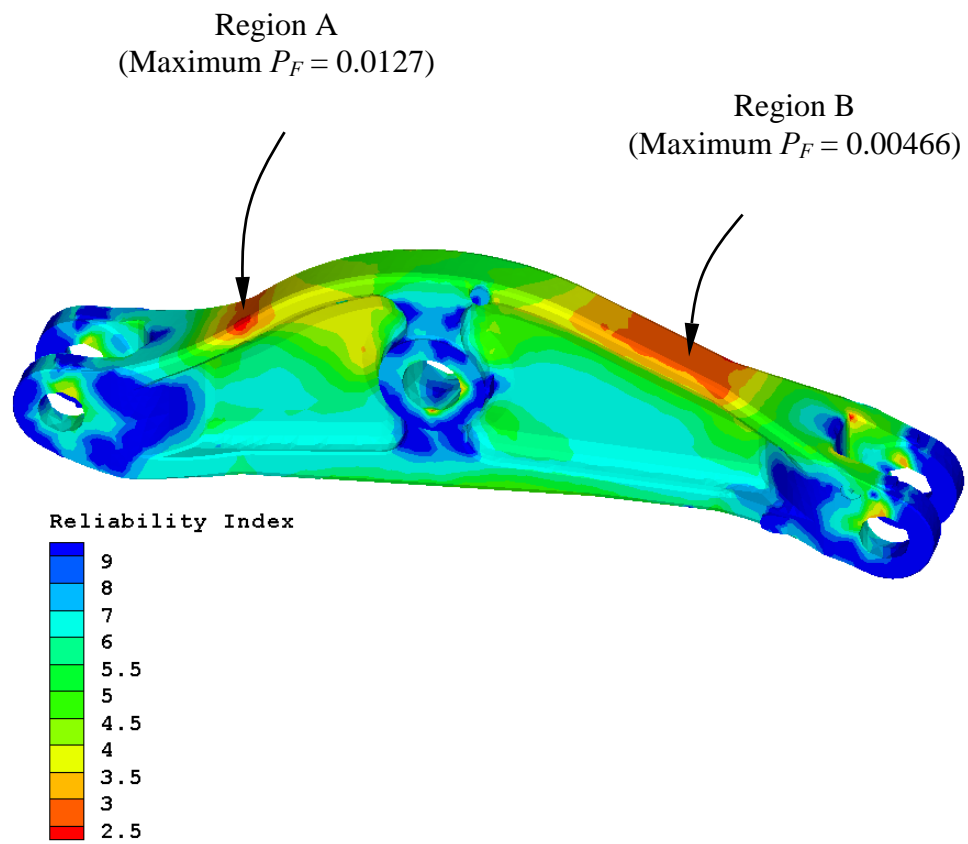
Figure 3.9 Fatigue life-based reliability index contour of lever arm

Location 1
($\mu_r = 14.4$ mm)   Location 2
($\mu_r = 5.5$ mm)

Location 3
($\mu_r = 11.5$ mm)

Porosity Fraction

0.4
0.36
0.32
0.28
0.24
0.2
0.16
0.12
0.08
0.04
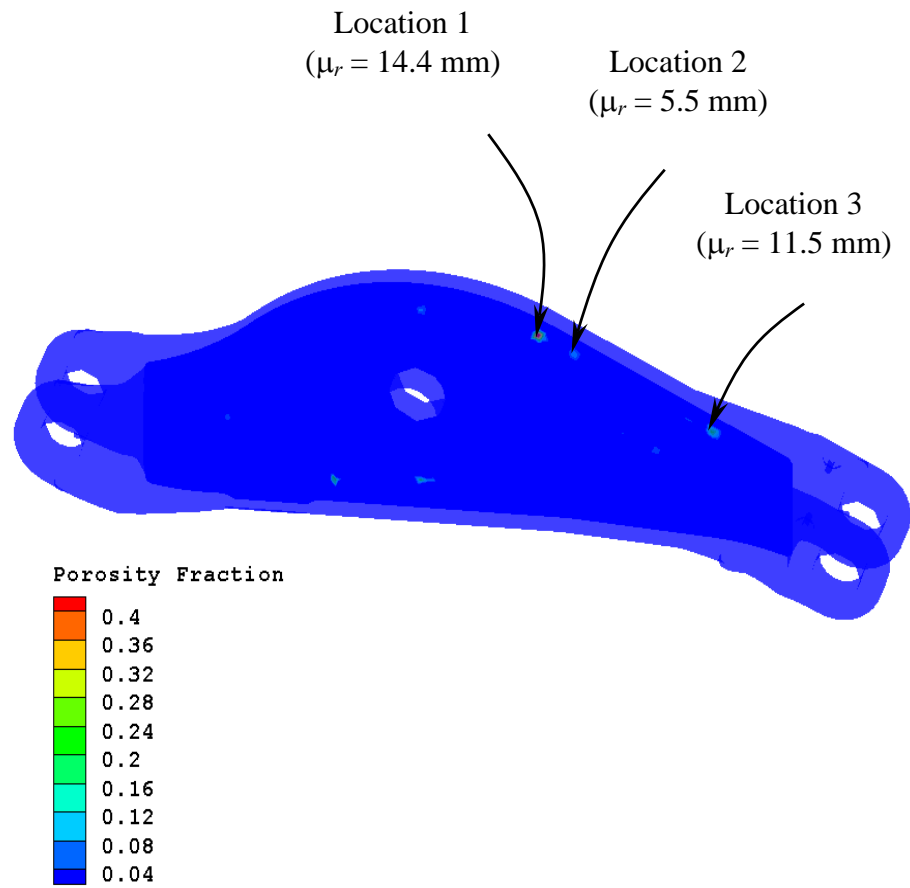
Figure 3.10 Porosity field of lever arm from casting simulation

CHAPTER 4

MPP-BASED UNIVARIATE METHOD WITH NUMERICAL INTEGRATION

4.1 Univariate Decomposition at MPP

The general case of multivariate function decomposition at MPP is described in Chapter 3. In this Chapter, a univariate decomposition at MPP is discussed further. Consider a univariate approximation of $y(\boldsymbol{v})$, denoted by

$$\hat{y}_1(\boldsymbol{v}) \equiv \hat{y}_1(v_1,\cdots,v_N) = \sum_{i=1}^{N} y(v_1^*,\cdots,v_{i-1}^*,v_i,v_{i+1}^*,\cdots,v_N^*) - (N-1)y(\boldsymbol{v}^*), \quad (4.1)$$

where each term in the summation is a function of only one variable and can be subsequently expanded in a Taylor series at MPP $\boldsymbol{v}^* = \left\{v_1^*,\cdots,v_{N-1}^*,v_N^*\right\}^T = \left\{0,\cdots,0,\beta_{HL}\right\}^T$, yielding

$$\hat{y}_1(\boldsymbol{v}) = y(\boldsymbol{v}^*) + \sum_{j=1}^{\infty}\frac{1}{j!}\sum_{i=1}^{N}\frac{\partial^j y}{\partial x_i^{\,j}}\left(\boldsymbol{v}^*\right)(v_i - v_i^*)^j . \quad (4.2)$$

In contrast, the Taylor series expansion of $y(\boldsymbol{v})$ at $\boldsymbol{v}^* = \left\{v_1^*,\cdots,v_N^*\right\}^T$ can be expressed by

$$y(\boldsymbol{v}) = y\left(\boldsymbol{v}^*\right) + \sum_{j=1}^{\infty}\frac{1}{j!}\sum_{i=1}^{N}\frac{\partial^j y}{\partial v_i^{\,j}}\left(\boldsymbol{v}^*\right)\left(v_i - v_i^*\right)^j + \mathcal{R}_2 \quad (4.3)$$

where the remainder $\mathcal{R}_2$ denotes all terms with dimension two and higher. A comparison of Equations (4.2) and (4.3) indicates that the univariate approximation of $\hat{y}_1(\boldsymbol{v})$ leads to a residual error $y(\boldsymbol{v}) - \hat{y}_1(\boldsymbol{v}) = \mathcal{R}_2$, which includes contributions from terms of dimension two and higher. For sufficiently smooth $y(\boldsymbol{v})$ with convergent Taylor series, the coefficients associated with higher-dimensional terms are usually much smaller than

that with one-dimensional terms. As such, higher-dimensional terms contribute less to the function, and therefore, can be neglected. Nevertheless, Equation (4.1) includes all higher-order *univariate* terms, as compared with FORM and SORM, which only retain *linear and quadratic univariate* terms, respectively.

It is worth noting that the univariate approximation in Equation (4.1) should not viewed as first- or second-order Taylor series expansions nor does it limit the nonlinearity of $y(\boldsymbol{v})$. According to Equation (4.2), *all* higher-order univariate terms of $y(\boldsymbol{v})$ are included in the proposed approximation.

4.2 Univariate Integration for Failure Probability Analysis

The proposed univariate approximation of the performance function can be rewritten as

$$\hat{y}_1(\boldsymbol{v}) = y_N(v_N) + \sum_{i=1}^{N-1} y_i(v_i) - (N-1)y(\boldsymbol{v}^*), \qquad (4.4)$$

where $y_i(v_i) \equiv y(v_1^*, \cdots, v_{i-1}^*, v_i, v_{i+1}^*, \cdots, v_N^*)$; $i = 1, N$. Due to rotational transformation of the coordinates (see Figure (3.1)), the univariate component function $y_N(v_N)$ in Equation (4.4) is expected to be a linear or a weakly nonlinear function of v_N. In fact, $y_N(v_N)$ is linear with respect to v_N in classical FORM/SORM approximations of a performance function in the v space. Nevertheless, if $y_N(v_N)$ is invertible, the univariate approximation $\hat{y}_1(\boldsymbol{v})$ can be further expressed in a form amenable to an efficient reliability analysis by one-dimensional numerical integration. In this work, both linear

and quadratic approximations of $y_N(v_N)$ and resultant equations for failure probability are derived, as follows.

4.2.1 Linear Approximation of $y_N(v_N)$

Consider a linear approximation: $y_N(v_N) = b_0 + b_1 v_N$, where coefficients $b_0 \in \mathbb{R}$ and $b_1 \in \mathbb{R}$ (non-zero) are obtained by least-squares approximations from exact or numerically simulated responses $\left\{ y_N(v_N^{(1)}), \cdots, y_N(v_N^{(n)}) \right\}$ at n sample points along the v_N coordinate. Applying the linear approximation, the component failure probability can be expressed by

$$P_F \equiv P\big[y(\mathbf{V}) < 0 \big] \cong P\big[\hat{y}_1(\mathbf{V}) < 0 \big] \cong P\left[b_0 + b_1 V_N + \sum_{i=1}^{N-1} y_i(V_i) - (N-1) y(\mathbf{v}^*) < 0 \right], \quad (4.5)$$

which on inversion yields

$$P_F \cong \begin{cases} P\left[V_N < \dfrac{(N-1)y(\mathbf{v}^*) - b_0}{b_1} - \dfrac{1}{b_1} \sum_{i=1}^{N-1} y_i(V_i) \right], & \text{if } b_1 > 0 \\[4mm] P\left[V_N \geq \dfrac{(N-1)y(\mathbf{v}^*) - b_0}{b_1} - \dfrac{1}{b_1} \sum_{i=1}^{N-1} y_i(V_i) \right], & \text{if } b_1 < 0 \end{cases} . \quad (4.6)$$

Since V_N follows standard Gaussian distribution, the failure probability can also be expressed by

$$P_F \cong \mathbb{E}\left[\Phi\left(\frac{(N-1)y(\mathbf{v}^*) - b_0}{|b_1|} - \frac{1}{|b_1|} \sum_{i=1}^{N-1} y_i(V_i) \right) \right], \quad (4.7)$$

where $\mathbb{E}$ is the expectation operator and $\Phi(u) = \left(1/\sqrt{2\pi}\right)\int_{-\infty}^{u} \exp\left(-\xi^2/2\right)d\xi$ is the cumulative distribution function of a standard Gaussian random variable. Note that Equation (4.7) provides higher-order estimates of failure probability if univariate component functions $y_i(v_i)$, $i = 1, N-1$ are approximated by higher than second-order terms. If $y_i(v_i)$, $i = 1, N-1$ retain only linear and quadratic terms fitted with appropriately selected sample points, Equation (4.7) can be further simplified to degenerate to the well-known FORM and SORM approximations.

4.2.2 Quadratic Approximation of $y_N(v_N)$

The linear approximation described in the preceding can be improved by a quadratic approximation: $y_N(v_N) = b_0 + b_1 v_N + b_2 v_N^2$, where coefficients $b_0 \in \mathbb{R}$, $b_1 \in \mathbb{R}$, and $b_2 \in \mathbb{R}$ (non-zero) are also obtained by least-squares approximations from exact or numerically simulated responses at n sample points along the v_N coordinate. Similarly, the quadratic approximation of $y_N(v_N)$ employed in Equation (4.4) leads to

$$P_F \equiv P\left[y(V) < 0\right] \cong P\left[\hat{y}_1(V) < 0\right] \cong P\left[b_0 + b_1 V_N + b_2 V_N^2 + \sum_{i=1}^{N-1} y_i(V_i) - (N-1)y(v^*) < 0\right]. \quad (4.8)$$

By defining $B(\tilde{V}) \equiv b_0 + \sum_{i=1}^{N-1} y_i(V_i) - (N-1)y(v^*)$, where $\tilde{V} = \{V_1, \cdots, V_{N-1}\}^T$ is an N-1-dimensional standard Gaussian vector, the following solutions are derived based on two cases:

(a) Case I – Trivial Solution ($b_1^2 - 4b_2 B < 0$; no real roots):

$$P_F \cong \begin{cases} 0, & \text{if } b_2 > 0 \\ 1, & \text{if } b_2 < 0 \end{cases} . \tag{4.9}$$

(b) Case II – Non-Trivial Solution ($b_1^2 - 4b_2 B \geq 0$; two real roots):

$$P_F \cong \begin{cases} P\left[\dfrac{-b_1 - \sqrt{b_1^2 - 4b_2 B(\tilde{\boldsymbol{V}})}}{2b_2} < V_N < \dfrac{-b_1 + \sqrt{b_1^2 - 4b_2 B(\tilde{\boldsymbol{V}})}}{2b_2} \right], & \text{if } b_2 > 0 \\[4mm] P\left[\dfrac{-b_1 + \sqrt{b_1^2 - 4b_2 B(\tilde{\boldsymbol{V}})}}{2b_2} < V_N < \dfrac{-b_1 - \sqrt{b_1^2 - 4b_2 B(\tilde{\boldsymbol{V}})}}{2b_2} \right], & \text{if } b_2 < 0 \end{cases}, \tag{4.10}$$

yielding

$$P_F \cong \frac{1 - b_2/|b_2|}{2} + \left\{ \mathbb{E}\left[\Phi\left(\frac{-b_1 + \sqrt{b_1^2 - 4b_2 B(\tilde{\boldsymbol{V}})}}{2b_2} \right) \right] - \mathbb{E}\left[\Phi\left(\frac{-b_1 - \sqrt{b_1^2 - 4b_2 B(\tilde{\boldsymbol{V}})}}{2b_2} \right) \right] \right\}. \tag{4.11}$$

Both Equations (4.7) and (4.11) can be employed for non-trivial solutions of failure probability. Improvement of the accuracy of results, if any, depends on how strongly $y_N(v_N)$ depends on v_N. Furthermore, it is possible to develop a generalized version of Equation (4.11) when $y_N(v_N)$ is highly nonlinear (*e.g.*, polynomial of an arbitrary order), but invertible. However, due to the rotational transformation from the $\boldsymbol{x}$ space to the $\boldsymbol{v}$ space, it is expected that the linear approximation of $y_N(v_N)$ (Equation (4.7)) should result in a very accurate solution. Hence, the present study is limited to only linear and quadratic approximations of $y_N(v_N)$. It is worth noting that unlike Equation (4.7), Equation (4.11) cannot be reduced to FORM/SORM equations as $y_N(v_N)$ includes a second-order term.

4.2.3 Univariate Integration

The failure probability expressions in Equations (4.7) and (4.11) involve calculation of expected values of several multivariate functions of an N-1 dimensional standard Gaussian vector $\tilde{V} = \{V_1, \cdots, V_{N-1}\}^T$. A generic expression of such calculation requires determining $\mathbb{E}\left[\Phi\left(f(\tilde{V})\right)\right]$, where $f : \mathbb{R}^{N-1} \mapsto \mathbb{R}$ is a general mapping of $\tilde{V}$ and depends on how univariate component functions $y_i(v_i)$, $i = 1, N-1$ are approximated. Unfortunately, the exact probability density function of $f(\tilde{V})$ is in general not available in closed form. For this reason, it is difficult to calculate $\mathbb{E}\left[\Phi\left(f(\tilde{V})\right)\right]$ analytically. Numerical integration is not efficient as $\Phi\left(f(\tilde{v})\right)$ is a multivariate function and becomes impractical when the dimension exceeds three or four.

In reference to Equation (4.1), consider again a univariate approximation of $\ln\left[\Phi\left(f(\tilde{v})\right)\right]$, expressed by

$$\ln\left[\Phi\left(f(\tilde{v})\right)\right] \cong \sum_{i=1}^{N-1} \ln\left[\Phi\left(f_i(v_i)\right)\right] - (N-2)\ln\left[\Phi\left(f(\tilde{v}^*)\right)\right], \qquad (4.12)$$

where $f_i(v_i) \equiv f(v_1^*, \cdots, v_{i-1}^*, v_i, v_{i+1}^*, \cdots, v_{N-1}^*)$ are univariate component functions and $f(\tilde{v}^*) \equiv f(v_1^*, \cdots, v_{N-1}^*)$. Hence,

$$
\begin{aligned}
\Phi\left(f(\tilde{v})\right) &= \exp\left\{\ln\left[\Phi\left(f(\tilde{v})\right)\right]\right\} \\
&\cong \exp\left\{\sum_{i=1}^{N-1} \ln\left[\Phi\left(f_i(v_i)\right)\right] - (N-2)\ln\left[\Phi\left(f(\tilde{v}^*)\right)\right]\right\} \quad (4.13) \\
&= \frac{\prod_{i=1}^{N-1} \Phi\left(f_i(v_i)\right)}{\Phi\left(f(\tilde{v}^*)\right)^{N-2}}
\end{aligned}
$$

yielding

$$\mathbb{E}\Big[\Phi\big(f(\tilde{\boldsymbol{V}})\big)\Big] \cong \frac{\prod_{i=1}^{N-1}\mathbb{E}\big[\Phi\big(f_i(V_i)\big)\big]}{\Phi\big(f(\tilde{\boldsymbol{v}}^*)\big)^{N-2}} = \frac{\prod_{i=1}^{N-1}\int_{-\infty}^{+\infty}\Phi\big(f_i(v_i)\big)\phi(v_i)dv_i}{\Phi\big(f(\tilde{\boldsymbol{v}}^*)\big)^{N-2}}\ , \quad (4.14)$$

which involves a product of *N-1 univariate* integrals with $\phi(\cdot)$ denoting standard Gaussian probability density function. Using Equation (4.14), the nontrivial expressions of failure probability in Equations (4.7) and (4.11) are

$$P_F \cong \frac{\prod_{i=1}^{N-1}\int_{-\infty}^{+\infty}\Phi\left(\frac{(N-1)y(\boldsymbol{v}^*)-b_0-y_i(v_i)}{|b_1|}\right)\phi(v_i)dv_i}{\left[\Phi\left(\frac{(N-1)y(\boldsymbol{v}^*)-b_0-\sum_{i=1}^{N-1}y_i(v_i^*)}{|b_1|}\right)\right]^{N-2}} \quad (4.15)$$

and

$$P_F \cong \frac{1-b_2/|b_2|}{2} + \left\{ \frac{\prod_{i=1}^{N-1}\int_{-\infty}^{+\infty}\Phi\left(\frac{-b_1+\sqrt{b_1^2-4b_2B_i(v_i)}}{2b_2}\right)\phi(v_i)dv_i}{\left[\Phi\left(\frac{-b_1+\sqrt{b_1^2-4b_2B(\tilde{\boldsymbol{v}}^*)}}{2b_2}\right)\right]^{N-2}} - \right.$$

$$\left. \frac{\prod_{i=1}^{N-1}\int_{-\infty}^{+\infty}\Phi\left(\frac{-b_1-\sqrt{b_1^2-4b_2B_i(v_i)}}{2b_2}\right)\phi(v_i)dv_i}{\left[\Phi\left(\frac{-b_1-\sqrt{b_1^2-4b_2B(\tilde{\boldsymbol{v}}^*)}}{2b_2}\right)\right]^{N-2}} \right\}$$

$$(4.16)$$

respectively, where $B_i(v_i) \equiv B(v_1^*,\cdots,v_{i-1}^*,v_i,v_{i+1}^*,\cdots,v_{N-1}^*)$. The univariate integration involved in Equations (4.15) or (4.16) can be easily evaluated by standard one-

dimensional Gauss-Hermite numerical quadrature (Abramowitz, 1972). The decomposition method involving univariate approximation (Equation (4.1)) and univariate integration (Equations (4.15) or (4.16)) is defined as the *MPP-based univariate method with numerical integration* in this chapter.

4.3 Computational Effort and Flow

Consider $y_i(v_i) \equiv y(v_1^*, \cdots, v_{i-1}^*, v_i, v_{i+1}^*, \cdots, v_N^*)$; $i = 1, N-1$, for which n function values $y_i(v_i^{(j)}) \equiv y(v_1^*, \cdots, v_{i-1}^*, v_i^{(j)}, v_{i+1}^*, \cdots, v_N^*)$; $j = 1, \cdots, n$ are required to be evaluated at integration points $v_i = v_i^{(j)}$ to perform an *n*-order Gauss-Hermite quadrature for *i*th integration in Equations (4.15) or (4.16). The same procedure is repeated for *N*-1 univariate component functions, *i.e.*, for all $y_i(v_i)$, $i = 1, \cdots, N-1$. Therefore, the total cost of the proposed univariate method including *n* function values of $y_N(v_N)$ required for its linear or quadratic approximation entails a *maximum* of $nN + 1$ function evaluations[1]. Note that the above cost is in addition to any function evaluations required for locating the MPP.

Figure 4.1 shows the computational flowchart of the MPP-based univariate method with numerical integration. The proposed effort in evaluating the failure probability has been transformed into numerically calculating univariate component functions at selected input determined by sample points in the v_N-coordinate and Gauss-

---

[1] The orders of numerical integration and the number of function values of $y_N(v_N)$ need not be the same. In addition, different orders of integration can be employed if desired.

Hermite integration points in the v_i-coordinate ($i = 1, N\text{-}1$). Compared with the previously developed univariate method (Rahman and Wei, 2006), no Monte Carlo simulation is required in the present method. The accuracy and efficiency of the new method depend on both the univariate approximation and numerical integration. They will be evaluated using several numerical examples in a forthcoming section.

In performing n-order Gauss-Hermite quadratures in Equations (4.15) or (4.16), two options for evaluating $y_i(v_i)$ are proposed. Option 1 involves calculating $y_i(v_i^{(j)})$ at integration points $(v_1^*, \cdots, v_{i-1}^*, v_i^{(j)}, v_{i+1}^*, \cdots, v_N^*)$; $j = 1, n$ from direct numerical analysis (*e.g.*, finite element analysis). When computing $y_i(v_i)$ is expensive, the first option is inefficient if n is required to be large for accurate numerical integration. The second option involves developing first a univariate response-surface approximation of $y_i(v_i)$ from selected samples points in the v_i-coordinate, followed by numerical integration of the response-surface approximation. Option 2 is computationally efficient, because no additional numerical analysis (*e.g.*, finite element analysis) is required if the order of integration is larger than the number of sample points. However, an additional layer of response surface approximation is involved in the second option. Both options were explored in numerical examples, as follows.

4.4 Numerical Examples

Five numerical examples involving explicit performance functions from mathematical or solid-mechanics problems (Examples 1 and 2) and implicit performance

functions from structural or solid-mechanics problems (Examples 3, 4, and 5), are presented to illustrate the MPP-based univariate method with numerical integration. Whenever possible, comparisons have been made with the previously developed MPP-based univariate method with simulation (Rahman and Wei, 2006), FORM/SORM, and direct Monte Carlo simulation to evaluate the accuracy and computational efficiency of the new method.

To obtain linear or quadratic approximation of $y_N(v_N)$, n (= 5, 7 or 9) sample points $v_N^* - (n-1)/2, v_N^* - (n-3)/2, \cdots, v_N^*, \cdots, v_N^* + (n-3)/2, v_N^* + (n-1)/2$ were deployed along the v_N-coordinate. The same value of n was employed as the order of Gauss-Hermite quadratures in Equations (4.15) or (4.16) of the proposed univariate method with numerical integration. Furthermore, option 1 was used in Examples 3 and 4 and option 2 was invoked in Examples 1,2 and 5. When using option 2, an nth-order polynomial equation was employed for generating response-surface approximation of various component functions $y_i(v_i)$, $i = 1, N-1$. For a consistent comparison, the same value of n was also employed as the number of sample points in the previously developed univariate method with simulation (Rahman and Wei, 2006). Hence, the total number of function evaluations required by both versions of the univariate method, in addition to those required for locating the MPP, is $(n-1)N$. When comparing computational efforts by various methods, the number of *original* performance function evaluations is chosen as the primary metric in this paper.

4.4.1 Example Set I: Explicit Performance Functions

4.4.1.1 Example 1 – Elementary Mathematical Functions

Consider a cubic and a quartic performance functions, expressed respectively by (Rahman and Wei, 2005)

$$g(X_1, X_2) = 2.2257 - \frac{0.025\sqrt{2}}{27}(X_1 + X_2 - 20)^3 + \frac{33}{140}(X_1 - X_2) \quad (4.17)$$

and

$$g(X_1, X_2) = \frac{5}{2} + \frac{1}{216}(X_1 + X_2 - 20)^4 - \frac{33}{140}(X_1 - X_2), \quad (4.18)$$

where $X_i \mapsto N(10, 3^2)$, $i = 1, 2$ are independent, Gaussian random variables, each with mean $\mu = 10$ and standard deviation $\sigma = 3$. From an MPP search, $v^* = \{0, 2.2257\}^T$ and $\beta_{HL} = \|v^*\| = 2.2257$ for the cubic function and $v^* = \{0, 2.5\}^T$ and $\beta_{HL} = \|v^*\| = 2.5$ for the quartic function. For both variants of the univariate method, a value of $n = 5$ was selected, resulting 9 function evaluations. Since both performance functions in the rotated Gaussian space are linear in v_2, the proposed method involving Equation (4.16) was employed to calculate the failure probability.

Tables 4.1 and 4.2 show the results of the failure probability calculated by FORM, SORM (Breitung, 1984; Hohenbichler, et al., 1987; Cai and Elishakoff, 1994), MPP-based univariate method with simulation (Rahman and Wei, 2006), proposed MPP-based univariate method with numerical integration, and direct Monte Carlo simulation using 10^6 samples. The univariate method with simulation, which yields exact limit-state

equations in this particular example, predicts the same probability of failure by the direct Monte Carlo simulation. The univariate method with numerical integration also yields exact limit-state equations and predicts very accurate estimates of failure probability when compared with simulation results. A slight difference in the failure probability estimates by two versions of the univariate method is due to approximations involved in Equations (4.5) and (4.13) of the proposed method. Nevertheless, other commonly used reliability methods, such as FORM and SORM, underpredict failure probability by 31 percent and overpredict failure probability by 117 percent when compared with the direct Monte Carlo results. The SORM results are the same as the FORM results, indicating that there is no improvement over FORM for problems involving inflection point (cubic function) or high nonlinearity (quartic function).

4.4.1.2 Example 2 – Burst Margin of a Rotating Disk

Consider an annular disk of inner radius R_i, outer radius R_o, and constant thickness $t \ll R_o$ (plane stress), as shown in Figure 3.3. The disk is subject to an angular velocity ω about an axis perpendicular to its plane at the center. The maximum allowable angular velocity ω_a when tangential stresses through the thickness reach the material ultimate strength S_u factored by a material utilization factor α_m is (Boresi and Schmidt, 2003)

$$\omega_a = \left[\frac{3\alpha_m S_u \left(R_o - R_i \right)}{\rho \left(R_o^{\ 3} - R_i^{\ 3} \right)} \right]^{1/2} , \tag{4.19}$$

where ρ is the mass density of the material. According to an SAE G-11 standard, the satisfactory performance of the disk is defined when the burst margin M_b, defined as

$$M_b \equiv \frac{\omega_a}{\omega} = \left[\frac{3\alpha_m S_u \left(R_o - R_i \right)}{\rho \omega^2 \left(R_o{}^3 - R_i{}^3 \right)} \right]^{1/2} , \qquad (4.20)$$

exceeds a critical threshold of 0.37473 (Penmetsa and Grandhi, 2003). If random

variables $X_1 = \alpha_m$, $X_2 = S_u$, $X_3 = \omega$, $X_4 = \rho$, $X_5 = R_o$, and $X_6 = R_i$, and have their

statistical properties defined in Table 3, the performance function becomes

$$g(X) = M_b(X_1, X_2, X_3, X_4, X_5, X_6) - 0.37473. \qquad (4.21)$$

Table 4.4 presents predicted failure probability of the disk and associated

computational effort using new and existing MPP-based univariate methods, FORM,

Hohenbichler's SORM (Hohenbichler, et al., 1987), and direct Monte Carlo simulation

(10^6 samples). For univariate methods, a value of $n = 7$ was selected. For the univariate

method with numerical integration, failure probabilities based on linear (Equation (4.15))

and quadratic (Equation (4.16)) approximations are almost identical, which verifies the

adequacy of the linear approximation of $y_N(v_N)$ in this example. The results also

indicate that the univariate methods using either simulation or numerical integration

produce the most accurate solution. FORM and SORM slightly underpredict the failure

probability. Both univariate methods surpass the efficiency of SORM in solving this

particular reliability problem.

4.4.1.3 Example 3 – Ten-Bar Truss Structure

A ten-bar, linear-elastic, truss structure, shown in Figure 3.4, was studied in this

example to examine the accuracy and efficiency of the proposed reliability method. The

Young's modulus of the material is 10^7 psi. Two concentrated forces of 10^5 lb are

applied at nodes 2 and 3, as shown in Figure 3.4. The cross-sectional area $X_i, i = 1, \cdots, 10$ for each bar follows truncated normal distribution clipped at $x_i = 0$ and has mean $\mu = 2.5$ in^2 and standard deviation $\sigma = 0.5$ in^2. According to the loading condition, the maximum displacement $[(v_3(X_1, \cdots, X_{10})]$ occurs at node 3, where a permissible displacement is limited to 18 in. Hence, the performance function is $g(X) = 18 - v_3(X_1, \cdots, X_{10})$.

From the MPP search involving finite-difference gradients, the reliability index is $\beta_{HL} = \|v^*\| = 1.3642$. Table 4.5 shows the failure probability of the truss, calculated using the proposed MPP-based univariate method with numerical integration, MPP-based univariate method with simulation (Rahman and Wei, 2006), FORM, three variants of SORM due to Breitung (1984), Hohenbichler (1987) and Cai and Elishakoff (1994), and direct Monte Carlo simulation (10^6 samples). For univariate methods, a value of $n = 7$ was selected. As can be seen from Table 4.5, both versions of the univariate method predict the failure probability more accurately than FORM and all three variants of SORM. This is because univariate methods are able to approximate the performance function more accurately than FORM/SORM. The univariate method with numerical integration involving the quadratic approximation of $y_N(v_N)$ yields slightly more accurate result than that based on its linear approximation. A comparison of the number of function evaluations, also listed in Table 4.5, indicates that the computational effort by the MPP-based univariate methods is slightly larger than FORM, but much less than SORM.

4.4.2 Example Set II: Implicit Performance Functions

4.4.2.1 Example 4 – Mixed-Mode Fracture-Mechanics Analysis

The fourth example involves an isotropic, homogeneous, edge-cracked plate, presented to illustrate mixed-mode probabilistic fracture-mechanics analysis using the proposed univariate method. As shown in Figure 3.5(a), a plate of length $L = 16$ units, width $W = 7$ units is fixed at the bottom and subjected to a far-field and a shear stress τ^∞ applied at the top. The elastic modulus and Poisson's ratio are 1 unit and 0.25, respectively. A plane strain condition was assumed. The statistical property of the random input $X = \left\{ a/W, \tau^\infty, K_{Ic} \right\}^T$ is defined in Table 4.6.

Due to the far-field shear stress τ^∞, the plate is subjected to mixed-mode deformation involving fracture modes I and II (Anderson, 1995). The mixed-mode stress-intensity factors $K_I(X)$ and $K_{II}(X)$ were calculated using an interaction integral (Yau, et al., 1980). The plate was analyzed using the finite-element method involving a total of 832 8-noded, regular, quadrilateral elements and 48 6-noded, quarter-point (singular), triangular elements at the crack-tip, as shown in Figure 3.5(b).

The failure criterion is based on a mixed-mode fracture initiation using the maximum tangential stress theory (Anderson, 1995), which leads to the performance function

$$g(X) = K_{Ic} - \left[K_I(X) \cos^2 \frac{\Theta(X)}{2} - \frac{3}{2} K_{II}(X) \sin \Theta(X) \right] \cos \frac{\Theta(X)}{2}, \qquad (4.22)$$

where K_{Ic} is statistically distributed fracture toughness and $\Theta_c(X)$ is the direction of crack propagation.

Failure probability estimates of $P_F = P[g(X) < 0]$, obtained using the proposed univariate method with numerical integration, univariate method using simulation, FORM, Hohenbichler's SORM, and direct Monte Carlo simulation, are compared in Figure 4.2 and are plotted as a function of $\mathbb{E}[\tau^\infty]$, where $\mathbb{E}$ is the expectation operator. For each reliability analysis (*i.e.*, each point in the plot), FORM and SORM require 29 and 42 function evaluations (finite-element analysis). Using $n = 9$, the MPP-based univariate methods require only 53 (= 29 + 24) function evaluations, whereas 50,000 finite-element analyses were employed in the direct Monte Carlo simulation. The results show that both versions of the univariate method are more accurate than other methods, particularly when the failure probability is low. The computational effort by univariate methods is slightly higher than that by FORM/SORM, but much lower than that by the direct Monte Carlo simulation.

4.4.2.2 Example 5 – Three-Span, Five–Story Frame Structure

The final example examines the accuracy and efficiency of the proposed univariate method for solving reliability problems involving correlated random variables. A three-span, five-story frame structure, originally studied by Liu and Kiureghian (1986), is subjected to horizontal loads, as shown in Figure 4.3. There are totally 21 random variables: (1) three applied loads, (2) two Young's moduli, (3) eight moments of inertia, and (4) eight cross-sectional areas. Tables 4.7-4.9 list the statistical properties of these

variables. The lognormally distributed load variables are independent and all other random variables are assumed to be jointly normal. Failure is defined when the horizontal component of the top floor displacement $u_1(X)$ exceeds 0.2 ft, leading to the limit-state function $g(X) = 0.2 - u_1(X)$.

The MPP-based univariate methods with numerical integration and simulation, FORM, Hohenbichler's SORM, and direct Monte Carlo simulation were employed to estimate the failure probability and are listed in Table 4.10. For the reliability analysis, FORM and SORM require 474 and 1143 function evaluations (frame analysis), respectively. Using $n = 7$, the univariate methods require 595 function evaluations, whereas 1,000,000 frame analyses are needed by the direct Monte Carlo simulation. For the univariate method with numerical integration, the linear approximation of $y_N(v_N)$ was employed. The results clearly show that both versions of the univariate method provide more accurate results than FORM and SORM. In terms of computational effort, the method developed is slightly more expensive than FORM, but significantly more efficient than SORM.

In all numerical examples presented, the number of function evaluations required by both versions of the univariate method is the same. However, the present univariate method developed does not require any Monte Carlo simulation embedded in its previous version. Instead, explicit forms of failure probability requiring only one-dimensional integrations have been formulated. Hence, the new method should be useful in deriving sensitivity (gradients) of failure probability for reliability-based design optimization, which is a subject of current research by the authors.

Table 4.1 Failure probability for cubic performance function

Method	Failure probability	Number of function evaluations[a]
MPP-based univariate method with numerical integration	0.01895	29[b]
MPP-based univariate method with simulation (Rahman and Wei, 2006)	0.01907	29[b]
FORM	0.01302	21
SORM (Hohenbichler et al., 1987)	0.01302	204
Direct Monte Carlo simulation	0.01907	1,000,000

(a) Total number of times the original performance function is calculated.

(b) $21 + (n-1) \times N = 21 + (5-1) \times 2 = 29$

Table 4.2 Failure probability for quartic performance function

Method	Failure probability	Number of function evaluations[a]
MPP-based univariate method with numerical integration	0.003030	29[b]
MPP-based univariate method with simulation (Rahman and Wei, 2006)	0.002886	29[b]
FORM	0.006209	21
SORM (Hohenbichler et al., 1987)	0.006208	212
Direct Monte Carlo simulation	0.002886	1,000,000

(a) Total number of times the original performance function is calculated.

(b) $21 + (n-1) \times N = 21 + (5-1) \times 2 = 29$

Table 4.3 Statistical properties of random input for rotating disk

Random variable	Mean	Standard deviation	Probability distribution
α_m	0.9377	0.0459	Weibull[a]
S_u, ksi	220	5	Gaussian
ω, rpm	24	0.5	Gaussian
ρ, lb-sec^2/in^4	$0.29/g$[b]	$0.0058/g$[b]	Uniform[c]
R_o, in	24	0.5	Gaussian
R_i, in	8	0.3	Gaussian

(a) Scale parameter = 25.508; shape parameter = 0.958

(b) g = 385.82 in/sec^2

(c) Uniformly distributed over (0.28,0.3).

Table 4.4 Failure probability of rotating disk

Method	Failure probability	Number of function evaluations[a]
MPP-based univariate method with numerical integration		
Linear (Equation (4.15))	0.00099	167[b]
Quadratic (Equation (4.16))	0.00099	167[b]
MPP-based univariate method with simulation (Rahman and Wei, 2006)	0.00101	167[b]
FORM	0.00089	131
SORM (Hohenbichler, et al., 1987)	0.00097	378
Direct Monte Carlo simulation	0.00104	1,000,000

(a) Total number of times the original performance function is calculated.

(b) $131 + (n-1) \times N = 131 + (7-1) \times 6 = 167$

Table 4.5 Failure probability of ten-bar truss structure

Method	Failure probability	Number of function evaluations[a]
MPP-based univariate method with numerical integration		
Linear (Equation (4.15))	0.1457	187[b]
Quadratic (Equation (4.16))	0.1400	187[b]
MPP-based univariate method with simulation (Rahman and Wei, 2006)	0.1465	187[b]
FORM	0.0862	127
SORM (Breitung, 1984)	0.1286	506
SORM (Hohenbichler, et al., 1987)	0.1524	506
SORM (Cai and Elishakoff, 1994)	0.1467	506
Direct Monte Carlo simulation	0.1394	1,000,000

(a)   Total number of times the original performance functions is calculated.

(b) $127 + (n-1) \times N = 127 + (7-1) \times 10 = 187$

Table 4.6 Statistical properties of random input for an edge-cracked plate

Random variable	Mean	Standard deviation	Probability distribution
a/W	0.5	0.2309	Uniform[a]
τ^{∞}	Variable [b]	0.1	Gaussian
K_{Ic}	200	0.1	Lognormal

(a) Uniformly distributed over (0.3, 0.7).

(b) Varies from 2.6 to 3.1.

Table 4.7 Frame element properties

Element	Young's modulus	Moment of inertia	Cross-sectional area
B_1	E_4	I_{10}	A_{18}
B_2	E_4	I_{11}	A_{19}
B_3	E_4	I_{12}	A_{20}
B_3	E_4	I_{13}	A_{21}
C_1	E_5	I_6	A_{14}
C_2	E_5	I_7	A_{15}
C_3	E_5	I_8	A_{16}
C_4	E_5	I_9	A_{17}

Table 4.8 Statistical properties of random input for frame structure[a]

Random variable	Mean	Standard deviation	Probability distribution
P_1	30	9	Lognormal
P_2	20	8	Lognormal
P_3	16	6.40	Lognormal
E_4	454,000	40,000	Normal
E_5	497,000	40,000	Normal
I_6	0.94	0.12	Normal
I_7	1.33	0.15	Normal
I_8	2.47	0.30	Normal
I_9	3.00	0.35	Normal
I_{10}	1.25	0.30	Normal
I_{11}	1.63	0.40	Normal
I_{12}	2.69	0.65	Normal
I_{13}	3.00	0.75	Normal
A_{14}	3.36	0.60	Normal
A_{15}	4.00	0.80	Normal
A_{16}	5.44	1.00	Normal
A_{17}	6.00	1.20	Normal
A_{18}	2.72	1.00	Normal
A_{19}	3.13	1.10	Normal
A_{20}	4.01	1.30	Normal
A_{21}	4.50	1.50	Normal

(a) The units of P_i, E_i, I_i, and A_i are kip, kip/ft^2, ft^4, and ft^2, respectively.

Table 4.9 Correlation coefficients of random input for frame structure

	P_1	P_2	P_3	E_4	E_5	I_6	I_7	I_8	I_9	I_{10}	I_{11}	I_{12}	I_{13}	A_{14}	A_{15}	A_{16}	A_{17}	A_{18}	A_{19}	A_{20}	A_{21}
P_1	1.0																				
P_2	0.	1.0																			
P_3	0.	0.	1.0																		
E_4	0.	0.	0.	1.0																	
E_5	0.	0.	0.	0.9	1.0																
I_6	0.	0.	0.	0.	0.	1.0															
I_7	0.	0.	0.	0.	0.	0.13	1.0														
I_8	0.	0.	0.	0.	0.	0.13	0.13	1.0													
I_9	0.	0.	0.	0.	0.	0.13	0.13	0.13	1.0												
I_{10}	0.	0.	0.	0.	0.	0.13	0.13	0.13	0.13	1.0											
I_{11}	0.	0.	0.	0.	0.	0.13	0.13	0.13	0.13	0.13	1.0										
I_{12}	0.	0.	0.	0.	0.	0.13	0.13	0.13	0.13	0.13	0.13	1.0									
I_{13}	0.	0.	0.	0.	0.	0.13	0.13	0.13	0.13	0.13	0.13	0.13	1.0								
A_{14}	0.	0.	0.	0.	0.	0.13	0.13	0.13	0.13	0.13	0.13	0.13	0.13	1.0							
A_{15}	0.	0.	0.	0.	0.	0.95	0.95	0.13	0.13	0.13	0.13	0.13	0.13	0.13	1.0						
A_{16}	0.	0.	0.	0.	0.	0.13	0.13	0.95	0.13	0.13	0.13	0.13	0.13	0.13	0.13	1.0					
A_{17}	0.	0.	0.	0.	0.	0.13	0.13	0.13	0.95	0.13	0.13	0.13	0.13	0.13	0.13	0.13	1.0				
A_{18}	0.	0.	0.	0.	0.	0.13	0.13	0.13	0.13	0.95	0.13	0.13	0.13	0.13	0.13	0.13	0.13	1.0			
A_{19}	0.	0.	0.	0.	0.	0.13	0.13	0.13	0.13	0.13	0.95	0.13	0.13	0.13	0.13	0.13	0.13	0.13	1.0		
A_{20}	0.	0.	0.	0.	0.	0.13	0.13	0.13	0.13	0.13	0.13	0.95	0.95	0.13	0.13	0.13	0.13	0.13	0.13	1.0	
A_{21}	0.	0.	0.	0.	0.	0.13	0.13	0.13	0.13	0.13	0.13	0.13	0.95	0.13	0.13	0.13	0.13	0.13	0.13	0.13	1.0

Table 4.10 Failure probability of frame structure

Method	Failure Probability	Number of function evaluations[a]
MPP-based univariate method with numerical integration	3.829×10^{-4}	600[b]
MPP-based univariate method with simulation (Rahman and Wei, 2006)	3.720×10^{-4}	600[b]
FORM	7.891×10^{-4}	474
SORM (Hohenbichler, et al., 1987)	1.402×10^{-4}	1,143
Direct Monte Carlo simulation	3.630×10^{-4}	1,000,000

(a) Total number of times the original performance functions is calculated.

(b) $474 + (n-1) \times N = 474 + (7-1) \times 21 = 600$
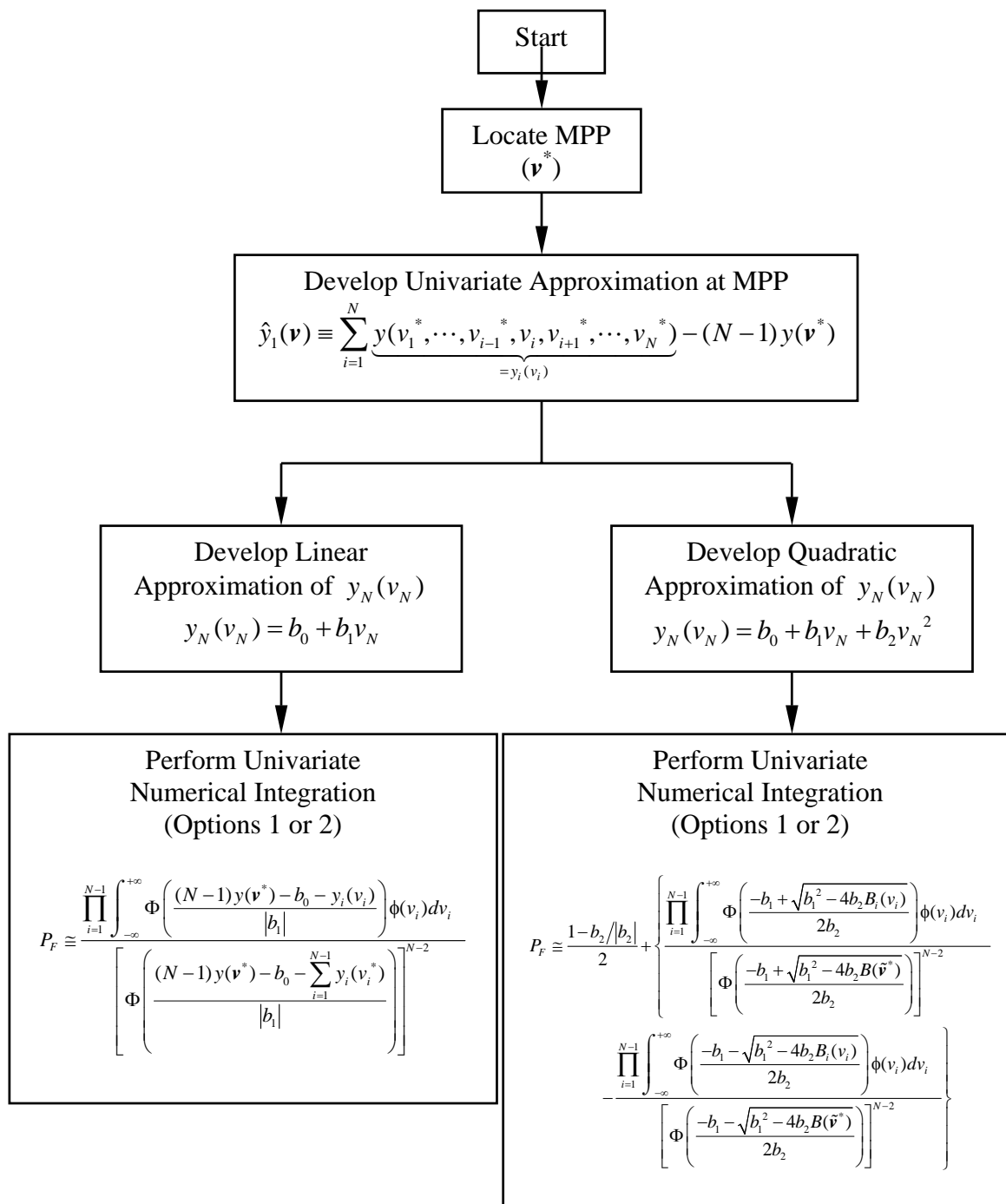
Figure 4.1 Flowchart of the MPP-based univariate method with numerical integration

The flowchart consists of the following boxes:

Start

↓

Locate MPP ($\boldsymbol{v}^*$)

↓

Develop Univariate Approximation at MPP

$$\hat{y}_1(\boldsymbol{v}) \equiv \sum_{i=1}^{N} \underbrace{y(v_1^*, \cdots, v_{i-1}^*, v_i, v_{i+1}^*, \cdots, v_N^*)}_{= y_i(v_i)} - (N-1)y(\boldsymbol{v}^*)$$

Branches into two:

Develop Linear Approximation of $y_N(v_N)$

$$y_N(v_N) = b_0 + b_1 v_N$$

↓

Perform Univariate Numerical Integration (Options 1 or 2)

$$P_F \cong \frac{\prod_{i=1}^{N-1} \int_{-\infty}^{+\infty} \Phi\left(\dfrac{(N-1)y(\boldsymbol{v}^*) - b_0 - y_i(v_i)}{|b_1|}\right)\phi(v_i)dv_i}{\left[\Phi\left(\dfrac{(N-1)y(\boldsymbol{v}^*) - b_0 - \sum_{i=1}^{N-1} y_i(v_i^*)}{|b_1|}\right)\right]^{N-2}}$$

Develop Quadratic Approximation of $y_N(v_N)$

$$y_N(v_N) = b_0 + b_1 v_N + b_2 v_N^2$$

↓

Perform Univariate Numerical Integration (Options 1 or 2)

$$P_F \cong \frac{1 - b_2/|b_2|}{2} + \left\{ \frac{\prod_{i=1}^{N-1} \int_{-\infty}^{+\infty} \Phi\left(\dfrac{-b_1 + \sqrt{b_1^2 - 4b_2 B_i(v_i)}}{2b_2}\right)\phi(v_i)dv_i}{\left[\Phi\left(\dfrac{-b_1 + \sqrt{b_1^2 - 4b_2 B(\tilde{\boldsymbol{v}}^*)}}{2b_2}\right)\right]^{N-2}} \right.$$

$$\left. - \frac{\prod_{i=1}^{N-1} \int_{-\infty}^{+\infty} \Phi\left(\dfrac{-b_1 - \sqrt{b_1^2 - 4b_2 B_i(v_i)}}{2b_2}\right)\phi(v_i)dv_i}{\left[\Phi\left(\dfrac{-b_1 - \sqrt{b_1^2 - 4b_2 B(\tilde{\boldsymbol{v}}^*)}}{2b_2}\right)\right]^{N-2}} \right\}$$

Figure 4.2 Probability of fracture initiation in an edge-cracked plate
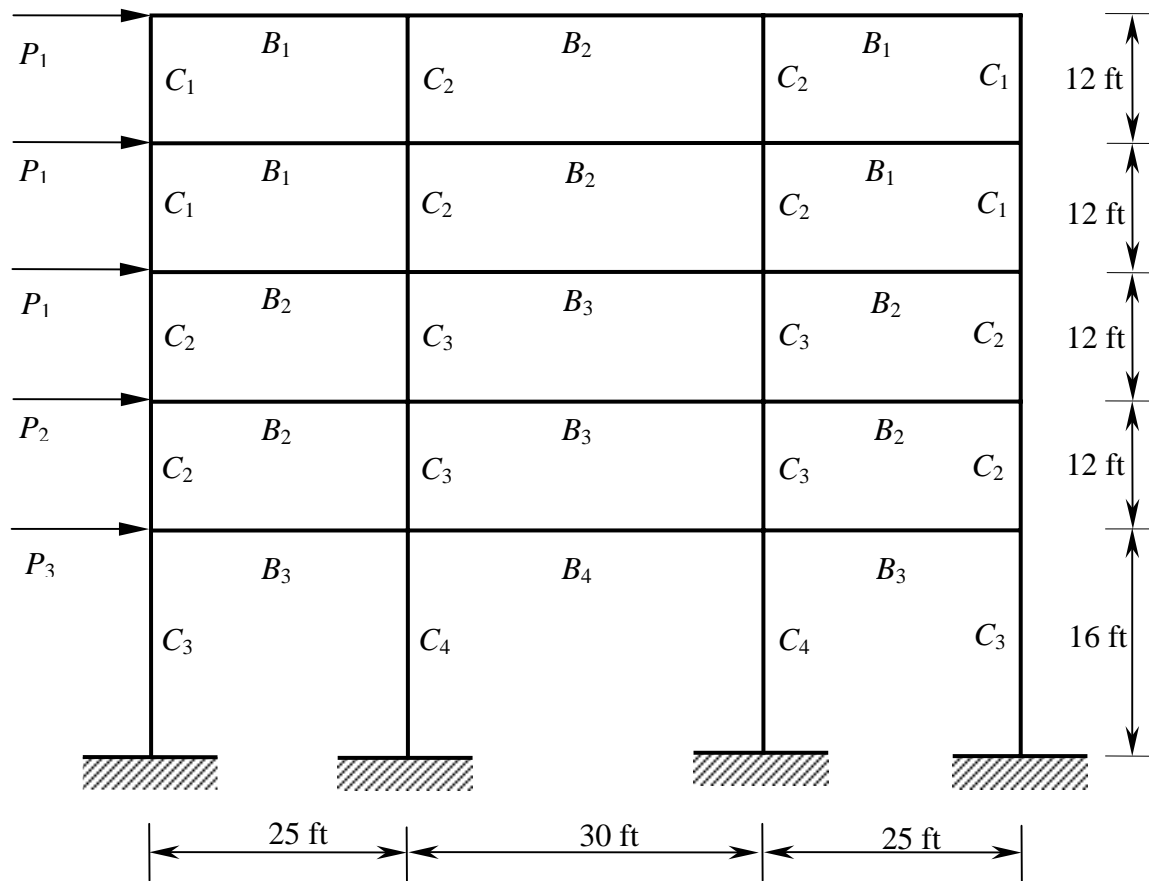
Figure 4.3 A three-span, five-story frame structure subjected to lateral loads

CHAPTER 5

MULTIPLE MPP PROBLEMS

This chapter presents extension of the univariate method for multiple most probable point (MPP) problems. If all MPPs can be identified, and a high nonlinearity exists in a limit state around some or all of these MPPs, then existing analytical methods, such as multipoint FORM/SORM, and simulation-based methods may not be accurate or provide computationally efficient solutions. It has been demonstrated that the MPP-based univariate decomposition method (Chapters 3 and 4) is more accurate than analytical methods, and more efficient than simulation methods. In this chapter, an integrated decomposition method with the barrier method to locate all MPPs, is proposed as a new strategy to solve multiple MPP problems. The barrier method is described in Appendix C.

5.1 Performance Function Decomposition at the *m*th MPP

Consider a continuous, differentiable, real-valued performance function $g(\boldsymbol{x})$ that depends on $\boldsymbol{x} = \{x_1, \cdots, x_N\}^T \in \mathbb{R}^N$. The transformed limit state $h(\boldsymbol{u}) = 0$ is the map of $g(\boldsymbol{x}) = 0$ in the standard Gaussian space (*u* space), as shown in Figure 5.1 for $N = 2$. Let the performance function contain M number of MPPs $\boldsymbol{u}_1^*, \cdots, \boldsymbol{u}_M^*$ with corresponding distances $\beta_1, \cdots, \beta_M$, as shown in Figure 5.1.

For the *m*th MPP, define an associated local coordinate system $\boldsymbol{v}_m = \{v_{m,1}, \cdots, v_{m,N}\}$, where $v_{m,N}$ is the coordinate in the direction of the MPP, as depicted in Figure 5.1. In the $\boldsymbol{v}_m$ space, denote the *m*th MPP by $\boldsymbol{v}_m^* = \{0, \cdots, 0, \beta_m\}$ and the

performance function by $y_m(\boldsymbol{v}_m) = 0$, which is also a map of the original limit state

$g(\boldsymbol{x}) = 0$. A decomposition of a general multivariate function $y_m(\boldsymbol{v}_m)$, described by

$$y_m(\boldsymbol{v}_m) = \underbrace{\underbrace{y_{m,0} + \sum_{i=1}^{N} y_{m,i}(v_{m,i})}_{=\hat{y}_{m,1}(\boldsymbol{v}_m)} + \sum_{\substack{i_1,i_2=1 \\ i_1<i_2}}^{N} y_{m,i_1 i_2}(v_{m,i_1}, v_{m,i_2})}_{=\hat{y}_{m,2}(\boldsymbol{v}_m)} + \cdots + y_{m,12\cdots N}(v_{m,1}, \cdots, v_{m,N}) \quad (5.1)$$

can be viewed as a finite hierarchical expansion of an output function in terms of its input

variables with increasing dimension, where $y_{m,0}$ is a constant, $y_{m,i}(v_{m,i}) : \mathbb{R} \mapsto \mathbb{R}$ is a

univariate component function representing individual contribution to $y_m(\boldsymbol{v}_m)$ by input

variable $v_{m,i}$ acting alone, $y_{m,i_1 i_2}(v_{m,i_1}, v_{m,i_2}) : \mathbb{R}^2 \mapsto \mathbb{R}$ is a bivariate component function

describing cooperative influence of two input variables v_{m,i_1} and v_{m,i_2}, and so on. If

$$\hat{y}_{m,S}(\boldsymbol{v}_m) = y_{m,0} + \sum_{i=1}^{N} y_{m,i}(v_{m,i}) + \sum_{\substack{i_1,i_2=1 \\ i_1<i_2}}^{N} y_{m,i_1 i_2}(v_{m,i_1}, v_{m,i_2}) + \cdots + \sum_{\substack{i_1,\cdots,i_S=1 \\ i_1<\cdots<i_S}}^{N} y_{m,i_1\cdots i_S}(v_{m,i_1}, \cdots, v_{m,i_S}) \quad (5.2)$$

represents a general S-variate approximation of $y_m(\boldsymbol{v}_m)$, the univariate ($S = 1$)

approximation $\hat{y}_{m,1}(\boldsymbol{v}_m)$ provides a two-term approximant of the finite decomposition in

Equation (5.1). Similarly, bivariate, trivariate, and other higher-variate approximations

can be derived by appropriately selecting the value of S. The fundamental conjecture

underlying this work is that component functions arising in the function decomposition

will exhibit insignificant S-variate effects cooperatively when $S \to N$, leading to useful

lower-variate approximations of $y_m(\boldsymbol{v}_m)$. In the limit, when $S = N$, $\hat{y}_{m,1}(\boldsymbol{v}_m)$ converges

to the exact function $y_m(\boldsymbol{v}_m)$. In other words, Equation (5.2) generates a hierarchical and

convergent sequence of approximations of $y_m(\boldsymbol{v}_m)$. Readers interested in the

fundamental development of the decomposition method are referred to authors' past work.

5.2 Multi-Point Univariate Decompostion Method

5.2.1 Univariate Decomposition of Performance Function

At the mth MPP, consider a univariate ($S = 1$) approximation of $y_m(\boldsymbol{v}_m)$, denoted by

$$\hat{y}_{m,1}(\boldsymbol{v}_m) \equiv \hat{y}_{m,1}(v_{m,1},\cdots,v_{m,N}) = \sum_{i=1}^{N} \underbrace{y_m(0,\cdots,0,v_{m,i},0,\cdots,\beta_m)}_{=y_{m,i}(v_{m,i})} \underbrace{-(N-1)y_m(\boldsymbol{v}_m^*)}_{=y_{m,0}}, \quad (5.3)$$

where $y_m(\boldsymbol{v}_m^*) \equiv y_m(0,\cdots,0,\beta_m)$ and $y_{m,i}(v_{m,i}) \equiv y_m(0,\cdots,0,v_{m,i},0,\cdots,\beta_m)$. Using a multivariate function theorem, it can be shown that the univariate approximation $\hat{y}_{m,1}(\boldsymbol{v}_m)$ leads to the residual error $y_m(\boldsymbol{v}_m) - \hat{y}_{m,1}(\boldsymbol{v}_m)$, which includes contributions from terms of dimension two and higher. For a sufficiently smooth $y_m(\boldsymbol{v}_m)$ with a convergent Taylor series, the coefficients associated with higher-dimensional terms are usually much smaller than that with one-dimensional terms. As such, higher-dimensional terms contribute less to the function, and therefore, can be neglected. Nevertheless, Equation (5.3) includes all higher-order *univariate* terms. In contrast, FORM and SORM also entail univariate approximations, but retain only *linear* and *quadratic univariate* terms, respectively. Hence, Equation (5.3) should provide in general a higher-order approximation of the performance function than those by commonly employed FORM/SORM.

5.2.2 Lagrange Interpolation and Return Mapping

Consider the univariate component function $y_{m,i}(v_{m,i}) \equiv y_m(0,\cdots,0,v_{m,i},0,\cdots,\beta_m)$

in Equation (5.3). If for sample points $v_{m,i} = v_{m,i}{}^{(j)}; j = 1,\cdots,n$, n function values

$A_{mi,j} \equiv y_m(0,\cdots,0,v_{m,i}{}^{(j)},0,\cdots,\beta_m)$; $j = 1,\cdots,n$ are given, the function value for an

arbitrary $v_{m,i}$ can be obtained by the Lagrange interpolation

$$y_{m,i}(v_{m,i}) = \sum_{j=1}^{n} \phi_j(v_{m,i}) y_m(0,\cdots,0,v_{m,i}{}^{(j)},0,\cdots,\beta_m) = \sum_{j=1}^{n} A_{mi,j}\phi_j(v_{m,i}), \quad (5.4)$$

where

$$\phi_j(v_{m,i}) = \frac{\displaystyle\prod_{k=1,k\neq j}^{n} \left(v_{m,i} - v_{m,i}{}^{(k)}\right)}{\displaystyle\prod_{k=1,k\neq j}^{n} \left(v_{m,i}{}^{(j)} - v_{m,i}{}^{(k)}\right)} \quad (5.5)$$

is the shape function. By using Equations (5.4) and (5.5), arbitrarily many values of

$y_i(v_{m,i})$ can be generated if n values of that component function are given. The same

procedure is repeated for all univariate component functions, *i.e.*, for all

$y_{m,i}(v_{m,i})$, $i = 1,\cdots,N$, leading to an explicit univariate approximation

$$\hat{y}_{m,1}(\boldsymbol{V}_m) \cong \sum_{i=1}^{N} \sum_{j=1}^{n} A_{mi,j}\phi_j(V_{m,i}) - (N-1)A_{m,0}, \quad (5.6)$$

where $A_{m,0} \equiv y_m(\boldsymbol{v}_m{}^*)$. By developing similar decompositions at all MPPs (*i.e.*, for all

$m = 1,\cdots,M$), univariate approximations $\hat{y}_{1,1}(\boldsymbol{V}_1),\cdots,\hat{y}_{M,1}(\boldsymbol{V}_M)$ associated with M number

of MPPs can be generated.

The functions $\hat{y}_{1,1}(\boldsymbol{V}_1),\cdots,\hat{y}_{M,1}(\boldsymbol{V}_M)$ represent M local approximations in vicinities

of MPPs $\boldsymbol{v}_1{}^*,\cdots,\boldsymbol{v}_M{}^*$ of $\boldsymbol{v}_1,\cdots,\boldsymbol{v}_M$ spaces, respectively. To describe these approximations

in a common space, such as the u space, consider a return mapping $u = R_m v_m$, where $R_m = [R_{m,ik}]$; $i, k = 1, \cdots, N$ is an $N \times N$ orthogonal rotation matrix associated with the mth MPP. Consequently, M local approximations of the performance function in the u space become

$$\hat{h}_{m,1}(U) = \sum_{i=1}^{N} \sum_{j=1}^{n} A_{mi,j} \phi_j \left(\sum_{k=1}^{N} R_{m,ki} U_k \right) - (N-1) A_{m,0}; \; m = 1, \cdots, M , \quad (5.7)$$

as schematically depicted in Figure 5.1. Therefore, the actual failure domain, defined by

$$\Omega_F \equiv \left\{ x : g(x) < 0 \right\} = \left\{ u : h(u) < 0 \right\} \quad (5.8)$$

and represented by the shaded area in Figure 5.1 can be approximated by a union of M failure sub-domains $\hat{h}_{1,1}(u) < 0, \cdots, \hat{h}_{M,1}(u) < 0$, thereby yielding the univariate approximation

$$\hat{\Omega}_F = \left\{ u : \bigcup_{m=1}^{M} \hat{h}_{m,1}(u) < 0 \right\} . \quad (5.9)$$

Note that the boundary of the failure domain $\hat{\Omega}_F$ can be highly nonlinear, which depends on how $\hat{y}_{m,1}(v_m)$ or $\hat{h}_{m,1}(u)$ are constructed. In contrast, FORM/SORM produce only multi-linear or multi-quadratic boundaries, also plotted in Figure 5.1. Therefore, the failure domain defined by Equation (5.9) with a Lagrange interpolation order $n > 2$ should provide a higher-order approximation than that by the multi-point FORM/SORM.

5.2.3 Monte Carlo Simulation

Once the Lagrange shape functions $\phi_j(v_{m,i})$ and deterministic coefficients $A_{mi,j}$; $j = 1, \cdots, n$ are generated for all $i = 1, \cdots, N$ and $m = 1, \cdots, M$, Equation (5.7)

provides explicit local approximations of the performance function in terms of the random input U. Therefore, any probabilistic characteristics of a response, including its moments and probability density function, can be easily evaluated by performing Monte Carlo simulation on Equation (5.7). For a component reliability analysis, the Monte Carlo estimate of the failure probability employing the proposed univariate approximation is

$$P_F \cong P\left(U \in \hat{\Omega}_F\right) \cong \frac{1}{N_S} \sum_{l=1}^{N_S} \mathbb{I}\left[\bigcup_{m=1}^{M} \hat{h}_{m,1}(u^{(l)}) < 0\right], \qquad (5.10)$$

where $u^{(l)}$ is the lth realization of U, N_S is the sample size, and $\mathbb{I}[\cdot]$ is an indicator function such that $\mathbb{I} = 1$ if $u^{(l)}$ is in the failure set (*i.e.*, when $u^{(l)} \in \hat{\Omega}_F$) and *zero* otherwise. Since Equations (5.7) and (5.9) are explicit and do not require additional numerical evaluations of response (*e.g.*, solving governing equations by expensive finite element analysis), the embedded Monte Carlo simulation can be efficiently conducted for any sample size.

The proposed method involving multi-point univariate approximation, *n*-point Lagrange interpolation, and Monte Carlo simulation is defined as the *multi-point univariate decomposition method* in this paper. Figure 5.2 shows the computational flowchart of the method developed.

5.3 Computational Effort

The multi-point univariate decomposition method requires evaluation of coefficients $A_{m,0} = y_m(v_m^*)$ and $A_{mi,j} = y_m(0, \cdots, 0, v_{m,i}^{(j)}, 0, \cdots, \beta_m)$; for $j = 1, \cdots, n$; $i = 1, \cdots, N$ and $m = 1, \cdots, M$. Hence, the computational effort required by the proposed

method can be viewed as numerically evaluating the original performance function at several deterministic input defined by user-selected sample points. For each MPP, there are n numerical evaluations of $y_m(\mathbf{v}_m)$ involved in Equation (5.4). Therefore, the total cost for the multi-point univariate method entails a *maximum* of $M[nN+1]$[1] function evaluations in addition to those required for locating all MPPs. If the sample points include a common point in each coordinate (see the forthcoming section), the number of function evaluations reduces to $M[(n-1)N+1]$.

5.4 Numerical Examples

Three numerical examples involving explicit performance functions from mathematical problems (Examples 1 and 2) and an implicit performance function from a structural dynamics problem (Example 3) are presented to illustrate the multi-point univariate decomposition method. Comparisons have been made with existing multi-point FORM/SORM and direct Monte Carlo simulation to evaluate the accuracy and efficiency of the new method. For the multi-point univariate decomposition method, n (= 3 or 5) uniformly distributed points $v_{m,i}^* - (n-1)/2, v_{m,i}^* - (n-3)/2, \cdots, v_{m,i}^*, \cdots, v_{m,i}^* + (n-3)/2, v_{m,i}^* + (n-1)/2$ were deployed at the $v_{m,i}$-coordinate of the mth MPP, leading to $M[(n-1)N+1]$ function evaluations in addition to those required for locating all MPPs. A barrier method developed by Der Kiureghian and Dakessian (1998) and the Hasofer-Lind-Rackwitz-Fiessler algorithm (Rackwitz, 2001) were employed to find multiple MPPs. The multi-

---

[1] The numeric 1 inside the parenthesis is due to a function evaluation $A_{m,0} = y_m(\mathbf{v}_m^*)$. It should be removed if an MPP search algorithm already has the information.

point FORM/SORM also involved Monte Carlo estimates of the failure probability using their respective approximate failure domains. When comparing computational efforts by various methods, the number of *original* performance function evaluations is selected as the primary metric in this paper.

5.4.1. Example 1 – Mathematical Functions with Gaussian Random Variables

Consider the performance function

$$g(X) = A + B(X_1 + D)^p - C(X_1 + D)^2 - X_2, \qquad (5.11)$$

where $X = \{X_1, X_2\}^T \in \mathbb{R}^2$ is a bivariate standard Gaussian random vector with the mean vector $\mu_X \equiv \mathbb{E}[X] = 0 \in \mathbb{R}^2$ and the covariance matrix $\Sigma_X \equiv \mathbb{E}[(X - \mu_X)(X - \mu_X)^T] = I \in \mathbb{R}^{2 \times 2}$; A, B, C, D are real-valued deterministic parameters; and p is an integer-valued deterministic parameter. By appropriately selecting these deterministic parameters, component reliability problems involving a single MPP or multiple MPPs can be constructed. Three cases involving quadratic, cubic, and quartic functions, each containing two MPPs, were studied, as follows.

Case I: $A = 5$, $B = 0.5$, $C = 1$, $D = -0.1$, $p = 2$ (Quadratic): For Case I, the quadratic limit-state surface has two MPPs: $u_1^* = (2.916, 1.036)$ with the Hasofer-Lind reliability index $\beta_1 = 3.094$, and $u_2^* = (-2.741, 0.966)$ with the index $\beta_2 = 2.906$, as shown in Figure 5.3. The failure probability was estimated by the proposed univariate method ($n = 3$), FORM, curvature- and point-fitted SORM, and direct Monte Carlo simulation (10^6 samples). The results considering either one MPP (single-point) or two MPPs (multi-point) and

associated computational efforts are listed in Table 5.1. Compared with the benchmark result of the Monte Carlo simulation, all single-point methods generate a large amount of error regardless of whether univariate, FORM, and SORM are employed. This is because both MPPs have significant contributions to the failure probability. Therefore, when two MPPs are accounted for, the proposed multi-point univariate method ($P_F \cong 0.00308$) and both variants of the multi-point SORM ($P_F \cong 0.00291$ and 0.00304) yield highly accurate results. The multi-point FORM ($P_F \cong 0.00276$), which slightly underpredicts the failure probability, is also fairly accurate. This is because, errors in approximating failure domains by various methods occur far away from the origin. Since the performance function is parabolic, no meaningful difference was observed between the results of the multi-point univariate method and the multi-point SORM. However, a comparison of computational efforts shows slightly or significantly better efficiency of the proposed univariate method when compared with the point-fitted or the curvature-fitted SORM, respectively.

Case II: $A = 5$, $B = 0.5$, $C = 1.5$, $D = 2$, $p = 3$ (Cubic): As shown in Figure 5.4, the limit-state surface for Case II also has two MPPs: $\boldsymbol{u}_1^* = (0,3)$ with $\beta_1 = 3$, and $\boldsymbol{u}_2^* = (-3.431, 0.466)$ with $\beta_2 = 3.462$. Table 5.2 presents similar comparisons of results and computational efforts by various methods stated earlier. For the univariate method, a value of $n = 5$ was selected to capture higher-order terms of the performance function. The results obtained from single-point and multi-point methods show a similar trend as in Case I. However, since the performance function in this case takes on a cubic form, the multi-point SORM no longer predicts highly accurate results as in Case I. Compared

with the Monte Carlo simulation (10^6 samples), the multi-point FORM overestimates the failure probability by 132 percent and the multi-point SORM underestimates the failure probability by 9 percent. Since the performance function is a univariate function (u space) and the first MPP lies on the u_2 axis (*i.e*, no rotation), the single-point univariate approximation at that MPP and the multi-point univariate approximation yield the exact failure domain. Hence, both single-point (first MPP) and multi-point univariate methods predict the same failure probability estimated by the direct Monte Carlo simulation. The multi-point univariate method is more accurate than either variant of the multi-point SORM and requires only a little more computational effort than the multi-point FORM.

Case III: $A = 3$, $B = 2$, $C = 1$, $D = -0.1$, $p = 4$ (Quartic): The final case involves a quartic limit-state function that also has two MPPs, as shown in Figure 5.5. The MPPs are: $u_1^* = (0.544, 2.881)$ with $\beta_1 = 2.932$, and $u_2^* = (-0.364, 2.877)$ with $\beta_2 = 2.9$. The failure probability estimates by various methods and their computational efforts are listed in Table 5.3. For the univariate method, a value of $n = 5$ was selected. Due to higher nonlinearity of the performance function in Case III than that in Cases I and II, the multi-point FORM/SORM fail to provide an accurate solution. Compared with the benchmark result of the Monte Carlo simulation (10^6 samples), the errors in calculating the failure probability by the multi-point FORM and the multi-point SORM are 139 and 23-26 percent, respectively. The multi-point univariate method is more accurate (error $\cong 2$ percent) than the multi-point FORM/SORM with a computational effort slightly higher than that required by the multi-point FORM. The higher accuracy of the univariate method is attributed to a higher-order approximation of the failure boundary that permits

an accurate representation of the flat region between two MPPs (see Figure 5.5). The underprediction of the multi-point SORM is due to its second-order approximation, which cannot capture the flatness of the failure boundary in that region. Although the multi-point FORM approximates that flat region well, it fails to capture the nonlinearity of the performance function on other sides of the MPPs, leading to a significant overprediction of the failure probability. Additional cases entailing higher-order nonlinearity of the performance function can be created in a similar manner to show a progressive loss of accuracy by the multi-point FORM/SORM.

The results of Cases I-III demonstrate that the multi-point univariate method can consistently handle higher-order reliability problems with multiple MPPs. For all three cases, the boundaries of failure domains plotted in Figures 5.3-5.5 indicate that the univariate method yields a better approximation than FORM/SORM, especially when the performance function is highly nonlinear. The point-fitted multi-point SORM exhibits a similar computational efficiency of the multi-point univariate method, because the analysis performed is only two-dimensional. For higher-dimensional reliability problems, the computational effort by the point-fitted SORM should grow larger than that by the univariate method. Nevertheless, the results of the multi-point SORM (curvature- or point-fitted), which captures at most a second-order approximation, should be carefully interpreted when a reliability problem is highly nonlinear.

5.4.2 Example 2 – Mathematical Function with Non-Gaussian Random Variables

A well-known performance function, originally introduced by Hohenbichler and Rackwitz (1981) and subsequently discussed by others (Madsen, 1986; Der Kiureghian, et al., 1998), is

$$g(X) = 18 - 3X_1 - 2X_2, \tag{5.12}$$

where $X = \{X_1, X_2\}^T \in \mathbb{R}^2$ is a bivariate random vector with the joint cumulative probability distribution function

$$F_{X_1 X_2}(x_1, x_2) = \begin{cases} 1 - \exp(-x_1) - \exp(-x_2) + \exp[-(x_1 + x_2 + x_1 x_2)], & x_1, x_2 \geq 0 \\ 0, & \text{otherwise} \end{cases}. \tag{5.13}$$

Due to the symmetry in Equation (5.13) between x_1 and x_2, there are two distinct Rosenblatt transformations (1952) depending on the ordering of variables $\{x_1, x_2\}$ and $\{x_2, x_1\}$, which lead to mappings

$$T_1 \equiv (x_1, x_2) \rightarrow (u_1, u_2) : \begin{cases} u_1 = \Phi^{-1}\{1 - \exp(-x_1)\} \\ u_2 = \Phi^{-1}\{1 - (1 + x_2)\exp[-x_2(1 + x_1)]\} \end{cases} \tag{5.14}$$

and

$$T_2 \equiv (x_2, x_1) \rightarrow (u_1, u_2) : \begin{cases} u_1 = \Phi^{-1}\{1 - \exp(-x_2)\} \\ u_2 = \Phi^{-1}\{1 - (1 + x_1)\exp[-x_1(1 + x_2)]\} \end{cases}, \tag{5.15}$$

respectively, where $\Phi(u) = \int_{-\infty}^{u} (1/\sqrt{2\pi})\exp(-\xi^2/2)d\xi$ is the cumulative distribution function of a standard Gaussian random variable. Due to the nonlinearity of transformations, the linear limit-state surface in the x space becomes nonlinear functions in the u space, as depicted in Figures 5.6(a) and 5.6(b) for transformations T_1 and T_2, respectively.

Regardless of the transformation, each limit-state surface possesses two distinct MPPs which are: $u_1^* = (2.782, 0.0865)$ with $\beta_1 = 2.784$, and $u_2^* = (-1.296, 3.253)$ with $\beta_2 = 3.501$ for transformation T_1; and $u_1^* = (-1.124, 2.399)$ with $\beta_1 = 2.649$, and

$u_2^* = (3.630, 0.142)$ with $\beta_2 = 3.633$ for transformation T_2.   The univariate decomposition method and FORM/SORM entailing single and multiple MPPs were applied to obtain estimates of the failure probability, which are presented in Tables 5.4 and 5.5 for transformations T_1 and T_2, respectively. Also listed is the reference solution obtained by the direct Monte Carlo simulation involving 10^6 samples. For the univariate method, a value of $n = 3$ was selected. The tabulated results indicate that the failure probability estimates based on a single MPP strongly depend on the selected transformation and the particular MPP that is found. If an optimization algorithm can find only one (*e.g.*, the second MPP) of these two MPPs, results based on that MPP may contain significant errors regardless of the reliability method employed. The multi-point FORM using the transformation T_1 yields an excellent result, but also produces an erroneous result when the transformation T_2 is chosen. In contrast, the multi-point univariate method and the multi-point curvature-fitted SORM yield excellent estimates of the failure probability regardless of the transformation invoked. The maximum errors by the multi-point univariate method, multi-point FORM, and multi-point SORM are 1.7, 40.9, and 2.7 percent, respectively. Although the univariate method and SORM have comparable accuracies, the multi-point univariate method is more computationally efficient than the multi-point SORM.

5.4.3 Example 3 – Seismic Dynamics of a Ten-Story Building-TMD System

In this example, consider a 10-story shear building subjected to seismic ground motion with a tuned mass damper (TMD) placed on the roof, as shown in Figure 5.7. A similar problem has been discussed by Der Kiureghian and Dakessian (1998) and Gupta

and Manohar (2004). The building has random floor masses M_i, $i = 1, \cdots, 10$ and random story stiffness K_i, $i = 1, \cdots, 10$. The TMD has a random mass M_0 and random stiffness K_0. The combined system has random modal damping ratios ζ_i, $i = 0, \cdots, 10$. The input motion is defined by a pseudo-acceleration response spectrum $A(T, \zeta) = SH(\zeta) a(T)$, where T is the period, $S = 0.61$ is a scale factor, $H(\zeta)$ is a damping–dependent correction factor defined by the *Applied Technology Council* (US Army Corps Engineering, 1995), and $a(T)$ is the pseudo-acceleration response spectrum shape for a 5 percent damping, as shown in Figure 5.8. The TMD is effective in reducing the dynamic response of the building over a narrow band of frequencies, providing best results when its natural frequency $\omega_0 = \sqrt{k_0/m_0}$ is perfectly tuned to the fundamental frequency of the building. In reality, due to uncertainties in mass, stiffness, and damping properties, perfect tuning between the TMD and the building may not occur. As a result, the TMD can be over-tuned or under-tuned, leading to two distinct MPPs when conducting reliability analysis of a combined building-TMD system.

For the present reliability analysis, consider the limit-state function

$$g(X) = V_0 - V_{\text{base}}(X), \tag{5.16}$$

where $X = \{M_0, M_1, \cdots, M_{10}, K_0, K_1, \cdots, K_{10}, \zeta_0, \zeta_1, \cdots, \zeta_{10}\}^T \in \mathbb{R}^{33}$ is a random vector consisting of 33 independent random variables, $V_{\text{base}}(X)$ is the base shear response of the building which is an implicit function of X, and $V_0 = 1000 \text{ kip}$ is an allowable threshold. Each of these random variable is lognormally distributed with respective means and coefficients of variations listed in Table 5.6. The base shear is computed by

combining modal responses of the 11-DOF building-TMD system using the CQC rule (Clough, 1993). Each realization of *X* involves an eigenvalue analysis of the system, the computation of the modal contributions to the base shear, and their combination according to the CQC rule.

Starting from the mean input, the first MPP was found with a value of the Hasofer-Lind reliability index $\beta_1 = 1.137$ (over-tuned). The second MPP was located with the corresponding index $\beta_2 = 1.846$ (under-tuned). Table 5.7 summarizes various estimates of the failure probability, based on single- and multi-point univariate decomposition method and FORM/SORM. These results are compared with the solution using the direct Monte Carlo simulation employing 5000 samples. For the univariate method, a value of $n = 3$ was selected. Failure probability estimates by all methods that are based on a single MPP improve when both MPPs are considered. Both the multi-point SORM (curvature-fitted) and multi-point univariate method provide very accurate results. However, by comparing the number of function evaluations, also listed in Table 5.7, the multi-point univariate decomposition method is more computationally efficient than the multi-point SORM.

Table 5.1 Failure probability for quadratic function in Example 1 (Case I)

MPP	Reliability Method	Failure probability	Number of function evaluations[a]
1st MPP $(\boldsymbol{u}_1^*)$	Single-point univariate method	0.00202	45
	Single-point FORM	0.00183	41
	Single-point SORM (curvature-fitted)	0.00195	186
	Single-point SORM (point-fitted)	0.00197	49
2nd MPP $(\boldsymbol{u}_2^*)$	Single-point univariate method	0.00113	50
	Single-point FORM	0.000987	46
	Single-point SORM (curvature-fitted)	0.00106	191
	Single-point SORM (point-fitted)	0.00107	54
Both MPPs $(\boldsymbol{u}_1^*$ and $\boldsymbol{u}_2^*)$	Multi-point univariate method	0.00308	95
	Multi-point FORM	0.00276	87
	Multi-point SORM (curvature-fitted)	0.00291	377
	Multi-point SORM (point-fitted)	0.00304	103
	Direct Monte Carlo simulation	0.00304	1,000,000

(a) Total number of times the original performance function is calculated.

Table 5.2 Failure probability for cubic function in Example 1 (Case II)

MPP	Reliability Method	Failure probability	Number of function evaluations[a]
1st MPP $(\boldsymbol{u}_1^*)$	Single-point univariate method	0.000721	29
	Single-point FORM	0.00135	21
	Single-point SORM (curvature-fitted)	0.000410	159
	Single-point SORM (point-fitted)	0.000410	29
2nd MPP $(\boldsymbol{u}_2^*)$	Single-point univariate method	0.000276	69
	Single-point FORM	0.000268	61
	Single-point SORM (curvature-fitted)	0.000277	437
	Single-point SORM (point-fitted)	0.000279	69
Both MPPs $(\boldsymbol{u}_1^*$ and $\boldsymbol{u}_2^*)$	Multi-point univariate method	0.000721	98
	Multi-point FORM	0.00167	82
	Multi-point SORM (curvature-fitted)	0.000646	596
	Multi-point SORM (point-fitted)	0.000651	98
	Direct Monte Carlo simulation	0.000721	1,000,000

(a) Total number of times the original performance function is calculated.

Table 5.3 Failure probability for quartic function in Example 1 (Case III)

MPP	Reliability Method	Failure probability	Number of function evaluations[a]
1st MPP (u_1^*)	Single-point univariate method	0.000954	154
	Single-point FORM	0.00169	146
	Single-point SORM (curvature-fitted)	0.000552	439
	Single-point SORM (point-fitted)	0.000519	154
2nd MPP (u_2^*)	Single-point univariate method	0.000938	134
	Single-point FORM	0.000186	126
	Single-point SORM (curvature-fitted)	0.000564	259
	Single-point SORM (point-fitted)	0.000527	134
Both MPPs $(u_1^*$ and $u_2^*)$	Multi-point univariate method	0.00101	288
	Multi-point FORM	0.00246	272
	Multi-point SORM (curvature-fitted)	0.000810	698
	Multi-point SORM (point-fitted)	0.000764	288
	Direct Monte Carlo simulation	0.00103	1,000,000

(a) Total number of times the original performance function is calculated.

Table 5.4 Failure probability for Example 2 (Transformation T_1)

MPP	Reliability Method	Failure probability	Number of function evaluations[a]
1st MPP (u_1^*)	Single-point univariate method	0.00285	45
	Single-point FORM	0.00269	41
	Single-point SORM	0.00280	182
2nd MPP (u_2^*)	Single-point univariate method	0.000157	105
	Single-point FORM	0.000232	101
	Single-point SORM	0.000145	244
Both MPPs (u_1^* and u_2^*)	Multi-point univariate method	0.00301	150
	Multi-point FORM	0.00290	142
	Multi-point SORM	0.00292	426
	Direct Monte Carlo simulation	0.00296	1,000,000

(a) Total number of times the original performance function is calculated.

Table 5.5 Failure probability for Example 2 (Transformation T_2)

MPP	Reliability Method	Failure probability	Number of function evaluations[a]
1st MPP (u_1^*)	Single-point univariate method	0.00281	85
	Single-point FORM	0.00404	81
	Single-point SORM	0.00273	224
2nd MPP (u_2^*)	Single-point univariate method	0.000180	55
	Single-point FORM	0.000140	51
	Single-point SORM	0.000150	196
Both MPPs (u_1^* and u_2^*)	Multi-point univariate method	0.00299	140
	Multi-point FORM	0.00417	132
	Multi-point SORM	0.00288	420
	Direct Monte Carlo simulation	0.00296	1,000,000

(a) Total number of times the original performance function is calculated.

Table 5.6 Statistical properties of random input for Example 3

Random variable	Mean	Coefficient of variation	Probability distribution
$M_1,\cdots,M_{10}$	193 kip/g	0.2	Lognormal
$K_1,\cdots,K_{10}$	1200 kip/in	0.2	Lognormal
M_0	158 kip/g	0.2	Lognormal
K_0	22 kip/in	0.2	Lognormal
$\zeta_0,\cdots, \zeta_{10}$	0.05	0.3	Lognormal

Table 5.7 Failure probability for Example 3

MPP	Reliability Method	Failure probability	Number of function evaluations[a]
1st MPP $(\boldsymbol{u}_1^*)$	Single-point univariate method	0.1422	536
	Single-point FORM	0.1278	470
	Single-point SORM	0.1401	1593
2nd MPP $(\boldsymbol{u}_2^*)$	Single-point univariate method	0.0314	737
	Single-point FORM	0.0324	671
	Single-point SORM	0.0295	1794
Both MPPs $(\boldsymbol{u}_1^*$ and $\boldsymbol{u}_2^*)$	Multi-point univariate method	0.163	1273
	Multi-point FORM	0.151	1141
	Multi-point SORM	0.161	3387
	Direct Monte Carlo simulation	0.163	5000

(a) Total number of times the original performance function is calculated.
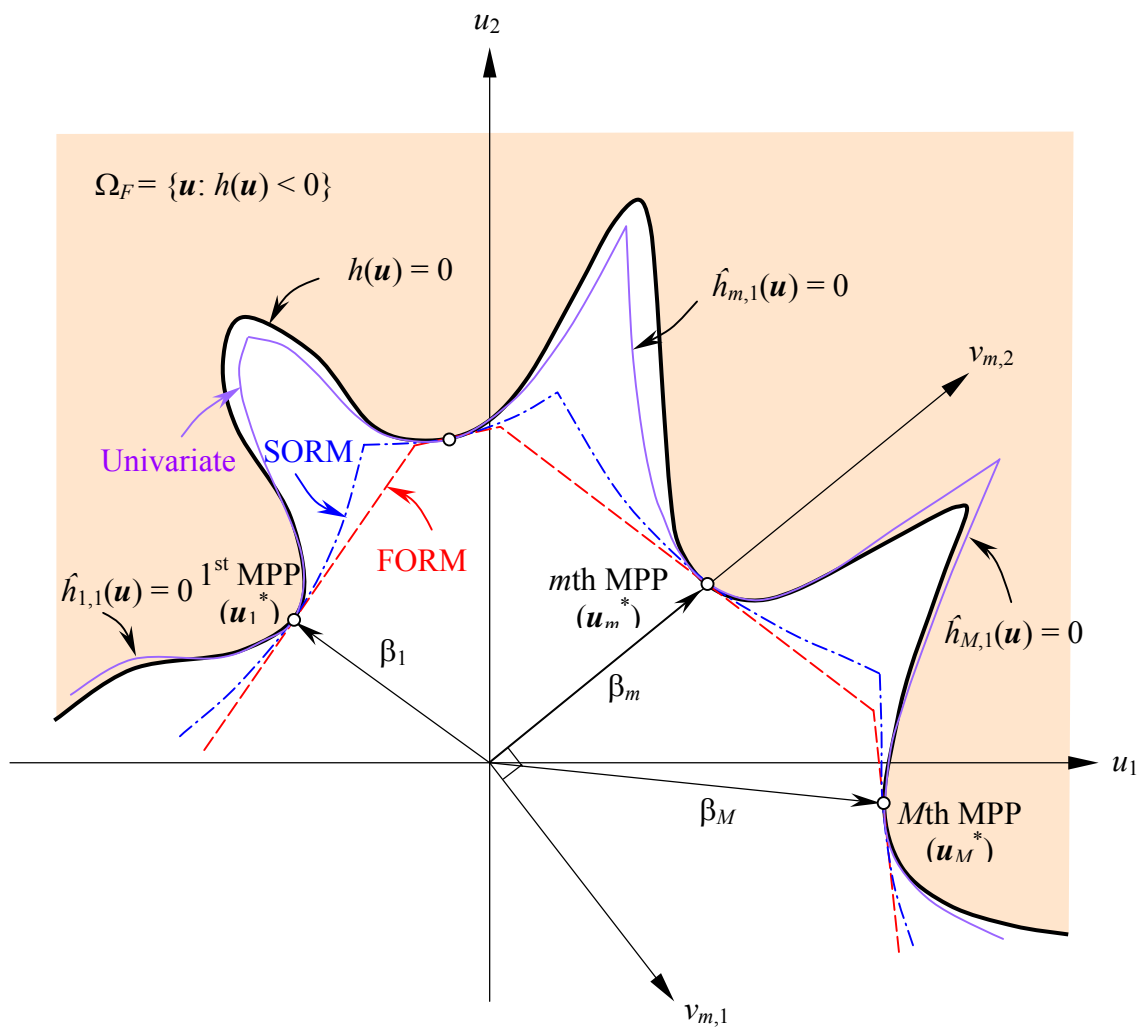
Figure 5.1 A performance function with multiple most probable points
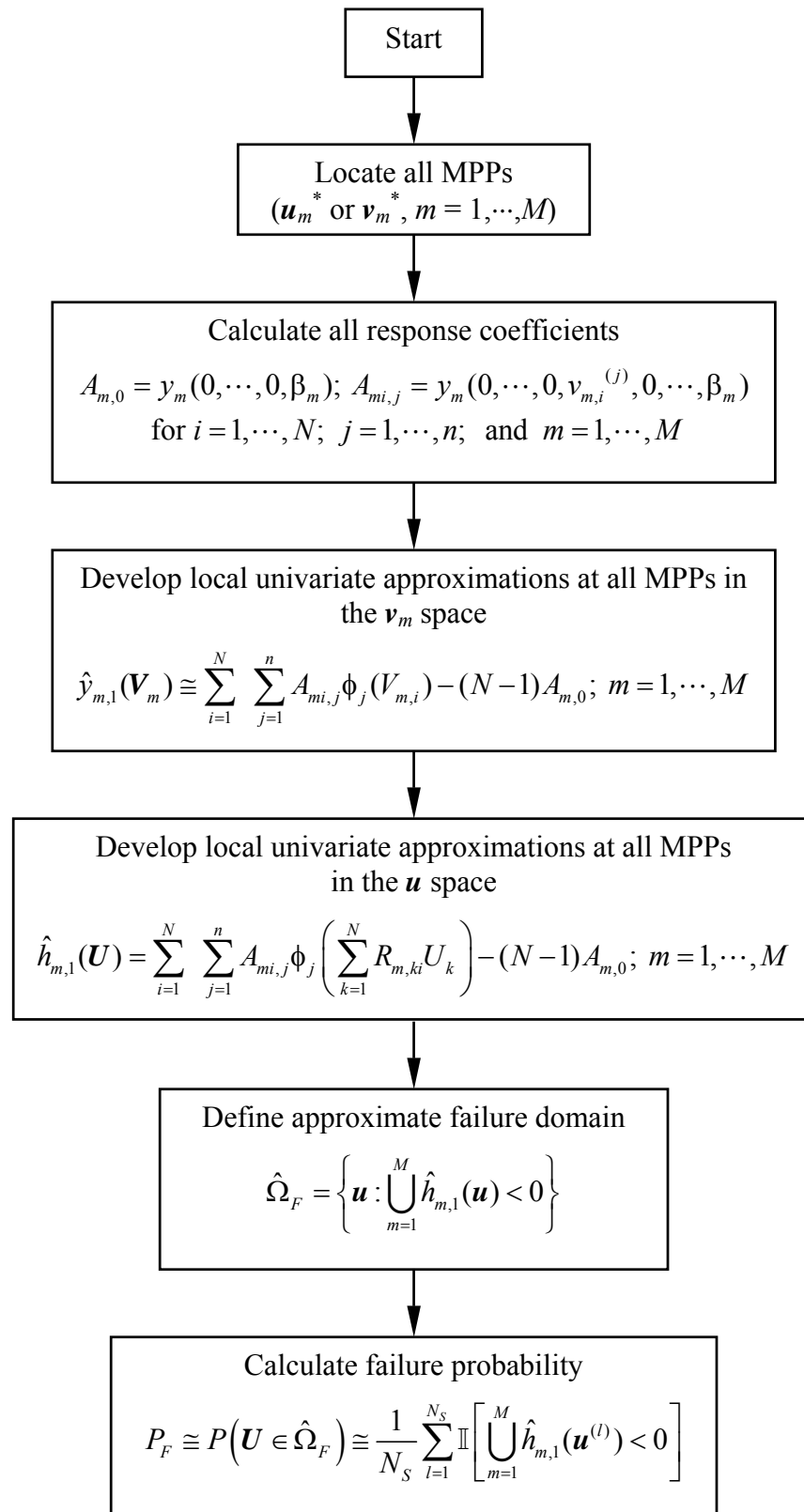
Figure 5.2 Flowchart of the multi-point univariate decomposition method

The flowchart contains the following elements:

Start

Locate all MPPs
$(\boldsymbol{u}_m^{\,*}$ or $\boldsymbol{v}_m^{\,*}$, $m = 1,\cdots,M)$

Calculate all response coefficients
$$A_{m,0} = y_m(0,\cdots,0,\beta_m); \; A_{mi,j} = y_m(0,\cdots,0,v_{m,i}^{(j)},0,\cdots,\beta_m)$$
$$\text{for } i = 1,\cdots,N; \; j = 1,\cdots,n; \; \text{and } m = 1,\cdots,M$$

Develop local univariate approximations at all MPPs in the $\boldsymbol{v}_m$ space
$$\hat{y}_{m,1}(\boldsymbol{V}_m) \cong \sum_{i=1}^{N} \sum_{j=1}^{n} A_{mi,j}\phi_j(V_{m,i}) - (N-1)A_{m,0}; \; m = 1,\cdots,M$$

Develop local univariate approximations at all MPPs in the $\boldsymbol{u}$ space
$$\hat{h}_{m,1}(\boldsymbol{U}) = \sum_{i=1}^{N} \sum_{j=1}^{n} A_{mi,j}\phi_j\left(\sum_{k=1}^{N} R_{m,ki}U_k\right) - (N-1)A_{m,0}; \; m = 1,\cdots,M$$

Define approximate failure domain
$$\hat{\Omega}_F = \left\{ \boldsymbol{u} : \bigcup_{m=1}^{M} \hat{h}_{m,1}(\boldsymbol{u}) < 0 \right\}$$

Calculate failure probability
$$P_F \cong P\left(\boldsymbol{U} \in \hat{\Omega}_F\right) \cong \frac{1}{N_S} \sum_{l=1}^{N_S} \mathbb{I}\left[\bigcup_{m=1}^{M} \hat{h}_{m,1}(\boldsymbol{u}^{(l)}) < 0\right]$$

Figure 5.3 Quadratic limit-state surface in Case I (Example 1)
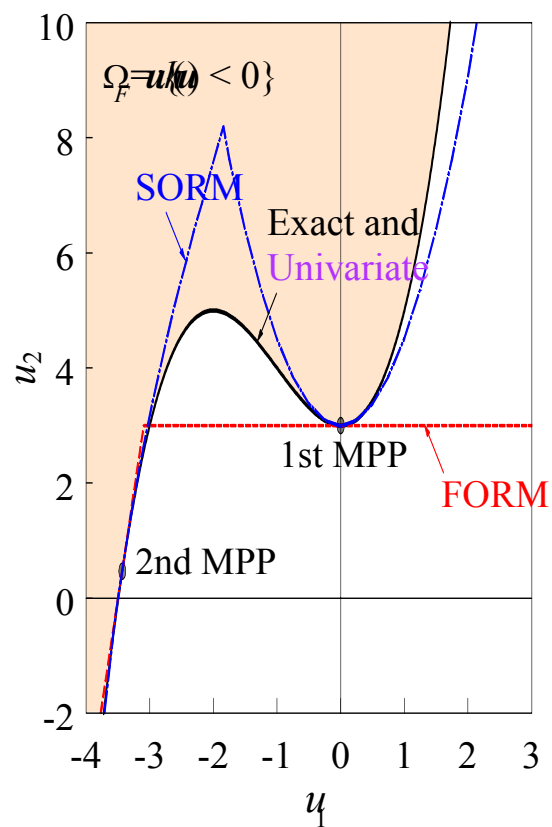
Figure 5.4 Cubic limit-state surface in Case II (Example 1)
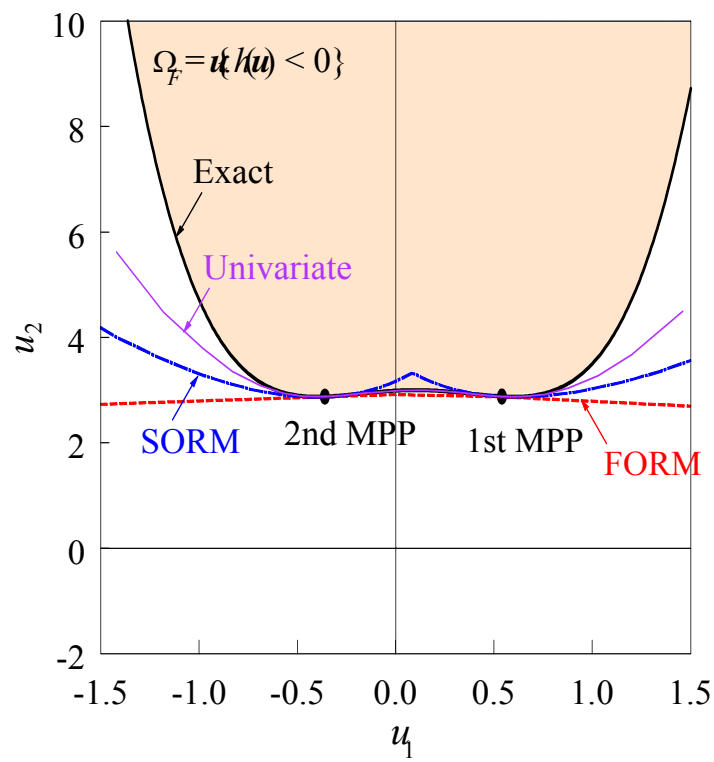
Figure 5.5 Quartic limit-state surface in Case III (Example 1)

(a)

(b)
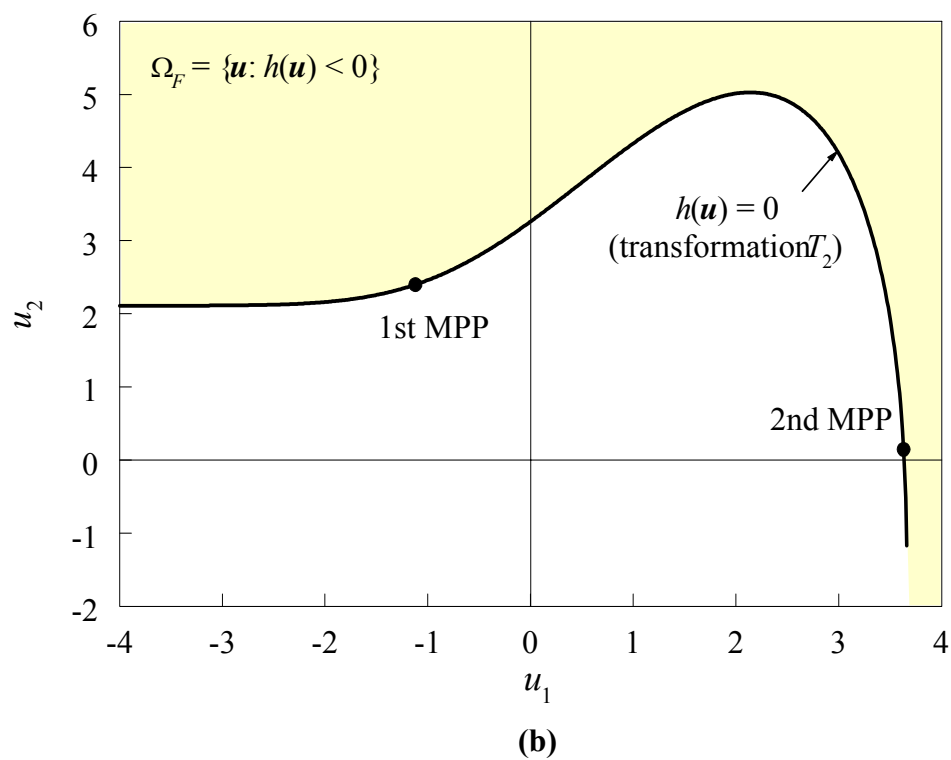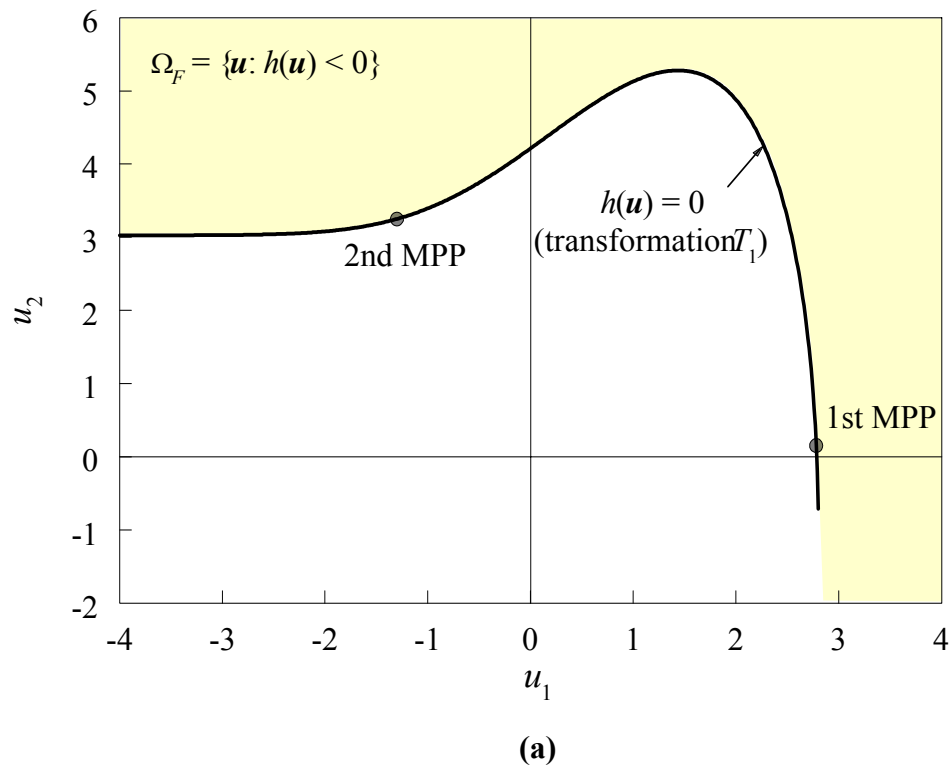
Figure 5.6 Limit-state surface of Example 2; (a) transformation T_1; (b) transformation T_2
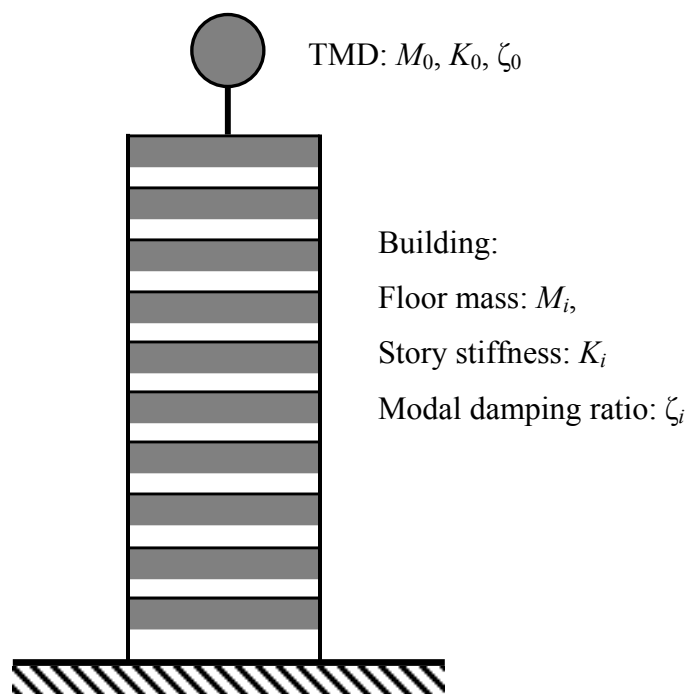
Figure 5.7 A ten-story building-TMD system (Example 3)
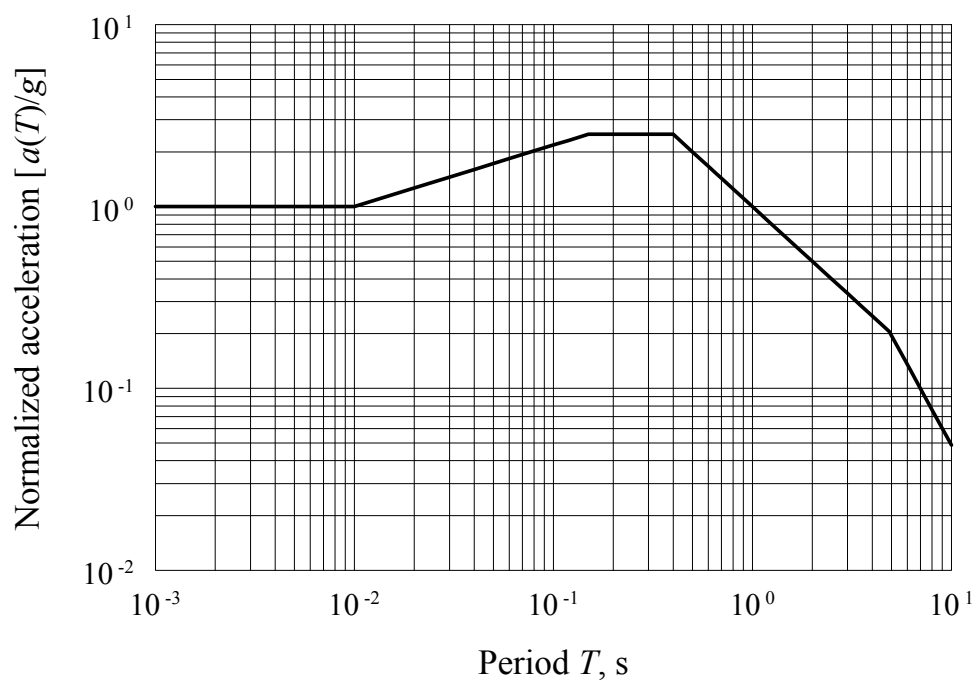
Figure 5.8 Normalized pseudo-acceleration response spectrum

CHAPTER 6

RELIABILITY-BASED DESIGN OPTIMIZATION BY

UNIVARIATE DECOMPOSITION

This chapter presents a univariate decomposition method for reliability-based design optimization of mechanical systems. The method involves: (1) higher-order, univariate approximation of performance functions for reliability analysis; (2) analytical sensitivities of failure probability with respect to design variables; (3) standard gradient-based optimization algorithms. The chapter begins with a brief exposition of the RBDO formulation in Section 6.1. Section 6.2 briefly summarizes the MPP-based univariate decomposition method for reliability analysis, presents new sensitivity equations for design variables, and design optimization. The computational flow and effort are described in Section 6.3. Two sets of examples, each involving mathematical functions and structural/solid-mechanics problems, illustrate the sensitivity analysis and RBDO method developed in section 6.4. Comparisons have been made with alternative FORM/SORM and simulation-based methods to evaluate the accuracy and computational efficiency of the new RBDO method. Finally, Section 6.5 provides conclusions and future outlook.

6.1 Reliability-Based Design Optimization

6.1.1 Generalized RBDO Problem

The mathematical formulation of a general stochastic optimization problem P_1 involving a single objective function and $1 \le K < \infty$ constraint functions entails the statement

$$P_1 : \begin{cases} \min_{\boldsymbol{d} \in \mathcal{D} \subseteq \mathbb{R}^M} & c_0(\boldsymbol{d}) \equiv \mathbb{B}\left[f_0(\boldsymbol{X}; \boldsymbol{d}) \right] \\ \text{subject to} & c_k(\boldsymbol{d}) \equiv P\left[\boldsymbol{X} \in \Omega_{F,k}(\boldsymbol{d}) \right] \leq p_k; \quad k = 1, \cdots, K \quad , \\ & \boldsymbol{d}_l \leq \boldsymbol{d} \leq \boldsymbol{d}_u \end{cases} \qquad (6.1)$$

in which $\boldsymbol{d} = \{d_1, \cdots, d_M\}^T \in \mathcal{D}$ is an M-dimensional design vector with non-empty closed set $\mathcal{D} \subseteq \mathbb{R}^M$; $\boldsymbol{X} = \{X_1, \cdots, X_N\}^T \in \mathbb{R}^N$ is an N-dimensional random vector with joint probability density function $f_X(\boldsymbol{x})$ defined on a probability space $(\Omega, \mathcal{F}, P)$, where Ω is the sample space, $\mathcal{F}$ is the σ-algebra, and P is the probability measure; $\Omega_{F,k}(\boldsymbol{d}) \subseteq \Omega, k = 1, \cdots, K$ is the kth failure domain that may depend on $\boldsymbol{d}$; and $0 \leq p_k \leq 1, k = 1, \cdots, K$ are target failure probabilities, and $\boldsymbol{d}_l$ and $\boldsymbol{d}_u$ are lower and upper bounds of $\boldsymbol{d}$. The design vector $\boldsymbol{d}$ can be deterministic parameters of objective and constraint functions and/or distribution parameters of $\boldsymbol{X}$ (*e.g.*, mean of $\boldsymbol{X}$). The objective function c_0 is obtained by applying an appropriate risk functional $\mathbb{B} : f_X \to \mathbb{R}$ on a random state function $f_0(\boldsymbol{X}; \boldsymbol{d})$. For example, a common characterization of c_0, obtained by applying the expectation operator $\mathbb{E} : f_X \to \mathbb{R}$, is $c_0(\boldsymbol{d}) = \mathbb{E}\left[f_0(\boldsymbol{X}; \boldsymbol{d}) \right]$, which involves statistical moment analysis. In contrast, the constraint functions c_k, depicted in Equation 6.1, requires reliability analysis. For component reliability analysis, the failure domain $\Omega_{F,k} = \{\boldsymbol{x} : g_k(\boldsymbol{x}; \boldsymbol{d}) \leq 0\}$, where $g_k(\boldsymbol{x}; \boldsymbol{d})$ is a single performance function for each constraint. Similar performance functions can be defined for system reliability analysis. Equation (6.1) defines a generic single-objective RBDO problem.

6.1.2 Special RBDO Problem

In engineering applications, RBDO is commonly formulated assuming a deterministic state function in the objective function and component failure probabilities in constraint functions, leading to the problem P_2 with the mathematical statement

$$P_2 : \begin{cases} \min_{\boldsymbol{d} \in \mathcal{D} \subseteq \mathbb{R}^M} & c_0(\boldsymbol{d}) \\ \text{subject to} & c_k(\boldsymbol{d}) \equiv P\big[g_k(\boldsymbol{X};\boldsymbol{d}) < 0\big] \le p_k; \ \ k = 1, \cdots, K \ , \\ & \boldsymbol{d}_l \le \boldsymbol{d} \le \boldsymbol{d}_u \end{cases} \qquad (6.2)$$

which is a special case of Problem P_1. Solving Problem P_2 requires only component reliability analysis in evaluating constraints, and is the focus of the current research. The scope of Problem P_2 can be expanded by including constraints involving system-reliability analysis, but they were not considered in this study. The optimal solution is denoted by $\boldsymbol{d}^* \in \mathbb{R}^M$.

6.2 Univariate Decomposition Method

Consider a continuous, differentiable, real-valued performance function $g_k(\boldsymbol{x};\boldsymbol{d}) = 0$ that depends on $\boldsymbol{x} = \{x_1, \cdots, x_N\}^T \in \mathbb{R}^N$ and $\boldsymbol{d} = \{d_1, \cdots, d_M\}^T \in \mathbb{R}^M$. If $\boldsymbol{u} = \{u_1, \cdots, u_N\}^T \in \mathbb{R}^N$ is the standard Gaussian space, let $\boldsymbol{u}_k^*$ denote the MPP or beta point, which is the closest point on the limit-state surface to the origin. The MPP has a distance β_k, which is commonly referred to as the Hasofer-Lind reliability index (Madsen, et al., 1986), is determined by a standard nonlinear constrained optimization. Construct an orthogonal matrix $\boldsymbol{R}_k \in \mathbb{R}^{N \times N}$ whose Nth column is $\boldsymbol{\alpha}_k^* \equiv \boldsymbol{u}_k^* / \beta_{HL}$, i.e., $\boldsymbol{R}_k = \big[\boldsymbol{R}_{k,1} \big| \boldsymbol{\alpha}_k^*\big]$, where $\boldsymbol{R}_{k,1} \in \mathbb{R}^{N \times N-1}$ satisfies $\boldsymbol{\alpha}_k^{*T} \boldsymbol{R}_{k,1} = \boldsymbol{0} \in \mathbb{R}^{1 \times N-1}$. The matrix $\boldsymbol{R}_{k,1}$ can

be obtained, for example, by Gram-Schmidt orthogonalization. For an orthogonal transformation $\boldsymbol{u} = \boldsymbol{R}_k \boldsymbol{v}_k$, let $\boldsymbol{v}_k = \{v_{k,1}, \cdots, v_{k,N}\}^T \in \mathbb{R}^N$ represent the rotated Gaussian space with the associated MPP $\boldsymbol{v}_k^* = \left\{v_{k,1}^*, \cdots, v_{k,N-1}^*, v_{k,N}^*\right\}^T = \{0, \cdots, 0, \beta_k\}^T$. The transformed limit states $h_k(\boldsymbol{u};\boldsymbol{d}) = 0$ or $y_k(\boldsymbol{v}_k;\boldsymbol{d}) = 0$ are therefore the maps of the original performance function $g_k(\boldsymbol{x};\boldsymbol{d}) = 0$ in the standard Gaussian space ($\boldsymbol{u}$ space) and the rotated Gaussian space ($\boldsymbol{v}_k$ space), respectively, as shown in Figure 6.1 for $N = 2$.

6.2.1 Reliability Analysis

6.2.1.1 MPP-based Univariate Decomposition of Performance Function

At the MPP, consider a univariate approximation of $y_k(\boldsymbol{v}_k;\boldsymbol{d})$, denoted by

$$\hat{y}_{k,1}(\boldsymbol{v}_k;\boldsymbol{d}) \equiv \hat{y}_{k,1}(v_{k,1}, \cdots, v_{k,N};\boldsymbol{d}) = \sum_{i=1}^{N} y_k(0, \cdots, 0, v_{k,i}, 0, \cdots, \beta_k;\boldsymbol{d}) - (N-1)y_k(\boldsymbol{v}_k^*;\boldsymbol{d}), \quad (6.3)$$

where $y_k(\boldsymbol{v}_k^*;\boldsymbol{d}) \equiv y_k(0, \cdots, 0, \beta_k;\boldsymbol{d})$ and $y_{k,i}(v_{k,i};\boldsymbol{d}) \equiv y_k(0, \cdots, 0, v_{k,i}, 0, \cdots, \beta_k;\boldsymbol{d}); \ i = 1, N$. From author's past work (Rahman and Wei, 2006), it can be shown that the univariate approximation $\hat{y}_{k,1}(\boldsymbol{v}_k;\boldsymbol{d})$ leads to the residual error $y_k(\boldsymbol{v}_k;\boldsymbol{d}) - \hat{y}_{k,1}(\boldsymbol{v}_k;\boldsymbol{d})$, which includes contributions from terms of dimension two and higher. For a sufficiently smooth $y_k(\boldsymbol{v}_k)$ with a convergent Taylor series, the coefficients associated with higher-dimensional terms are usually much smaller than that with one-dimensional terms. As such, higher-dimensional terms contribute less to the function, and therefore, can be neglected. Nevertheless, Equation (6.3) includes all higher-order *univariate* terms. In contrast, FORM and SORM also entail univariate approximations, but retain only *linear* and *quadratic univariate* terms, respectively. Hence, Equation (6.3) should provide in

general a higher-order approximation of the performance function than those by commonly employed FORM/SORM.

6.2.1.2 Failure Probability Analysis for Constraint Evaluations

The univariate approximation in Equation (6.3) can be rewritten as

$$\hat{y}_{k,1}(\boldsymbol{v}_k;\boldsymbol{d}) = y_{k,N}(v_{k,N};\boldsymbol{d}) + \sum_{i=1}^{N-1} y_{k,i}(v_{k,i};\boldsymbol{d}) - (N-1)y_k(\boldsymbol{v}_k^*;\boldsymbol{d}), \qquad (6.4)$$

where, due to the rotational transformation of the coordinates (see Figure 6.1), the univariate component function $y_{k,N}(v_{k,N};\boldsymbol{d})$ in Equations (6.3) or (6.4) is expected to be a linear or a weakly nonlinear function of v_N. In fact, $y_{k,N}(v_{k,N};\boldsymbol{d})$ is linear with respect to $v_{k,N}$ in classical FORM/SORM approximations of a performance function in the $\boldsymbol{v}_k$ space. Hence, consider a linear and quadratic approximation: $y_{k,N}(v_{k,N};\boldsymbol{d}) = b_{k,0}(\boldsymbol{d}) + b_{k,1}(\boldsymbol{d})v_{k,N}$ and $y_{k,N}(v_{k,N};\boldsymbol{d}) = b_{k,0}(\boldsymbol{d}) + b_{k,1}(\boldsymbol{d})v_{k,N} + b_{k,2}(\boldsymbol{d})v_{k,N}^2$, where coefficients $b_{k,0} \in \mathbb{R}$, $b_{k,1} \in \mathbb{R}$ and $b_{k,2} \in \mathbb{R}$ (non-zero) are obtained by least-squares approximations from exact or numerically simulated responses $\left\{ y_{k,N}(v_{k,N}^{(1)}), \cdots, y_{k,N}(v_{k,N}^{(n)}) \right\}$ at n sample points along the $v_{k,N}$ coordinate. Applying the linear and quadratic approximation respectively and noting that $V_{k,N}$ follows standard Gaussian distribution, the component failure probability embedded in the kth constraint can be expressed by

$$c_k(\boldsymbol{d}) = P\left[y_k\left(\boldsymbol{V}_k;\boldsymbol{d}\right) < 0 \right] \cong \mathbb{E}\left[\Phi\left(\frac{(N-1)y_k(\boldsymbol{v}_k^*;\boldsymbol{d}) - b_{k,0}(\boldsymbol{d}) - \sum_{i=1}^{N-1} y_{k,i}(V_{k,i};\boldsymbol{d})}{\left| b_{k,1}(\boldsymbol{d}) \right|} \right) \right], \quad (6.5a)$$

and

$$c_k(\boldsymbol{d}) = P\big[\, y_k(\boldsymbol{V}_k;\boldsymbol{d}) < 0 \big] \cong \frac{1 - b_{k,2}\big/\big|b_{k,2}\big|}{2}$$

$$+ \mathbb{E}\left[\Phi\left(\frac{-b_{k,1}(\boldsymbol{d}) + \sqrt{b_{k,1}{}^2(\boldsymbol{d}) - 4 b_{k,2}(\boldsymbol{d}) B\big(\tilde{\boldsymbol{V}}_k;\boldsymbol{d}\big)}}{2 b_{k,2}(\boldsymbol{d})} \right) \right], \quad (6.5b)$$

$$- \mathbb{E}\left[\Phi\left(\frac{-b_{k,1}(\boldsymbol{d}) - \sqrt{b_{k,1}{}^2(\boldsymbol{d}) - 4 b_{k,2}(\boldsymbol{d}) B\big(\tilde{\boldsymbol{V}}_k;\boldsymbol{d}\big)}}{2 b_{k,2}(\boldsymbol{d})} \right) \right]$$

where $\Phi(z) = \left(1\big/\sqrt{2\pi}\right) \int_{-\infty}^{z} \exp\left(-\xi^2\big/2\right) d\xi$ is the cumulative distribution function of a standard Gaussian random variable. In Equation (6.5b) $B\big(\tilde{\boldsymbol{V}}_k,\boldsymbol{d}\big) \equiv b_{k,0}(\boldsymbol{d}) + \sum_{i=1}^{N-1} y_{k,i}\big(V_{k,i};\boldsymbol{d}\big) - (N-1) y_k\big(\boldsymbol{v}_k^*;\boldsymbol{d}\big)$, where $\tilde{\boldsymbol{V}}_k = \big\{V_{k,1},\cdots,V_{k,N-1}\big\}^T$ is an N-1-dimensional standard Gaussian vector. Note that Equation (6.5) provides higher-order estimates of failure probability than that by FORM/SORM if univariate component functions $y_{k,i}(v_{k,i})$, $i = 1, N-1$ are approximated by higher than second-order terms. By integrating with respect to $\tilde{\boldsymbol{v}}_k = \{v_{k,1},\cdots,v_{k,N-1}\}^T \in \mathbb{R}^{N-1}$,

$$c_k(\boldsymbol{d}) \cong \int_{\mathbb{R}^{N-1}} \underbrace{\Phi\left(\frac{(N-1) y_k\big(\boldsymbol{v}_k^*(\beta_k);\boldsymbol{d}\big) - b_{k,0}(\boldsymbol{d}) - \sum_{i=1}^{N-1} y_{k,i}(v_{k,i};\boldsymbol{d})}{\big|b_{k,1}(\boldsymbol{d})\big|} \right)}_{f_k(\tilde{\boldsymbol{v}})} \prod_{i=1}^{N-1} \phi(v_{k,i}) dv_{k,i}, \quad (6.6a)$$

and

$$c_k(\boldsymbol{d}) \cong \frac{1 - b_{k,2}/|b_{k,2}|}{2} + \int_{\mathbb{R}^{N-1}} \Phi\left(\frac{-b_{k,1}(\boldsymbol{d}) + \sqrt{b_{k,1}^{\,2}(\boldsymbol{d}) - 4b_{k,2}(\boldsymbol{d})B(\tilde{\boldsymbol{V}}_k;\boldsymbol{d})}}{2b_{k,2}(\boldsymbol{d})}\right) \prod_{i=1}^{N-1} \phi(v_{k,i})dv_{k,i}$$
$$- \int_{\mathbb{R}^{N-1}} \Phi\left(\frac{-b_{k,1}(\boldsymbol{d}) - \sqrt{b_{k,1}^{\,2}(\boldsymbol{d}) - 4b_{k,2}(\boldsymbol{d})B(\tilde{\boldsymbol{V}}_k;\boldsymbol{d})}}{2b_{k,2}(\boldsymbol{d})}\right) \prod_{i=1}^{N-1} \phi(v_{k,i})dv_{k,i}$$

$$(6.6b)$$

where $\phi(v_{k,i}) \equiv d\Phi(v_{k,i})/dv_{k,i} = \left(1/\sqrt{2\pi}\right)\exp\left(-v_{k,i}^{\,2}/2\right)$ is the probability density function of a standard Gaussian random variable.

6.2.2 Design Sensitivity Analysis

In gradient-based optimization algorithms, derivatives of both objective and constraint functions with respect to each design variable are required. For the RBDO problem P_2, calculating such derivatives of the objective function is trivial. However, the formulation of gradients for a constraint function is dependent on how the underlying reliability analysis is performed. A new analytically derived sensitivity analysis of general constraint functions $c_k(\boldsymbol{d}); \; k = 1, K$ was conducted as follows.

The integrand of the multi-dimensional integration (Equation (6.6)) depends on $\beta_k(\boldsymbol{d})$ and $\tilde{\boldsymbol{v}}_k(\boldsymbol{d})$, each of which in turn depends on design $\boldsymbol{d}$. By applying the chain rule in Equation (6.6), the partial derivative of the constraint function $c_k(\boldsymbol{d})$ with respect to design variable d_i is

$$\frac{\partial c_k(\boldsymbol{d})}{\partial d_i} = \frac{\partial c_k(\boldsymbol{d})}{\partial \beta_k}\frac{\partial \beta_k}{\partial d_i} + \sum_{j=1}^{N-1}\frac{\partial c_k(\boldsymbol{d})}{\partial v_{k,j}}\frac{\partial v_{k,j}}{\partial d_i}, \tag{6.7}$$

which involves four partial derivatives described as follows.

6.2.2.1 Partial Derivative of $c_k(d)$ with Respect to β_k

Using the univariate approximation of $y_k(\boldsymbol{v}_k;\boldsymbol{d})$ in Equation (6.4) and linear approximation of the component function $y_{k,N}(v_{k,N};\boldsymbol{d})$,

$$\begin{aligned}
\frac{\partial y_k\left(\boldsymbol{v}_k^{\,*}(\beta_k);\boldsymbol{d}\right)}{\partial\beta_k} &= \left.\frac{\partial y_k\left(\boldsymbol{v}_k;\boldsymbol{d}\right)}{\partial\beta_k}\right|_{v_k=v_k^*} \\
&\cong \frac{\partial}{\partial\beta_k}\left[b_{k,0}(\boldsymbol{d})+b_{k,1}(\boldsymbol{d})v_{k,N}+\sum_{i=1}^{N-1}y_{k,i}(v_{k,i};\boldsymbol{d})-(N-1)y_k(\boldsymbol{v}_k^{\,*};\boldsymbol{d})\right]\Bigg|_{v_k=v_k^*}
\end{aligned} \qquad (6.8)$$

which yields

$$\frac{\partial y_k\left(\boldsymbol{v}_k^{\,*}(\beta_k);\boldsymbol{d}\right)}{\partial\beta_k} \cong \frac{\partial}{\partial\beta_k}\left[b_{k,0}(\boldsymbol{d})+b_{k,1}(\boldsymbol{d})\beta_k+\sum_{i=1}^{N-1}y_{k,i}(0;\boldsymbol{d})-\left(N-1\right)y_k\left(\boldsymbol{v}_k^{\,*}\right)\right]. \quad (6.9)$$

For a variation in β_k, coefficients $b_{k,0}(\boldsymbol{d})$, $b_{k,1}(\boldsymbol{d})$, and $y_{k,i}(0;\boldsymbol{d})$ employed in representing the component function $y_{k,N}(v_{k,N};\boldsymbol{d})$ is not expected to change significantly. In addition, the term $(N-1)y_k(\boldsymbol{v}_k^{\,*};\boldsymbol{d})$ in Equation (6.4) is a constant, which does not change with β_k in Equation (6.9). Hence, it can be assumed that $\partial b_{k,0}/\partial\beta_k = \partial b_{k,1}/\partial\beta_k = \partial y_{k,i}(0;\boldsymbol{d})/\partial\beta_k = \partial y_k(\boldsymbol{v}^*;\boldsymbol{d})/\partial\beta_k = 0$ in Equation (6.9), yielding

$$\frac{\partial y_k\left(\boldsymbol{v}_k^{\,*}(\beta_k);\boldsymbol{d}\right)}{\partial\beta_k} \cong b_{k,1}(\boldsymbol{d}). \qquad (6.10a)$$

For quadratic approximation of the component function $y_{k,N}(v_{k,N};\boldsymbol{d})$, with the assumption $\partial b_{k,0}/\partial\beta_k = \partial b_{k,1}/\partial\beta_k = \partial b_{k,2}/\partial\beta_k = \partial y_{k,i}(0;\boldsymbol{d})/\partial\beta_k = \partial y_k(\boldsymbol{v}^*;\boldsymbol{d})/\partial\beta_k = 0$, Equation (6.10a) is also satisfied. Further derivation leads to

$$\frac{\partial B\left(\tilde{\boldsymbol{V}}_k;\boldsymbol{d}\right)}{\partial\beta_k} \cong -\left(N-1\right)\frac{\partial y_k\left(\boldsymbol{v}_k^{\,*}(\beta_k);\boldsymbol{d}\right)}{\partial\beta_k} \cong -\left(N-1\right)b_{k,1}(\boldsymbol{d}). \qquad (6.10b)$$

Taking partial derivative of Equation (6.6) with respect to β_k,

$$\frac{\partial c_k(\boldsymbol{d})}{\partial \beta_k} \cong \int_{\mathbb{R}^{N-1}} \phi\left(\frac{(N-1)y_k\left(\boldsymbol{v}_k^*(\beta_k);\boldsymbol{d}\right) - b_{k,0}(\boldsymbol{d}) - \sum_{i=1}^{N-1} y_{k,i}(v_{k,i};\boldsymbol{d})}{\left|b_{k,1}(\boldsymbol{d})\right|}\right) (N-1)\frac{\frac{\partial y_k\left(\boldsymbol{v}_k^*(\beta_k);\boldsymbol{d}\right)}{\partial \beta_k}}{\left|b_{k,1}(\boldsymbol{d})\right|} \times \quad (6.11a)$$
$$\prod_{i=1}^{N-1} \phi(v_{k,i})dv_{k,i}$$

and

$$\frac{\partial c_k(\boldsymbol{d})}{\partial \beta_k} \cong \int_{\mathbb{R}^{N-1}} \phi\left(\frac{-b_{k,1}(\boldsymbol{d}) + \sqrt{b_{k,1}^2(\boldsymbol{d}) - 4b_{k,2}(\boldsymbol{d})B\left(\tilde{\boldsymbol{V}}_k;\boldsymbol{d}\right)}}{2b_{k,2}(\boldsymbol{d})}\right) \frac{-\frac{\partial B\left(\tilde{\boldsymbol{V}};\boldsymbol{d}\right)}{\partial \beta_k}}{\sqrt{b_{k,1}^2(\boldsymbol{d}) - 4b_{k,2}(\boldsymbol{d})B\left(\tilde{\boldsymbol{V}}_k;\boldsymbol{d}\right)}} \times \prod_{i=1}^{N-1} \phi(v_{k,i})dv_{k,i}$$
$$-\int_{\mathbb{R}^{N-1}} \phi\left(\frac{-b_{k,1}(\boldsymbol{d}) - \sqrt{b_{k,1}^2(\boldsymbol{d}) - 4b_{k,2}(\boldsymbol{d})B\left(\tilde{\boldsymbol{V}}_k;\boldsymbol{d}\right)}}{2b_{k,2}(\boldsymbol{d})}\right) \frac{\frac{\partial B\left(\tilde{\boldsymbol{V}};\boldsymbol{d}\right)}{\partial \beta_k}}{\sqrt{b_{k,1}^2(\boldsymbol{d}) - 4b_{k,2}(\boldsymbol{d})B\left(\tilde{\boldsymbol{V}}_k;\boldsymbol{d}\right)}} \times \prod_{i=1}^{N-1} \phi(v_{k,i})dv_{k,i}$$
,

$$(6.11b)$$

which when combined with Equation (6.10), yields

$$\frac{\partial c_k(\boldsymbol{d})}{\partial \beta_k} \cong \int_{\mathbb{R}^{N-1}} \underbrace{\phi\left(\frac{(N-1)y_k\left(\boldsymbol{v}_k^*(\beta_k);\boldsymbol{d}\right) - b_{k,0}(\boldsymbol{d}) - \sum_{i=1}^{N-1} y_{k,i}(v_{k,i};\boldsymbol{d})}{\left|b_{k,1}(\boldsymbol{d})\right|}\right)}_{f_k(\tilde{\boldsymbol{v}})} (N-1)\operatorname{sgn}\left(b_{k,1}(\boldsymbol{d})\right) \prod_{i=1}^{N-1} \phi(v_{k,i})dv_{k,i}$$

$$(6.12a)$$

and

$$\frac{\partial c_k(\boldsymbol{d})}{\partial \beta_k} \cong (N-1)b_{k,1}(\boldsymbol{d}) \int_{\mathbb{R}^{N-1}} \underbrace{\left[\phi\left(\frac{-b_{k,1}(\boldsymbol{d}) + \sqrt{b_{k,1}^2(\boldsymbol{d}) - 4b_{k,2}(\boldsymbol{d})B(\tilde{V}_k;\boldsymbol{d})}}{2b_{k,2}(\boldsymbol{d})} \right) + \phi\left(\frac{-b_{k,1}(\boldsymbol{d}) - \sqrt{b_{k,1}^2(\boldsymbol{d}) - 4b_{k,2}(\boldsymbol{d})B(\tilde{V}_k;\boldsymbol{d})}}{2b_{k,2}(\boldsymbol{d})} \right) \right] \frac{1}{\sqrt{b_{k,1}^2(\boldsymbol{d}) - 4b_{k,2}(\boldsymbol{d})B(\tilde{V}_k;\boldsymbol{d})}}}_{f_k(\tilde{\boldsymbol{v}})} \cdot \\ \times \prod_{i=1}^{N-1} \phi(v_{k,i}) dv_{k,i}$$

$$(6.12b)$$

6.2.2.2 Partial Derivative of $c_k(d)$ with Respect to $v_{k,i}$

The partial derivative of failure probability defined by constraint function $c_k(\boldsymbol{d})$ with respect to the realization $v_{k,j}$ of the ith rotated Gaussian random variable $V_{k,j}$ is

$$\frac{\partial c_k(\boldsymbol{d})}{\partial v_{k,j}} \cong \int_{\mathbb{R}^{N-1}} \left[\underbrace{\left(\phi\left(\frac{(N-1)y_k\left(\boldsymbol{v}_k^*(\beta_k);\boldsymbol{d}\right) - b_{k,0}(\boldsymbol{d}) - \sum_{i=1}^{N-1} y_{k,i}(v_{k,i};\boldsymbol{d})}{\left|b_{k,1}(\boldsymbol{d})\right|} \right) \right) \left(-\frac{\frac{\partial y_{k,j}(v_{k,j};\boldsymbol{d})}{\partial v_{k,j}}}{\left|b_{k,1}(\boldsymbol{d})\right|} \right)}_{f_k(\tilde{\boldsymbol{v}})} \right. $$
$$\left. \underbrace{-\Phi\left(\frac{(N-1)y_k\left(\boldsymbol{v}_k^*(\beta_k);\boldsymbol{d}\right) - b_{k,0}(\boldsymbol{d}) - \sum_{i=1}^{N-1} y_{k,i}(v_{k,i};\boldsymbol{d})}{\left|b_{k,1}(\boldsymbol{d})\right|} \right) v_{k,j}}_{f_k(\tilde{\boldsymbol{v}})} \right] \prod_{i=1}^{N-1} \phi(v_{k,i}) dv_{k,i}.$$

$$(6.13a)$$

and

$$\frac{\partial c_k(\boldsymbol{d})}{\partial v_{k,j}} \cong \int_{\mathbb{R}^{N-1}} \left[\underbrace{\left(\phi\left(\frac{-b_{k,1}(\boldsymbol{d}) + \sqrt{b_{k,1}{}^2(\boldsymbol{d}) - 4b_{k,2}(\boldsymbol{d})B(\tilde{V}_k;\boldsymbol{d})}}{2b_{k,2}(\boldsymbol{d})} \right) \right) \left(-\frac{\dfrac{\partial B(\tilde{V}_k;\boldsymbol{d})}{\partial v_{k,j}}}{\sqrt{b_{k,1}{}^2(\boldsymbol{d}) - 4b_{k,2}(\boldsymbol{d})B(\tilde{V}_k;\boldsymbol{d})}} \right)}_{f_k(\tilde{\boldsymbol{v}})} \right.$$

$$\left. \underbrace{-\Phi\left(\frac{-b_{k,1}(\boldsymbol{d}) + \sqrt{b_{k,1}{}^2(\boldsymbol{d}) - 4b_{k,2}(\boldsymbol{d})B(\tilde{V}_k;\boldsymbol{d})}}{2b_{k,2}(\boldsymbol{d})} \right) v_{k,j}}_{f_k(\tilde{\boldsymbol{v}})} \right] \prod_{i=1}^{N-1} \phi(v_{k,i}) dv_{k,i}$$

$$-\int_{\mathbb{R}^{N-1}} \left[\underbrace{\left(\phi\left(\frac{-b_{k,1}(\boldsymbol{d}) - \sqrt{b_{k,1}{}^2(\boldsymbol{d}) - 4b_{k,2}(\boldsymbol{d})B(\tilde{V}_k;\boldsymbol{d})}}{2b_{k,2}(\boldsymbol{d})} \right) \right) \left(\frac{\dfrac{\partial B(\tilde{V}_k;\boldsymbol{d})}{\partial v_{k,j}}}{\sqrt{b_{k,1}{}^2(\boldsymbol{d}) - 4b_{k,2}(\boldsymbol{d})B(\tilde{V}_k;\boldsymbol{d})}} \right)}_{f_k(\tilde{\boldsymbol{v}})} \right.$$

$$\left. \underbrace{-\Phi\left(\frac{-b_{k,1}(\boldsymbol{d}) - \sqrt{b_{k,1}{}^2(\boldsymbol{d}) - 4b_{k,2}(\boldsymbol{d})B(\tilde{V}_k;\boldsymbol{d})}}{2b_{k,2}(\boldsymbol{d})} \right) v_{k,j}}_{f_k(\tilde{\boldsymbol{v}})} \right] \prod_{i=1}^{N-1} \phi(v_{k,i}) dv_{k,i} \; .$$

$$(6.13\mathrm{b})$$

6.2.2.3 Partial Derivatives of β_k and $v_{k,j}$ with Respect to d_i

Of the two remaining gradients, the partial derivative of reliability index β_k with respect to design variable d_i is

$$\frac{\partial \beta_k}{\partial d_i} = -\left[\frac{\nabla h_k(\boldsymbol{u};\boldsymbol{d})^T}{\|\nabla h_k(\boldsymbol{u};\boldsymbol{d})\|} \frac{\partial \boldsymbol{u}}{\partial d_i} \right]_{\boldsymbol{u}=\boldsymbol{u}_k{}^*}, \qquad (6.14)$$

where $\nabla h_k = \{\partial h_k/\partial u_1, \cdots, \partial h_k/\partial u_N\}^T$, $\|\cdot\|$ is the $\mathbb{L}_2$ norm, and the vector derivative $\partial \boldsymbol{u}/\partial d_i = \{\partial u_1/\partial d_i, \cdots, \partial u_N/\partial d_i\}^T$ is obtained from the *x-u* transformation. In Equation

(6.14), $\nabla h_k(\boldsymbol{u};\boldsymbol{d})^T$ represents a vector of structural response sensitivities, is problem dependent, and is calculated either analytically or numerically by a finite-difference approximation. Finally, the partial derivative $\partial v_{k,j}/\partial d_i$ included in Equation (6.7) is obtained from the $\boldsymbol{x}\text{-}\boldsymbol{v}_k$ transformation. Both $\boldsymbol{x}\text{-}\boldsymbol{u}$ and $\boldsymbol{x}\text{-}\boldsymbol{v}_k$ transformations depend on the probability distribution of $\boldsymbol{X}$ and hence on a specific RBDO problem to be solved.

6.2.3 Univariate Numerical Integration for Reliability and Sensitivity Analyses

The expressions of constraint function in Equation (6.6) and their partial derivatives in Equations (6.12) and (6.13) involve multivariate integrations over $\mathbb{R}^{N-1}$. A generic evaluation of these integrals requires calculating $\int_{\mathbb{R}^{N-1}} f_k(\tilde{\boldsymbol{v}})\prod_{i=1}^{N-1} q(v_{k,i})d\tilde{\boldsymbol{v}}$, where $f_k : \mathbb{R}^{N-1} \mapsto \mathbb{R}$ is the multivariate part of the integrand and depends on how univariate component functions $y_{k,i}(v_{k,i})$, $i=1, N-1$ are constructed, and $q : \mathbb{R} \mapsto \mathbb{R}$ is the remaining univariate part of the integrand. The exact calculation of this integral is not possible in general. Numerical integration is not efficient as $f_k(\tilde{\boldsymbol{v}})$ is a multivariate function and becomes impractical when the dimension exceeds three or four.

In reference to Equation (6.3), consider again a univariate approximation of $\ln\left[f_k(\tilde{\boldsymbol{v}})\right]$ at $\tilde{\boldsymbol{v}}^* \equiv \{0,\cdots,0\}^T = \boldsymbol{0} \in \mathbb{R}^{N-1}$, expressed by

$$\ln\left[f_k(\tilde{\boldsymbol{v}})\right] \cong \sum_{i=1}^{N-1} \ln\left[f_{k,i}(v_{k,i})\right] - (N-2)\ln\left[f_k(\boldsymbol{0})\right], \qquad (6.15)$$

where $f_{k,i}(v_{k,i}) \equiv f_k(0,\cdots,0,v_{k,i},0,\cdots,0)$ are univariate component functions and $f_k(\boldsymbol{0}) \equiv f_k(0,\cdots,0)$. Hence

$$
\begin{aligned}
f_k(\tilde{\boldsymbol{v}}) &= \exp\left\{\ln\left[f_k(\tilde{\boldsymbol{v}})\right]\right\} \\
&\cong \exp\left\{\sum_{i=1}^{N-1}\ln\left[f_{k,i}(v_{k,i})\right]-(N-2)\ln\left[f_k(\mathbf{0})\right]\right\}, \qquad (6.16) \\
&= \frac{\displaystyle\prod_{i=1}^{N-1}f_{k,i}(v_{k,i})}{f_k(\mathbf{0})^{N-2}}
\end{aligned}
$$

yielding

$$
\int_{\mathbb{R}^{N-1}}f_k(\tilde{\boldsymbol{v}})\prod_{i=1}^{N-1}q(v_{k,i})d\tilde{\boldsymbol{v}}\cong\frac{\displaystyle\prod_{i=1}^{N-1}\int_{-\infty}^{+\infty}f_{k,i}(v_{k,i})q(v_{k,i})dv_{k,i}}{f_k(\mathbf{0})^{N-2}}, \qquad (6.17)
$$

which involves a product of *N*-1 *univariate* integrals. Using Equation (6.17) with appropriately defined $f(\tilde{\boldsymbol{v}})$ in Equations (6.6), (6.12), and (6.13), the failure probability by linear approximation of component function $y_{k,N}(v_{k,N};\boldsymbol{d})$ and their derivatives becomes

$$
c_k(\boldsymbol{d})\cong\frac{\displaystyle\prod_{i=1}^{N-1}\int_{-\infty}^{+\infty}\Phi\left(\frac{(N-1)y_k\left(\boldsymbol{v}_k^*(\beta_k);\boldsymbol{d}\right)-b_{k,0}(\boldsymbol{d})-y_{k,i}(0;\boldsymbol{d})}{\left|b_{k,1}(\boldsymbol{d})\right|}\right)\phi(v_{k,i})dv_{k,i}}{\Phi\left(\dfrac{(N-1)y_k\left(\boldsymbol{v}_k^*(\beta_k);\boldsymbol{d}\right)-b_{k,0}(\boldsymbol{d})-\displaystyle\sum_{i=1}^{N-1}y_{k,i}(0;\boldsymbol{d})}{\left|b_{k,1}(\boldsymbol{d})\right|}\right)^{N-2}}, \qquad (6.18)
$$

$$
\frac{\partial c_k(\boldsymbol{d})}{\partial\beta_k}\cong\frac{(N-1)\mathrm{sgn}\left(b_{k,1}(\boldsymbol{d})\right)\displaystyle\prod_{i=1}^{N-1}\int_{-\infty}^{+\infty}\phi\left(\frac{(N-1)y_k\left(\boldsymbol{v}_k^*(\beta_k);\boldsymbol{d}\right)-b_{k,0}(\boldsymbol{d})-y_{k,i}(v_{k,i};\boldsymbol{d})}{\left|b_{k,1}(\boldsymbol{d})\right|}\right)\phi(v_{k,i})dv_{k,i}}{\phi\left(\dfrac{(N-1)y_k\left(\boldsymbol{v}_k^*(\beta_k);\boldsymbol{d}\right)-b_{k,0}(\boldsymbol{d})-\displaystyle\sum_{i=1}^{N-1}y_{k,i}(0;\boldsymbol{d})}{\left|b_{k,1}(\boldsymbol{d})\right|}\right)^{N-2}},
$$

$$
(6.19)
$$

and

$$\frac{\partial c_k(\boldsymbol{d})}{\partial v_{k,j}} \cong \frac{\displaystyle\prod_{i=1,i\neq j}^{N-1}\int_{-\infty}^{+\infty}\phi\left(\frac{(N-1)y_k\left(\boldsymbol{v}_k^*(\beta_k);\boldsymbol{d}\right)-b_{k,0}(\boldsymbol{d})-y_{k,i}(v_{k,i};\boldsymbol{d})}{\left|b_{k,1}(\boldsymbol{d})\right|}\right)\phi(v_{k,i})dv_{k,i}}{\left[\phi\left(\dfrac{(N-1)y_k\left(\boldsymbol{v}_k^*(\beta_k);\boldsymbol{d}\right)-b_{k,0}(\boldsymbol{d})-\displaystyle\sum_{i=1}^{N-1}y_{k,i}(0;\boldsymbol{d})}{\left|b_{k,1}(\boldsymbol{d})\right|}\right)\right]^{N-2}}\times$$

$$\int_{-\infty}^{+\infty}\phi\left(\frac{(N-1)y_k\left(\boldsymbol{v}_k^*(\beta_k);\boldsymbol{d}\right)-b_{k,0}(\boldsymbol{d})-y_{k,j}(v_{k,j};\boldsymbol{d})}{\left|b_{k,1}(\boldsymbol{d})\right|}\right)\left(-\frac{\dfrac{\partial y_{k,j}(v_{k,j};\boldsymbol{d})}{\partial v_{k,j}}}{\left|b_{k,1}(\boldsymbol{d})\right|}\right)\phi(v_{k,j})dv_{k,j}-$$

$$\frac{\displaystyle\prod_{i=1,i\neq j}^{N-1}\int_{-\infty}^{+\infty}\Phi\left(\frac{(N-1)y_k\left(\boldsymbol{v}_k^*(\beta_k);\boldsymbol{d}\right)-b_{k,0}(\boldsymbol{d})-y_{k,i}(v_{k,i};\boldsymbol{d})}{\left|b_{k,1}(\boldsymbol{d})\right|}\right)\phi(v_{k,i})dv_{k,i}}{\left[\Phi\left(\dfrac{(N-1)y_k\left(\boldsymbol{v}_k^*(\beta_k);\boldsymbol{d}\right)-b_{k,0}(\boldsymbol{d})-\displaystyle\sum_{i=1}^{N-1}y_{k,i}(0;\boldsymbol{d})}{\left|b_{k,1}(\boldsymbol{d})\right|}\right)\right]^{N-2}}\times$$

$$\int_{-\infty}^{+\infty}\Phi\left(\frac{(N-1)y_k\left(\boldsymbol{v}_k^*(\beta_k);\boldsymbol{d}\right)-b_{k,0}(\boldsymbol{d})-y_{k,j}(v_{k,j};\boldsymbol{d})}{\left|b_{k,1}(\boldsymbol{d})\right|}\right)v_{k,j}\phi(v_{k,j})dv_{k,j},$$

$$(6.20)$$

respectively. The univariate integration involved in each of Equations (6.18), (6.19), and (6.20) can be easily evaluated by standard one-dimensional Gauss-Hermite numerical quadrature. The failure probability by quadratic approximation of component function $y_{k,N}(v_{k,N};\boldsymbol{d})$ and their derivatives can be evaluated by the similar forms. Equation (6.7) with partial derivatives formulated in Equations (6.19) and (6.20) provide design sensitivities for a gradient-based design optimization.

6.3 Computational Flow and Effort

In summary, the overall process for solving the RBDO problem P_2 can be described by the following steps:

(1) Define an initial design with $d = d_0$. Use the final result of mean- or other relevant reference-point-based optimization if available.

(2) Evaluate both objective and constraint functions for the current design vector. For constraint functions, use the proposed univariate decomposition method (Equation (6.18)) for reliability analysis.

(3) Evaluate gradients of both objective and constraint functions for the current design vector. For gradients constraint functions, use the proposed univariate decomposition method (Equations (6.7), (6.19), and (6.20)) for design sensitivity analysis.

(4) Perform deterministic optimization to solve Equation (6.2) by a selected gradient-based algorithm.

(5) Check for the convergence of the objective function and design vector. If the convergence is reached, stop. If not, update the design vector to find the next design vector and repeat steps 2 through 4.

Figure 6.2 depicts the flowchart of the proposed RBDO process. New methods were developed in the shaded areas.

For determining computational effort, consider $y_{k,i}(v_{k,i};d) \equiv y_k(0,\cdots,0,v_{k,i},0,\cdots,0;d)$; $i = 1, N$, for which n function values $y_{k,i}(v_{k,i}^{(j)};d) \equiv y(0,\cdots,0,v_{k,i}^{(j)},0,\cdots,0;d)$; $j = 1,\cdots,n$ are required to be evaluated at integration points $v_{k,i} = v_{k,i}^{(j)}$ to perform an n-order Gauss-Hermite quadrature for ith

integration in Equations (6.18)-(6.20). The same procedure is repeated for N-1 univariate component functions for each constraint, *i.e.*, for all $y_{k,i}(v_{k,i};\boldsymbol{d})$, $i=1,\cdots,N$ and for K constraint functions, *i.e.*, for all $y_k(\boldsymbol{v}_k;\boldsymbol{d})$, $k=1,\cdots,K$. Therefore, the total cost of the proposed univariate method entails a *maximum* of *nNK* function evaluations. Note that the above cost is in addition to any function evaluations required for locating the MPP in each constraint.

Design sensitivities using FORM/SORM approximations of failure probability in evaluating constraints are described in Appendix D. For linear approximations of $c_k(\boldsymbol{d})$ at MPP, Equation (6.7) can be further simplified to degenerate to FORM sensitivity equations.

6.4 Numerical Examples

Two example sets, one involving two design sensitivity problems, and the other involving four RBDO problems, are presented to illustrate the proposed univariate decomposition method. Constraints associated with both mathematical functions (Examples 1 and 3) and structural/solid-mechanics (Examples 2, 4, 5, and 6) problems were employed. Whenever possible, comparisons have been made with the FORM/SORM, and direct Monte Carlo simulation to evaluate the accuracy and efficiency of the new method. In solving RBDO problems (Examples 4-6), all approximate methods employ the nested double loop for design and reliability iterations. No single-loop FORM-based methods, although available in the current literature, were included, as the objective was to determine how the accuracy and efficiency of a reliability analysis influence the optimization process. All structural sensitivities

$(\nabla h_k(\boldsymbol{u};\boldsymbol{d})^T)$ were obtained by the finite-difference method involving 1 percent perturbations.

To obtain linear approximation of $y_{k,N}(v_{k,N};\boldsymbol{d})$; $k=1,K$, n (= 5 or 7) sample points $v_{k,N}^{*}-(n-1)/2, v_{k,N}^{*}-(n-3)/2, \cdots, v_{k,N}^{*}, \cdots, v_{k,N}^{*}+(n-3)/2, v_{k,N}^{*}+(n-1)/2$ were deployed along the $v_{k,N}$-coordinate. The same value of n was employed as the order of Gauss-Hermite quadratures in Equations (6.6), (6.12), or (6.13) of the proposed univariate method. Hence, the total number of function evaluations required by the univariate method, in addition to those required for locating the MPP, is $(n-1)NK$. When comparing computational efforts by various RBDO methods, the number of *original* performance function evaluations was chosen as the primary metric in this work.

The optimization algorithms employed were sequential quardratic programming in Example 3, 4, and 6; and sequential linear programming in Example 5.

6.4.1 Example Set I – Design Sensitivity Analysis

6.4.1.1 Example 1 – Elementary Mathematical Functions

Consider two constraint functions $c_k(\boldsymbol{d})=P[g_k(\boldsymbol{X};\boldsymbol{d})<0]$; $k=1,2$, where the cubic and quartic performance functions are respectively expressed by

$$g_1(\boldsymbol{X};\boldsymbol{d})=2.2257-\frac{0.025\sqrt{2}}{27}\left(X_1(d_1)+X_2(d_2)-20\right)^3+\frac{33}{140}\left(X_1(d_1)-X_2(d_2)\right) \quad (6.21)$$

and

$$g_2(\boldsymbol{X};\boldsymbol{d})=\frac{5}{2}+\frac{1}{216}\left(X_1(d_1)+X_2(d_1)-20\right)^4-\frac{33}{140}\left(X_1(d_1)-X_2(d_2)\right), \quad (6.22)$$

in which, $\boldsymbol{X}(\boldsymbol{d}) = \{X_1(d_1), X_2(d_2)\}^T$ is a bivariate, independent, Gaussian random vector with means $\mu_i = 10$ and standard deviations $\sigma_i = 3$; $i = 1,2$. From an MPP search, $\boldsymbol{v}_1^* = \{0, 2.2257\}^T$ and $\beta_1 = \|\boldsymbol{v}_1^*\| = 2.2257$ for the cubic function and $\boldsymbol{v}_2^* = \{0, 2.5\}^T$ and $\beta_2 = \|\boldsymbol{v}_2^*\| = 2.5$ for the quartic function. For the univariate method, a value of $n = 5$ was selected, resulting 9 function evaluations. The design vector is $\boldsymbol{d} = \{\mu_1, \mu_2\}^T = \{10,10\}^T$ for both functions.

Table 6.1 presents partial derivatives $\partial c_1(\boldsymbol{d})/\partial d_i$; $i = 1,2$ and $\partial c_2(\boldsymbol{d})/\partial d_i$; $i = 1,2$, calculated by FORM/SORM, proposed univariate decomposition method, and Monte Carlo simulation using 10^6 samples. The univariate method yields very accurate estimates of gradients of both constraints with a maximum error of less than 1 percent when compared with simulation results. In contrast, existing FORM/SORM for this particular example contains maximum errors of 64 and 113 percent for cubic and quartic performance functions, respectively. The SORM results are the same as the FORM results, indicating that there is no improvement over FORM for problems involving inflection point (cubic function) or high nonlinearity (quartic function).

6.4.1.2 Example 2 – Ten-Bar Truss Structure

A ten-bar, linear-elastic, truss structure, shown in Figure 6.3, was studied in this example to examine the accuracy and efficiency of the proposed univariate method for calculating gradients. The Young's modulus of the material is 10^7 psi. Two concentrated forces of 10^5 lb are applied at nodes 2 and 3. The cross-sectional area $X_i(\boldsymbol{d})$ for each bar is independent, follows normal distribution, and has means $\mu_i = 2.5$ in^2 and standard

deviation $\sigma_i = 0.5$ in^2; $i = 1, \cdots, 10$. According to the loading condition, the maximum displacement $[(v_3(X_1(d_1), \cdots, X_{10}(d_{10})))]$ occurs at node 3, where a permissible displacement is limited to 18 in. Hence, the constraint function is

$$c(\boldsymbol{d}) = P\left[18 - v_3\left(X_1(d_1), \cdots, X_{10}(d_1)\right) < 0\right].$$

From an MPP search, the reliability index is $\beta = \|\boldsymbol{v}^*\| = 1.3642$. Table 6.2 lists ten gradients of the failure probability of the truss, i.e., $\partial c(\boldsymbol{d})/\partial d_i$; $i = 1, \cdots, 10$, which were calculated using the proposed univariate method (linear and quadratic approximation), FORM, SORM, and direct Monte Carlo simulation (10^6 samples). For the univariate method, a value of $n = 7$ was selected. As can be seen from Table 6.2, both SORM and the univariate method predict derivatives of the failure probability more accurately than FORM. This is because univariate methods and SORM are able to approximate the performance function embedded in the constraint more accurately than FORM. The computational efforts to obtain these sensitivities are described in Table 6.3. For all methods, no additional function evaluations other than that for reliability analysis were required in obtaining these sensitivities. In other words, the same computational effort is needed to obtain both reliability and sensitivity results.

6.4.2 Example Set II – Reliability-based Design Optimization

6.4.2.1 Example 3 – Mathematical Functions

Consider a mathematical example with two independent Gaussian random variables and three nonlinear constraints. The RBDO problem is defined by

$$\min_{\boldsymbol{d} \in \mathbb{R}^2} \qquad c_0(\boldsymbol{d}) = d_1 + d_2$$

$$\text{subject to} \quad c_1(\boldsymbol{d}) = P\left[\frac{X_1^2(d_1)X_2(d_2)}{20} - 1 < 0 \right] \leq \Phi(-3)$$

$$c_2(\boldsymbol{d}) = P\left[\frac{\left(X_1(d_1) + X_2(d_2) - 5\right)^2}{30} + \frac{\left(X_1(d_1) - X_2(d_2) - 12\right)^2}{120} - 1 < 0 \right] \leq \Phi(-3),$$

$$c_3(\boldsymbol{d}) = P\left[\frac{80}{\left(X_1^{5/2}(d_1) + 8X_2(d_2) + 5\right)} - 1 < 0 \right] \leq \Phi(-4)$$

$$0 \leq d_i \leq 10; \ i = 1, 2$$

$$(6.23)$$

where $\boldsymbol{X}(\boldsymbol{d}) = \{X_1(d_1), X_2(d_2)\}^T \in \mathbb{R}^2$ is an independent, bivariate, Gaussian random vector with means μ_i and standard deviations $\sigma_i = 0.3$; $i = 1, 2$. The design vector is $\boldsymbol{d} = \{d_1, d_2\}^T = \{\mu_1, \mu_2\}^T$.

Using the initial design point $\boldsymbol{d}_0 = \{5, 5\}^T$, Figure 6.4 depicts the optimization history when the constraints are evaluated by the proposed univariate decomposition method, FORM, SORM, and Monte Carlo simulation involving 10^6 samples for each failure probability calculation. The detailed results presented in Table 6.4 suggest that all four methods are able to reach an optimum state in 4-6 iterations, which yield very close optimal solutions. Hence, each method can be used to solve this optimization problem. It is interesting to note that SORM requires fewer function evaluations than FORM, which is somewhat counter-intuitive because reliability analysis by SORM is generally more expensive than that by FORM. However, an exception may occur, when SORM leads to fewer design iterations than FORM in the outer loop, which was observed in this particular RBDO problem. Nevertheless, the univariate method is more efficient than

FORM or SORM, because of the fewest number of function evaluations required to solve this example.

6.4.2.2 Example 4 – Cantilever Beam

In this example, the design of a fixed cantilever beam, which has a deterministic length $L = 100$ inches, a random vertical load X_1, a random lateral load X_2, shown in Figure 6.5, was studied. The beam is made of a material with random uniaxial yield strength X_3 and random elastic modulus X_4. The width d_1 and height d_2 of the prismatic cross-section are two design variables. The objective is to minimize the area of the beam cross-section so that its total volume is minimized. Two nonlinear failure modes were examined. The first failure mode is due to yielding at the fixed end of the cantilever; and the second failure mode is associated with the tip displacement exceeding a permissible value of 2.5 inches. The RBDO problem is stated as

$$\min_{\boldsymbol{d} \in \mathbb{R}^2} \quad c_0(\boldsymbol{d}) = d_1 d_2$$

$$\text{subject to} \quad c_1(\boldsymbol{d}) = P\left[X_3 - \frac{600}{d_1 d_2}\left(\frac{X_1}{d_2} + \frac{X_2}{d_1} \right) < 0 \right] \leq \Phi(-2.5)$$

$$c_2(\boldsymbol{d}) = P\left[2.5 - \frac{4 \times 10^6}{X_4 d_1 d_2}\sqrt{\frac{X_1^2}{d_2^4} + \frac{X_2^2}{d_1^4}} < 0 \right] \leq \Phi(-3.5)$$

$$0 \leq d_i \leq 5 \text{ inches}; \; i = 1, 2 \qquad (6.24)$$

where $\boldsymbol{X} = \{X_1, X_2, X_3, X_4\}^T \in \mathbb{R}^4$ is an independent, four-dimensional, Gaussian random vector, in which each random variable has mean and standard deviation listed in Table 6.5. The design vector is $\boldsymbol{d} = \{d_1, d_2\}^T$. The proposed RBDO method starts with the initial design vector $\boldsymbol{d}_0 = \{2, 4\}^T$ in.

Figure 6.6 illustrates the optimization history of the proposed univariate method, FORM, SORM, and Monte Carlo simulation. Table 6.6 compares the accuracy and efficiency of three approximate methods by using the Monte Carlo benchmark solution. The results suggest that all three methods attain the same optimum value (≈ 9.21 inch^2) of the objective function. The univariate method is slightly more expensive than FORM, because of (1) additional function evaluations required after locating MPPs and (2) larger design iterations involved in this particular example. Even if the numbers of design iterations are the same, the univariate method will require slightly more function evaluations than FORM. In this example, both FORM and univariate methods are more efficient than SORM, a trend that is expected unless the number of design iterations required by SORM is significantly fewer than others.

Since the univariate method and FORM/SORM entails approximate reliability analysis, the constraints associated with the optimal design generated by each method were evaluated using the Monte Carlo simulation (10^6 samples). Table 6.7 presents the values of failure probability embedded in each constraint. It appears that both FORM and SORM slightly violates the second constraint with a maximum error of 18 and 9 percent in calculating the failure probability. In contrast, no such violations were observed in the univariate method. This is because the proposed univariate method is more accurate than FORM/SORM in performing reliability analysis in this example.

6.4.2.3 Example 5 – 10-Bar Truss

A ten-bar truss, illustrated in Figure 6.3, was designed by minimizing its total volume given that the truss reliability is no less than a target value of $\Phi(2) = 0.9772$. The RBDO formulation is

$$\min_{\boldsymbol{d} \in \mathbb{R}^{10}} \quad c_0(\boldsymbol{d}) = 360 \Big[d_1 + d_2 + d_3 + d_4 + d_5 + d_8 + \sqrt{2}\big(d_6 + d_7 + d_9 + d_{10}\big) \Big]$$

$$\text{subject to} \quad c_1(\boldsymbol{d}) = P \Big[14 - v_3 \big(X_1(d_1), \cdots, X_{10}(d_{10}) \big) < 0 \Big] \le \Phi(-2) \qquad , \quad (6.25)$$

$$0 \le d_i \le 5 \text{ inches; } i = 1,10$$

where $\boldsymbol{X} = \{X_1(d_1), \cdots, X_{10}(d_{10})\}^T \in \mathbb{R}^{10}$ is an independent, Gaussian random vector with each component representing a random cross-section of the truss. The random variable X_i follows Gaussian distribution, and has means μ_i and standard deviation $\sigma_i = 0.2$ in^2; $i = 1, \cdots, 10$. The design vector is $\boldsymbol{d} = \{d_1, \cdots, d_{10}\}^T = \{\mu_1, \cdots, \mu_{10}\}^T$. The initial design point is $\boldsymbol{d}_0 = \{3, \cdots, 3\}^T$ in^2.

Figure 6.7 and Table 6.8 present the optimization history and optimization results by various methods. The optimal volumes achieved by the univariate method, SORM, and Monte Carlo vary from 9327 to 9340 inch^3. In contrast, FORM leads to a lower optimal volume, which is 9282 inch^3. A Monte Carlo reliability analysis at optimal designs obtained by FORM, SORM, and univariate method reveals that the failure probability estimates have associated absolute errors of 55%, 5%, and 1%, respectively. Hence, FORM violates the constraint leading to the lower optimum volume of the truss. Both SORM and univariate method satisfy the constraint and hence provide acceptable designs. However, the univariate method proposed is more efficient than SORM in solving the truss problem.

6.4.2.4 Example 6 – Torque Arm

The final example involves designing a torque-arm, where eight random shape parameters $X_i(d_i)$; $i = 1,8$ describe its outer and inner boundaries, as shown in Figure 6.8 for the mean input at the initial design.   The left hole of the structure is fixed and two deterministic forces F_1 = 2789 N and F_2 = 5066 N are applied at the center of the right hole. The torque-arm material has mass density ρ = 7800 kg/m^3, elastic modulus E = 207 GPa, Poisson's ratio ν = 0.3, and uniaxial yield strength S_y = 400 MPa. The objective is to minimize the mass of the structure $m(\boldsymbol{d})$ by changing the shape of the geometry (i.e., by $\boldsymbol{X}(\boldsymbol{d}) \in \mathbb{R}^8$) such that the von Mises stresses at five selected points do not exceed S_y. Locations of these five points, marked as finite element nodes 90, 98, 106, 173, and 175, are illustrated in Figure 6.9. Mathematically,

$$\min_{\boldsymbol{d} \in \mathbb{R}^{10}} \quad c_0(\boldsymbol{d}) = m(\boldsymbol{d})$$

$$\text{subject to} \quad c_k(\boldsymbol{d}) = P\left[S_y - \sigma_{k,e}(\boldsymbol{X};\boldsymbol{d}) < 0 \right] \le \Phi(-3);\ k = 1,5$$
$$-1 \text{ mm} \le d_1 \le 1 \text{ mm}$$
$$-1 \text{ mm} \le d_2 \le 1 \text{ mm}$$
$$-1 \text{ mm} \le d_3 \le 1 \text{ mm}$$
$$-2 \text{ mm} \le d_4 \le 1 \text{ mm}$$
$$-5 \text{ mm} \le d_5 \le 1 \text{ mm}$$
$$-0.5 \text{ mm} \le d_6 \le 2 \text{ mm}$$
$$-1 \text{ mm} \le d_7 \le 6 \text{ mm}$$
$$-0.5 \text{ mm} \le d_8 \le 1 \text{ mm}$$

$$, \quad (6.26)$$

where $\sigma_{k,e}(\boldsymbol{X};\boldsymbol{d})$ is the von Mises equivalent stress at the kth selected point. The finite element mesh includes 657 nodes and 177 eight-noded quadrilateral elements. A plane stress condition was assumed.   The independent random vector $\boldsymbol{X}$, which represents manufacturing variability, follows Gaussian distribution. The components X_i has means

μ_i and standard deviations $\sigma_i = 0.2$ mm; $i = 1, \cdots, 10$. The design vector is

$$\boldsymbol{d} = \{d_1, \cdots, d_8\}^T = \{\mu_1, \cdots, \mu_8\}^T.$$

The initial design point is $\boldsymbol{d}_0 = \{0, \cdots, 0\}^T$ mm with the corresponding finite element mesh depicted in Figure 6.8. Following linear-elastic stress analysis, Figure 6.10 presents the contour plot of the von Mises stress at the initial design when shape parameters assume their mean values. Due to conservative initial design, the maximum von Mises stress of 130 MPa, which occurs at node 98, is much lower than the uniaxial yield strength ($S_y = 400$ MPa). During design iterations, the movement of nodes, which control shape parameters $X_i(d_i)$; $i = 1, 8$, was performed by design velocity field involving an isoparametric mapping (Choi and Chang, 1994).

For computational efficiency, the optimal design was obtained in two steps. In the first step, a coarse RBDO was performed using the initial design $\boldsymbol{d}_0 = \{0, \cdots, 0\}^T$ and an approximate reliability method, known as the mean-value first-order second moment method. The resultant design after 10 iterations in the first step (coarse RBDO) is $\bar{\boldsymbol{d}}_0 = \{-0.427, -1, -0.063, -2, -0.327, 2, 0.234, 0.875\}^T$ mm. In the second step, a refined RBDO involving the proposed univariate method and the result of step 1 as the initial design (i.e., $\boldsymbol{d}_0 = \bar{\boldsymbol{d}}_0$) was employed. After 9 iterations, the final design was attained, which is $\boldsymbol{d}^* = \{-0.709, -0.721, -0.077, -2, -0.247, 2, 0.258, 0.524\}^T$ mm with the corresponding mean shape presented in Figure 6.11. The optimal mass of the torque arm is 2.035 kg – a 30 percent reduction from the initial mass of 2.915 kg. Figure 6.11 also displays the contour plot of the von Mises stress at the optimal design when the shape parameters assume their mean values. Compared with the conservative initial design of

Figure 6.10, larger stresses, for example 256, 247, and 226 MPa at nodes 98, 106, and 173, respectively, can be safely tolerated in the final design of Figure 6.11. The larger area of the slotted hole and movement of outer boundaries have led to significant alteration of the shape of the initial design. Figure 6.12 shows the optimization history of the objective function.

If the uncertainty of X is ignored and the constraints in Equation 6.26 is replaced by $S_y - \sigma_{k,e}(d;d) < 0;\ k = 1,5$, as commonly adopted in traditional design optimization, 13 iterations led to $d^* = \{-1, -1, -0.062, -2, -1.785, 2, 1.676, 0.795\}^T$ mm and a corresponding optimal mass of 1.861 kg – a 36 percent reduction from the initial mass. Therefore, a traditional risk-ignoring optimization process may lead to a smaller mass than that obtained from RBDO, however with the higher stresses, as depicted in the contour plot of Figure 6.13. If uncertainties are included, the optimal design in Figure 6.13 is highly likely to violate the reliability constraints. By comparing optimal designs from RBDO (Figure 6.11) and risk-ignoring optimization (Figure 6.13), it appears that the outer boundaries generated by both designs are similar. However, the inner slot from the RBDO is smaller than that from the risk-ignoring optimization. The primary reason is that the latter optimization does not account for variability of shape parameters and of the performance function. In addition, the sensitivity of the von Mises stress with respect to shape parameters in the inner boundary is much larger than that in the outer boundary.

In summary, the univariate method consistently provides very accurate RBDO solutions. Of the three methods studied, the FORM-based RBDO is the most efficient method; however, it may lead to infeasible or inaccurate designs. Both SORM and univariate method have comparable accuracies, but the univariate method is less

expensive than SORM. Nevertheless, for industrial-scale design applications, further research is required in making the proposed univariate method computationally more efficient by potentially decoupling the design and reliability iterations or exploring the possibility of single-loop formulations.

Table 6.1 Gradients of two mathematical constraint functions

Gradients	Methods			
	FORM	**SORM**	**Univariate**	**Monte Carlo**[a]
$\partial c_1(\boldsymbol{d})/\partial d_1$	0.007896	0.007896	0.01390	0.01389
$\partial c_1(\boldsymbol{d})/\partial d_2$	-0.007896	-0.007896	-0.00475	-0.00482
$\partial c_2(\boldsymbol{d})/\partial d_1$	0.004132	0.004132	0.001945	0.001944
$\partial c_2(\boldsymbol{d})/\partial d_2$	-0.004132	-0.004132	-0.001945	-0.001944

(a) Sample size = 10^6 for each simulation; finite difference with 1% perturbation.

Table 6.2 Gradients of the constraint in 10-bar truss

Gradients	Methods				
	FORM	**SORM**	**Univariate (linear)**	**Univariate (Quadratic)**	**Monte Carlo**[a]
$\partial c(\boldsymbol{d})/\partial d_1$	-0.2107	-0.3156	-0.3038	-0.3063	-0.2976
$\partial c(\boldsymbol{d})/\partial d_2$	-0.0155	-0.0232	-0.0217	-0.0226	-0.0272
$\partial c(\boldsymbol{d})/\partial d_3$	-0.0086	-0.0129	-0.0121	-0.0122	-0.0144
$\partial c(\boldsymbol{d})/\partial d_4$	-0.0086	-0.0129	-0.0121	-0.0122	-0.0142
$\partial c(\boldsymbol{d})/\partial d_5$	-0.2005	-0.3003	-0.2850	-0.2891	-0.2788
$\partial c(\boldsymbol{d})/\partial d_6$	-0.0729	-0.1092	-0.1042	-0.1053	-0.1138
$\partial c(\boldsymbol{d})/\partial d_7$	-0.0769	-0.1152	-0.1094	-0.1105	-0.1218
$\partial c(\boldsymbol{d})/\partial d_8$	0.0007	0.0010	0.0010	0.0010	0.0008
$\partial c(\boldsymbol{d})/\partial d_9$	-0.0250	-0.0375	-0.0357	-0.0363	-0.0386
$\partial c(\boldsymbol{d})/\partial d_{10}$	-0.0464	-0.0695	-0.0664	-0.0673	-0.0730

(a) Sample size = 10^6 for each simulation; finite difference with 1% perturbation.

Table 6.3 Computational efforts for 10-bar truss

Methods	Number of function evaluations
FORM	127
SORM	365
Univariate[a]	187
Monte Carlo	10^6

(a) $127 + (n-1) \times N = 127 + (7-1) \times 10 = 187$.

Table 6.4 Optimization results by various methods for mathematical functions

	Methods[a]			
	FORM	**SORM**	**Univariate**	**Monte Carlo**
No. of iterations	6	5	4	4
No. of function evaluations	1406	1226	949	26×10^6
Final design: $\boldsymbol{d}^* = \{d_1{}^*, d_2{}^*\}^T$				
$d_1{}^*$	3.4391	3.4544	3.4544	3.4547
$d_2{}^*$	3.2867	3.2760	3.2740	3.2741
Constraint functions:				
$c_1(\boldsymbol{d}^*)$ - $\Phi(-3)$	1.35×10^{-4}	-9.00×10^{-6}	4.00×10^{-6}	0
$c_2(\boldsymbol{d}^*)$ - $\Phi(-3)$	-2.33×10^{-4}	-2.80×10^{-5}	-2.90×10^{-5}	-5.00×10^{-6}
$c_3(\boldsymbol{d}^*)$ - $\Phi(-4)$	-1.17×10^{-5}	-5.67×10^{-5}	-5.67×10^{-6}	-5.67×10^{-6}
Objective function:				
$c_0(\boldsymbol{d}^*)$	6.7258	6.7304	6.7284	6.7288

(a) Initial design $\boldsymbol{d}_0 = \{5,5\}^T$.

**Table 6.5 Statistical properties of random input
for cantilever beam**

Random variable	Mean	Standard deviation	Probability distribution
X_1, lb	1000	100	Gaussian
X_2, lb	500	100	Gaussian
X_3, psi	40,000	200	Gaussian
X_4, psi	29×10^6	1.45×10^6	Gaussian

Table 6.6 Optimization results by various methods for the cantilever beam

	Methods[a]			
	FORM	**SORM**	**Univariate**	**Monte Carlo**
No. of iterations	4	5	6	6
No. of function evaluations	992	1412	1373	29×10^6
Final design: $\boldsymbol{d}^* = \{d_1{}^*, d_2{}^*\}^T$				
$d_1{}^*$, in	2.4530	2.4580	2.4683	2.4629
$d_2{}^*$, in	3.7550	3.7476	3.7326	3.7403
Constraint function:				
$c_1(\boldsymbol{d}^*) - \Phi(-3)$	0	-9.00×10^{-6}	-2.80×10^{-5}	-5.00×10^{-6}
$c_2(\boldsymbol{d}^*) - \Phi(-3.5)$	4.24×10^{-5}	2.14×10^{-5}	-2.26×10^{-5}	-2.40×10^{-6}
Objective function:				
$c_0(\boldsymbol{d}^*)$, in^2	9.2109	9.2117	9.2132	9.2119

(a) Initial design $\boldsymbol{d}_0 = \{2,4\}^T$ in.

Table 6.7 Failure probabilities for cantilever beam

Methods	$c_1(\boldsymbol{d}^*)$	$c_2(\boldsymbol{d}^*)$
FORM	0.006210	0.0002750
SORM	0.006201	0.0002540
Univariate	0.006182	0.0002100
Monte Carlo	0.006205	0.0002350

Table 6.8 Optimization results by various methods for the 10-bar truss

	Methods[a]			
	FORM	**SORM**	**Univariate**	**Monte Carlo**
No. of iterations	15	12	13	11
No. of function evaluations	2694	4894	3113	117×10^5
Final design: $\boldsymbol{d}^* = \{d_1^*,\ldots,d_{10}^*\}^T$				
d_1^*, in^2	3.998	4.072	3.935	4.21
d_2^*, in^2	1.944	1.968	1.947	1.918
d_3^*, in^2	1	1	1	1
d_4^*, in^2	1	1	1	1
d_5^*, in^2	4.388	4.384	4.381	4.268
d_6^*, in^2	2.827	2.783	2.94	2.669
d_7^*, in^2	2.225	2.284	2.117	2.436
d_8^*, in^2	1	1.001	1	1.001
d_9^*, in^2	1	1	1	1.039
d_{10}^*, in^2	2.754	2.77	2.743	2.728
Constraint function: $c_1(\boldsymbol{d}^*) - \Phi(-2)$	1.25×10^{-2}	-1.13×10^{-3}	2.3×10^{-4}	2.3×10^{-5}
Objective function: $c_0(\boldsymbol{d}^*)$, in^3	9282	9332	9327	9340

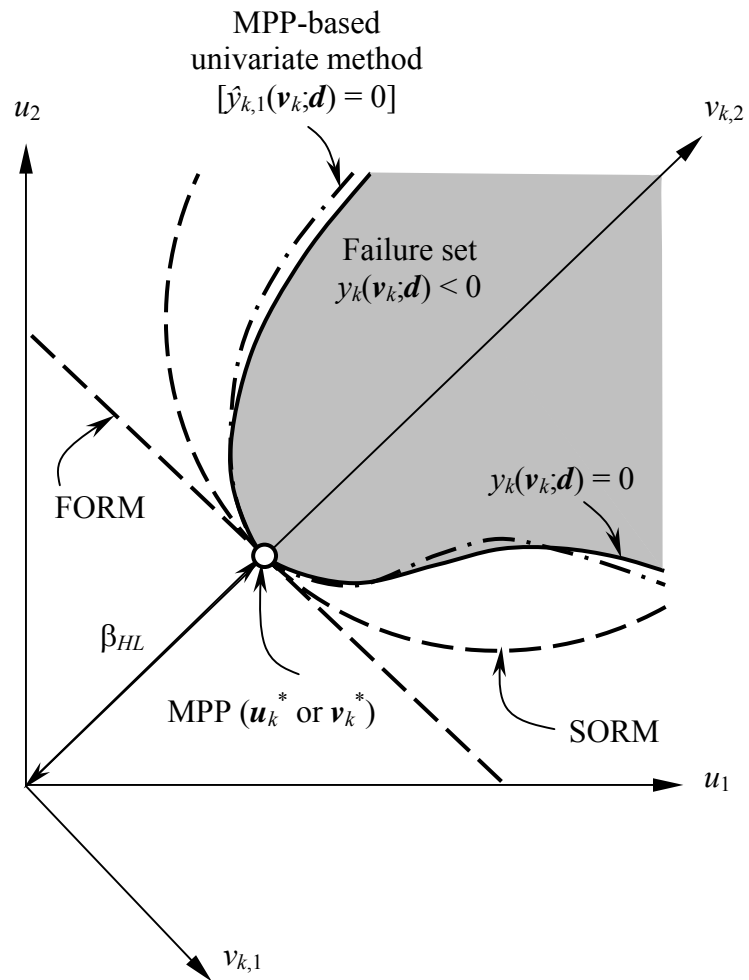(a) Initial design $\boldsymbol{d}_0 = \{3,\ldots,3\}^T$ in^2.

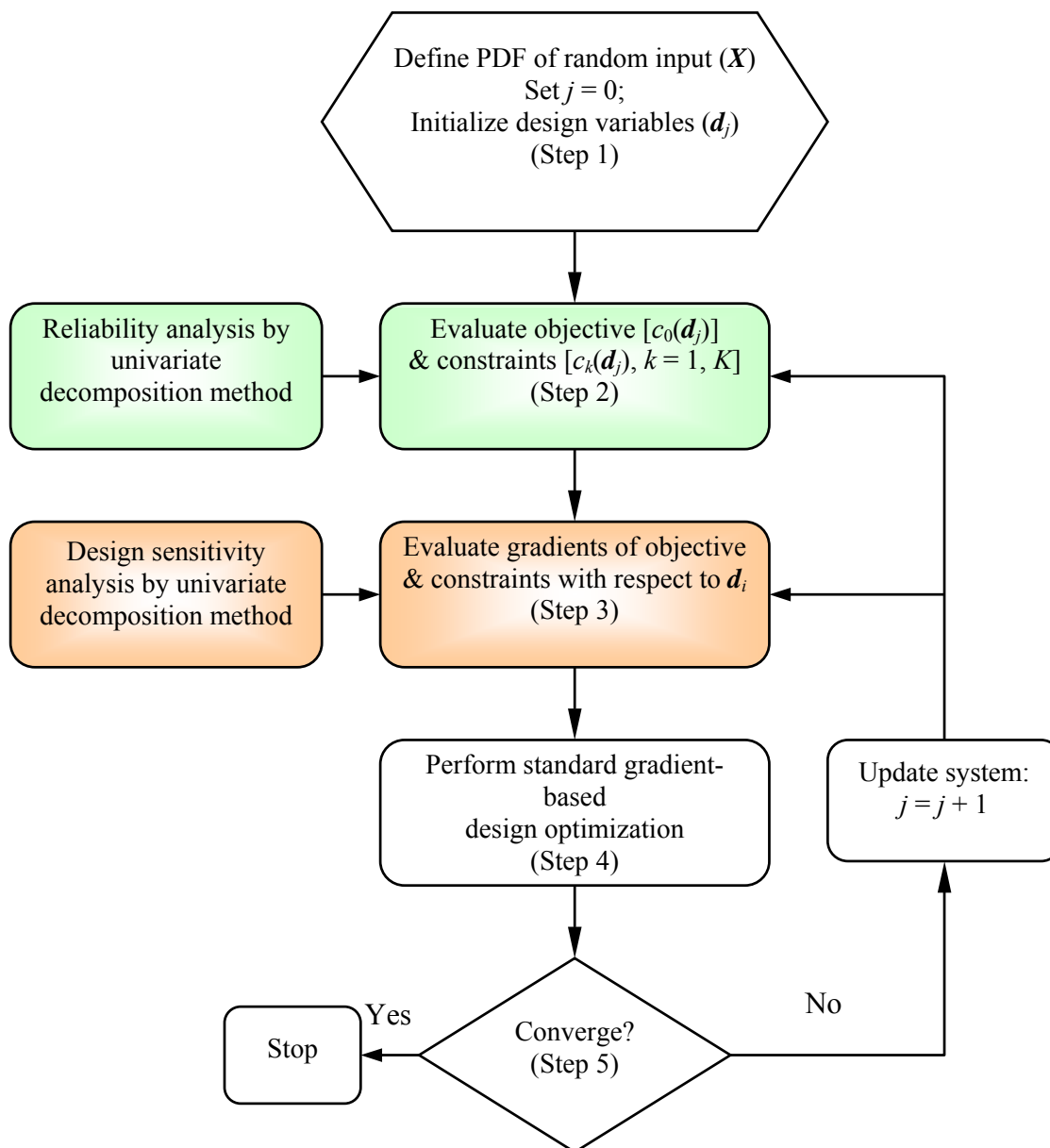**Figure 6.1 Various approximations of the performance function of _k_th constraint**

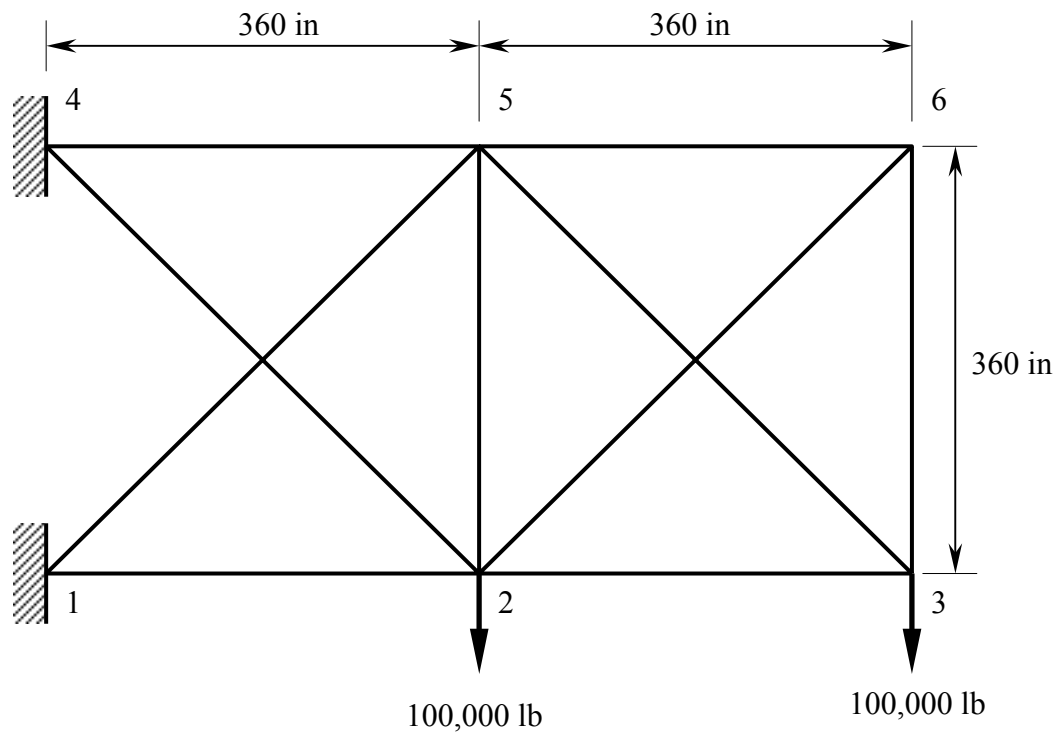**Figure 6.2 Flowchart of the proposed RBDO process**

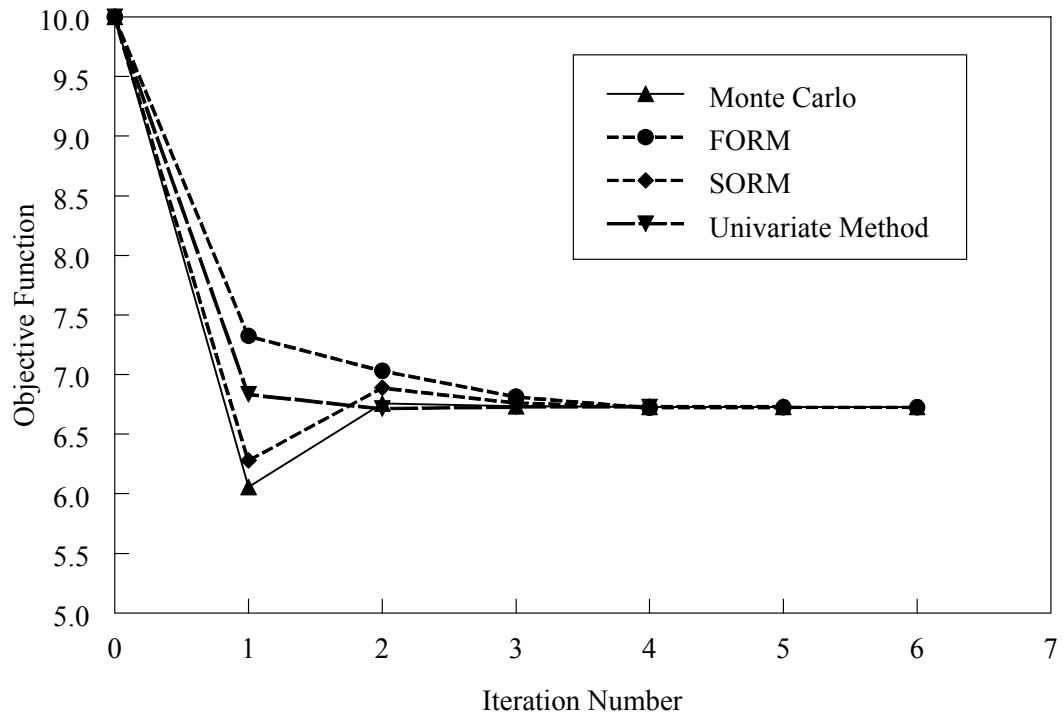**Figure 6.3 A ten-bar truss structure (Repeating Figure 3.4)**

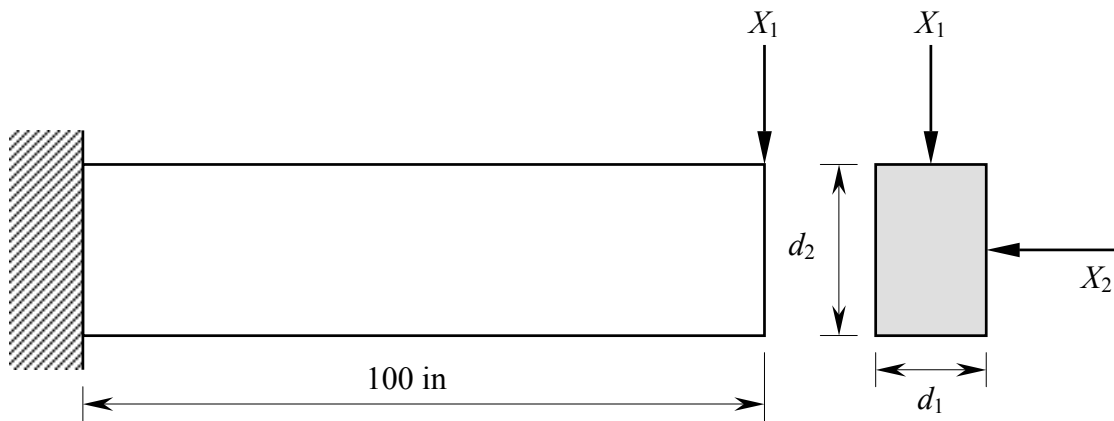**Figure 6.4 History of mathematical objective function**

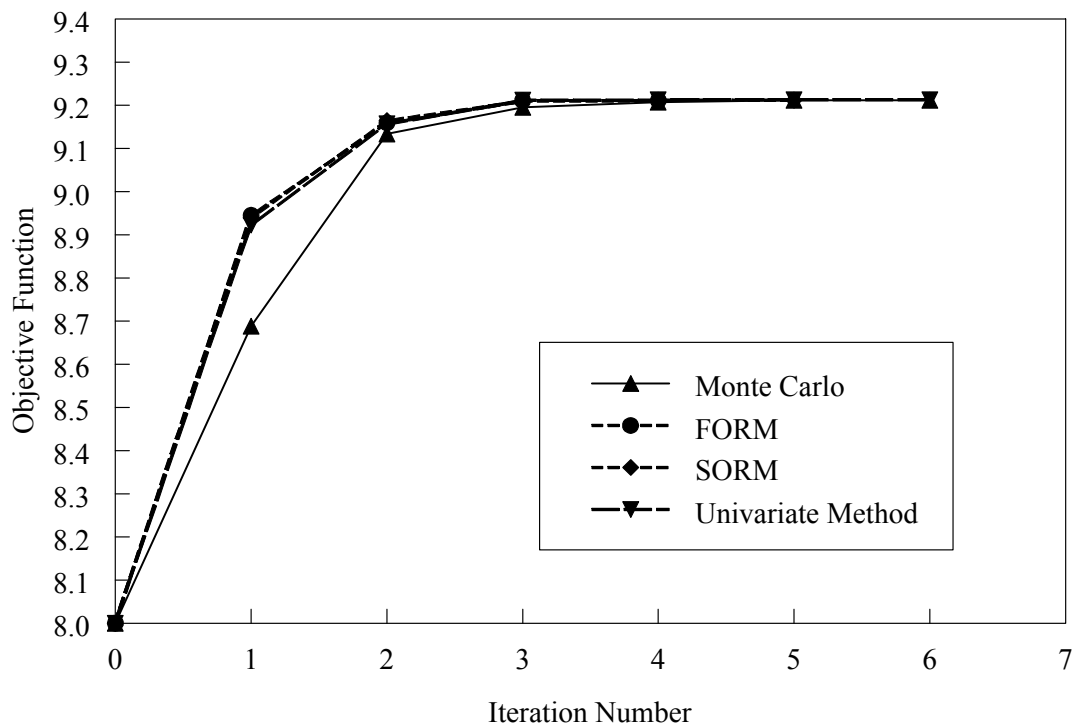**Figure 6.5 A cantilever beam subjected to end loads**

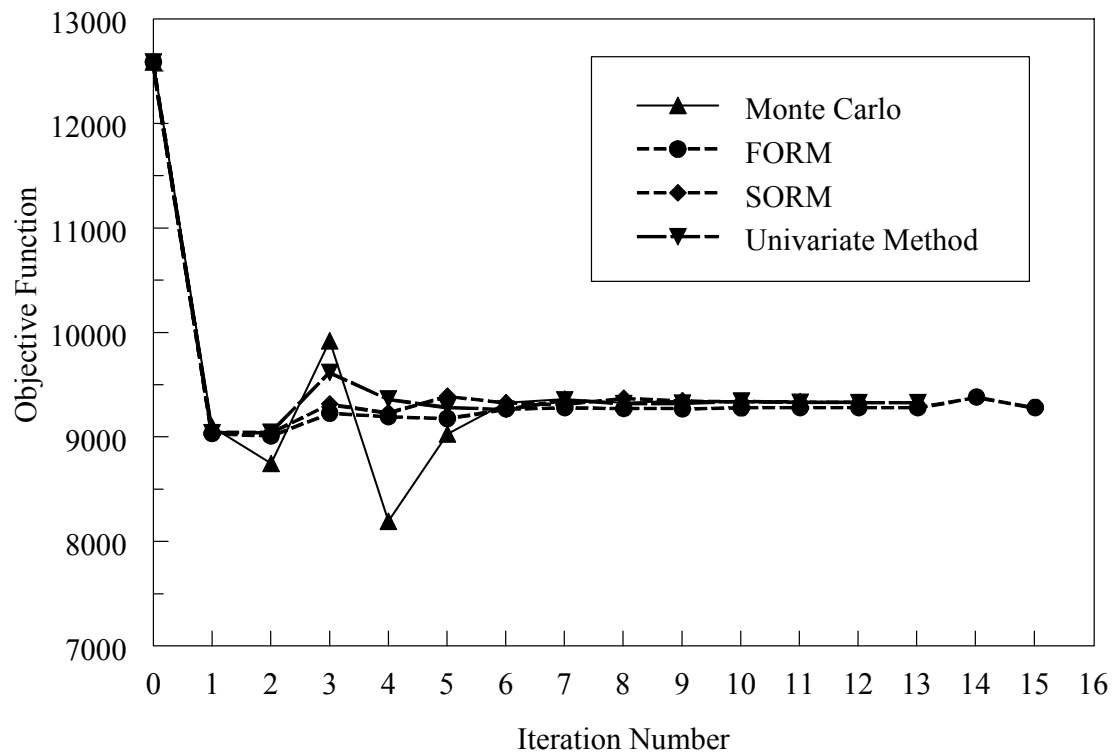**Figure 6.6 History of objective function for cantilever beam**

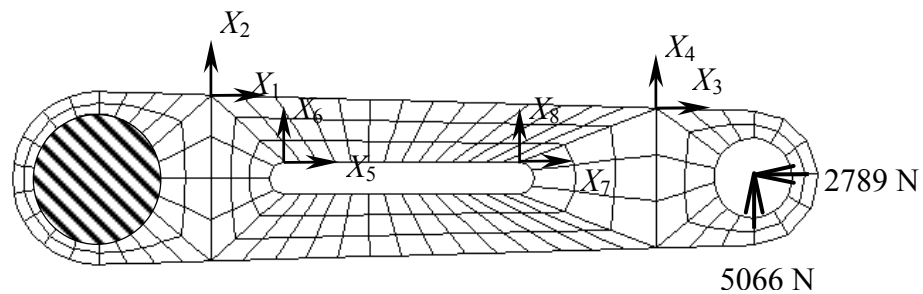**Figure 6.7 History of objective function for 10-bar truss**

Figure 6.8 Initial design of torque arm geometry at mean values of shape parameters
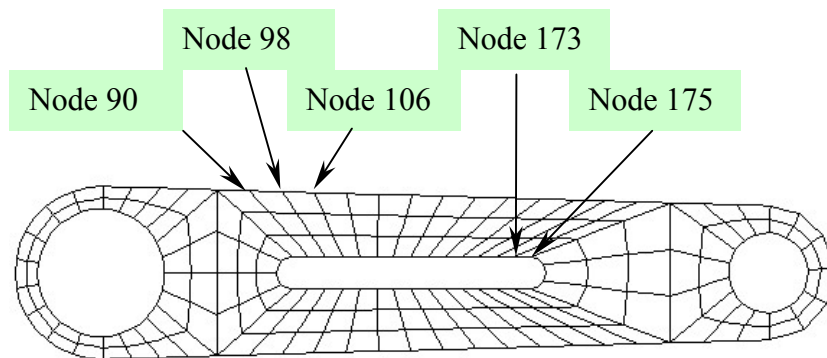

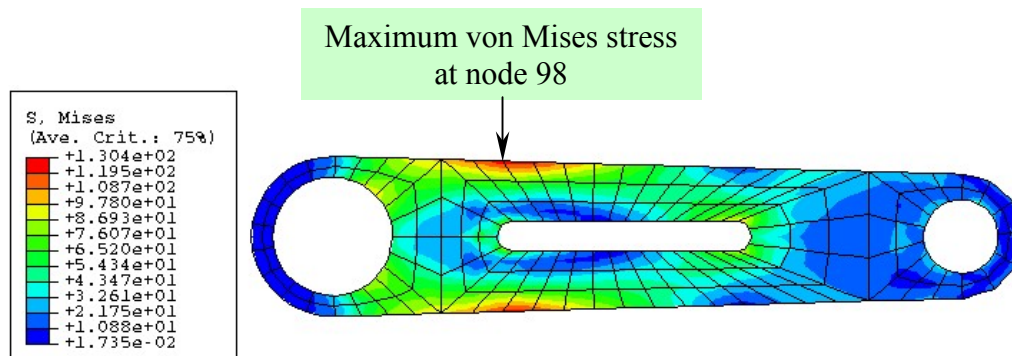**Figure 6.9 Locations of points for prescribing constraints**

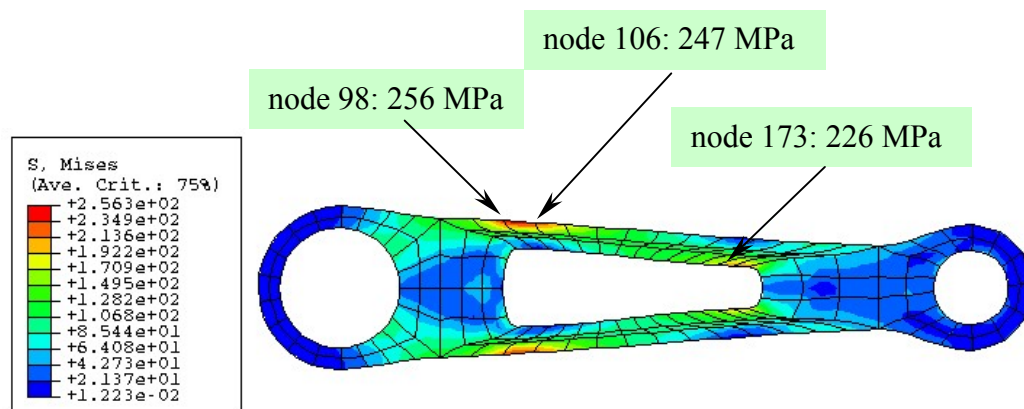**Figure 6.10 Contour of von Mises stress at mean values of shape parameters for initial design**

Figure 6.11 Contour of von Mises stress at mean values of shape parameters for RBDO design
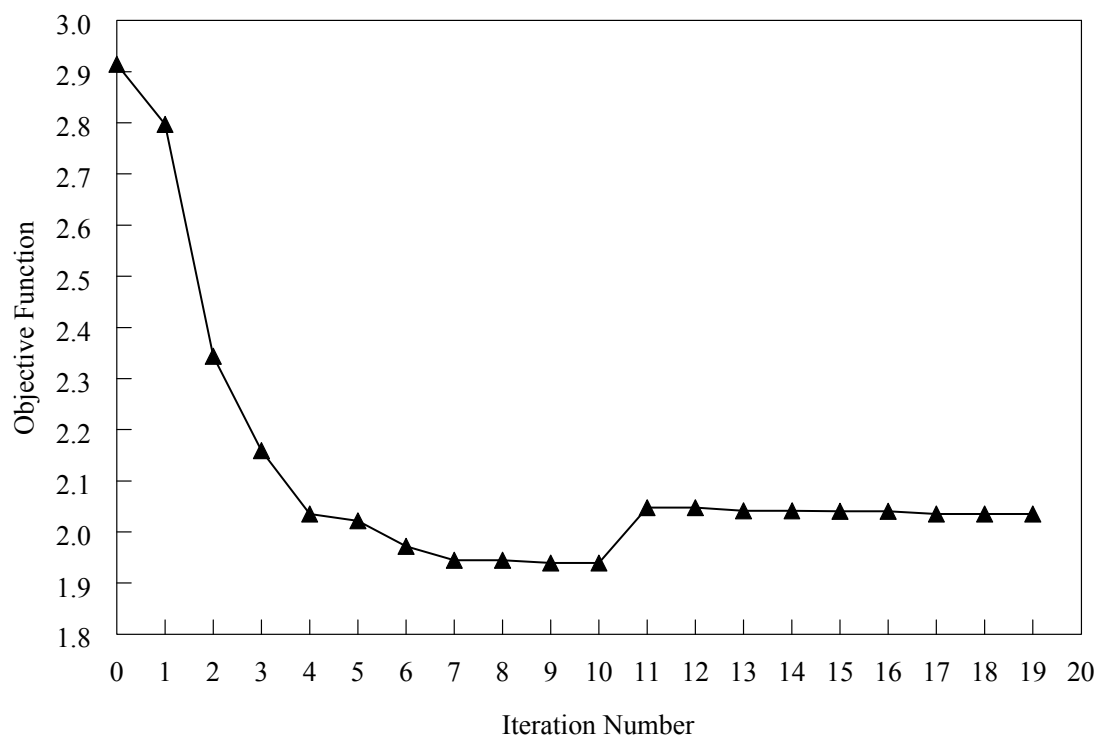
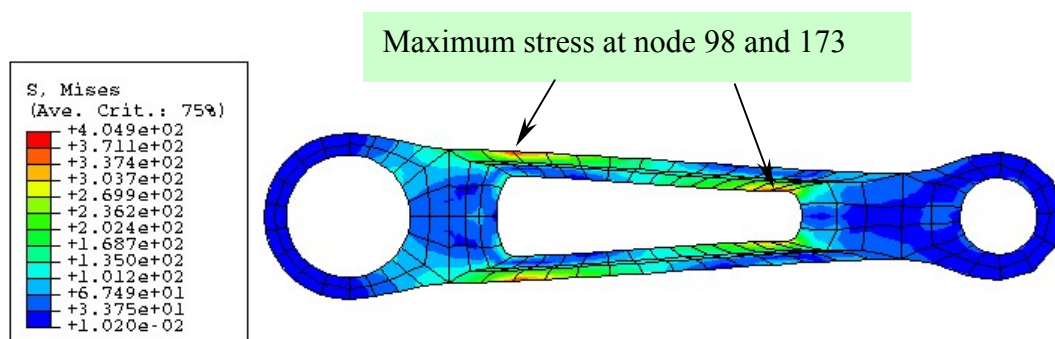**Figure 6.12 Optimization history of objective function for torque arm**

Figure 6.13 Contour of von Mises stress at mean values of shape parameters for risk-ignoring optimum design

CHAPTER 7

CONCLUSIONS AND RECOMMENDATIONS FOR

FUTURE WORK

7.1 Summary and Conclusions

The primary objective of this study is to develop a new stochastic method to solve highly nonlinear reliability problems, referred to as the most probable point (MPP)-based decomposition method, for reliability analysis and subsequent design optimization of complex engineering systems. The following four research directions have been pursued: (1) development of an MPP-based univariate method with simulation; (2) development of an MPP-based univariate method with numerical integration; (3) development of an MPP-based univariate method for solving multiple MPPs problems; (4) sensitivity analysis and reliability-based design optimization involving the new univariate method. The conclusions from above four studies are summarized in the following subsections.

7.1.1 MPP-based Univariate Method with Simulation

A new univariate decomposition method employing the most probable point as the reference point was developed for predicting failure probability of uncertain structural and mechanical systems. The method involves novel decomposition at most probable point that facilitates a univariate approximation of a general multivariate function, response surface generation of the univariate function, and Monte Carlo simulation. In addition to the effort of identifying the MPP, the method requires a small number of exact or numerical evaluations of the performance function at selected input. Four numerical examples involving mathematical functions and structural/solid-mechanics problems

illustrate the proposed method. Comparisons were made with alternative approximate and simulation methods to evaluate the accuracy and computational efficiency of the univariate response-surface method developed. Results indicate that the proposed method provides accurate and computationally efficient estimates of probability of failure. Finally, the fatigue failure of lever arm in a wheel loader was evaluated, demonstrating the ability of the new method in solving industrial-scale fatigue reliability problems.

7.1.2 MPP-based Univariate Method with Numerical Integration

A new and alternative univariate method was developed for predicting component reliability of mechanical systems. This method involves novel function decomposition at most probable point that facilitates univariate approximation of a general multivariate function in the rotated Gaussian space and one-dimensional integrations for calculating the failure probability. Based on linear and quadratic approximations of the univariate component function in the direction of most probable point, two mathematical expressions of the failure probability were derived. In both expressions, the proposed effort in evaluating the failure probability involves calculating conditional responses at selected input determined by sample points and Gauss-Hermite integration points. Results of five numerical examples involving elementary mathematical functions and structural/solid-mechanics problems indicate that the proposed method provides accurate and computationally efficient estimates of the probability of failure. Compared with the previous work, no Monte Carlo simulation is required in the present version of the

univariate method developed. Although both versions of the univariate method have comparable computational efficiency, the new method should be useful in deriving sensitivity of failure probability for reliability-based design optimization, which is the ultimate goal of probabilistic mechanics.

7.1.3 Multi-Point Univariate method

A multi-point univariate decomposition method was developed for solving component reliability problems involving multiple most probable points (MPPs). The method is based on: (1) a novel function decomposition at all MPPs that facilitates local univariate approximations of a performance function in the rotated Gaussian space, (2) Lagrange interpolation for univariate component functions and return mapping to the standard Gaussian space, and (3) Monte Carlo simulation. The proposed decomposition results in an approximate failure domain that is constructed by a union of failure sub-domains associated with all MPPs. The boundary of the approximate failure domain can be highly nonlinear, which consists of explicit functions of random input variables. Hence, the embedded Monte Carlo simulation can be conducted for an arbitrarily large sample size. In addition to the effort in identifying all MPPs, the computational effort in the multi-point method developed can be viewed as performing deterministic response analysis at user-selected input defined by sample points. Compared with the multi-point FORM/SORM available in the current literature, the multi-point univariate method provides higher-order approximations of the boundary of the failure domain. Three numerical examples involving elementary mathematical functions and a structural

dynamics problem illustrate the proposed method. Comparisons were made with existing multi-point FORM/SORM and direct Monte Carlo simulation to evaluate the accuracy and computational efficiency of the univariate method developed. Results indicate that the multi-point univariate method consistently provides an accurate and computationally efficient estimate of the probability of failure.

7.1.4 Design Sensitivity Analysis and RBDO by Univariate Method

A new univariate decomposition method was developed for design sensitivity analysis and reliability-based design optimization of mechanical systems subject to uncertain performance functions in constraints. The method involves a novel univariate approximation of a general multivariate function in the rotated Gaussian space for reliability analysis; analytical sensitivity of failure probability with respect to design variables; and standard gradient-based optimization algorithms. In both reliability and sensitivity analyses, the proposed effort can be viewed as performing multiple one-dimensional integrations. The evaluation of these one-dimensional integrations requires calculating only conditional responses at selected deterministic input determined by sample points and Gauss-Hermite integration points. Results of two numerical examples involving mathematical functions and truss problems indicate that the proposed method provides accurate and computationally efficient estimates of the sensitivity of failure probability. Subsequent results of four design problems, entailing mathematical functions and structural/solid-mechanics applications, indicates that the new sensitivity

equations developed facilitate an accurate and/or efficient method for reliability-based design optimization of mechanical systems.

7.2 Recommendations for Future Work

1. The accuracy of the univariate approximation in the MPP-based univariate method may depend on the orientation of first N-1 axes. In the current work, the orientation is defined by the matrix R obtained from the Gram-Schmidt orthogonalization. However, an improved approximation may be possible by selecting an orientation that is optimal in some sense. Future efforts should be expended to define relevant criteria that lead to an optimal choice for defining the first N-1 axes.

2. The high accuracy of the univariate method developed has been demonstrated in conjunction with the double-loop formulation for solving simple RBDO problems. However, for solving industrial-scale design problems, the double-loop approach is very expensive because of the coupled inner (reliability) and outer (design) iterations of an RBDO process. Therefore, further research is required in making the proposed univariate method computationally more efficient by potentially decoupling the design and reliability iterations or exploring the possibility of single-loop formulations.

3. The class of RBDO problems studied entails a single deterministic objective function and constraints that are associated with only component reliability analysis. A major future effort should focus on solving a generalized RBDO

problem, where there are multiple objective functions that require stochastic analysis and constraint functions that include both component and system reliability analyses.

APPENDIX A. APPROXIMATE EVALUATIONS OF σ_m AND $\Delta\varepsilon$

For a uniaxial stress state, let S_{max}, ΔS, e_{max}, and Δe denote elastically calculated maximum stress, stress range, maximum strain, and strain range at an arbitrary point, which are typically evaluated using linear-elastic FEM. Define σ_{max}, $\Delta\sigma$, ε_{max}, and $\Delta\varepsilon$ as maximum stress, stress range, maximum strain, and strain range at the same point that are evaluated using appropriate elastic-plastic analysis. Using Neuber's rule and linear-elastic calculations, the inelastic maximum stress σ_{max} and inelastic strain range $\Delta\varepsilon$ can be estimated by solving the following two pairs of equations (Stephens et al., 2001)

$$
\begin{aligned}
\sigma_{max}\varepsilon_{max} &= K_f^2 S_{max} e_{max} \\
\varepsilon_{max} &= \frac{\sigma_{max}}{E} + \left(\frac{\sigma_{max}}{K'}\right)^{1/n'}
\end{aligned}
\tag{A.1}
$$

and

$$
\begin{aligned}
\Delta\sigma\Delta\varepsilon &= K_f^2 \Delta S \Delta e \\
\Delta\varepsilon &= \frac{\Delta\sigma}{E} + 2\left(\frac{\Delta\sigma}{2K'}\right)^{1/n'},
\end{aligned}
\tag{A.2}
$$

respectively, where $K' = \sigma_f'/\varepsilon_f'^{\,b/c}$ and $n' = b/c$ are Ramberg-Osgood parameters,

$$
K_f = \begin{cases} 1, & \text{without defect} \\ 1 + \dfrac{K_t + 1}{1 + a/r}, & \text{with defect} \end{cases},
\tag{A.3}
$$

is the fatigue notch factor, $K_t = 2.05$ is the elastic stress concentration factor due to a spherical notch, and $a = 0.0274\left(2070/S_u\right)^{1.8}$ with S_u in MPa and a in mm (Stephens et al., 2001). The inelastic mean stress can be easily estimated from $\sigma_m = \sigma_{max} - \Delta\sigma/2$. For a

multiaxial stress state, the simplest approach involves following the same procedure using von Mises equivalent stresses and strains. Note that there are other rules, such as linear rule, Glinka's strain energy density rule, for estimating inelastic stresses and strains (Stephens et al., 2001). They were not considered in this study.

APPENDIX B. POROSITY FIELD AND DEFECT SIZE

Casting simulation codes, such as MAGMASOFT (2002), are currently available that allow the size and location of shrinkage discontinuities to be predicted before a mechanical component is actually cast.   Consider a three-dimensional mechanical component with physical domain $\Omega \subset \mathbb{R}^3$ and a small subdomain $\Omega_x \subset \Omega$ in the vicinity of a spatial point $\boldsymbol{x} \in \Omega \subset \mathbb{R}^3$.   If $p(\boldsymbol{x})$ represents the porosity field over Ω_x, the equivalent mean radius μ_r of a spherical hole (*i.e.*, with porosity = 1) can be obtained from

$$\mu_r = \left[\frac{3 \int_{\Omega_x} p(\boldsymbol{x}) d\boldsymbol{x}}{4\pi} \right]^{1/3} . \tag{B.1}$$

Using Equation B.1 and predicted porosity field from casting simulation, the mean size of a casting-induced defect can be estimated.

APPENDIX C. BARRIER METHOD FOR FINDING MULTIPLE MPPS

The basic idea behind barrier method (Kiureghian, et al, 1998) is that by constructing artificial barriers around previously identified MPPs, the searching algorithm is forced to seek a new MPP. Since the objective function is the distance $\|\boldsymbol{u}\|$ between limit state and origin, a "barrier" around the first MPP $\boldsymbol{u}_1^*$ can be constructed by moving the limit state surface in the neighborhood of $\boldsymbol{u}_1^*$ away from the origin. By adding a "bulge" to the limit state surface, the modified limit state function $h_1(\boldsymbol{u})$ is described by $h_1(\boldsymbol{u}) = h(\boldsymbol{u}) + b_1(\boldsymbol{u})$, where $h(\boldsymbol{u})$ is the transformed limit state function in the standard normal space ($\boldsymbol{u}$-space), and $b_1(\boldsymbol{u})$ defines the bulge function fitted at $\boldsymbol{u}_1^*$. Solving the optimization problem with the limit state function $h_1(\boldsymbol{u})$ leads to a second MPP $\boldsymbol{u}_2^*$. A bulge $b_2(\boldsymbol{u})$ is now added at $\boldsymbol{u}_2^*$, resulting to the limit state function $h_2(\boldsymbol{u}) = h_1(\boldsymbol{u}) + b_2(\boldsymbol{u})$, which can be used to seek a third MPP $\boldsymbol{u}_3^*$. This process is continued until all MPPs are identified (See Figure C.1). Thus, the limit state function for finding the mth MPP is

$$h_{m-1}(\boldsymbol{u}) = h_{m-2}(\boldsymbol{u}) + b_{m-1}(\boldsymbol{u}) = h(\boldsymbol{u}) + \sum_{i=1}^{m-1} b_i(\boldsymbol{u}). \qquad (C.1)$$

To define the bulge, it is important to make sure that the foot of the bulge has a strong outward curvature. Furthermore, the starting point for subsequent searching iterations is selected in the direction away from previous bulges to reduce the possibility of convergence at the bulges' feet. The following considerations lead to a definition of a bulge $b_i(\boldsymbol{u})$ at a MPP $\boldsymbol{u}_i^*$:

(1) $b_i(\boldsymbol{u})$ must have a positive value in the neighborhood of $\boldsymbol{u}_i^*$ (in order to move the limit state surface away from the origin), and zero elsewhere.

(2) It is desirable that the bulge has a strong outward curvature at its feet.

(3) Each of the modified limit state functions must be continuous and differentiable. That means each bulge function $b_i(\boldsymbol{u})$ must be continuous and differentiable. Based on the proceeding considerations, select

$$b_i(\boldsymbol{u}) = \begin{cases} s_i \left(r_i^2 - \left\| \boldsymbol{u} - \boldsymbol{u}_i^* \right\|^2 \right)^2, & \left\| \boldsymbol{u} - \boldsymbol{u}_i^* \right\| \le r_i \\ 0, & \text{elsewhere} \end{cases} \tag{C.2}$$

where r_i is the radius of the bulge and s_i is a positive scale factor. The profile of the bulge is shown in Figure C.2. The second-order derivative of $b_i(\boldsymbol{u})$ at the foot is

$$\left. \frac{\partial^2 b_i}{\partial \boldsymbol{u}^2} \right|_{\left\| \boldsymbol{u} - \boldsymbol{u}_i^* \right\| = r_i} = -4 s_i r_i^2 + 12 s_i \left\| \boldsymbol{u} - \boldsymbol{u}_i^* \right\|^2 \Big|_{\left\| \boldsymbol{u} - \boldsymbol{u}_i^* \right\| = r_i} = 8 s_i r_i^2. \tag{C.3}$$

It follows that s_i and r_i must be large in order to have a strong curvature at the foot of the bulge.

(4) If multiple MPPs exist, they are usually far apart. If not, then owing to the smoothness of the limit state surface, the corresponding tangent planes must be nearly coincident, which implies that one of these points needs to be considered. Select r_i as $\gamma \beta_i$, where γ is a parameter. A small γ is conservative but may produce insufficient curvature at the foot of the bulge, whereas a large γ may result in a bulge that conceals other significant MPPs.

(5) The scale parameter s_i controls the height of the bulge and, therefore, the distance by which the limit state surface around $\boldsymbol{u}_i^*$ moves away from the origin. s_i must be

sufficiently large to assure a strong curvature at the foot of the bulge. Suppose that the design is pushed away from the origin by the amount $\delta\beta_i$, where $0 < \delta < \gamma$. The necessary height of the bulge at that point is approximated by $\delta\beta_i \tan\theta = \delta\beta_i \left\|\nabla h\left(\boldsymbol{u}_i^*\right)\right\|$. Using Equation (C.2), s_i can be written as

$$s_i = \frac{\delta\beta_i \left\|\nabla h\left(\boldsymbol{u}_i^*\right)\right\|}{\left[\left(\gamma\beta_i\right)^2 - \left(\delta\beta_i\right)^2\right]^2}. \tag{C.4}$$

Equation (C.2) and (C.4) together with parameters γ and δ completely define the bulge at each MPP $\boldsymbol{u}_i^*$ in terms of the quantities β_i and $\left\|\nabla h\left(\boldsymbol{u}_i^*\right)\right\|$.

Initial point $\boldsymbol{u}_0$ also needs to be chosen at the beginning of each search. At first, set $\boldsymbol{u}_0 = 0$ for all MPPs, and $\gamma \neq 1$. Then, it is more efficient if $\boldsymbol{u}_0$ is chosen on the opposite side of previous bulges. For example, select $\boldsymbol{u}_0$ for finding the mth MPP as

$$\boldsymbol{u}_0 = -\varepsilon\left(\boldsymbol{u}_1^* + \boldsymbol{u}_2^* + \cdots + \boldsymbol{u}_{m-1}^*\right), \tag{C.5}$$

where ε is a small positive number in the range 0.2-0.5.

As shown in Figure C.3, define φ_i as the angle between $\boldsymbol{u}_i^*$ and line from the origin to the foot of the bulge $b_i\left(\boldsymbol{u}\right)$. The largest value of φ_i occurs when the limit state surface is spherical (the distance from the foot of the bulge to the origin is also equal to β_i). Using the cosine rule for the triangle in Figure C.4, φ_i satisfies

$$\varphi_i \leq \cos^{-1}\left(1 - 0.5\gamma^2\right), \tag{C.6}$$

which defines the half-angle of a hyper-cone that completely contains the bulge. Any MPP found within this cone is potentially spurious. Convergence to a spurious MPP is usually an indication that no more genuine MPPs exist.
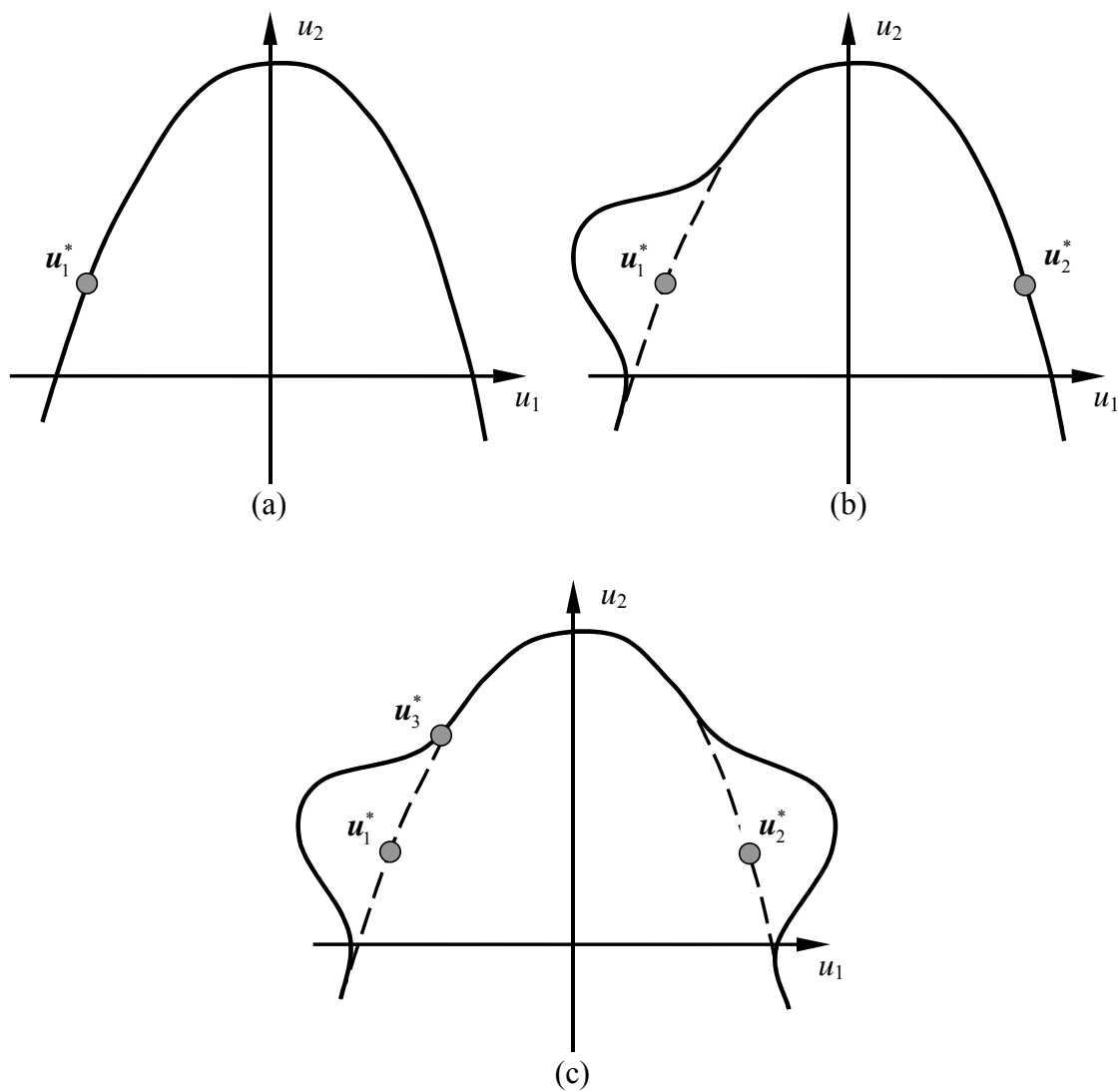
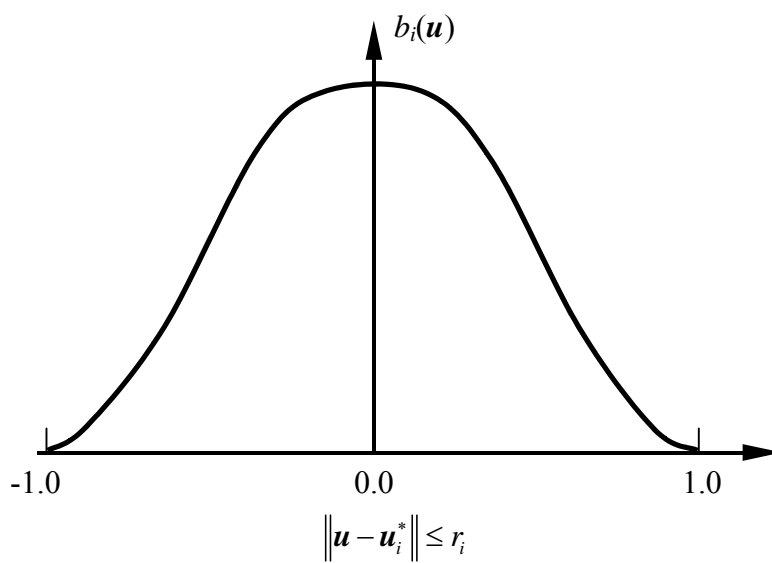**Figure C.1 Successive uses of bulges to find multiple MPPs**

$$\|\bm{u} - \bm{u}_i^*\| \le r_i$$
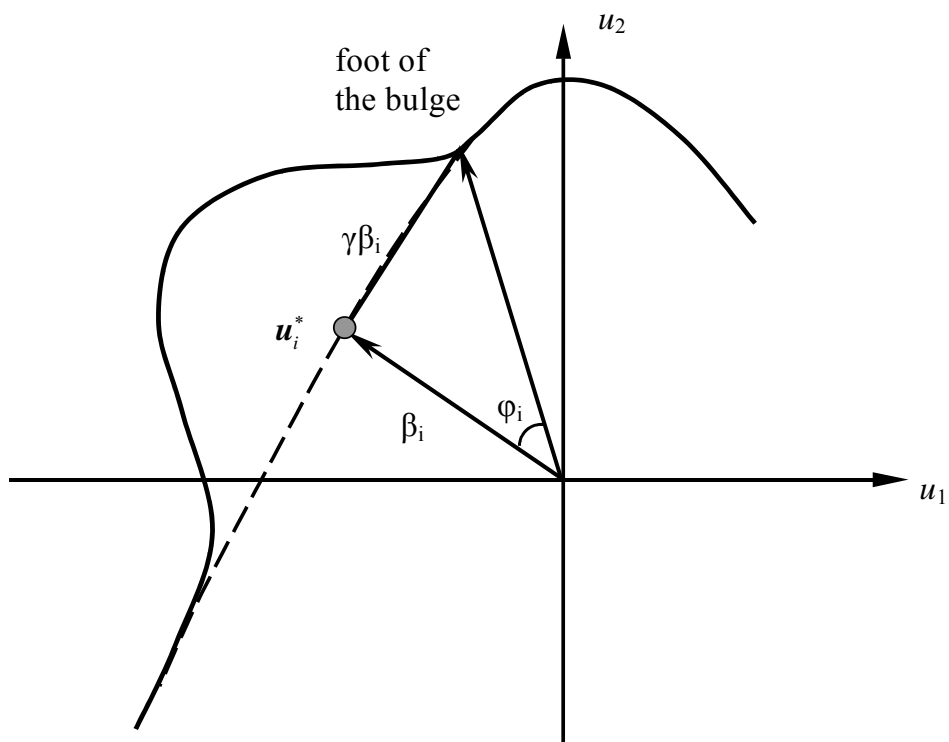
Figure C.2 Profile of the bulge

Figure C.3 Definition of cone containing the bulge

APPENDIX D. SENSITIVITY ANALYSIS BASED ON FORM/SORM

When gradient-based optimization algorithm is used in RBDO, the analytical sensitivity for reliability analysis should be provided. Here assuming reliability analysis is based on FORM or SORM.

If using FORM, the derivative of failure probability with respect to ith design variable in x-space using chain rule and Equation (6.14) is

$$\frac{\partial P_{F,1}}{\partial d_i} = -\phi\left(-\beta_{HL}\right)\frac{\partial \beta_{HL}}{\partial d_i} = \phi\left(-\beta_{HL}\right)\left[\frac{\nabla h\left(u;d\right)^T}{\left\|\nabla h\left(u;d\right)\right\|}\frac{\partial u}{\partial d_i}\right]_{u=u^*} , \qquad \text{(D.1)}$$

where β_{HL} is Hasofer-Lind reliability index, $\nabla h = \left\{\partial h/\partial u_1, \cdots, \partial h/\partial u_N\right\}^T$, $\left\|\bullet\right\|$ is the $\mathbb{L}_2$ norm, $\partial u/\partial d_i = \left\{\partial u_1/\partial d_i, \cdots, \partial u_N/\partial d_i\right\}^T$ is obtained from the x-u transformation, and u^* is the MPP in u-space.

If using SORM, the derivative of failure probability with respect to ith design variable in x-space is

$$\frac{\partial P_{F,II}}{\partial d_i} = \frac{\partial P_{F,II}}{\partial \beta_{HL}}\frac{\partial \beta_{HL}}{\partial d_i} = -\frac{\partial P_{F,II}}{\partial \beta_{HL}}\left[\frac{\nabla h\left(u;d\right)^T}{\left\|\nabla h\left(u;d\right)\right\|}\frac{\partial u}{\partial d_i}\right]_{u=u^*} , \qquad \text{(D.2)}$$

where $\partial P_{F,II}/\partial \beta_{HL}$ depends on different type of SORM methods. For example, if Breitung's asymptotic solution (Breitung, 1984) is used to obtain failure probability, then its derivative with respect to β_{HL} can be estimated by

$$\frac{\partial P_{F,II}}{\partial \beta_{HL}} = -\left[\phi\left(\beta_{HL}\right)\prod_{i=1}^{N-1}\left(1+\kappa_i\beta_{HL}\right)^{-1/2} + \frac{1}{2}\Phi\left(-\beta_{HL}\right)\sum_{i=1}^{N-1}\frac{\kappa_i}{1+\kappa_i\beta_{HL}}\prod_{j=1,j\neq i}^{N-1}\left(1+\kappa_j\beta_{HL}\right)^{-1/2}\right],$$
$$\text{(D.3)}$$

where κ_i, $i=1,\cdots,N-1$ is the main curvature at MPP. κ_i is assumed as a constant which does not change with β_{HL}, that is, $\partial \kappa_i/\partial \beta_{HL} = 0$.

REFERENCES

1.   ABAQUS, User's Guide and Theoretical Manual, Version 6.3, Hibbitt, Karlsson, and Sorenson, Inc., Pawtucket, RI, 2002.

2.   Abramowitz, M. and Stegun, I., Handbook of Mathematical Functions, 9th Edition, Dover Publications, Inc., New York, NY, 1972.

3.   Adhikari, S. "Reliability Analysis using Parabolic Failure Surface Approximation," *ASCE Journal of Engineering Mechanics*, Vol. 130, No. 12, pp. 1407-1427, 2004.

4.   Agarwal H., Renaud J.E., Lee, J.C. and Watson, L.T., "A Unilevel Method for Reliability Based Design Optimization," Proceedings of *45th AIAA/ASME/ASCE/AHS/ASC Structures, Structural Dynamics and Materials Conference*, Palm Springs, CA, April 19-22, 2004.

5.   Agarwal H., Reliability Based Design Optimization: Formulations and Methodologies, Ph. D dissertation, The University of Notre Dame, 2004.

6.   Allen, M. and Vlahopoulos, N., "Numerical Probabilistic Analysis of Structural/Acoustic Systems," *Mech. Struct. & Mach.*, Vol. 30, pp. 353-280, 2002.

7.   Allen, M. and Maute, K., "Reliability-Based Design Optimization of Aeroelastic Structures," *Struct. Multidisc. Optim.*, Vol. 27, pp. 228-242, 2004.

8.   Anderson, T.L., Fracture Mechanics: Fundamentals and Applications, Second Edition, CRC Press Inc., Boca Raton, Florida, 1995.

9.   Arora, J.S., Introduction to Optimal Design, Second Edition, Elsevier Academic Press, San Diego, CA, 2004.

10.   Au, S. K. and Beck, J.L., "Estimation of Small Failure Probabilities in High Dimensions by Subset Simulation," *Probabilistic Engineering Mechanics*, Vol. 16, No. 4, pp. 263-277, 2001.

11.   Barbato, M. and Conte, J.P., "Finite Element Response Sensitivity Analysis: a Comparison between Force-Based and Displacement-Based Frame Element Models," *Journal of Comput. Methods Appl. Mech. Engrg.*, Vol. 194, pp. 1479-1512, 2005.

12.   Bjerager, P., "Probability Integration by Directional Simulation," *ASCE Journal of Engineering Mechanics*, Vol. 114, No. 8, pp. 1285-1302, 1988.

13. Bjerager, P., "On Computational Methods for Structural Reliability Analysis," *Structural Safety*, Vol. 9, No. 2, pp. 79-96, 1990.

14. Boresi, A.P. and Schmidt, R.J., Advanced Mechanics of Materials, 6th Edition, John Wiley & Sons, Inc., New York, NY, 2003.

15. Breitung, K., "Asymptotic Approximations for Multinormal Integrals," *ASCE Journal of Engineering Mechanics*, Vol. 110, No. 3, pp. 357-366, 1984.

16. Bucher C.G. and Bourgund, U., "A fast and Efficient Response Surface Approach for Structural Reliability Problems," *Structural Safety*, Vol. 7, pp. 57-66, 1990.

17. Cai, G.Q. and Elishakoff, I., "Refined Second-Order Reliability analysis," *Structural Safety*, Vol. 14, pp. 267-276, 1994.

18. Chen, X., Hasselman, T.K. and Neill, D.J., "Reliability Based Design Optimization for Practical Applications," Proceedings of *38th AIAA/ASME/ASCE/AHS/ASC Structures, Structural Dynamics, and Materials Conference and Exhibit*, Kissimmee, FL, 1997.

19. Chiralaksanakul, A. and Mahadevan, S., "First-Order Approximation Methods in Reliability-Based Design Optimization," *ASME Journal of Mechanical Design*, Vol. 127, pp. 851-857, 2005.

20. Choi, K.K. and Chang, K., "A study of Design Velocity Field Computation for Shape Optimal Design," *Finite Elements in Analysis and Design*, Vol. 15, pp. 317-341, 1994.

21. Choi, S.K., Grandhi, R.V. and Canfield, R.A., "Structural Reliability under Non-Gaussian Stochastic Behavior," *Computers and Structures*, Vol. 82, pp. 1113-1121, 2004.

22. Clough, R.W. and Penzien, J., Dynamics of Structures, 2nd Edition, McGraw-Hill, Inc., New York, NY, 1993.

23. Cornell, C.A., "A Probability-Based Structural Code," *Journal of American Concrete Institution*, Vol. 66, pp. 974-985, 1969.

24. Das, P.K. and Zheng, Y., "Cumulative Formation of Response Surface and its Use in Reliability Analysis," *Probabilistic Engineering Mechanics*, Vol. 15, No. 4, pp. 309-315, 2000.

25. Der Kiureghian, A., Lin, H.Z. and Hwang, S.J., "Second-Order Reliability Approximations," *ASCE Journal of Engineering Mechanics*, Vol. 113, No. 8, pp.1208-1225, 1987.

26. Der Kiureghian, A., "Structural Reliability Methods for Seismic Safety Assessment: a Review," *Journal of Engineering Structures*, Vol. 18, No. 6, pp.412-424, 1996.

27. Der Kiureghian, A. and Dakessian, T., "Multiple Design Points in First and Second-Order Reliability," *Structural Safety,* Vol. 20, No. 1, pp. 37-49, 1998.

28. Ditlevsen, O., Melchers, R.R. and Gluver, H., "General Multi-Dimensional Probability Integration by Directional Simulation," *Computers and Structures*, Vol. 36, No. 2, pp. 355-368, 1990.

29. Ditlevsen, O. and Madsen, H.O., Structural Reliability Methods, John Wiley & Sons Ltd., Chichester, 1996.

30. Du, X. and Chen, W., "Sequential Optimization and Reliability Assessment Method for Efficient Probabilistic Design," *ASME Journal of Mechanical Design*, Vol. 126, pp. 225-233, 2004.

31. Elegbede, C., "Structural Reliability Assessment Based on Particles Swarm Optimization," *Structural Safety*, Vol. 27, pp. 171-186, 2005.

32. Engelund, S. and Rackwitz, R., "A Benchmark Study on Importance Sampling Techniques in Structural Reliability," *Structural Safety*, Vol. 12, No. 4, pp. 255-276, 1993.

33. Faravelli, L., "Response Surface Approach for Reliability Analysis," *ASCE Journal of Engineering Mechanics*, Vol. 115, No. 12, pp. 2763-2781, 1989.

34. Fiessler, B. Neumann, H. J. and Rackwitz, R., "Quadratic Limit States in Structural Reliability," *ASCE Journal of the Engineering Mechanics Division*, Vol. 105, pp. 661-676, 1979.

35. Fishman, G. S., Monte Carlo: Concepts, Algorithms, and Applications, Springer, New York, NY, 1996.

36. Fitzgerald, W. J., "Markov Chain Monte Carlo Methods with Applications to Signal Processing," *Signal Processing*, Vol.81, pp.3-18, 2001.

37. Frangopol D. M and Maute K., "Life-Cycle Reliability-Based Optimization of Civil and Aerospace Structures," *Computers and Structures*, Vol. 81, pp. 397-410, 2003.

38. Grandhi, R. and Wang, L., "Reliability-Based Structural Optimization Using Improved Two-Point Adaptive Nonlinear Approximations," *Finite Elements in Analysis and Design*, Vol. 29, pp. 35-48, 1998.

39. Grandhi, R. and Wang, L., "Higher-Order Failure Probability Calculation using Nonlinear Approximations," *Computer Methods in Applied Mechanics and Engineering*, Vol. 168, pp. 185-206, 1999.

40. Guan, X.L. and Melchers, R.E., "Effect of Response Surface Parameter Variation on Structural Reliability Estimates," *Structural Safety*, Vol. 23, pp. 429-444, 2001.

41. Gupta, S. and Manohar, C.S., "An Improved Response Surface Method for the Determination of failure Probability and Importance Measures," *Structural Safety*, Vol.26, pp.123-139, 2004.

42. Haldar, A. and Mahadevan, S., Reliability Assessment using Stochastic Finite Element Analysis, John Wiley & Sons, Inc., New York, NY, 2000.

43. Hasofer A.M. and Lind N.C., "An Exact and Invariant First Order Reliability Format," *ASCE Journal of the Engineering Mechanics Division*, Vol. 100, No. 1, pp. 111-121, 1974.

44. Hohenbichler M. and Rackwitz, R., "Non-Normal Dependent Vectors in Structural Safety," *ASCE Journal of the Engineering Mechanics Division*, Vol. 107, pp. 1227-1238, 1981.

45. Hohenbichler, M., Gollwitzer, S., Kruse, W., and Rackwitz, R., "New Light on First- and Second-Order Reliability Methods," *Structural Safety*, Vol. 4, pp. 267-284, 1987.

46. Hohenbichler, M and Rackwitz, R., "Improvement of Second-Order Reliability Estimates by Importance Sampling," *ASCE Journal of Engineering Mechanics*, Vol. 114, No. 12, pp. 2195-2199, 1988.

47. Hurtado, J.E. and Barbat, A. H., "Monte Carlo Techniques in Computational Stochastic Mechanics," *Archives of Computational Methods in Engineering*, Vol. 5, No. 1, pp. 3-30, 1998.

48. Kaymaz, I. And McMahon C. A., "A Response Surface Method Based on Weighted Regression for Structural Reliability Analysis," *Probabilistic Engineering Mechanics*, Vol. 20, pp. 11-17, 2005.

49. Kharmanda, G., Mohamed, A. and Lemaire, M., "Efficient Reliability-Based Design Optimization Using a Hybrid Space with Application to Finite Element Analysis," *Struct. Multidisc. Optim.*, Vol. 24, pp. 233-245, 2002.

50. Kim, N.H., Choi, K.K. and Botkin, M.E., "Numerical Method for Shape Optimization Using Meshfree Method," *Struct. Multidisc. Optim.*, Vol. 24, pp. 418-429, 2003.

51. Kim, S. and Na, S., "Response Surface Method using Vector Projected Sampling Points," *Structural Safety*, Vol. 19, No. 1, pp. 3-19, 1997.

52. Kodiyalam, S. and Thanedar, P.B., "Some Practical Aspects of Shape Optimization and its Influence on intermediate Mesh Refinement," *Finite Elements in Analysis and Design*, Vol. 15, pp. 125-133, 1993.

53. Lemaire, M, "Finite Element and Reliability - Combined Methods by Response Surface," in PROBAMAT-21st century: Probabilities and materials - Tests, models and applications for the 21st century; Proceedings of *the NATO Advanced Research Workshop*, pp. 317-331, Kluwer Academic Publishers, Netherlands, 1997.

54. Li, H. and Foschi, R.O., "An Inverse Reliability Method and its Application," *Structural Safety*, Vol. 20, pp. 257-270, 1998.

55. Liang, J. Mourelatos, Z. P. and Tu, J., " A Single-Loop Method for Reliability-Based Design Optimization," Proceedings of *DETC' 04 ASME 2004 Design Engineering Technical Conferences and Computers and Information in Engineering Conference*, Salt Lake City, UT, September 28- October 2, 2004.

56. Liu, P. L. and Der Kiureghian, A., " Optimization Algorithms for Structural Reliability Analysis," Report No. UCB/SESM-86/09, Berkeley, CA, 1986.

57. Liu, P. L. and Der Kiureghian, A., "Optimization Algorithms for Structural Reliability," *Structural Safety*, Vol. 9, pp. 161-177, 1991.

58. Luenberger, D., Introduction to Linear and Non Linear Programming, Addison & Wesley, Reading, MA, 1986.

59. Mckay, M. D., Conover, W. J. and Beckman, R. J., "A Comparison of Three Methods for Selecting Values of Input Variables in the Analysis of Output from a Computer Code," *Technometrics*, Vol. 21, No. 2, pp. 239-245, 1979.

60. Madsen, H. O., Krenk, S, and Lind, N. C., Methods of Structural Safety, Prentice-Hall, Inc., Englewood Cliffs, NJ, 1986.

61. Madsen, H.O. and Hansen, P.F., "A Comparison of Some Algorithms for Reliaiblity Based Structural Optimization and Sensitivity Analysis," Proceedings of 4th *IFIP WG 7.5 Conference*, Munich, Germany, September 11-13, 1991.

62. Mahadevan, S. and Shi, P., " Multiple Linearization Method for Nonlinear Reliability Analysis," *ASCE Journal of Engineering Mechanics*, Vol. 127, Vol. 11, pp. 1165-1173, 2001.

63. MAGMASOFT, User Manual, MAGMA Foundry Technology Inc., Arlington Heights, IL, 2002.

64. Mansour, A.E. and Wirsching, P.H., "Sensitivity Factors and their Application to Marine Structures," *Marine Structures*, Vol. 8, pp. 229-255, 1995.

65. Melchers, R.E., Structural Reliability Analysis and Prediction, 2nd Edition, John Wiley & Sons, Inc., New York, NY, 1999.

66. Melchers, R.E. and Ahammed, M., "A Fast Approximate Method for Parameter Sensitivity Estimation in Monte Carlo Structural Reliability," *Computers and Structures*, Vol. 82, pp. 55-61, 2004.

67. Metropolis, N., Rosenbluth, A.W., Rosenbluth, M. N. and Teller, A. H., "Equations of State Calculations by Fast Computing Machines," *Journal of Chemical Physics*, Vol. 21, No. 6, pp. 1087-1092, 1953.

68. Nataf, A., "Determination des distribution dont les marges sont donnees," *Comptes Rendus de l'Academic des Sciences*, Vol. 225, pp. 42-43, 1962.

69. Nie, J. and Ellingwood, B.R., "Directional Methods for Structural Reliability Analysis," *Structural Safety,* Vol. 22, pp. 233-249, 2000.

70. Olsson, A. and Sandberg, G.E., "Latin Hypercube Sampling for Stochastic Finite Element Analysis," *ASCE Journal of Engineering Mechanics*, Vol. 128, No. 1, pp. 121-125, 2002.

71. Olsson, A. and Sandberg, G.E. and Dahlblom, O., "On Latin Hypercube Sampling for Structural Reliability Analysis," *Structural Safety*, Vol. 25, No. 1, pp. 47-68, 2003.

72. Papadimiriou, C., Beck, J.L. and Katafygiotis, L.S., "Asymptotic Expansions for Reliability and Moments of Uncertain Systems," *ASCE Journal of Engineering Mechanics*, Vol. 123, No. 12, pp. 1219-1229, 1997.

73. Penmetsa, R. and Grandhi, R., "Adaptation of Fast Fourier Transformations to Estimate Structural Failure Probability," *Finite Elements in Analysis and Design*, Vol. 39, pp. 473-485, 2003.

74. Qu, X., Venkataraman, S., Haftka, R. T. and Johnson, T. F., "Reliability, Weight, and Cost Tradeoffs in the Design of Composite Laminates for Cryogenic Environments," *42nd AIAA/ASME/ASCE/AHS/ASC Structures, Structural Dynamics, and Materials Conference and Exhibit*, AIAA-2001-1237, Seattle, WA, Apr. 16-19, 2001.

75. Qu, X. and Haftka, R. T., "Deterministic and Reliability-Based Optimization of Composite Laminates for Cryogenic Environments," *AIAA Journal*, Vol. 41, No. 10, pp. 2029-2036, 2003.

76. Rackwitz, R. and Fiessler, B., "Structural Reliability under Combined Load Sequences," *Computers and Structures*, Vol. 9, pp. 489-494, 1978.

77. Rackwitz, R. "Methods of System Reliability in Multidimensional Spaces," in Probabilistic Methods for Structural Design, Soares C.G. (ed.), pp. 161-212, Kluwer Academic Publishers, the Netherlands, 1997.

78. Rackwitz, R., "Reliability Analysis – A Review and Some Perspectives," *Structural Safety,* Vol. 23, No. 4, pp. 365-395, 2001.

79. Rahman, S. and Wei, D. "A Univariate Approximation at Most Probable Point for Higher-Order Reliability Analysis," *International Journal of Solids and Structures*, Vol. 43, pp. 2820-2839, 2006.

80. Rahman, S. and Xu, H. "A Univariate Dimension-Reduction Method for Multi-Dimensional Integration in Stochastic Mechanics," *Probabilistic Engineering Mechanics*, Vol. 19, pp. 393-408, 2004.

81. Rajashekhar M.R. and Ellingwood, B.R., "A New Look at the Response Surface Approach for Reliability Analysis," *Structural Safety*, Vol. 12, pp. 205-220, 1993.

82. Rosenblatt, M., "Remarks on a Multivariate Transformation," *Annals of Mathematical Statistics*, Vol. 23, pp. 470-472, 1952.

83. Royset, J.O., Der Kiureghian A. and Polak, E., "Reliability-Based Optimal Structural Design by the Decoupling Approach," *Reliability Engineering and System Safety*, Vol. 73, pp. 213-221, 2001.

84. Royset, J.O. and Polak, E., "Reliability-Based Optimal Design using Sample Average Approximations," *Probabilistic Engineering Mechanics*, Vol. 19, pp. 331-343, 2004.

85. Royset, J.O., Der Kiureghian A. and Polak, E., "Optimal Design with Probabilistic Objective and Constraints," Journal of Engineering Mechanics, Vol. 132, pp. 107-118, 2006.

86. Schueller, G. I. and Stix, R., "A Critical Appraisal of Methods to determine Failure Probabilities," *Structural Safety*, Vol. 4, No. 4, pp. 293-309, 1987.

87. Shao, S. and Morutso, Y., "Structural Reliability Analysis using a Neural Network," *JSME International Journal, Series A*, Vol. 40, No. 3, pp. 242-246, 1997.

88. Stein, M., "Large Sample Properties of Simulations using Latin Hypercube Sampling," *Technometrics*, Vol. 29, No. 2, pp. 143-151,1987.

89. Stephens, R.I., Fatemi, A., Stephens, R.R., and Fuchs, H. O., Metal Fatigue in Engineering, 2nd Edition, John Wiley & Sons, Inc., New York, NY, 2001.

90. Sudret, B. and Der Kiureghian, A., "Stochastic Finite Element Methods and Reliability - State-of-the-Art Report," Report No. UCB/SEMM-2000/08, Berkeley, CA, 2000.

91. Thacker, B.H., Riha, D.S. Millwater, H.R. and Enright, M.P., "Errors and Uncertainties in Probabilistic Engineering Analysis," *42nd AIAA/ASME/ASCE/AHS/ASC Structures, Structural Dynamics and Materials Conference and Exhibit*, AIAA-2001-1239, Seattle, WA, April 16-19, 2001.

92. Tu, J. Choi, K.K. and Park, Y.H., "A New Study on Reliability-Based Design Optimization," *Journal of Mechanical Design*, Vol. 121, pp. 557-564, 1999.

93. Tu, J. Choi, K.K. and Park, Y.H., "Design Potential Method for Robust System Parameter Design," *AIAA Journal*, Vol. 39, No. 4, pp. 667-677, 2001.

94. Tvedt, L., "Distribution of Quadratic Forms in Normal Space − Application to Structural Reliability," *ASCE Journal of Engineering Mechanics*, Vol. 116, No. 6, pp. 1183-1197, 1990.

95. US Army Corps Engineering, "Engineering and Design - Seismic Design Provisions for Roller Compacted Concrete Dams," Report No. EP 1110-2-12, 1995.

96. Wei, D. and Rahman R., "Structural Reliability Analysis by Univariate Decomposition and Numerical Integration," accepted in *Probabilistic Engineering Mechanics*, 2006.

97. Wu, Y.T., Millwater H.R., and Cruse T.A., "Advanced Probabilistic Structural Analysis Method for Implicit Performance Functions," *AIAA Journal*, Vol. 28, No. 9, pp.1663-1669, 1990.

98. Wu, Y.T., "Computational Methods for Efficient Structural Reliability and Reliability Sensitivity Analysis," *AIAA Journal*, Vol. 32, No. 8, pp.1717-1723, 1994.

99. Wu, Y.T., Shin, Y., Sues, R. and Cesare, M., "Safety-Factor Based Approach for Probability-Based Design Optimization," *42nd AIAA/ASME/ASCE/AHS/ASC Structures, Structural Dynamics and Materials Conference and Exhibit*, AIAA-2001-1239, Seattle, WA, April 16-19, 2001.

100. Wu, Y.T., Enright, M.P. and Millwater, H.R., "Probabilistic Methods for Design Assessment of Reliability with Inspection," *AIAA Journal*, Vol. 40, No. 5, pp.937-946, 2002.

101. Wu, Y.T., Shah, C.R. and Deb Baruah, A.K., "Progressive Advanced-Mean-Value Method for CDF and Reliability Analysis," *International Journal of Materials & Product Technology*, Vol. 17, No. 5/6, pp. 303-318, 2002.

102. Xu, H. and Rahman, S., "A Generalized Dimension-Reduction Method for Multi-Dimensional Integration in Stochastic Mechanics," *International Journal for Numerical Methods in Engineering*, Vol. 61, pp. 1992-2019, 2004.

103. Xu, H., Dimension-Reduction Methods in Computational Stochastic Mechanics and Reliability, Ph. D dissertation, The University of Iowa, 2004.

104. Xu, H. and Rahman, S., "Decomposition Methods for Structural Reliability Analysis," *Probabilistic Engineering Mechanics*, Vol. 20, pp. 239-250, 2005.

105. Yang, R.J. and Gu, L., "Experience with Approximate Reliability-Based Optimization Methods," *Struct. Multidisc. Optim.*, Vol. 26, pp. 152-159, 2004.

106. Yau, J.F., Wang, S.S., and Corten, H.T., "A Mixed-Mode Crack Analysis of Isotropic Solids using Conservation Laws of Elasticity," *Journal of Applied Mechanics*, Vol. 47, pp. 335-341, 1980.

107. Youn, B.D., Advances in Reliability-Based Design Optimization and Probability Analysis, Ph. D dissertation, The University of Iowa, 2001.

108. Youn, B.D., Choi, K.K. and Park, Y.H., "Hybrid Analysis Method for Reliability-Based Design Optimization," *ASME Journal of Mechanical Design*, Vol. 125, pp. 221-232, 2003.

109. Youn, B.D. and Choi, K.K., "A New Response Surface Methodology for Reliability-Based Design Optimization," *Computers and Structures*, Vol. 82, pp. 241-256, 2004.

110. Zhang, T., Choi, K.K. and Rahman, S., "A Hybrid Method Using Response Surface and Pattern Search for Design Optimization," Proceedings of *IDETC/CIE* 2005, *ASME 2005 Design Engineering Technical Conference & Computer and Information in Engineering Conference*, Long Beach, CA, September 24-28, 2005.

111. Zhang, Y. and Der Kiureghian, A., "Two Improved Algorithms for Reliability Analysis," in Proceedings of *6th IFIP WG7.5* "*Reliability and Optimization of Structural Systems*", 1995.

112. Zhang, Y. and Der Kiureghian, A., "Finite Element Reliability Methods for Inelastic Structures," Report No. UCB/SEMM-97/05, Berkeley, CA, 1997.

113. Zou, T. and Mahadevan, S., Mourelatos and Meernik, P., "Reliability Analysis of Automotive Body-Door Subsystem," *Reliability Engineering and System Safety*, Vol. 78, pp. 315-324, 2002.

114. Zou, T. and Mahadevan, S., "A direct Decoupling Approach for Efficient Reliability-Based Design Optimization," *Struct. Multidisc. Optim.*, Vol. 31, pp. 190-200, 2006.